



# LIBRARIES

UNIVERSITY OF WISCONSIN-MADISON

## **A simple stochastic model predicting conservative mass transport through the unsaturated zone into ground water. [DNR-001] c1986**

Brasino, John Sheldon

[Place of publication not identified]: [publisher not identified],  
c1986

<https://digital.library.wisc.edu/1711.dl/JLK5HC2F3GPBA8B>

<http://rightsstatements.org/vocab/InC/1.0/>

For information on re-use see:

<http://digital.library.wisc.edu/1711.dl/Copyright>

The libraries provide public access to a wide range of material, including online exhibits, digitized collections, archival finding aids, our catalog, online articles, and a growing range of materials in many media.

When possible, we provide rights information in catalog records, finding aids, and other metadata that accompanies collections or items. However, it is always the user's obligation to evaluate copyright and rights issues in light of their own use.

050 833

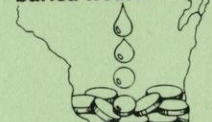
# Wisconsin Groundwater Management Practice Monitoring Project No. 1

Water Resources Center  
University of Wisconsin - MSN  
1975 Willow Drive  
Madison, WI 53706



Wisconsin Department of Natural Resources

**GROUNDWATER**  
Wisconsin's  
buried treasure







**A SIMPLE STOCHASTIC MODEL PREDICTING CONSERVATIVE MASS TRANSPORT  
THROUGH THE UNSATURATED ZONE INTO GROUND WATER**

**by**

Water Resources Center  
University of Wisconsin - MSN  
1975 Willow Drive  
Madison, WI 53706

**JOHN SHELDON BRASINO**

**A thesis submitted in partial fulfillment of the  
requirements for the degree of**

**Doctor of Philosophy  
(Civil and Environmental Engineering)**

**at the**

**UNIVERSITY OF WISCONSIN - MADISON**

**1986**



**A SIMPLE STOCHASTIC MODEL PREDICTING CONSERVATIVE MASS TRANSPORT  
THROUGH THE UNSATURATED ZONE INTO GROUND WATER**

**by**

**JOHN SHELDON BRASINO**

**A thesis submitted in partial fulfillment of the  
requirements for the degree of**

**Doctor of Philosophy  
(Civil and Environmental Engineering)**

**at the**

**UNIVERSITY OF WISCONSIN - MADISON**

**1986**

## Abstract

The development of a Randomized Plug Flow (RPF) model is motivated by the problem of large spatial variability in unsaturated zone parameters. The model utilizes a one-dimensional plug flow concept with conservative tracer applied as a delta function at  $i=0$ . Flow is defined as  $d = i/\theta$  where  $d(L)$  is the depth to the tracer,  $i(L)$  is the net infiltration, and  $\theta(L^3/L^3)$  is the field capacity of the soil.  $d$ ,  $i$  and  $\theta$  are defined as random variables  $D$ ,  $I$ , and  $\Theta$  respectively. The percent of mass applied that has reached the water table as a function of  $i$  is determined by  $F_\Theta(i/z)$ , where  $F_\Theta(\ )$  is the cumulative distribution function of  $\theta$  and  $z$  is the depth to ground water. Similar results are presented using distributions of  $i$  and  $d$ .

Five experiments conducted at the Hancock Experimental Station in the central sands region of Wisconsin are presented. The first experiment compares the transport of tracer to pesticide Aldicarb. Soil water samplers were installed in triplicate at depths of 3, 6 and 9 feet directly beneath potato hills in a 50' x 150' plot. Three wells with 2 foot screens at the water table were installed in furrows. Potassium bromide and Aldicarb were applied in narrow strips over the emerging plants and immediately hilled. Samples were taken over 372 days. Transport of Aldicarb is similar to bromide at the experimental plot. Both substances were transported to the water table in significant quantities far in advance of average rates of transport through the unsaturated zone.



The second experiment tests the accuracy of model transport predictions. Samplers were installed and tracer applied in a 60' x 60' plot as in Experiment 1. Samples were collected from 6 soil water samplers at 3 feet and 7 samplers at 6 feet for 180 days to determine the distribution of  $I$ . Ninety-one days after tracer application 23 soil cores were taken. Bromide and moisture content were determined to define the distributions of  $D$  and  $\Theta$  respectively. Wells surrounding the field with two foot screens at the water table were sampled for 237 days after application of the tracer to estimate transport of bromide to the water table. Comparisons are made assuming log normal or normal distribution of  $I$ ,  $D$  and  $\Theta$  and using Jury's Transfer Function Model, (TFM) (1982) to adjust distribution parameters. Normal distributions and distributions adjusted using the TFM show good agreement with the percent of mass transported to the ground water determined using well samples.

The utility of the method is illustrated in Experiments 3, 4 and 5. All three experiments use soil water samplers installed in triplicate at 3 and 6 feet to determine  $f_I(i)$ . Potassium bromide is applied as in Experiment 1. Experiment 3 compares mass transport to the ground water under 3 methods of potato cultivation; 20 inch disk hills, Lilliston cultivator hills and bed cultivation. Results are inconclusive due to large natural variability and problems with sample apparatus. Experiment 4 compares the effects of over irrigation on the three methods of potato cultivation. Transport under the hill treatments which apparently shed the excess water is not affected by 60% more irrigation. In contrast 200% more mass is predicted to reach the water table under the over irrigated

bed treatment within 300 days of tracer application. Experiment 5 compares in furrow placement of tracer to the placement described in Experiment 1. Five hundred percent more mass is predicted to reach the water table within 300 days after application of bromide in the furrow.

The RPF model may be calibrated using estimates of readily obtained parameters. It will probably provide good estimates of conservative mass transport to ground water in sandy soils.



## **Acknowledgments**

The author would like to thank Professor John Hoopes for encouragement and guidance which led to the development of this work. Appreciation is also expressed to Professors K. Potter, E. Miller, C. Tanner, M. Anderson, D. Armstrong and P. Bosscher for their help in various technical aspects of this report. Special thanks to my wife Terry for so much support and help in producing this document. This thesis was supported under grants from Wisconsin Department of Natural Resources, Wisconsin Geologic and Natural History Survey and Union Carbide Agricultural Products Division.

## Table of Contents

I. Introduction .....	1
II. Background .....	5
Physics of Transport .....	5
A. Water .....	5
B. Flow of Tracers Through Porous Media .....	9
Heterogeneity of Transport.....	15
Modeling.....	18
1. Advection-Dispersion.....	18
2. Advection-Dispersion with Storage.....	21
3. Simple Algebraic Models.....	23
4. Stochastic Differential Equations.....	27
III. Randomized Plug Flow and the Transfer Function Model .....	30
The Physical Model - Randomized Plug Flow .....	31
The Transfer Function Model .....	36
IV. Field Tests of the Models .....	42
Materials and Methods .....	43
A. Site Characterization .....	43
B. Tracer Selection .....	43
C. Soil Water Samplers .....	44
D. Wells .....	47
E. Chemistry .....	48
Experiment 1 .....	49
A. Methods .....	51
B. Results and Discussion .....	53
1. Breakthrough Curves.....	55
2. Tracer Movement.....	59
3. The Determination of Net Infiltration.....	66
4. Total Mass.....	69
5. Center of Mass and Peaks.....	71
6. The Transfer Function Model.....	72
7. Ergodicity.....	82
8. Conclusions.....	85



Experiment 2 .....	87
A. Methods .....	89
B. Results and Discussion .....	90
1. The Flow Pattern.....	90
2. Tests of Assumptions in the RPF Model.....	93
3. Breakthrough Curves.....	100
4. Transfer Function Model.....	102
5. Prediction of Mass Transported to the Water Table.....	114
C. Conclusions .....	126
V. Model Applications .....	129
Prologue .....	129
Experiment 3 .....	129
Results and Discussion .....	131
Conclusions .....	136
Experiment 4 .....	137
Results and Discussion .....	137
Conclusions .....	144
Experiment 5 .....	145
Results and Discussion .....	146
Conclusions .....	151
VI. Summary of Conclusions .....	152
VII. Comments and Recommendations for Further Work .....	155
Enhancements to the Model .....	156

VIII. Appendices .....	158
Appendix A .....	158
Solutions to the TFM .....	158
Predictions of Mass Transported to the Water Table ..	161
Appendix B .....	164
Appendix C .....	169
Appendix D .....	179
Addendum to Appendix D .....	186
Appendix E .....	187
Appendix F .....	188
Appendix G .....	195
Appendix H .....	197
Appendix I .....	202
Appendix J .....	216
Appendix K .....	223
Appendix L .....	229
IX. Bibliography .....	242



## I. Introduction

The importance of ground water should not be underestimated. Ground water is used as a primary source of drinking water by nearly half the population of the United States. Industrialization, population density, and agricultural activity all contribute to the problem of ground water contamination. Once contaminated, it is complicated, time-consuming, expensive and often not feasible to rehabilitate an aquifer. Therefore, the best solution to ground water pollution is prevention (Pye and Patrick, 1983).

In order to prevent ground water pollution, it is necessary to understand the influence of certain physical processes on the transport and fate of substances beneath the ground surface. This "understanding" may then be incorporated into a model of the movement and behavior of pollutants which allows prediction and quantification of contamination occurring under circumstances which have never before been studied. This is the power of a model. However, models do not offer a panacea. Even if a model is correct the quality of output is directly related to the quality of input. Errors or variability in initial conditions, parameters or boundary conditions may lead to totally false conclusions.

This research deals with ground water pollution via the application of agricultural chemicals at the ground surface. Any substance placed on an agricultural field moves through the unsaturated zone at a rate which is variable in space. Spatially variable transport rates in the unsaturated zone cause spatially variable concentrations of a substance in the unsaturated zone. Thus, if any of this substance reaches the water table

it will not arrive as it was applied to the surface (e.g., as a square pulse). Some of the total mass applied at the surface will arrive earlier and some later relative to the mean rate of movement through the unsaturated zone.

### The Problem

Many substances are used in agriculture that are undesirable as constituents of ground water. Suppose some substance (e.g., a pesticide) with particular plant uptake, decay, and adsorption rates is applied uniformly as a pulse on the surface. The problem then is to find the mass of the substance entering the ground water as a function of time. The most thorough approach would be to deterministically define the concentration of the substance entering the water table as a function of both space and time. At the other extreme a simple black box model calibrated to field data could be used to describe the concentrations averaged over space that are entering the ground water at a particular time.

My thesis employs a middle ground between a totally empirical "black box" method and a completely deterministic method. A conservative, non-adsorptive tracer (bromide) is used to test the method.

Solving the problem stated above for the case of bromide offered many advantages over investigating the behavior of a particular pollutant, such as aldicarb. Bromide and its analysis are inexpensive. Hence, resources could be concentrated on other aspects of experimental design, such as increasing the number of replicates. Due to savings in analysis, whole

new experiments were undertaken. The use of bromide simplified the problem, as the affects of adsorption and breakdown were removed. Thus, bromide provided a worst case scenario of possible contamination. This simplification also allows the method to be used to isolate and compare the affects of various agricultural management practices or soils on the advection of substances through the unsaturated zone.

From a regulatory point of view a worst case scenario is often desirable. However, adsorption and breakdown change dramatically for particular substances under various agriculture management practices or soils. In this case the use of bromide for comparisons may be misleading. The correlation of bromide movement to the movement of many substances of interest should change over the course of the experiment. The early transport of the bromide should correlate relatively well with simultaneous transport of degradable and adsorbable substances. The longer the bromide remains in a zone where adsorption or breakdown is pronounced, the poorer the correlation between the mass of bromide and mass of reactable substance. For this reason, the ability of the model to predict the distribution of contaminant early in the experiment is considered crucial.

### Thesis

The early arrival of tracer at the water table, far in advance of the center of mass of a square pulse of a conservative, non-adsorbing tracer, can be predicted by introducing random variables, derived from field experiments, into a physically based, mathematical model of transport.

## Outline

The first portion of this work is devoted to providing a background understanding of the physics and various models of solute transport in the unsaturated zone. A randomized plug flow model is then developed. The Randomized Plug Flow model and the method for determining the transport of mass to the water table which follows from it constitute new and original contributions to theory in this work. Next, Jury's transport function (1982) is introduced and defined in the context of the plug flow model. These two models, randomized plug flow and the modified transport function, are used to support the thesis.

Five experiments were conducted at Hancock Experimental Station to test and illustrate the utility of the models. The first experiment was conducted as preliminary research. The movement of bromide was compared to the movement of aldicarb through the unsaturated zone over a period of 372 days. The results of this experiment form the basis for understanding the problem stated above.

The second experiment was designed to test the model predictions of mass transport to the water table. In addition, the physical basis of the Randomized Plug Flow model is tested by comparing three independently derived estimates of the volumetric moisture content distribution.

The remaining experiments were designed to show the utility of the models. They are used to compare the effects on advection of two different irrigation rates, three different surface morphologies and furrow versus hill placement of tracer.

## II. Background

### Physics of Transport in the Unsaturated Zone

#### A. Water

The transport of a conservative tracer through the unsaturated zone occurs in solution and, neglecting diffusion and vapor transport, may be interpreted as the transport of particular parcels of water that have been "marked" by the tracer. For this reason, a brief review of the movement of water through the unsaturated zone, neglecting diffusion and vapor transport, is presented.

The movement of water within the soil may be classified into three distinct stages after E.E. Miller and A. Klute (1967):

- 1) Infiltration, the process whereby water enters into the soil through the surface;
- 2) Redistribution, usually resulting in a quasi-equilibrium or slow moving distribution; and
- 3) Withdrawal, due to evapotranspiration.

During these three stages, water flows in the direction of decreasing potential and the rate of flow is proportional to the potential gradient, so that a form of Darcy's Law describes the flow. As in saturated flow, the hydraulic conductivity is related to the geometric properties of the pore channels through which flow takes place (Hillel, 1982). However, the similarity between saturated and unsaturated flow stops here. Bear (1972) treats unsaturated flow as the flow of two immiscible fluids (soil



gas and water) simultaneously flowing through a porous medium. He points out three important aspects of unsaturated flow:

- 1) Each fluid establishes its own set of tortuous paths to form very stable channels;
- 2) A unique set of channels corresponds to every degree of saturation; and
- 3) Any fluid that has become discontinuous cannot flow.

From 2) above and Hillel's observation that the hydraulic conductivity ( $K$ ) is related to the geometric properties of the pore channels, we might expect  $K$  to be a function of the moisture content ( $\theta$ ) of a soil. This is indeed the case. A function  $K(\theta)$  can be found for any soil where  $K$  increases with increases in  $\theta$ .

Water in the unsaturated zone is at a lower potential than water in the saturated zone at the same height. For example, where a zone of saturation meets the unsaturated zone, the unsaturated zone pulls water out of the zone of saturation resulting in a capillary fringe of saturated water under tension. This tension ( $\psi$ ) is continuous and exists to some extent throughout the unsaturated zone. It is related to the radii of curvature of the soil water by

$$\psi = -\sigma_{GL} (r_1^{-1} + r_2^{-1})$$

where  $\sigma_{GL}$  is the surface tension between the gas and the liquid phase and  $r_1$  and  $r_2$  are the two radii of curvature as illustrated in Figure 1 (White et al., 1976).

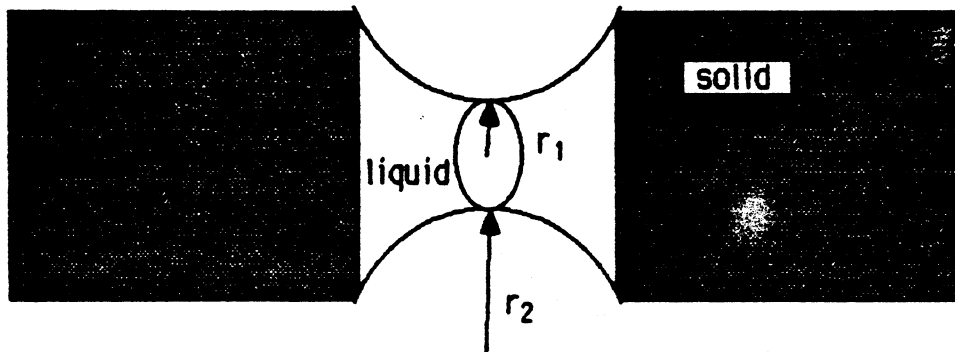


Figure 1. Radii of curvature.

Since  $\phi$  is continuous and assuming a constant  $\sigma_{GL}$  and no other forces, there is a tendency for water to move until  $(r_1^{-1} + r_2^{-1})$  are the same everywhere. If we consider a generalized pore geometry as in Figure 2, we can see that there are two positions, A and B, corresponding to a mostly full and mostly empty pore where a single  $\phi$  may be satisfied.

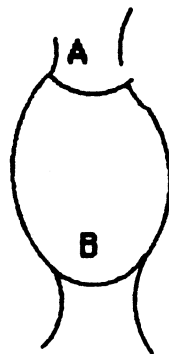


Figure 2. Generalized pore geometry

Thus,  $\theta$  is a hysteretic function of  $\phi$  and since  $K$  is a function of  $\theta$ ,  $K$  is also a hysteretic function of  $\phi$ . As expected from Figure 2, this hysteretic behavior depends on whether the soil is wetting or drying.

### Governing Partial Differential Equation

Darcy's Law for unsaturated flow in the  $x$  direction, in an isotropic soil is:

$$v_x = -K_H(\phi) \partial h / \partial x$$

where  $v_x$  is the velocity in the  $x$  direction,  $K_H(\phi)$  is the hydraulic conductivity as a hysteretic function of the local potential  $\phi$ , and  $h$  is the total potential =  $(\phi + Z)$  (Freeze and Cherry, 1979; Childs, 1969).

Substituting Darcy's Law into the conservation of mass of the volumetric soil water content (Miller and Klute, 1967; Schwartzendruber and Hillel, 1973) we find the Buckingham-Darcy flux equation:

$$\frac{\partial \theta}{\partial t} = - \frac{\partial}{\partial x} \left[ K_H(\phi) \frac{\partial \phi}{\partial x} \right] + \frac{\partial}{\partial y} \left[ K_H(\phi) \frac{\partial \phi}{\partial y} \right] + \frac{\partial}{\partial z} \left[ K_H(\phi) \left[ \frac{\partial \phi}{\partial z} + 1 \right] \right]$$

where  $\theta$  is the volumetric water content and  $x$ ,  $y$ , and  $z$  are coordinates in the horizontal and vertical (upward) directions, respectively.

## B. Flow of Tracers Through Porous Media

The four physical processes involved in the movement of a non-volatile tracer through the unsaturated zone are advection, diffusion, dispersion, and physical, chemical and biological reactions between and within stationary and moving phases. Advection is the transport of the tracer with the mean flow of the soil solution. Diffusion is the flow of tracer within the solution in response to concentration gradients. Dispersion is the spread and mixing of tracer between portions of the soil solution due to the distribution of velocities and the tortuosity of the paths of the soil solution. Reactions between and within stationary and moving phases include adsorption, desorption, transformation, degradation, electrostatic repulsion and attraction.

Consider the unsaturated advection of a step concentration change of a conservative tracer through a column of soil, freely drained to some moisture content. As the tracer solution moves through the column, the water initially in the pores is displaced to some extent so that a moisture front moves ahead of the tracer (Ghumand et al., 1975; Bressler, 1973; Warwick et al., 1971; Gelhar, 1983). The velocity distribution within a single pore, and the flow and velocity distribution at junctions of pores, some of which may be blind and exhibit no movement, cause an uneven penetration of the tracer solution. In addition, in unsaturated flow, the variations in the degree of saturation create an extremely wide range in pore velocities. These variations in pore velocity, which are also

enhanced by spatial variations in pore structure (heterogeneity), cause dispersive mixing (Gardner and Brooks, 1956). The velocity distributions effectively increase the surface area between the tracer and initial soil water solution. The increased surface area allows for more rapid diffusion or "dispersion enhanced diffusion" (Nielsen and Biggar, 1961, 1962a, 1962b, 1963). Since diffusion is a relatively slow process, the amount of diffusive versus dispersive mixing is dependent on the flow rate. The combined effects of dispersion and diffusion will cause tracer to appear at the bottom of a column of soil when only a fraction of the pore volume has infiltrated. Also, the breakthrough of the 50% concentration will occur significantly before one pore volume has infiltrated. It is useful to note that these facts point to the conclusion that there is an amount of water moving slowly or not moving in unsaturated soils, and this volume is inversely proportional to the water content.

Consider a pulse application of conservative tracer to a packed column of sandy loam soil previously drained to some soil moisture content. This application is followed by infiltration and redistribution of tracer-free water. Ghuman et al. (1975) used chloride as a tracer in packed columns of sandy loam to verify the results of Warwick et al. (1971). As expected from the above discussion, he found that the salt front coincided with the water front in the initially dry soil and lagged behind it in the initially wet soil (Figure 3).



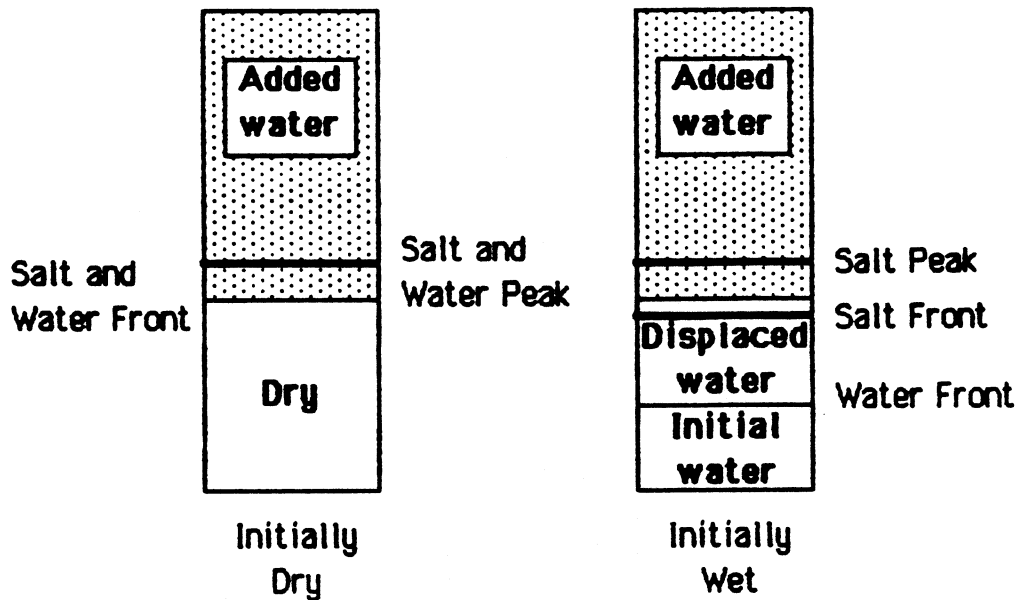
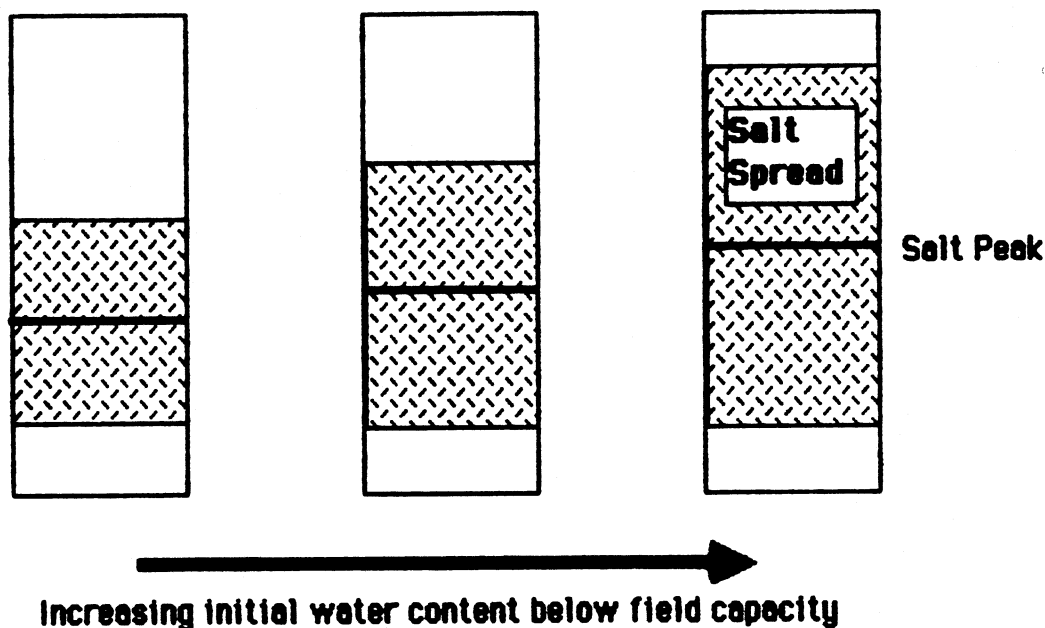


Figure 3. Comparison of salt and water front movement.

This lag in the wet soil is apparently due to the displacement of tracerless water in front of the infiltrating water. In addition, he found that the salt peak was above the depth at which the total water storage equalled the added water (Figure 3). Neglecting absorption or electrostatic attraction, this result is probably due to dispersion and/or dispersion enhanced diffusion. Holding the initial moisture content of the media below field capacity, the depth to the peak was found to be inversely proportional to the initial water content of the soil, and the salt spread in the profile increased as the initial water content increased (Figure 4). These observations are probably due to increased soil water storage and a change from diffusion-dominated to dispersion-dominated mixing with increased moisture.



**Figure 4. Salt spread and depth to peak as a function of initial water content.**

Assuming a one-dimensional advection-dispersion model and steady infiltration, the breakthrough curve of a degrading tracer applied as a pulse at the surface is shifted as compared to a conservative tracer (see Figure 5). Measured at a single point in space, the peak concentrations arrive earlier in time. Measured at a single point in time, the peak of the degrading tracer is reduced in magnitude but remains at the same point in space. The breakthrough curve of an adsorbed tracer is also shifted (see Figure 5). For an adsorbed tracer, the peak will be shifted to a longer time (relative to a non-adsorbed tracer) when measured at a single point in space. When measured at a single point in time, the peak will be shifted (relative to a non-adsorbed tracer) to a shorter distance in space respectively.

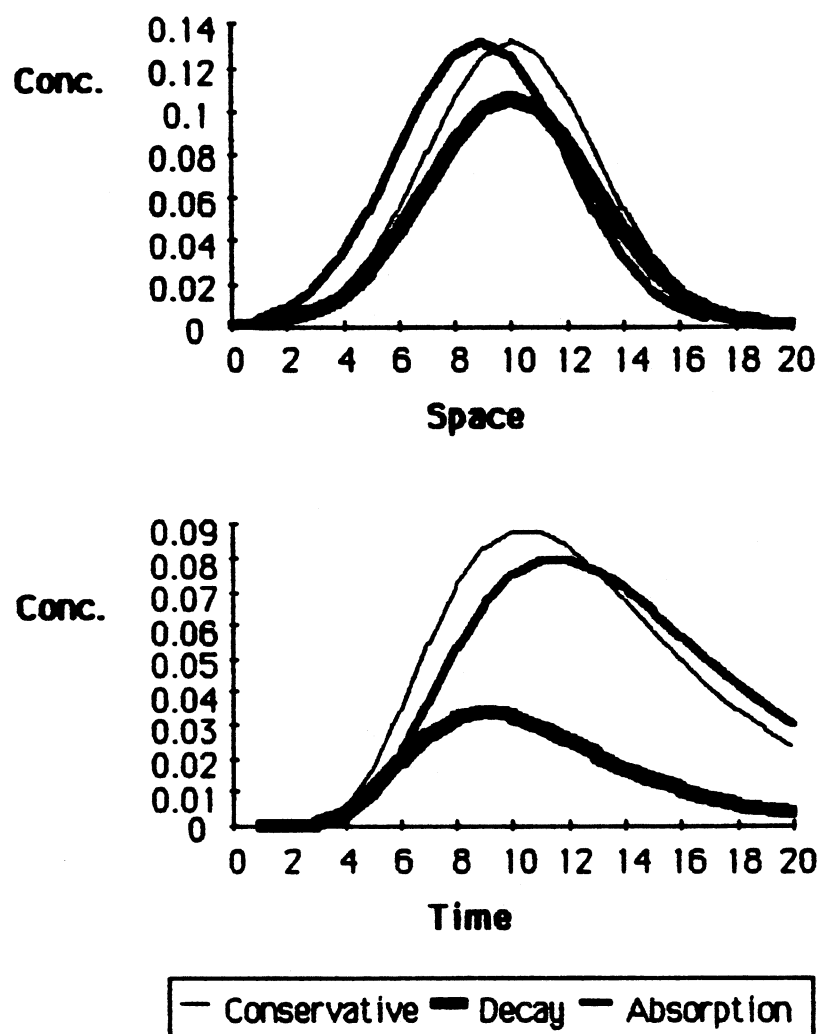


Figure 5. Theoretical breakthrough curves.

The extent to which the soil affects the transport of a tracer is mostly related to soil surface area and surface charge (Bohn et al., 1979). Charge development in soils results from either permanent isomorphous substitution during formation of the crystal lattice or an ionization of the functional groups on the surface of solids that make up the soil matrix. Although isomorphous substitution need not result in the development of a negative charge, a negative charge is far more common in most soil

minerals. The gain or loss of  $H^+$  from functional groups on the surface of soil solids accounts for pH dependent charge in soils. Some highly weathered soils dominated by hydrous oxides may actually have a net positive charge at low pH. However, most soils have a net negative charge.

The reaction of a negatively charged tracer such as  $Br^-$  in solution with a negatively charged solid is dependent on the thickness and potential of the electrochemical double layer. Stern (Stumm and Morgan, 1981) divided this region near the solid surface into two parts. The first Stern layer consists of a compact region of specifically adsorbed ions while the second Gouy layer is more diffuse. Sterns' model allows for a change in thickness of the Gouy layer with changes in ionic composition of the solution. In addition, if specific interaction outweighs electrostatic interaction, the inner layer may become more positive than the surface is negative, resulting in a negative Gouy layer.

A negative tracer may react with a negatively charged surface by being excluded from or negatively adsorbed to the electric bilayer. However, adsorption of  $NO_3^-$  and  $Cl^-$  is believed to be of minor consequence in the northern United States (Kurtz and Melstead, 1973). In addition, Bressler (1973) found that including anion exclusion of  $Cl^-$  in his model only slightly improved the fit to field data obtained in a Panoche clay loam. He also found no improvement in the fit to laboratory data obtained from columns of loam soil from Gilat Israel (Bressler et al., 1974).

The relatively low surface area, organic and clay content of the Plainfield sandy loam in which experiments were conducted minimizes any effects resulting from reactions between stationary and moving phases.

The aldicarb that was applied in Experiment 1 should be adsorbed to the 0.8% by weight organic fraction in the upper two feet. Because of the low organic content this effect should be small. Aldicarb should degrade with a half-life between 20 and 100 days in the unsaturated zone (Jones, 1984). Since aldicarb is a systemic pesticide, a large amount should be taken up by the potato plant roots. Potassium bromide used as a tracer in all experiments should behave conservatively. However, it also may be taken up in small amounts by the roots.

#### Heterogeneity of Transport

In the previous section, dispersion, diffusion, convection, moving and stationary interactions, and the physics of the soil system have been discussed. When we apply these concepts to transport in an entire field, there is a "very serious and certainly not yet solved problem of severe lateral variability in soil physical properties" (Miller, 1981). Although vertical variability presents important complications, these complications may be solved by discretizing the domain into horizontal planes with varying properties. With the use of digital computers and appropriate boundary conditions for each plane, a variety of problems, including vertical stratification, may be solved. It is the lateral or horizontal variability which seems to present overwhelming problems in the application of deterministic models.



Cassel et al. (1975), in studying the displacement of  $\text{NO}_3$  and  $\text{Cl}^{36}$  from disturbed and undisturbed cores of Aberdeen loam, found that using depth dependent values of water content and bulk density increased the accuracy of prediction of anion movement. It is important to note that in the same paper the authors point out that this improvement in accuracy may be less than the variation in solute movement among replicate cores. Indeed, horizontal variations of soil properties affecting transport may be huge. Hillel (1980) shows a table of estimated means, standard deviations and coefficients of variation found in the literature for ten soil properties within the same soil type. Coefficients of variation of saturated hydraulic conductivity range from 86% to 190%; unsaturated hydraulic conductivity from 170% to 400%; pore water velocity from  $1.7 \times 10^{-4}$ % to  $1.1 \times 10^{-4}$ %; and the apparent diffusion coefficient is given a single coefficient of variation of  $6.5 \times 10^5$ %.

Biggar and Nielsen (1976) show that the average position of a solute peak within a  $6.5 \text{ m}^2$  plot may be found within  $\pm 40\%$  of the true value when 20 soil cores are used to calculate the mean. In a 150 ha. (375 acre) field, 20 cores would allow the true mean to be estimated within an order of magnitude; 100 cores, within  $\pm 50\%$ ; and 1000 cores within  $\pm 10\%$ . Biggar and Nielsen (1976) claim that once the distribution of soil property is known, the parameters of the distribution may be used to estimate the mean with greater efficiency than a simple mean of all the samples. It is not clear that this is true if the distribution and parameters are not known and are merely assumed to have some distribution.

Jury et al. (1977) also found "a great deal of variability" between depth-equivalent solute movement measurements. In a subsequent sensitivity analysis, using a one-dimensional model, they found that large horizontal variations in several parameters including hydraulic conductivity had little effect on solute movement but variations in water uptake in the top 60 cm created large variations in concentrations at depth.

The structure of soil and in particular, the occurrence of macropores in a soil, may account for the large amount of variability in soil properties. In a review of macropores and water flow in soils, Beven and Germann (1982) show that the macropore concept has been used with pores of 30 micrometers to 10,000 micrometers equivalent diameter. Macropores are relatively larger continuous pores in a soil. They may be formed by animals, roots, or even water flow itself. The occurrence of macropores may explain large reductions in time of transport through undisturbed, as compared to disturbed, cores (McMahon and Thomas, 1974). Beven and Germann (1982) claim that "macropores may make up only a small portion of the soil voids but may dominate vertical flow rates during infiltration under some conditions".

An entirely different cause for the large variability in solute transport is the possibility that unsaturated flow, under certain conditions, may be unstable. Diment and Watson (1985) show graphically with soil columns that a fine over coarse stratified profile may result in very unstable flow. This instability was greatest in flow introduced into completely dry soils and decreased sharply with increases in initial water

content. However, they point out that their experimental systems were free from any local irregularities, such as macropores which might trigger instability when the initial water content is higher. White et al. (1977), using a Hele-Shaw model, showed that a gradual increase in saturated hydraulic conductivity in the direction of flow may cause instability. This instability may also occur in unsaturated flow. It should be noted that the fields in which these experiments were conducted probably exhibit an increase in saturated hydraulic conductivity with depth as the soil composition changes to almost 100% sand.

### Modeling

The purpose of this section is to review available models so that the reader may see where the modeling proposed in this report fits into the current literature. There are hundreds of models available which describe the flow of contaminants through the unsaturated zone. In this presentation they are organized into four categories:

- A) Advection-Dispersion
- B) Advection-Dispersion with Storage
- C) Simple Algebraic Models
- D) Stochastic Differential Models

#### A) Advection-Dispersion

The general equation for transport of solute through the unsaturated zone is derived from continuity considerations. The processes modeled

are advection, diffusion, dispersion, stationary-moving phase interactions and degradation. In Cartesian tensor notation, the equation is:

$$\frac{\partial}{\partial t} (\theta C + (1-n)S) + \frac{\partial}{\partial x_i} (q_i C) - Q = \frac{\partial}{\partial x_i} \left[ \theta (D + D_{ij}) \frac{\partial C}{\partial x_j} \right]$$

where:  $x_i$ , ( $i=1,2,3$ ) are Cartesian coordinates (L)

$\theta$  is the volumetric water content in interconnected pores ( $L^3/L^3$ )

$C$  is the concentration of chemical in solution ( $M/L^3$ )

$S$  is the concentration of chemical adsorbed onto soil ( $M/L^3$ )

$D_{ij}$  is the apparent dispersion tensor

$D_{ij}$  is the diffusion tensor

$q_i$  is the specific discharge vector

$Q$  is the rate of addition by sources or sinks

$n$  is the pore volume ( $L^3/L^3$ ).

This solute mass balance equation requires the complete description of the flow field, so that this must be determined before transport is modeled. Dispersion is represented as a Fickian (diffusion) process in the model. It should be noted that the validity of this representation is presently being debated in the literature (Molz, Guven and Melville, 1983). Two reasons for this debate are given at the beginning of the next section.

A review of several models employing some version of the advection-dispersion equation was offered by Boast (1973).  $S$  may be described using an equilibrium  $S = S(C_i)$  or non-equilibrium model.

$$\frac{\partial S}{\partial t} = \theta(S_i, C_i)$$

$Q$  may also be represented as a function of space  $Q = Q(x_i)$  or concentration  $Q = Q(S_i, C_i)$ . Analytical and numerical solutions have been found for a variety of boundary conditions and governing equations, including unsteady, non-uniform velocities (Boast, 1973; Enfield et al., 1982; Wilson and Gelhar, 1981; Bressler, 1973; Warrick et al., 1971).

The greatest value this model has is in conceptualization. Problems arise in the actual use of the model in a predictive mode in a field situation. First the flow field must be known. This involves finding the potential as a function of moisture content  $\phi(\theta)_H$  and hydraulic conductivity as a function of potential  $K(\phi)$ . Then the field must be monitored for  $\phi$  at various depths. The functions of  $S$  or  $Q$  must be found and calibrated. Finally,  $(D+D)_{ij}$  must be determined for the porous media. Considerable simplifications may be made to these methods. For example, coordinates may be arranged and diffusion may be neglected or lumped so that  $(D+D)_{ij}$  is reduced to transverse dispersivity ( $E_T$ ), and longitudinal dispersivity ( $E_L$ ).

These models only employ and produce horizontal spatial average values because the parameters (i.e.  $q_i$ ,  $E_L$ ,  $E_T$ ) are not known functions of

position in the horizontal plane. This is particularly disappointing since horizontal heterogeneity is very large. Hence, perhaps the greatest problem in applying these models to field situations is that they do not estimate the horizontal spatial heterogeneity of concentration profiles.

#### B. Advection-Dispersion with Storage

In general, the advection-dispersion models assume the applicability of a simple diffusion equation to the dispersion process. The coefficients of diffusion and dispersion are usually lumped together and must be found experimentally as some "effective" diffusion coefficient which is used as a fitted parameter in the advection-dispersion equation. Two problems arise in this process:

- 1) The "effective" diffusion coefficient has been found not to be constant but rather to increase with increasing scale of experiment; and
- 2) The advection-dispersion equation predicts breakthrough curves that are symmetric about the mean in space but many investigators have found asymmetrical concentration curves in laboratory and field experiments.

As a result of these problems with the advection-dispersion equation, there is interest in a reformulation of pollutant transport into an advection-diffusion equation. This model consists of areas of flow adjacent to dead end pores, and allows for diffusion of substance to and from these pores. It is interesting to note that this same concept of advection with diffusion into storage has been used in solute transport



stream models (Westrich, 1976; Rand and Tsai, 1984) and in saturated groundwater (Gillham et al., 1984). Coats and Smith (1964) used such a model to analyze transport of calcium chloride and sodium chloride through consolidated and unconsolidated cores. They found that it matched the data significantly better than the advection-dispersion model. They state this "model allows determination of the amount of dead end pore space in a porous matrix and the effect of velocity on the rate of diffusion into this space". The model in saturated, one-dimensional, steady uniform flow describes the transport of a conservative tracer through a column of length  $L$ .

$$nD \frac{\partial^2 C}{\partial x^2} - q \frac{\partial C}{\partial x} = fn \frac{\partial C}{\partial t} + (1-f)n \frac{\partial C^*}{\partial t}$$

and;

$$n(1-f) \frac{\partial C^*}{\partial t} = \frac{aq}{L} (C - C^*) \quad (\text{first order mass transfer})$$

where:  $f$  = fraction of pore space occupied by mobile fluid

$C^*$  = concentration in stagnant fluid

$n$  = pore volume

$a$  = rate constant (found by experiment)

$L$  = core length

and all other parameters are as previously defined. Coats and Smith (1964) give an analytical solution to this model for a particular set of

boundary conditions. They state that one of the major problems of the study was finding a unique set of the three parameters  $\alpha$ ,  $f$ , and  $D$ . Gaudet et al. (1977) modified the model for unsaturated flow, calibrated it at one depth in a uniform column and predicted concentrations of sodium chloride at other depths and the bottom of the column. They found very good agreement between predicted and actual concentrations. In addition, they found that a small reduction of 5.6% in the unsaturated moisture content increased the dead end water an order of magnitude and decreased the effective dispersion coefficient a factor of 6 (Figure 4). These results illustrate the strength of this model in the formation of a concept of unsaturated solute flow. However, assuming the model can be generalized, the problems are the same as with the advection-dispersion equation. The model uses and produces horizontal spatial averages which may be very difficult to determine as input parameters, and as the preliminary results in this report suggest, these averages may actually be unimportant as output parameters.

### C. Simple Algebraic Models

The rate of drainage and redistribution of water through the unsaturated zone in a sandy soil becomes very slow within a few days of an infiltration event. The moisture content that the media has drained to at this point is referred to as the field capacity of the soil. This rather loosely defined quantity is used to predict transport in many simple

algebraic models. Rao et al. (1976) present a model of one-dimensional solute transport given the following assumptions:

- i) Soil water in all pores participates in the transport process (no dead end or non-connected pores);
- ii) Soil water initially present in the profile is completely and instantaneously moved ahead of the water entering from above (piston flow);
- iii) All soil water instantly drains to field capacity;
- iv) Adsorption-desorption processes are modeled by assuming a linear and reversible equilibrium model.

The model is given by:

$$i = Z\theta_{fC}R$$

$$R = 1 + (\rho_B K_d / \theta_{fC})$$

where:  $i$  is the net amount of water added after a pulse of tracer is applied

$Z$  is the depth at which the tracer has arrived

$\theta_{fC}$  is the moisture content at field capacity

$R$  is the solute retention factor

$\rho_B$  is soil bulk density

$K_d$  is the soil adsorption coefficient (from experiment)

Time is introduced into the model through  $i$ .  $i$  may be input as an average rate of infiltration. The model does not predict solute concentration but estimates the position of the peak concentration. The authors found that

this simplified model was in agreement with the predicted solute front location using a transient, one-dimensional, advection-dispersion model and the actual field data for chloride movement in a sandy soil. Wehjte et al. (1984) in studying the movement of atrazine in an irrigated field under corn used the model to determine if atrazine found at depth was applied prior to the beginning of the study.

Burns (1975, 1976) offers a simple model which predicts the fraction of surface applied solute that leaches below any depth. This one-dimensional, solute transport model, excluding any moving-stationary phase interactions, is based upon the following assumptions:

- i) All soil water participates in transport as in Rao's model;
- ii) Soil water initially contained in the porous media is uniformly mixed with incoming water in discrete layers. This may result in transient supersaturation in these layers; and
- iii) Once totally mixed, the water in the upper layer drains to field capacity into the layer immediately below it.

As in Rao's model, dispersion is not included and time is introduced through  $i$ . But unlike Rao's model, the resulting concentration profile is dispersed. This apparent dispersion is due to the mixing in each layer.

The basic model developed from a set of perfectly mixed cells is given by:

$$f = \left[ \frac{i(L)}{i(L) + (\theta_{rc}(L^3/L^3)/100(L))} \right]^{z/t}$$

where:  $f$  is the fraction of surface applied solute leached below depth  $Z$ ;  
 $t$  is the thickness of each mixing layer and must be an integer multiple of  $Z$ .

Burns (1975, 1976), using  $t = 1$ , found good agreement between the model and field and laboratory observations.

These two models, which use the field capacity concept are certainly very easy to calibrate and use. They require a measurement of net infiltration ( $i = \text{gross infiltration} - \text{evapotranspiration}$ ) and field capacity ( $\theta_{fc}$ ). The Burns model also requires some decision about the mixing layer thickness ( $t$ ). Either a value may be assumed as Burns did ( $t = 1$ ), or it may be used as a calibration parameter. While the value of the advection-dispersion equations is in the representation of transport through the unsaturated zone, the value of these models is in the ease that they may be calibrated and used. Indeed, if the horizontal heterogeneity of the unsaturated systems is great, then these simple models may produce results just as reliable as models which are more difficult to calibrate. Although Rao's or Burn's models use and produce average values, the simplicity of these models makes Monte Carlo simulation techniques readily feasible. In such simulations, input parameters are considered random variables in space. Hence, a one-dimensional model may produce a distribution of concentrations at a single depth. Assuming a series of vertical, parallel, one-dimensional models may be used to represent three-dimensional space, the distribution of concentrations may be reported as distributions in the horizontal plane.

#### D. Stochastic Differential Models

Field observations show significant horizontal spatial heterogeneity of hydraulic properties in soil. For this reason, many authors have employed random variables as input parameters to the Buckingham-Darcy flux and the advection-dispersion equations. Yeh, Gelhar and Gutjahr (1985a, 1985b, 1985c) examined the Buckingham-Darcy flux equation under steady flow. Following Gardner, they model the relation between hydraulic conductivity ( $K$ ) and capillary pressure head ( $\phi$ ) as:

$$K(\phi, x_i) = K_S(x_i) \exp(-\alpha(x_i) \phi)$$

where saturated hydraulic conductivity ( $K_S$ ) and a fitted soil parameter ( $\alpha$ ) are represented by three-dimensional, statistically homogeneous (weakly stationary) fields. The specific goal of the analysis is to determine the mean and variance of the effective  $K(\phi)$  relation which will apply to a large area as well as the resulting behavior of the heterogeneous system. Weakly stationary implies:

- 1) That all one-dimensional distribution functions must be identical. That is, the mean of  $K$  or  $\alpha$  is not dependent on position. In general;

$$F_t(x) = P \{ \eta(t) < x \}$$

is identical for all  $t$  where  $\eta(t)$  is a finite family of random variables. Where  $F_t$  is the cumulative distribution function of  $t$  and  $P\{ \}$  is the probability of the quantity in the brackets;

- 2) All two-dimensional distribution functions can only depend on  $(t_1 - t_2)$ . That is, the covariance of  $(x_1, x_2)$  is only dependent upon the distance between the positions of  $x_1$  and  $x_2$ , not on their location. In general;

$$F_{t_1, t_2}(x_1, x_2) = P \{ \eta(t_1) < x_1, \eta(t_2) < x_2 \}$$

can only depend on  $(t_1 - t_2)$ ; and

- 3) All higher joint probability functions must be invariant also (Yaglom, 1962).

The assumption of stationarity in this model may be a source of contention because it seems reasonable that the mean and variance of hydraulic conductivity are functions of space. The theory developed by Yeh, Gelhar, and Gutjahr indicated increased capillary head variance as the soil becomes drier and substantially varying anisotropy if the mean of  $\alpha$  is large.

Bressler and Dagan (1982) state that

"although solutions of simultaneous transient flow and transport problems in three space coordinates and time in a spatially variable field are computationally impossible or at least impractical estimations of expectations and variances of  $\theta$  and  $C$  over a horizontal plane  $(x, y)$  as a function of time  $(t)$  and vertical coordinate  $(z)$  is relatively simple".

To illustrate their point they compare two models considering a single infiltration and redistribution of a conservative tracer in a soil of initially constant moisture content and concentration. In one model they used the advection-dispersion equation and a one-dimensional Buckingham-

Darcy equation. In a second model, they used a plug-flow estimate of flow and a simplified model for solute transport. The models require the input of ten parameters. All parameters except saturated hydraulic conductivity ( $K_S$ ) are constant.  $K_S$  is input as a weakly stationary, log normal, random variable. Analytical expressions are found for the means and standard deviations of  $\theta(Z,t)$  and  $C(Z,t)$  using the plug flow model. Expressions for the means and standard deviations of  $\theta(Z,t)$  and  $C(Z,t)$  are found for the advection-dispersion model by numerical integration. Using data from a highly variable Panoche soil and a less variable Bet Degan soil, Bressler and Dagan found that the plug flow model gave good estimates of the mean and standard deviation of  $\theta$  and  $C$  in both soils. They conclude that since stochastic modeling represents more realistically the actual water flow and salt transport phenomena, and provides the main statistical moments by simplified models, refinements of existing models or derivations of more complicated ones are unnecessary.

This simple approach is very powerful. However, the acquisition of ten input variables on a regular basis in many field situations would be difficult. The proposed modeling in the next section represents an effort to further simplify both the physical and mathematical model and the calibration procedure.



### III. Randomized Plug Flow and the Transfer Function Model

Due to the large spatial variability of the unsaturated zone and the need for models which may be calibrated without tremendous data requirements, many workers have stopped trying to represent material transport through the unsaturated zone in exact detail. Jury (1982) and Jury and Stolzy (1982) have proposed a transfer function model (TFM) of solute transport. They presented the TFM because the many causes of spatial variability of water solute transport (i.e. macropore flow, aggregate structure, permeability variations, unstable flow, flow barriers) make the calibration of a deterministic model very difficult, if not impossible, costly and time-consuming. In addition, because of the great variability of transport, the determination of average transport behavior may be inadequate.

The transfer function model is a black box approach. In the form given, it describes the transport of a conservative tracer through the unsaturated zone. It should be noted, however, that the TFM can be modified to include the movement of non-conservative solutes (Jury et.al., 1983, 1985b; White et.al., 1985; Sposito et.al., 1985). In the TFM, transport of a solute is characterized by a distribution (log normal generally) of residence (travel) times to any depth. The input data are the average ( $\mu$ ) and the variance ( $\sigma$ ) of the natural log of the net water (water applied - evapotranspiration) required to move the peak concentration of the solute to a depth  $d_c$ . The output of the model is the concentration of

solute at any time and depth. Because of its inclusion of heterogeneity, its flexibility and relative simplicity, a TFM will be used in this study to calculate distributions which will then be used to predict the amount of mass transported to the water table.

There is no single, unique set of physical mechanisms occurring in the unsaturated zone which are implicit in the TFM. Physical interpretations are given only as an aid to understanding a soil transport system that is consistent with the TFM.

In the following pages a physical model of randomized plug flow is developed and is tested in Experiment 2. The physical model is consistent with the TFM.

#### The Physical Model - Randomized Plug Flow

The reason for developing the physical model is that it allows the use of the spatial distribution of three independent parameters to predict the percent of mass delivered to the water table as a function of net infiltration.

- i. The unsaturated zone is modeled as a series of parallel separate vertical tubes packed with porous media.
- ii. There is no dispersion or diffusion of solute in a tube. The flow in each tube is plug flow and instantaneous.
- iii. Each tube has a different uniform field capacity,  $\theta_{fc}$  ( $L^3/L^3$ ).  $\theta_{fc}$  is defined as a random variable given by

$$\theta \approx \ln(\mu_x, \sigma_x)$$

where the subscript has been dropped and

$$x = \ln \theta,$$

$$\mu_x = E(x),$$

$$\sigma_x = \text{standard deviation of } x.$$

The above notation means that  $\theta$  is lognormally distributed with parameters  $\mu_x$  and  $\sigma_x$ .

- iv. The entire process of flow in a single vertical tube is defined by

$$d = i/\theta \dots\dots\dots (1)$$

where

$i$  = the sum of net water added (precipitation - evaporation) at the top of a tube ( $L$ )

$d$  = the depth which the leading edge of the added water reaches ( $L$ )

$\theta$  = the moisture content (field capacity) in a single tube ( $L^3/L^3$ ).

It is interesting to note that  $f_I(i)$  and  $f_D(d)$  have simple relations to  $f_\theta(\theta)$  since the function which relates the random variables is monotonic and single-valued. With  $I$  as a random variable,  $i$  as a particular value of  $I$ , and  $i_c$  as a single-valued variable, we have

$$f_\theta(\theta) = |dd/d\theta| f_D(i_c/\theta) \qquad f_\theta(\theta) = (i_c/\theta^2) f_D(i_c/\theta) \dots\dots\dots (2)$$

$$f_\theta(\theta) = |di/d\theta| f_I(d_c\theta) \qquad f_\theta(\theta) = d_c f_I(d_c\theta) \dots\dots\dots (3)$$

$$f_D(i) = |d\theta/dd| f_\theta(i_c/D) \qquad f_D(d) = (i_c/d^2) f_\theta(i_c/d) \dots\dots\dots (4)$$

$$f_I(i) = |d\theta/di| f_\theta(i/d_c) \qquad f_I(i) = (1/d_c) f_\theta(i/d_c) \dots\dots\dots (5)$$

$$f_I(i) = |dd/di| f_D(d/\theta_c) \qquad f_I(i) = (1/\theta_c) f_D(d/\theta_c) \dots\dots\dots (6)$$

Depending on the design of an experiment, either Equation 2, 3, 4, or 5 may be used. Equation 2 is used where  $D$  and  $\theta$  are defined as random variables and  $I$  is a constant ( $i_C$ ). For example, consider a pulse tracer applied to a field followed by spatially uniform net infiltration of fresh water. After a certain time, soil cores are taken and the peak concentration or center of mass of tracer is determined as a function of depth in each core. The distribution of  $D$ ,  $f_D(d)$  may be determined from these data. Also,  $I$  is a known constant ( $i_C$ ) at the time the cores were taken. Thus  $f_\theta(\theta)$  may be calculated.

Equation 3 may be used where  $I$  and  $\theta$  are defined as random variables and  $D$  is constant ( $d_C$ ). Consider a similar experiment as given above. However, in this experiment, soil water samplers placed at a single depth are used to define the time when the center of mass or tracer peak arrives at each of the samplers. Because a particular time corresponds to a particular  $i$ , the distribution of  $I$ ,  $f_I(i)$  may be calibrated from these data.  $D$ , the depth of the samplers, is a constant ( $d_C$ ) throughout the experiment. Using equation 3,  $f_\theta(\theta)$  may be calculated.

Finally, if  $f_\theta(\theta)$  is determined for a field,  $f_I(i)$  may be determined at any depth  $d_C$  or  $f_D(d)$  may be determined after any total net precipitation  $i_C$  has been applied. Consider several soil cores taken in a field. If an average  $\bar{\theta}$  can be determined for each core, the distribution of  $f_\theta(\theta)$  can be calibrated. Then equations 4 and 5 may be used to determine  $f_I(i)$  at some  $d_C$  or  $f_D(d)$  after some  $i_C$  is applied.

Occasionally in this thesis it will be desirable to relate  $f_D(d)$  to  $f_I(i)$  (Equation 6). In this case,  $\theta_C$  is defined as the average  $\theta$  in the field.

A change in the physical model is required to handle this situation. Each parallel tube is defined to have the same  $\theta_c$ .  $I$  is defined as a log normal random variable representing different amounts of net infiltration added to each tube.  $D$  is defined as before. It is generally not desirable to combine results derived from mutually exclusive physical models in a single method or approach. I believe it is justifiable in this case because the physical model is clearly an invention of convenience. It is presented here as a compromise between purely deterministic and empirical models. Assume  $f_I(i)$  has been estimated at some depth  $d_c$ .  $f_I(i)$  defines the probability that the leading edge of water will reach  $d_c$  after  $i$  has been added at the surface.  $f_I(i)$  also defines the percent of tubes where the leading edge of added water  $i$  is exactly at  $d_c$ . This is very useful information, for if  $d_c$  is the depth to the water table and tracer is applied as a delta function at  $i = 0$  then the cumulative distribution function,  $F_I(i)$ , defines the percent of tubes that contribute tracer to the ground water after  $i$  is applied at the surface. The percent of tubes is also the percent of area in the field. Thus

$$(\% \text{ area}) * (\text{mass applied/area}) = \% \text{ mass applied.}$$

Assuming the mass is applied uniformly,  $F_I(i)$  evaluated at the water table defines the percent of mass applied at the surface that enters the ground water after  $i$  has been applied at the surface.

In the TFM section, a method is given to transform  $F_I(i)$  determined at  $d_C$  to  $F_I(i)$  at the water table. An analagous method usind  $F_D(d)$  is presented in Appendix A.

To use  $f_\theta(\theta)$  to predict the percent of mass transmitted to the water table,  $F_\theta(i/d_C)$  is evaluated where  $d_C$  is the depth to the water table.

### Problems and Restrictions

The physical model does not include any mechanisms for redistribution of soil moisture following an infiltration event other than instantaneous plug flow. For this reason, the model is expected to perform poorly in fine soils (where capillary effects are strong) or at small times following infiltration (while the moisture is being redistributed). The porous media is considered vertically uniform so that the model may perform poorly in highly stratified soils. Perhaps the most difficult question concerning the use of the model is the problem of scale. What scale should be sampled to define  $f_\theta(\theta)$ ? What area of influence is appropriate for the soil water samplers to define  $f_I(i)$ ? How often should they be sampled? How large a diameter core should be used to define  $f_D(d)$ ? If the scale of sampling is much larger than the scale of heterogeneity, information will be lost because parameter values from several points in space will be averaged. This would result in under

estimates of  $\sigma_x$ . For the most part, the problem of scale is ignored in this thesis. Sampling scales have been determined by convenience. The resulting error is unknown.

### The Transfer Function Model

The reason for presenting the TFM model is because it is used in later sections to calibrate distributions of  $I$ ,  $\theta$  and  $D$  to the shapes of the unsaturated breakthrough curves. The calibration compensates for the underestimates of  $\sigma_x$  described above. As a result, more accurate predictions are made of the mass arriving at the water table. The model is based on a simple scaling of  $I$  to transform the distribution of  $I$  found at the calibration depth to any other depth. Using this scaling technique,  $F_I(i)$  is described at the water table. An analogous method using  $F_D(d)$  is described in Appendix A.

Instead of investigating the movement of the leading edge of added water  $i$ , it is more interesting to discuss the movement of tracer. However, with no diffusion, breakdown, dispersion or adsorption, the tracer marks a parcel of infiltrating water. The parcel is pushed ahead of all following additions of water.

All experiments discussed in this work involve tracer applied as a square pulse followed by tracerless irrigation water.  $C_{in}(i_c)$  is defined as the concentration of tracer added at the top of all tubes as a function of  $i_c$ . The use of  $i_c$  means that a known amount of water has been added to each tube.

The square pulse input is given by:

$$\begin{aligned} C_{in}(i_c) &= 0 & i_c &= 0 \\ C_{in}(i_c) &= C_0 & 0 < i_c \leq \Delta i_c \\ C_{in}(i_c) &= 0 & i_c > \Delta i_c \end{aligned}$$

where  $C_0$  is the initial concentration of tracer solution,  $i_c = 0$  prior to tracer application and  $\Delta i_c$  is the amount of tracer solution applied. In a single tube, this square pulse is transported deterministically according to  $d_c = i_c / \theta_c$ . However, over the entire field, at a single depth  $d_c$  from which  $f_I(i)$  has been determined, an average concentration  $C_{dc}(i_c)$  in the tubes is described as a function of  $i_c$  by superposition.

$$C_{dc}(i_c) = \int_0^{i_c} C_{in}(i_c - i) f_I(i) di = \int C_{in}(i_c - i) f_I(i) di \quad (7)$$

Using  $C_{in}(i_c)$  as the step function above

$$C_d(i_c) = C_0 ( F_I(i_c) - F_I(i_c - \Delta i_c) ) \quad (8)$$

To extend the model to predict the average concentration at any depth  $z$ , given a single distribution of  $f_I(i)$  at a single depth  $d_c$ , Jury (1982) proposed the change of variable



$$I(z/d_c) = I_z$$

where

$d_c$  is the calibration depth.

$I$  is the random variable describing the net amount of added water required to move the peak concentration to  $d_c$ .

$z$  is the depth of interest.

$I_z$  is the random variable describing the net amount of added water required to move the peak concentration to  $z$ .

This change of variable is the heart of the model and leads to great flexibility in the model output. It is based upon the assumption of vertically uniform  $\theta$  (field capacity in each tube). Thus the probability of a tracer reaching  $d = 60$  cm when  $i_c = 10$  cm is the same as the probability of reaching  $d = 120$  cm at  $i_c = 20$  cm. Making the change of variable in Equation (7)

$$i = I_z d_c/z \quad \text{and} \quad di/dI_z = d_c/z$$

results in

$$C(i_c, z) = \int_0^{\infty} (d_c/z) C_{In}(i_c - I_z) f_I(I_z d_c/z) dI_z \quad (9)$$

where  $C(i_c, z)$  is the average concentration at  $z$  after  $i_c$  is added.

Using  $C_{In}(i_c)$  as the step function above,

$$C(i_c, z) = C_0 (F_I(i_c d_c/z) - F_I((i_c - \Delta i_c) d_c/z)) \quad (10)$$

The change of variable is the same as multiplying the random variable  $I$  by  $z/d_c$ . Thus the mean of  $\mu_{Iz}$  of  $I$  at depth  $z$  is simply shifted to  $(z/d_c) \mu_I$  and the variance  $\sigma_{Iz}$  of  $I$  at depth  $z$  is  $(z^2/d_c^2)\sigma_I^2$ . For a log normal distribution of  $I$ ,  $\mu_{Iz}$  and  $\sigma_{Iz}$  may be expressed in terms of  $\mu_x$  and  $\sigma_x$ , the mean and variance of  $x$ , respectively, at depth  $d_c$  using

$$\sigma_I^2 = \exp(2\mu_x + \sigma_x^2) (\exp(\sigma_x^2) - 1)$$

$$\mu_I = \exp(\mu_x + .5\sigma_x^2)$$

(Benjamin and Cornell, 1970).

The TFM as presented here, can be used to predict solute concentration  $C(z, I_z)$ , at a particular depth after any  $I_z$  has been added at the surface, given  $f_I(i)$  at some  $d_c$ . In addition, the model also finds the distribution of  $I_z$  at any depth. As stated above this allows estimation of extremely low probability infiltration events taking place within a specified area. If, for instance,  $z$  is the depth to ground water, the distribution  $I$  at  $z$  can be used to estimate when any percent of a field transmits solute to the water table.

Calibration of the model requires the description of the distribution of  $I$  at some depth  $d_c$ . Assuming that  $I$  is log normally distributed, two parameters,  $\mu_x$  and  $\sigma_x$  must be estimated. From the discussion of the Randomized Plug Flow model, there are three methods of determining  $\mu_x$  and  $\sigma_x$ .

- 1) The different depths to the center of mass taken from replicate soil cores taken after  $i_c$ .
- 2) The different amounts of net infiltration required to move the center of mass to replicate soil water samplers located at  $d_c$ .
- 3) The horizontal space distribution of vertically averaged  $\theta$ .

These methods will be tested and compared using data from Experiment 2. The representations of  $C(i_c, z)$  using error functions which are more convenient for calculation are given in Appendix A using  $f_1(i)$ ,  $f_D(d)$  and  $f_\theta(\theta)$  to calibrate the model.

### Problems and Limitations

The transfer function model without the physical model is a purely black box approach which is calibrated by a simple empirical experiment. Because of this approach, the model is useful only under particular circumstances for which it has been calibrated. For example, significant errors may result if the model is calibrated in a dry year and then used in a wet year.

The model relies on the determination of total net infiltration as a parameter. Time varying errors in this parameter or errors different from those encountered during calibration will result in misleading model predictions. However, consistent or constant errors in this variable are more tolerable. This is a direct result of the empirical black box approach. Although the model appears limited by the use of  $(z/d_c) \mid = \mid z$ , it requires very little modification for a different function of  $d_c$  and  $z$  to

be used to transform  $I$  to  $I_z$ .

#### IV Field Tests of the Models

The work reported here began in the fall of 1983 and is composed of two experiments. The first experiment was conducted as a preliminary investigation to test equipment and methods. Because of the preliminary nature of this work, much was done to elucidate possible avenues for future investigation. The focus of the first experiment was to compare the transport of the pesticide, aldicarb, to a conservative tracer through the unsaturated zone and into the ground water. To analyze these data, the flow patterns in the unsaturated zone and the net infiltration directly under the potato hill must be known. In addition, it is necessary to determine  $f_I(i)$  to use the TFM. Problems which arose in determining these quantities and the simplification of the flow parameters are discussed in Experiment 1.

The purpose of the second experiment was to test predictions of mass transport to the ground water. Thus, data were required to determine  $f_I(i)$ ,  $f_D(d)$  and  $f_\theta(\theta)$ . These distributions were used to predict mass transport to the water table. The mass flowing past wells down gradient from the field were compared to predicted values.

The third, fourth and fifth experiments presented in Section V illustrate the use of the proposed method to evaluate the effects of irrigation rates and of surface morphology and placement on the transport of tracer to the groundwater. Although each experiment is considered separately, many of the methods and materials employed are similar. To minimize repetition, these are discussed in the following section.

## Materials and Methods

### A. Site Characterization

Tests were conducted in three plots of potato plants at the Hancock Agricultural Research Station in the central sands region of Wisconsin. The hydrogeology there is characterized by the presence of a shallow water table aquifer made up of glacial outwash. The aquifer varies in depth from a few feet to more than 100 feet. The sands that compose the aquifer vary from medium to very coarse and most usually lie above Cambrian sandstones. Crystalline rocks of Precambrian origin form a hydraulic barrier under the sandstones. Shallow depths to the water table make this unconfined aquifer an important agricultural resource. At Hancock, the soil is a Plainfield loamy sand, 90% sand by weight in the upper two feet and essentially 100% sand below four feet. The organic content ranges from approximately 0.8% by weight in the top foot to only trace amounts below the surface layer (Wyman, 1985). Depth to ground water at two plots averaged about 19 feet and averaged about 8 feet at the third plot.

### B. Tracer Selection

Bromide was selected as an appropriate conservative tracer in flow through Plainfield sand for the following reasons:

- 1) Bromide is neither negatively or positively adsorbed in sandy soil with low silt, clay and organic fractions such as Plainfield sand; and

- 2) Bromide has very low background concentrations in both ground and soil water so that fairly low application concentrations are required.

Fluorescent dyes, often employed as ground water tracers, were considered because they can be detected at very low concentrations using a fluorometer (Davis and Thompson, 1980; Yates and Akesson, 1963; Vincent and Clarke, 1982; Smart and Laidlaw, 1977; Reynolds, 1966). No fluorescent dye was found that did not adsorb to sand, and none were found that completely resisted chemical and biological degradation in the unsaturated zone. Chloride was also considered as a tracer but high background levels of chloride would have dictated very high application rates. Because background levels of bromide are below detection in the soil and water at Hancock, there is no doubt that the bromide found in the ground water or soil solution at a particular plot is directly from the tracer application on that plot and not from some other source.

### C. Soil Water Samplers

Soil water samplers (suction lysimeters) were chosen to collect samples of soil water at various depths. The sampler shown in Figure 6 employs a ceramic cup attached with epoxy to the end of a 2" x 2' PVC pipe. The design is similar to those described by Wood (1976) and Wilson (1979). Nylon tubing was used in the preliminary experiment as sample vacuum ports. However, the nylon apparently leached some substance which caused interference with the analysis of aldicarb mentioned below. For this reason, in all subsequent experiments, polyethylene tubing was used as sample and vacuum ports. The soil water samplers were installed

directly into the porous media. A bucket auger was used to dig a hole to the appropriate depth. The lysimeter was then lowered into the hole and carefully pressed down to ensure maximum contact between the soil and the porous cup. The hole was backfilled and tamped, returning the soil in approximately the same order in which it was removed. Prior to installation, the samplers were cleaned using deionized water (0.1 - 0.01  $\mu\text{mhos}$  conductivity) until the conductivity of the water remained within an order of magnitude after passing through the sampler. This procedure was found to be preferable to recommended procedures by Wood (1973) involving cleaning with 8 N HCl and rinsing with distilled water. This extensive cleaning was found to make the porous cups very absorptive. Passing tap water through an extensively cleaned cup reduced the conductivity of the tap water significantly.

The materials chosen for the construction of the soil water samplers minimized reactions between bromide or aldicarb and the solid surfaces. Teflon was considered as a suitable material for construction of sample ports and the porous cup. Teflon has been reported as having the least adsorption and leaching problems (Barcelona, Helfrich and Garske, 1985). However, the relative expense of Teflon combined with the lack of reactivity of both aldicarb and bromide to polyethylene and nylon were the reasons polyethylene and nylon were chosen in place of Teflon.

The soil water samplers were operated by applying a suction to the vacuum port and allowing the vacuum to decay over a sample period. At the end of a sample period, a sample was removed under suction through the sample port, and a vacuum was applied to the sampler. The samples



represent both a spatial and temporal average of the soil water solution *in situ*. Due to the decay in vacuum and the unknown nature of the porous cup contact with porous media, the spatial and temporal averages involve some unknown weighting function. This lack of certainty as to exactly where or when samples were being withdrawn may be seen as a major fault with suction lysimeter derived data. England (1974) recommended caution in interpreting data due to problems with ceramic type samplers;

- 1) The sampler may empty only certain pores in the porous media that hold water at a lower tension than is applied in the suction lysimeter.
- 2) Leaching adsorbed species from the cup may delay peak times.
- 3) Screening or salt sieving may reduce solutes in the sample.

Hanson and Harris (1975) in controlled laboratory and field tests, found leaching to be of minor importance. Wood (1973) found no significant salt sieving in field tests. Problem 1) above may lead to samples that are representative of only some fraction of soil water held in a particular range of pore sizes. To address this problem, soil solution samplers were set at various suctions. No correlation was found with pH, bromide, alkalinity, aldicarb or conductivity with changes in suction. Wood, in a reply to England (1974), comments that the exchange capacity of the cups is very small and that there is sufficient sample taken (10 to 100 ml.) to ensure equilibrium with exchange sites with little change in sample concentration.

The maximum radius of influence of the soil water samplers used in the experiments was calculated using the method of A.W. Warrick and A.

Amoozegar-Fard (1977). The method involves solving the steady state moisture equation in cylindrical coordinates for homogeneous and isotropic media. The boundary conditions are:

- 1) the surface of the sampler is modelled as a constant matrix flux potential; and
- 2) the domain is surrounded by a constant matrix flux potential.

The hydraulic conductivity  $K$  is modelled as;  $K = K_S \exp(\alpha h)$  where  $K_S$  is the saturated hydraulic conductivity,  $\alpha$  is a constant, and  $h$  is the local suction head. Using data from Kimbel (1983) and Leszczynski (1969)  $\alpha$  was found to vary from 0.097 to 0.14 at Hancock Experimental Station. The resulting range of influence for the soil water samplers is 1.0 cm to 7.2 cm. Assuming an order of magnitude error in  $K_S$ , the maximum radius of influence is 16.8 cm from the center of the soil water samplers.

#### D. Wells

PVC wells were installed with two foot screens at the water table. The wells were developed by pumping until the samples were free of fines. Prior to sampling, the wells were bailed to remove stagnant water in the well screen (Schuller, Gibb and Griffin, 1981). The wells were sampled by inserting a nylon or polyethylene tube down the casing and pulling the sample out with a hand pump under suction.

## E. Chemistry

Aldicarb, aldicarb sulfoxide and aldicarb sulfone samples were analyzed by Union Carbide Agricultural Products Co. using a high pressure liquid chromatography technique with a post-column reaction and fluorescence detector (Krause, 1980). The system is capable of detecting concentrations down to 1 ppb. Bromide was analysed using an Orion bromide selective ion electrode with a single junction reference electrode and micro-sample dishes. This technique allows for quick detection of bromide down to 5 micromoles/liter (with a precision of  $\pm 2$  micromoles/liter). The method is very sensitive to the ionic strength of solution. Hence all standards were adjusted to the mean ionic strength of the samples. This was accomplished by first measuring the conductivity of the samples. Then a relationship was used between conductivity and ionic strength,  $z = 0.013 \text{ EC}$ , (Lindsay, 1979), where  $z$  is the ionic strength in moles/liter and EC is electrical conductivity in millimhos/cm at  $25^\circ \text{C}$ . This procedure may cause an error within the range of -5 to +10%.



agricultural management practices. A conservative tracer should move as fast or faster than other substances, thus determining a worst case scenario for transport of many other substances. Recent work in Florida citrus fields has shown there is a general similarity between bromide and aldicarb movement (Jones, 1985). It is important to note that the use of bromide in place of a degradable substance such as aldicarb cannot take into consideration possible changes in aldicarb degradation under different circumstances. The comparison is only useful in defining potential transport rates of a substance.

Recent tests conducted by the University of Wisconsin, Wisconsin State Agencies, and Union Carbide Agricultural Products Co. have shown that traces of aldicarb residues may appear in potable well water from shallow wells located near agricultural land (Chesters, 1982; Rothschild, Manser and Anderson, 1982). In Wisconsin, aldicarb is applied primarily to potato plants to control a variety of pests. Aldicarb is formulated as a granular product for incorporation into the soil. In the unsaturated zone, aldicarb is rapidly oxidized to aldicarb sulfoxide. Aldicarb sulfoxide may be further degraded to aldicarb sulfone. The sulfoxide and sulfone are then simultaneously metabolized or chemically hydrolyzed to low toxicity compounds (Figure 7). Aldicarb, aldicarb sulfoxide and aldicarb sulfone are biologically active carbamates and will be reported, combined as ppb of aldicarb sulfone. Transport of all these compounds through the unsaturated zone is retarded by the presence of organic matter in the soil.

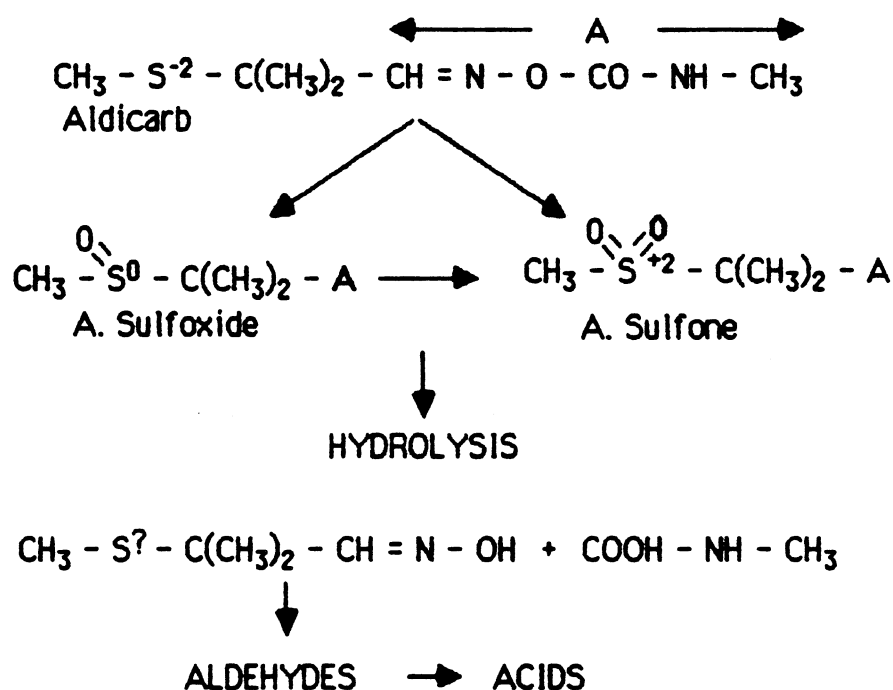


Figure 7. Oxidation of Aldicarb.

#### A. Methods

Potato plants were planted in late April 1984. On May 18, 1984, soil water samplers were installed in triplicate at 3, 6 and 9 feet in a 50' x 150' plot (Figure 8). The plot had not had aldicarb applied to it for at least three years and to our knowledge had never had bromide applied to it. The lysimeters were placed directly beneath the emerging potato plants. On May 19, 1984, aldicarb was applied in granular form at a rate of 2 lb./ acre in bands on top of the plants. Immediately following, in a single procedure, a 1.7 molar solution of potassium bromide was sprayed onto the seedlings at a rate of 0.94 ml/ft, and the plants were hilled using 20 inch disks. In this way, both the tracer and pesticide were incorporated into hills which were approximately one foot high and three

feet apart. Three wells were installed in early June 1984 in the furrows with two foot screens at the water table. The field was irrigated throughout the summer using the Wisconsin Irrigation Scheduling Program which irrigates at a rate approximately equal to the evapotranspiration rate while avoiding plant stress. The potatoes were not harvested and the field was not disturbed; sampling which began in late May continued through the winter and into the summer of 1985.

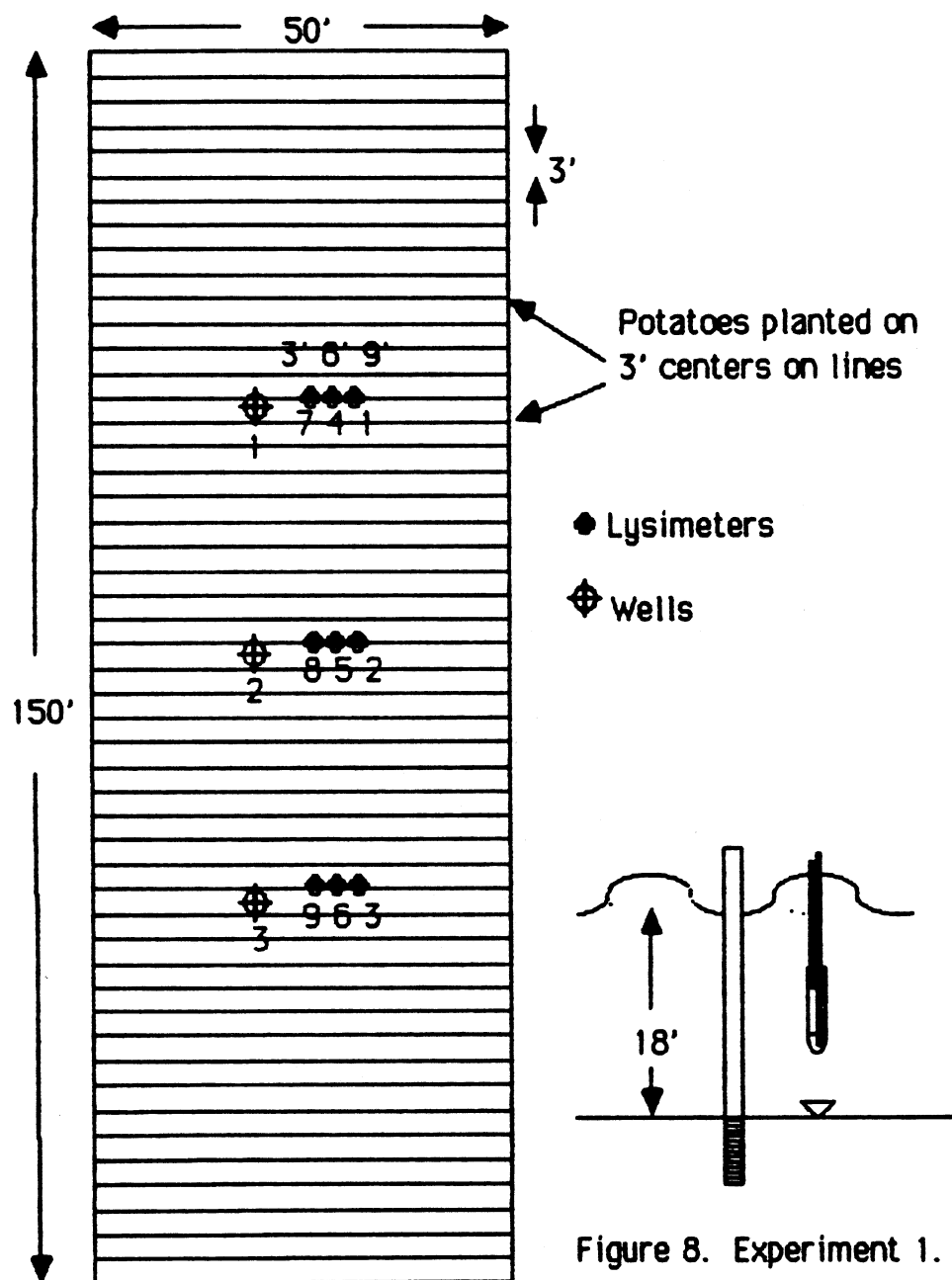


Figure 8. Experiment 1.

## B. Results

During the first two months of operation in Spring 1984, a contaminant was present in the samples obtained from the soil water



samplers. The contaminant passed through the high pressure liquid chromatography column in approximately the same amount of time as the species of aldicarb. However, the peak produced by the contaminant was not similar to the aldicarb peaks. We believe that new nylon tubing employed in the construction of the lysimeters leached the contaminant into the samples during the first two months of operation. For this reason, these samples were excluded from the data. In addition, four outliers were removed from the data. The outliers were obvious because they were large spikes between samples of low concentration. The sample obtained from each suction lysimeter represents a weighted average over the time between samples and a weighted average over some region around the lysimeter cup. Unfortunately, the weighting factor in either case is unknown. In addition, the samplers are not completely evacuated at each sampling. The remaining sample along with averaging causes smoothing of the data.

One question that must be addressed when using soil water samplers is whether the samples are representative of the soil water *in situ*. To partially answer this question, the lysimeters were operated at different suctions (5 inches to 20 inches Hg) throughout the summer. Using regression analysis, no correlation was found between pH and the suction at which the sample was extracted. Further, no evidence was found in the conductivity, bromide, or aldicarb data to suggest that pressure affected the results. Although these negative results do not definitely prove that the samples are representative of the soil water,

they strongly suggest that this is true. Any positive correlation would have cast doubt on the validity of the aldicarb/bromide comparison.

Some difficulty was found in operating the nine lysimeters. One lysimeter at a depth of nine feet ceased operation shortly after the experiment began. Two lysimeters, both at a depth of three feet, became temporarily clogged with a biological film. They were both revived by applying 26 inches of Hg vacuum over a sampling period.

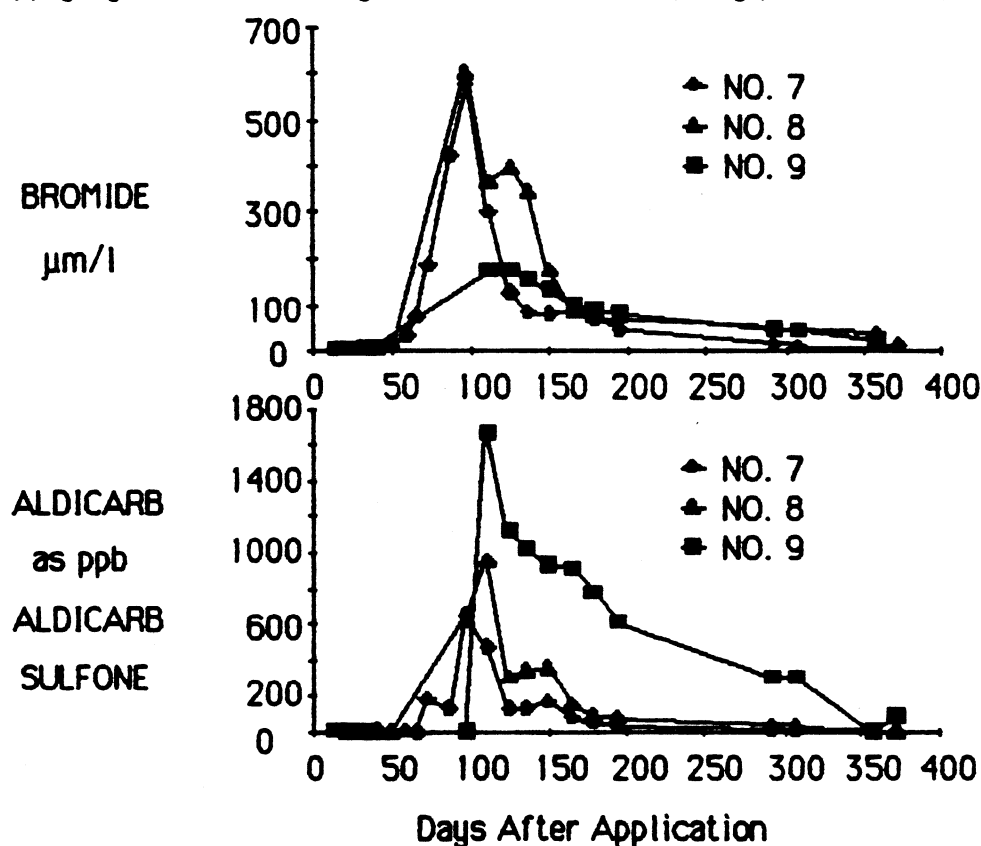


Figure 9. Aldicarb and bromide data from lysimeters at 3 feet

#### 1. Breakthrough Curves

The patterns of bromide and aldicarb concentrations versus time are generally similar (Figures 9, 10, 11 and 12). The variation among the samplers in each figure apparently reflects the natural heterogeneity in

transport. Both substances show a range of peak concentrations between 95 and 110 days at 3 feet deep (Figure 9). If the aldicarb were absorbed to the organic matter above 3 feet, the concentration peak would be shifted to greater time. However, there is little evidence of this in Figure 9. The aldicarb is also degraded; this process would shift the concentration peak to smaller time. This effect is evident at the 6

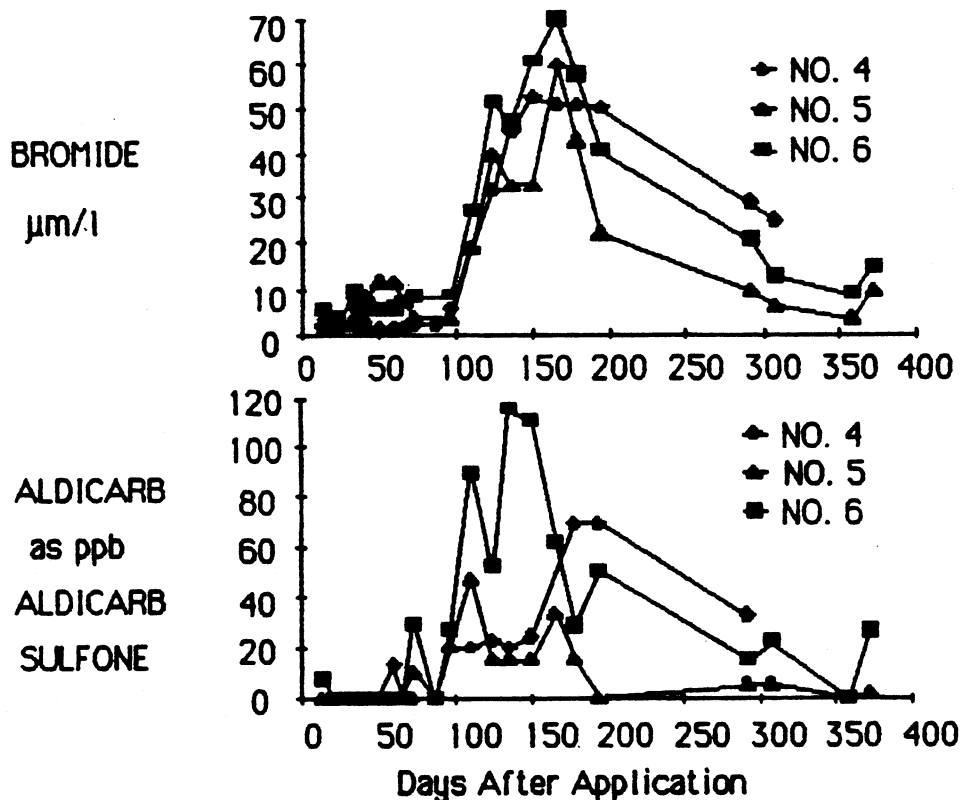


Figure 10. Aldicarb and bromide data from lysimeters at 6 feet.

foot depth (Figure 10). Comparing Figures 9 and 10, an increase in the rate of transport through the second three feet of soil can be seen (peak concentrations occur between 110 and 180 days at 6 feet). This result is probably due to an increase in infiltration caused by the death of potato

plants coupled with rainfall at 100 to 120 days after application of the tracer and pesticide. The behavior at 9 feet (Figure 11) is very different than that at 3 feet and 6 feet. This appears to be due to the prolonged winter months during which the ground was frozen.

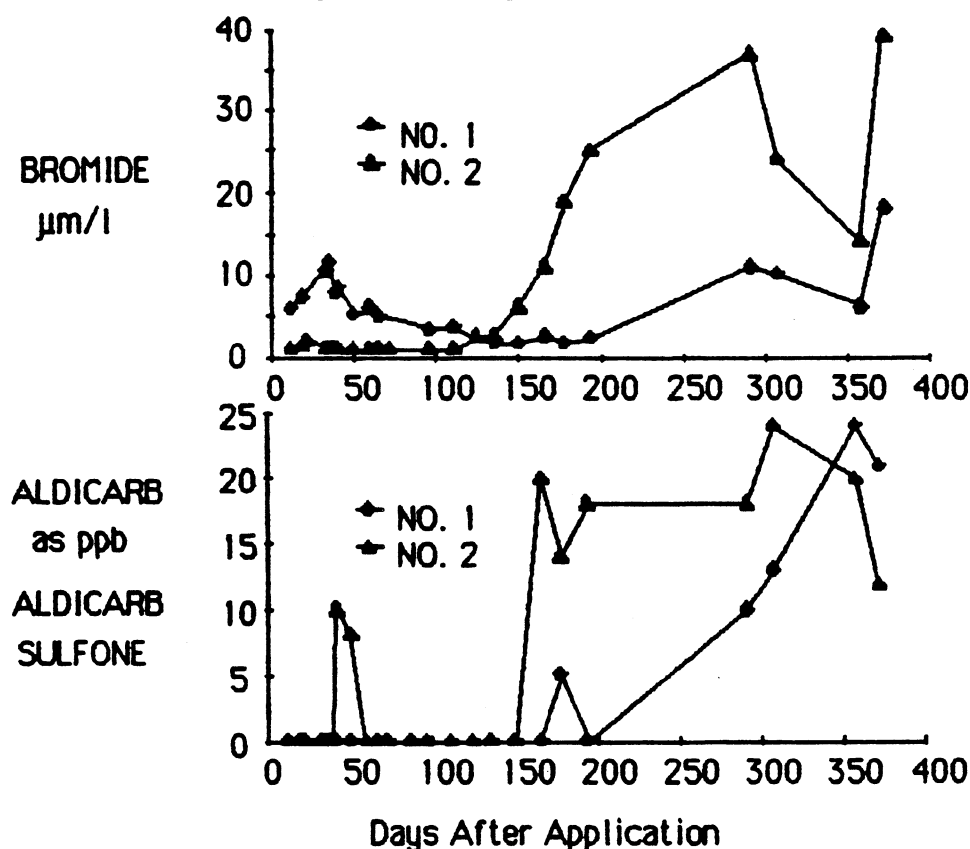


Figure 11. Aldicarb and bromide data from lysimeters at 9 feet.

The well data (Figure 12) clearly show the effect of the aldicarb degradation. Aldicarb peaks are displaced to the left of bromide peaks. The aldicarb peaks are also followed by a significant decrease in concentrations; this behavior is not observed with bromide. However the large gap in the data during the winter months and the heterogeneity of responses makes analysis of the data difficult. In contrast with the

lysimeter data which show that the concentration peaks at greater depths, at greater times (Figures 9, 10, and 11), the wells show an aldicarb (and bromide) peak much earlier than expected. Indeed the peaks of aldicarb (and bromide) at the wells are most comparable to those found at a depth of 6 feet.

The well data represent an integration of vertical transport through the unsaturated zone to the water table occurring up-gradient of the well. This transport may be a rare event not represented by average rates of transport in the unsaturated zone. Instead of average transport rates, Figure 12 shows the importance of the distribution of transport rates due to heterogeneity in solute movement (Biggar and Nielsen, 1976; Jury, Stolzy and Fluhler, 1977).

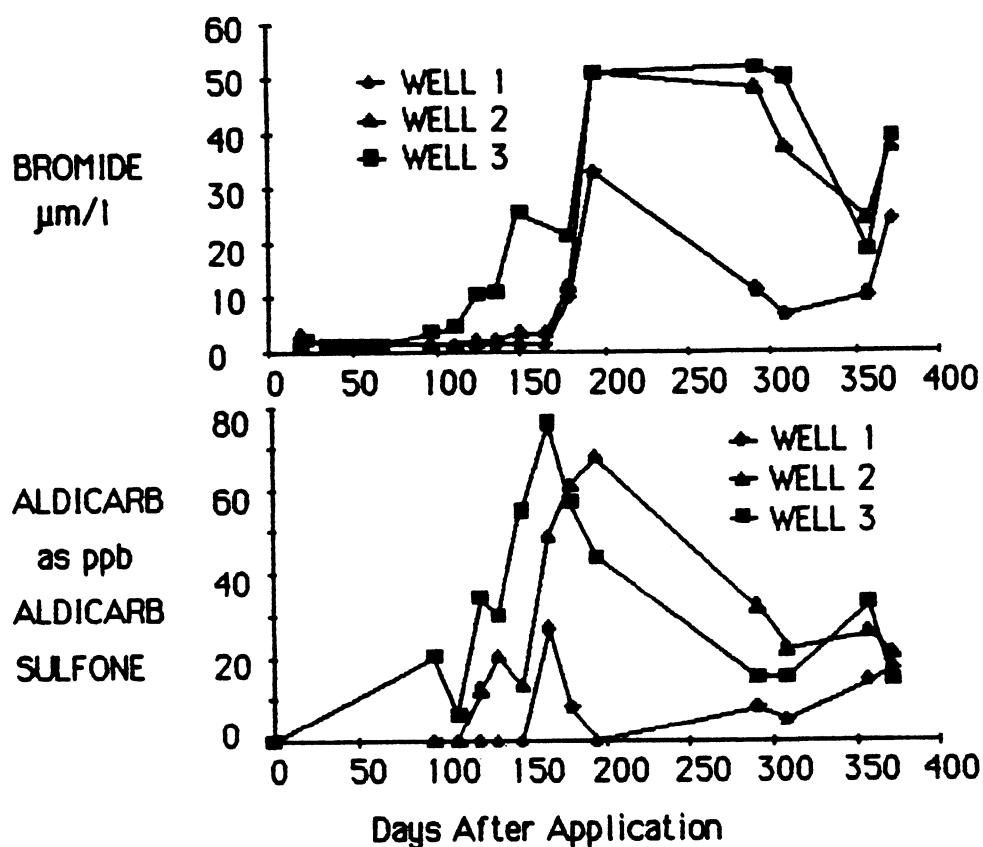


Figure 12. Aldicarb and bromide data from wells with two foot screens at the water table.

## 2. Tracer Movement

To determine the mass of aldicarb or bromide which passes by each sampler and to better understand the data already presented, it is necessary to describe the tracer movement and flow patterns under the potato hills.

From the discussion above, we can expect the radius of influence of each sampler to be no greater than 15 cm. We expect higher percentages of the sample removed to originate from distances closer to the sampler within the radius of influence. As the tracer is advected towards the

water table, it is dispersed and diffused longitudinally (downward) and transversely (horizontally) across the flow. If there is no horizontal variability in advection and no transverse dispersivity, the problem becomes one-dimensional. Then the total mass passing the sampler can be found by integrating sample concentrations over the net infiltration. This method is used in later sections. The error in ignoring the transverse dispersivity may be significant. Assuming no interaction between adjacent strips, an analogy may be drawn between the transverse dispersion of the bromide sprayed in a strip on the hills and the cooling of an infinite strip in a planar homogeneous isotropic medium. From Carslaw and Jaeger (1959) the solution to this problem for all  $x$  is

$$C(x,t) = 1/2 C_0 \{ \text{erf} ([a-x] / [2 D_t t]) + \text{erf} ([a+x] / [2 D_t t]) \} \quad (10)$$

where

$x$  is measured from the center of the strip outwards;

$C(x,t)$  is the concentration as a function of  $x$  and  $t$ ;

$C_0$  is the input concentration;

$a$  is 1/2 the strip width;

$D_t$  is the transverse dispersivity;

$t$  is time.

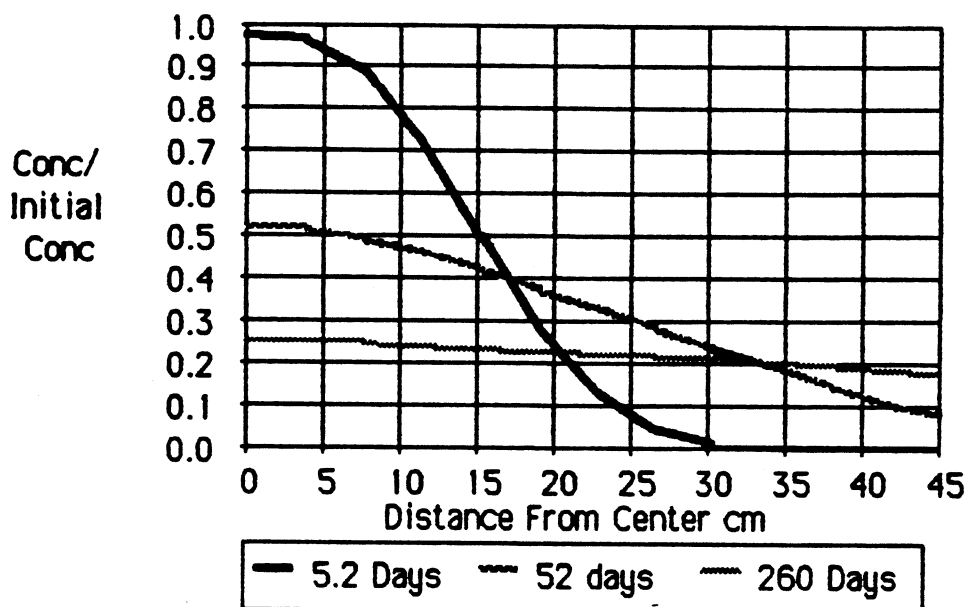


Figure 13. Effects of transverse dispersivity.

Figure 13 shows a graph of the solution. Each line is the concentration profile for a particular time after the start of the experiment. Yule and Gardner (1978) found transverse dispersion for chloride in the unsaturated Plainfield sand to be essentially independent of pore velocity. They found a value of  $0.0031 \text{ cm}^2/\text{min}$ . Because chloride is similar to bromide, this same transverse dispersion coefficient was used in preparing Figure 13. This value is approximately one order of magnitude greater than the molecular diffusion coefficient of bromide. The figure shows the spread of the tracer pulse with time. During the experiment, the pulse moves down toward the water table at the same time it spreads out horizontally. Thus, time in Figure 13 is related to depth in the experiments. The concentrations found at the sampler are reduced by the effect of transverse dispersivity. This in turn causes a reduction in the mass calculation as discussed above. Concentrations



from the samples may be corrected for this error using Equation (10). Assuming the sample is taken close to  $x=0$ , the corrected concentration  $C_C$  is

$$C_C = \beta (x) C_S, \quad \beta = C_0/C(x,t) \quad (12)$$

where

$C_0$  is the initial concentration;

$C_S$  is the concentration of the sample;

$C(x,t)$  is determined for  $x=0$  at the time the sample is taken using Equation (10).

Horizontal variability in advection results in more complicated problems. In particular, the hypothetical hill-furrow system shown in Figure 14 and used in several experiments results in higher net infiltration under the furrow and lower net infiltration under the hill. Saffignia, Tanner and Keeney (1976) documented this phenomenon in the upper 60 cm of soil using Rhodamine WT dye as a tracer. They found deep movement of the dye beneath the surface of the furrows caused by leaf drip and runoff. In addition, they found 20 to 46 percent of the irrigation and 4 to 23 percent of the rain flowed down the stems of the potatoes. This stem flow caused deep penetration of the dye directly under the plants to depths of 45 cm within 4 days following application and heavy irrigation. These short studies show the spatial heterogeneity of infiltration. However, spatial heterogeneity is only part of the cause of heterogeneity of net infiltration. Evapotranspiration may alter the effects that the heterogeneity of infiltration has on net infiltration. Appendix C

shows root density data from Tanner and Weis (1986). Two important conclusions are apparent from the data: 1) Root depth is always greatest under the hill and increases as the plants grow; and 2) The root density per unit surface area is greater under the hill than the furrow and is stationary during the growth of the plants. With all other factors remaining the same, root depth should be proportional to the amount of water required to advect a substance past the root zone. Thus we expect this amount of water to be less in the furrow and when the plants are young. Roots in moist soil should take up more water than roots in dry soil. For this reason, stem flow may be adaptive. It actually delivers water to the highest density of roots. In general, the roots probably mitigate the effects of heterogeneity of infiltration by removing water preferentially from the moist areas.

The higher net infiltration in the furrow is a result of greater infiltration combined with lower evapotranspiration due to shading, wind protection and shallow root growth. This should cause higher rates of advection under the furrows that would quickly transport any tracer that entered this path to the ground water. This effect will be illustrated in Experiment 5. It is particularly interesting to note that the "fast lanes" (Figure 14) between the parallel strips of tracer effectively isolate each strip. This isolation enhances the transverse dispersivity. Without isolation, the maximum effect of transverse dispersivity would be to spread the tracer mass evenly across the area perpendicular to flow. This is because the parallel strips would begin to overlap. Isolation of the

strips of tracer ensures infinite dilution in the horizontal plane at infinite time. Hence the analysis given above is more accurate.

Higher infiltration into the furrow may also cause flow from under the furrow to under the hill. This flow would occur as a result of tension gradients pulling moisture at lower tension under the furrows to lower moisture areas at higher tension under the ridges. The flow would be enhanced by gradients caused by operation of the samplers. Even though this additional flow from the side acts against the transverse dispersion discussed above, it would result in diluted samples. Diluted samples cause an underestimate of total mass at the sampler. Because of the rapid draining of the sandy soil, this effect should be effective only during and immediately following heavy infiltration at shallow depths.

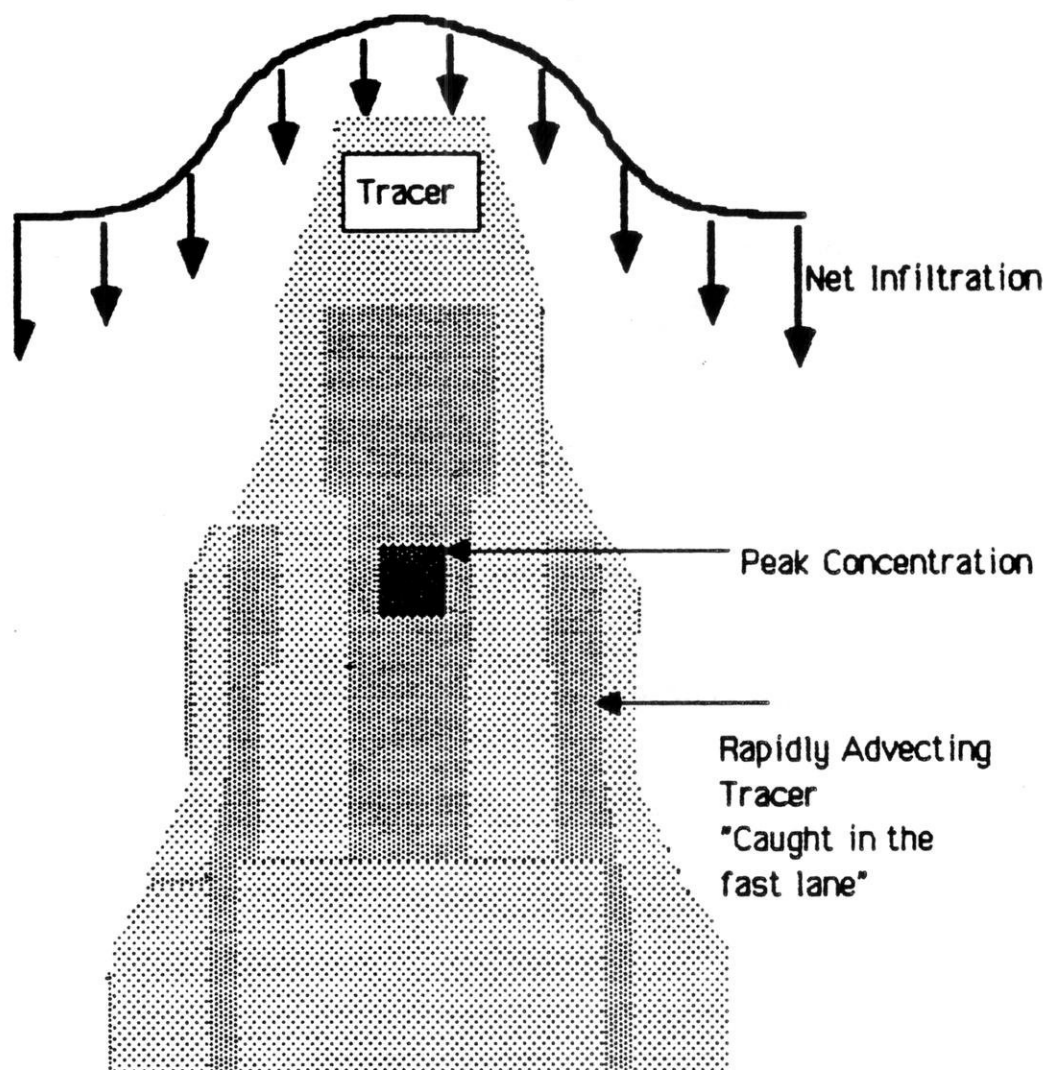


Figure 14. Possible transport under the hill furrow system. The complicated tracer pattern is a result of longitudinal and transverse dispersion combined with accelerated transport under the furrows. Thus tracer transported laterally by transverse dispersivity may be advected ahead of tracer remaining under the hills.

### 3. The Determination of Net Infiltration.

Net infiltration was initially calculated using data generated by the Wisconsin Irrigation Scheduling Program. The net infiltration during a sample period was found by subtracting evapotranspiration from the sum of precipitation and irrigation during the period. Evapotranspiration (ET) is found by first calculating the potential ET using a Priestley-Taylor model as described by Linsley, Kohler and Paulhaus (1982). The potential ET is then modified using the percent cover of the crop to yield the actual ET. The values determined using this method are the average net infiltration over the entire field. For reasons mentioned above the average net infiltration is an overestimate of the actual net infiltration occurring under the hills and an underestimate of the actual net infiltration occurring under the furrows. Furthermore, the advection of the tracer under the hill is determined by the net infiltration under the hill. Thus the first problem is to correct the average net infiltration over the field to that under the hill. The second problem is that values for ET are only available for the months of May through mid-September. Some estimate of ET is required for other months.

Three estimates of net infiltration are compared in analyzing the data from Experiment 1. The first estimate  $I_1$  is found using uncorrected, average values for the growing months and assuming no ET during all other months. The total net infiltration,  $I$ , required to move the center of the mass of solute to 3 feet is  $P_3$  and to 6 feet is  $P_6$ .

The second estimate of net infiltration ( $I_2$ ) is made by assuming that all errors in  $I_1$  due to water distribution under the plants occur between emergence of the crop in May and death of the plants in September. Fortuitously, the death of the plants in September correlates well with the time the center of mass passes 3 feet. Thus all of the error occurs in  $P_3$  and  $P_6 - P_3$  is unaffected.  $P_6 - P_3$  is the net amount of water required to move the center of mass of the tracer from three to six feet. Assuming a homogeneous one-dimensional system,  $P_6 - P_3$  should be equal to  $P_3$ . Thus

$$\begin{array}{ll} 0 < I_1 < P_3 & I_2 = I_1 \alpha_0 \\ I_1 = P_3 & I_2 = (P_6 - P_3) \\ I_1 > P_3 & I_2 = I_1 - (P_3 - (P_6 - P_3)) = I_1 - (2P_3 - P_6) \end{array}$$

$$\text{where } \alpha_0 = (P_6 - P_3) / P_3 \text{ and } I(t) = \sum_0^t i_i \text{ where}$$

$I(t)$  is the total net infiltration  $t$  sample periods after application of the tracer and  $i_i$  is the net infiltration occurring during a sample period.

The third estimate of net infiltration involves correcting  $I_1$  for evaporation during the months outside the growing season. Appendix D shows weighing lysimeter data for two lysimeters at Hancock Experimental Station from 1966 to 1978. The values shown are for potatoes, bare ground (possibly with some weeds) and crops left standing. During Experiment 1, corrections need to be made for evaporation

occurring from October 1984 through June 1985. After death of the potato vines in September 1984, the potatoes were left in the field. During the spring of 1985, some weeds grew but the plot was left mostly bare. Using weighing lysimeter data for similar conditions, the factor  $\alpha_{00}$  is calculated for each month from  $\alpha_{00} = 1 - (ET / \text{Gross } i)$  and is given in the last column of Appendix E.

Thus

$$i_3' = i_1 \alpha_{00} \quad \text{for October through June}$$

$$i_3' = i_1 \quad \text{for May through September}$$

where

$$I(t) = \sum_{t=0}^t i_t' \text{ and}$$

$i_t'$  = net infiltration in an sample period

$t$  = the number of sample periods.

Once  $I_3'$  is determined,  $P_3'$  and  $P_6'$  are determined and corrections are made as in  $I_2$ .

Hence, when

$$0 < I_3' < P_3' \quad I_3 = I_3' \alpha_0$$

$$I_3' = P_3' \quad I_3 = P_6' - P_3'$$

$$I_3' > P_3' \quad I_3 = I_3' - (2P_3' - P_6')$$

$$\text{where } \alpha_0 = (P_6' - P_3') / P_3'$$

The values of  $\alpha_{00}$ ,  $\alpha_0$ ,  $I_1$ ,  $I_2$  and  $I_3$  are given in Appendix E. Figure 15 shows  $I_1$ ,  $I_2$  and  $I_3$  plotted as a function of time.

In the addendum to Appendix D, the coefficients of variation of ET, Gross  $i$  and the ratio ET/Gross  $i$  are given for each month. All three parameters show similar variability in this record. In general it is expected that Gross  $i$  would have a higher variability than ET. Therefore, it would be preferable to subtract average monthly ET from  $i_1$  to obtain  $i_3'$ . Given the lack of correlation and similar coefficients of variation found in the lysimeter data, either method is suitable.

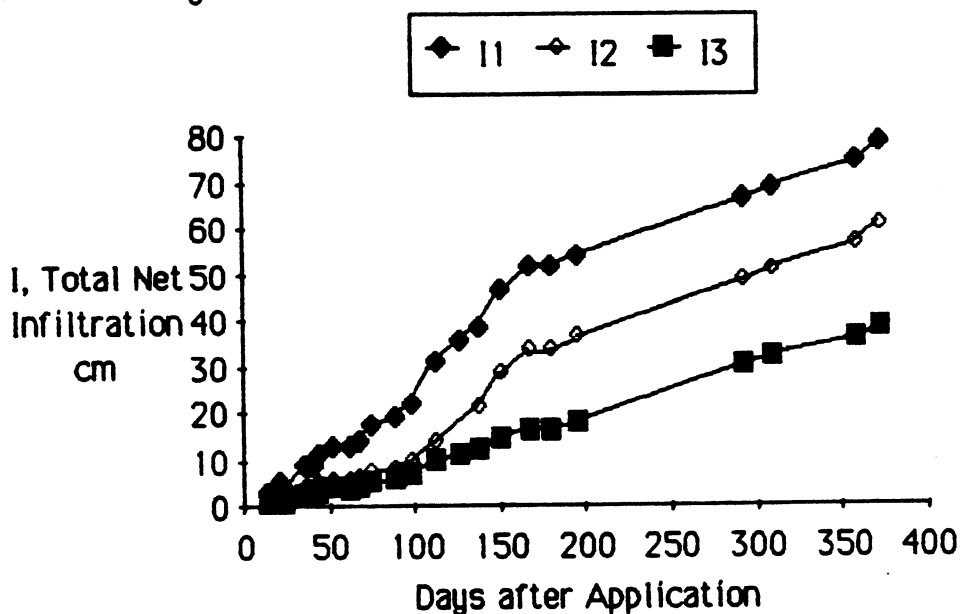


Figure 15. The total net infiltration during Experiment 1.

#### 4. Total Mass

Although the total mass of a substance that has passed a particular lysimeter is not utilized by the transfer function or randomized plug flow models the estimation of this parameter provides insight into the flow system. Appendix F shows the total mass calculations for all three



estimates of net infiltration. To calculate total mass, the concentration of samples are plotted against net infiltration and the area under the curve determined by integration. The result is the total mass per unit area intercepted by the sampler. The sample concentrations used in these calculations are the same for each estimate of net infiltration. Since the net infiltration is highest in  $I_1$  and lowest in  $I_3$ , the total mass calculated using  $I_1$  is greater than  $I_3$ . Appendix G shows the percent mass recovered which is the total mass divided by the applied mass. The decrease in total mass with each net infiltration estimate ( $I_1$ ,  $I_2$ ,  $I_3$  respectively) is apparent.

In a uniform, one-dimensional flow field, 100% of the applied mass should be recovered by the samplers. Appendix G illustrates that the percent of mass recovered is, in general, very low (1% to 31% for  $I_3$ ) and decreases with depth. One conclusion based upon this trend is that transverse dispersivity is an important factor. Using Equation (11), sample concentrations were adjusted to remove the effects of transverse dispersivity. The "corrected" recovered mass using  $I_3$  and these adjusted concentrations are given in Appendix G. Removing the effects of transverse dispersion on sample concentration shifts the percent mass recovered towards 100% in all cases. However, Figure 16 shows that the trend of decreased recovery with depth is still apparent. This is probably caused by several mechanisms. Depth in the field is directly proportional to time in Equation (11). Hence many errors due to deviations from assumptions made in developing Equation (11) are greater at greater depths. One assumption is that the samples are taken from a point at the

middle of the band of tracer. In reality, the sampler is probably not at the exact center of the band. Also the samples are taken out of some finite volume. The tracer concentrations are averaged from soil water removed some distance away from the sampler. Both of these errors cause the correction factor,  $\beta$ , in Equation (12) to be underestimated. At early times or shallow depth, this error would be relatively small. The error would increase with depth.

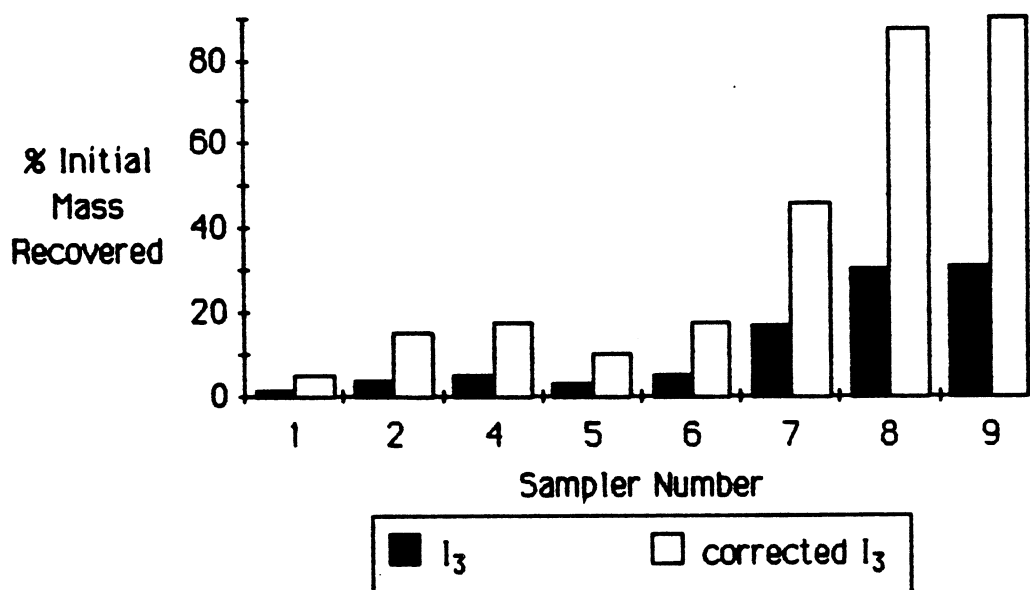


Figure 16. A comparison of the percent mass recovered from all soil water samplers used in Experiment 1. Samplers 1 and 2 were at 9 feet. Samplers 4, 5, and 6 were at 6 feet. Samplers 7, 8, and 9 were at 3 feet.

## 5. Center of Mass and Peaks.

The center of mass or centroid of concentration in terms of net infiltration is given in Appendix F for each sampler and for each of the three models of net infiltration. The calculation of center of mass is estimated as shown in Appendix F. The center of mass is the amount of infiltration required to move half the total mass past the sampler. For

example, if  $C(l)$  were symmetric about some  $l_c$ , then  $l_c$  would be the center of mass.

The center of mass is an important input parameter in the transfer function and randomized plug flow models. The average of the natural log of the center of mass for the samplers at a particular depth is  $\mu_x$ . Jury suggests using the position of the peak concentration,  $l = \max C(l)$ , as an estimate of the center of mass. Appendix F illustrates that peak position and the center of mass are in poor agreement. This is partly because the definition of the peak position makes it highly reliant on sample period. The peak is constrained to occur when a sample is taken. As shown in Figure 5, theoretical breakthrough curves of concentration versus time are asymmetric. Assuming a constant infiltration rate,  $C(t)$  would have the same shape as  $C(l)$ . For these asymmetric breakthrough curves, the peak position is not coincident with the center of mass of the sampler. Although peak position is not a good estimate of the centroid of a breakthrough curve, sometimes it is the best estimate. This is clear from the data obtained in the 9 foot samplers. The breakthrough curves at 9 feet are more irregular and at 372 days do not seem completed. Thus, the center of mass, found by numerical integration, is too small. Here the peak position is probably the better estimate of the actual center of mass.

## 6. The Transfer Function Model

A listing of the program used to run the transfer function model (TFM) is given in Appendix H. The model requires the input of 8 parameters; given  $x = \ln$  centroid in terms of  $l$ .

$C_0$  is the initial concentration;

$\Delta l$  is the width of the square pulse input or the depth of solution with concentration  $C_0$  applied;

$\mu_x$  is the mean of  $x$  at the calibration depth;

$\sigma_x$  is the standard deviation of  $x$  at the calibration depth;

$d_c$  is the calibration depth;

$z$  is the depth of interest;

$\bar{I}$  is the average daily net infiltration;

$N$  is the number of days to be simulated.

The model was calibrated at 3 feet using all three estimates of net infiltration. The calibration procedure involved using  $\sigma_x$  as a fitting parameter to match  $C(l)$  at three feet.  $\sigma_x$  was chosen as the variable because out of all the parameters derived from the data,  $\sigma_x$  is probably the most unreliable. This lack of reliability is due to:

- 1) The sample size of 3 is too small;
- 2) The samples represent average concentrations over the sample period; and
- 3) The length of the sample period arbitrarily decreases  $\sigma_x$ .

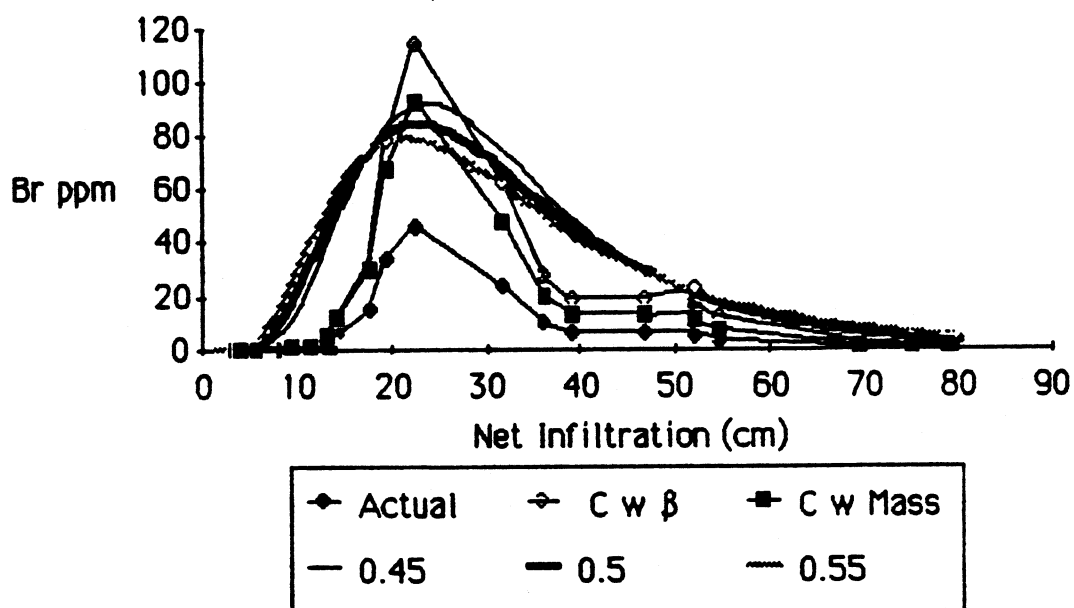


Figure 17. Calibration at 3 feet using  $I_1$ . Values of  $\sigma_x$  are shown for each of the curves produced by the model.

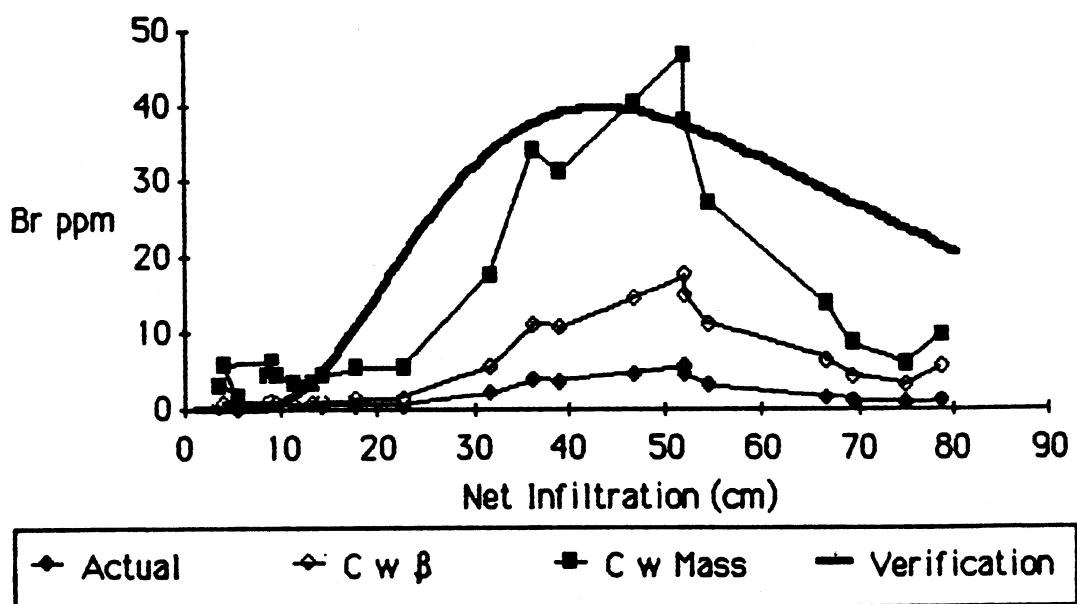


Figure 18. Verification at 6 feet using  $I_1$ .

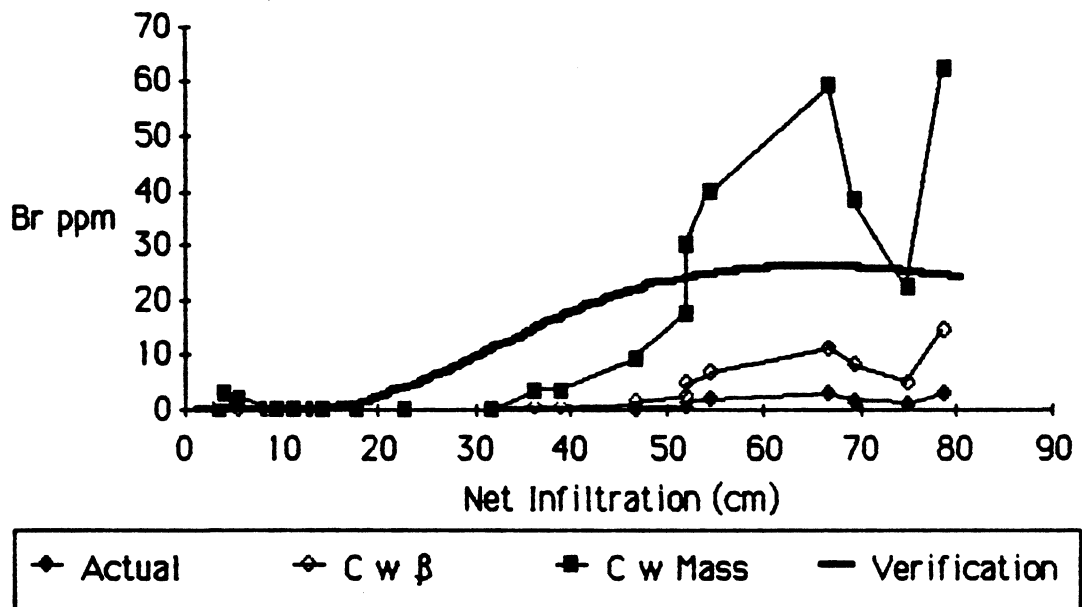


Figure 19. Verification at 9 feet using  $I_1$ .

The model was calibrated to data from sampler 7. This is the most complete set of data at 3 feet. Calibrations are shown for  $I_1$ ,  $I_2$  and  $I_3$  in Figures 17, 20 and 23 respectively. The standard deviation is used to calibrate the model at 3 feet. The model is then verified at 6 feet. Three curves are presented with each calibration and verification run. 1) The average breakthrough curve; 2) The average curve adjusted with  $\beta$ ; and 3) The average curve adjusted with mass. Calibration is accomplished by running the TFM for various  $\sigma_x$  until the "best fit" to the average breakthrough curve at 3 feet is obtained. The "best fit" might have been determined with a least squares test. However, given all sources of error and natural heterogeneity of the system, the curve which looked like the best fit was chosen. Verification runs use the calibrated parameters from the best fit.

The figures show that calibration was not successful unless the sample concentrations were adjusted to remove the effects of transverse dispersion. The values were adjusted in two ways;  $C_w\beta$  and  $C_w\text{Mass}$ . The data presented as  $C_w\beta$  show the sample concentrations (labeled "Actual") multiplied by  $\beta$  as defined in Equation (11) and given in Appendix G. This adjustment underestimates the "corrected" concentrations as described above. The values labeled  $C_w\text{Mass}$  are obtained using

$$(1 / \% \text{ Mass recovered}) * \text{Actual concentration} = C_w\text{Mass}$$

Thus the data presented as  $C_w\text{Mass}$  are  $C(l)$  adjusted so that the area under the curve is the mass per unit area applied at the surface. This completely removes the effects of transverse dispersion on the total mass recovered by the sampler. However, this adjustment uses a crude, "brute force" method and produces some unwanted effects. In particular, samples taken after small amounts of net infiltration are treated the same as samples taken after large net infiltration. This produces too large an adjustment at small times and too small an adjustment at large times. A still better fit of the model would be obtained by adjusting  $C_w\beta$  to have an area under the curve of the mass per unit area applied at the surface. This may be "guilding the lily".

The model was calibrated using the parameters in Table 1. The model was then verified using data at 6 feet from sampler 6 and at 9 feet from sampler 2.

Table 1

	I1	I2	I3
$C_0$	136000	136000	136000
$\Delta I$	0.02	0.02	0.02
$\mu_x$	3.365	2.89	2.38
$\sigma_x$	0.55	0.70	0.60
$\bar{T}$	0.2115	0.164	0.1446
$d_c$	91	91	91
$z$	91	91	91
$N$	380	380	380

Verification involves changing  $z$  to the verification depth. All other parameters remain unchanged. Figures 18, 21 and 24 show the comparison of model output (labeled verification) to a representative breakthrough curve at 6 feet for models using  $I_1$ ,  $I_2$  and  $I_3$ . The model seems very robust, showing that it verifies equally well for three different estimates of net infiltration if concentrations are adjusted to remove effects of transverse dispersion. Figures 19, 22 and 25 illustrate similar comparisons at 9 feet. Figures 19 and 22 only show fair agreement between model and adjusted samples. This is probably due to large errors in  $I_1$  and  $I_2$  which occur from October 1984 to June 1985. In contrast, Figure 25 shows good agreement between model and corrected concentrations. This seems to be due to lower estimates of net infiltration, especially during the spring of 1985. Figure 26 compares the model output at 9 feet to data from the other sampler at 9 feet corrected



using the mass method. This is presented to illustrate the worst fit using  $I_3$  in Experiment 1. Natural spatial or temporal heterogeneity of all input parameters and complicated soil water and tracer movement during winter months are probable reasons for the "worst fit".

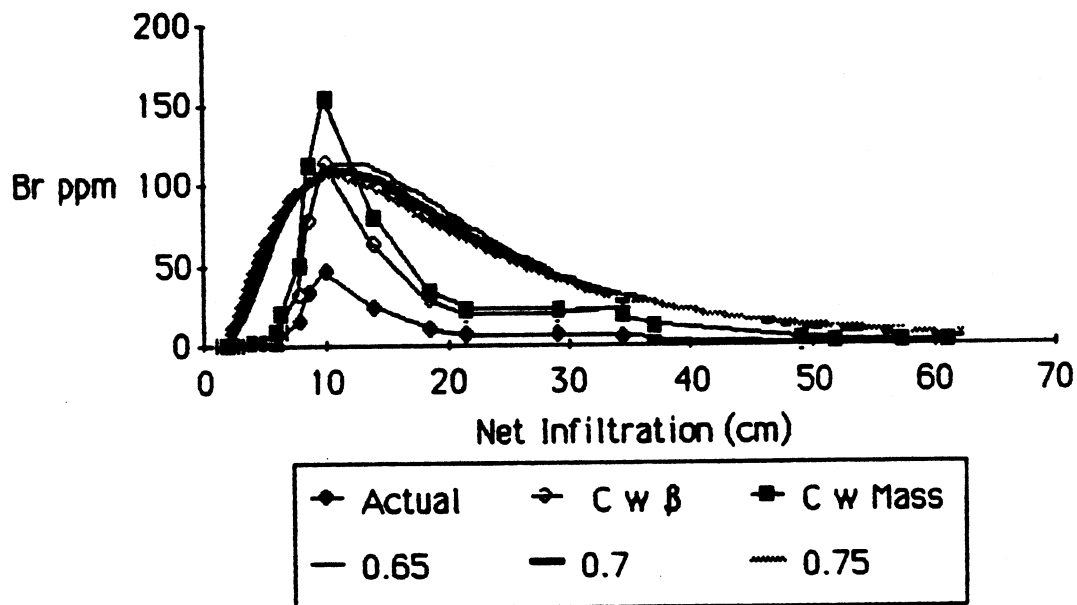


Figure 20. Calibration at 3 feet using  $I_2$ . Values of  $\sigma_x$  are shown for each of the curves produced by the model.

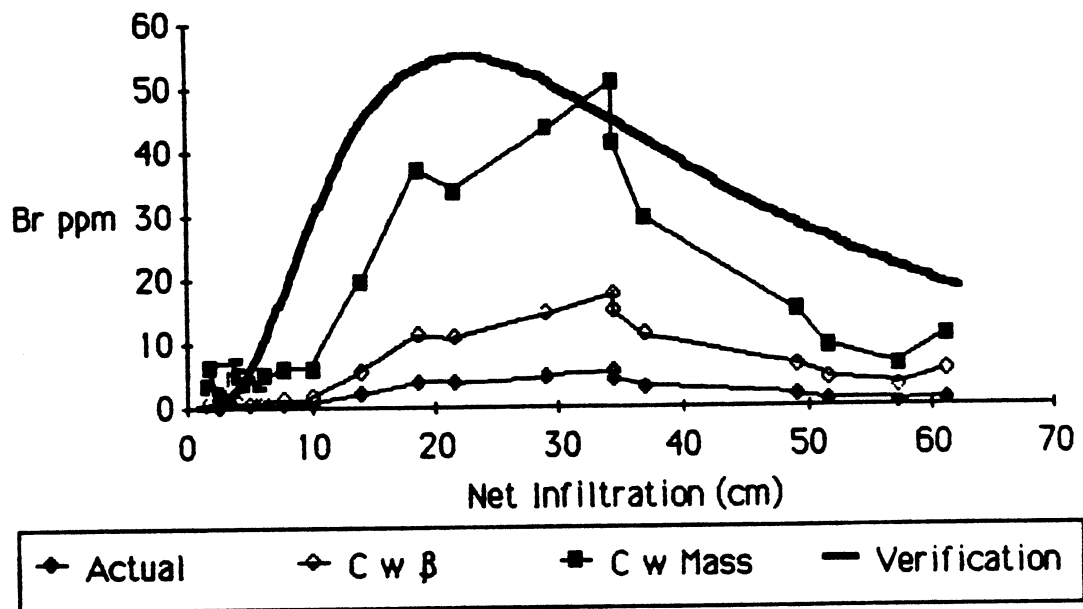


Figure 21. Verification at 6 feet using  $I_2$ .

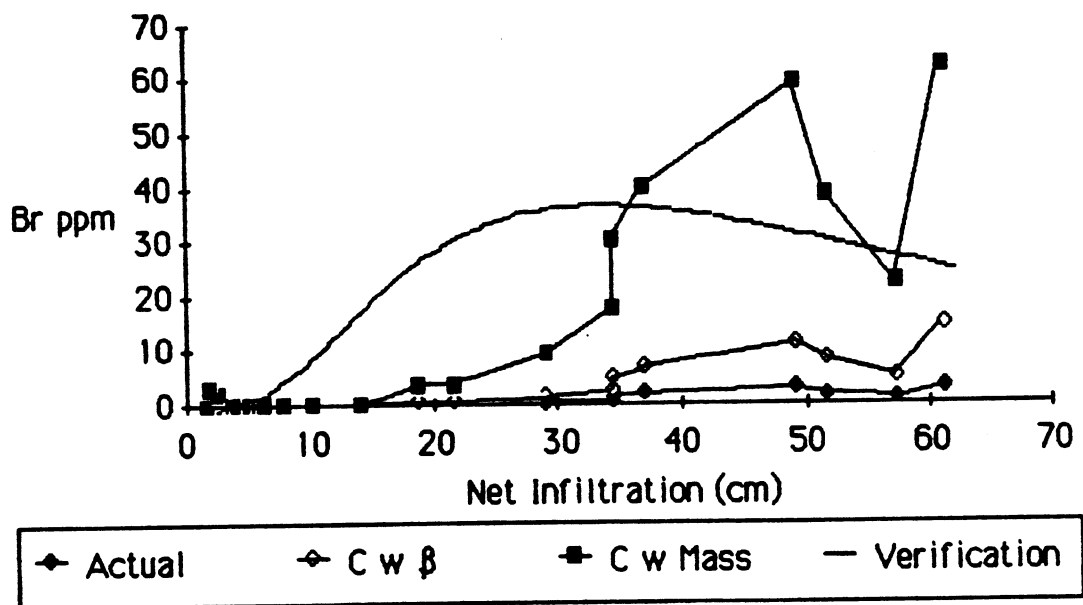


Figure 22. Verification at 9 feet using  $I_2$ .

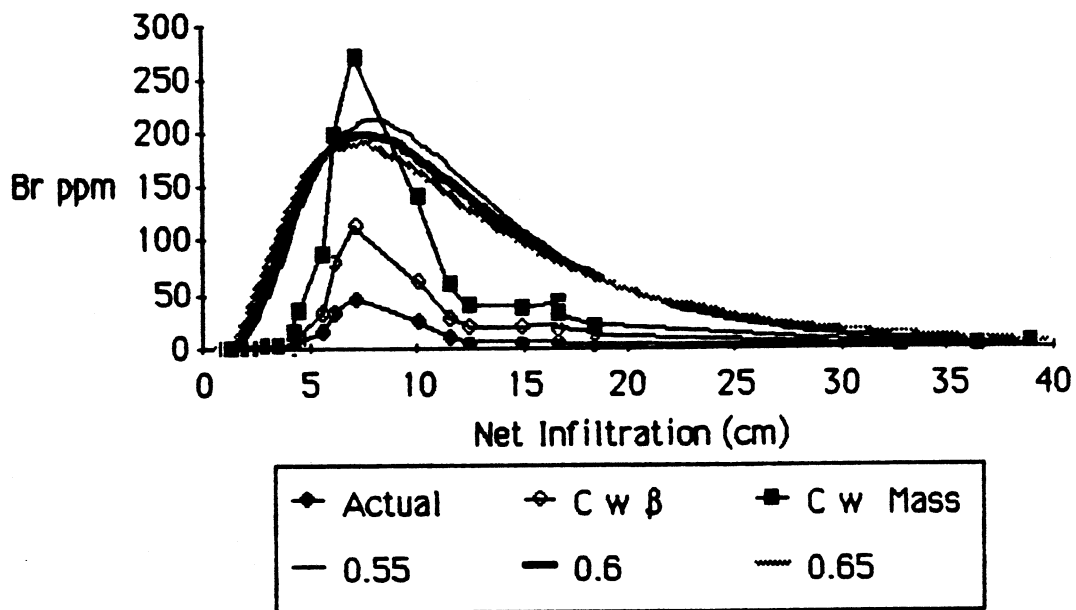


Figure 23. Calibration at 3 feet using  $I_3$ . Values of  $\sigma_x$  are shown for each of the curves produced by the model.

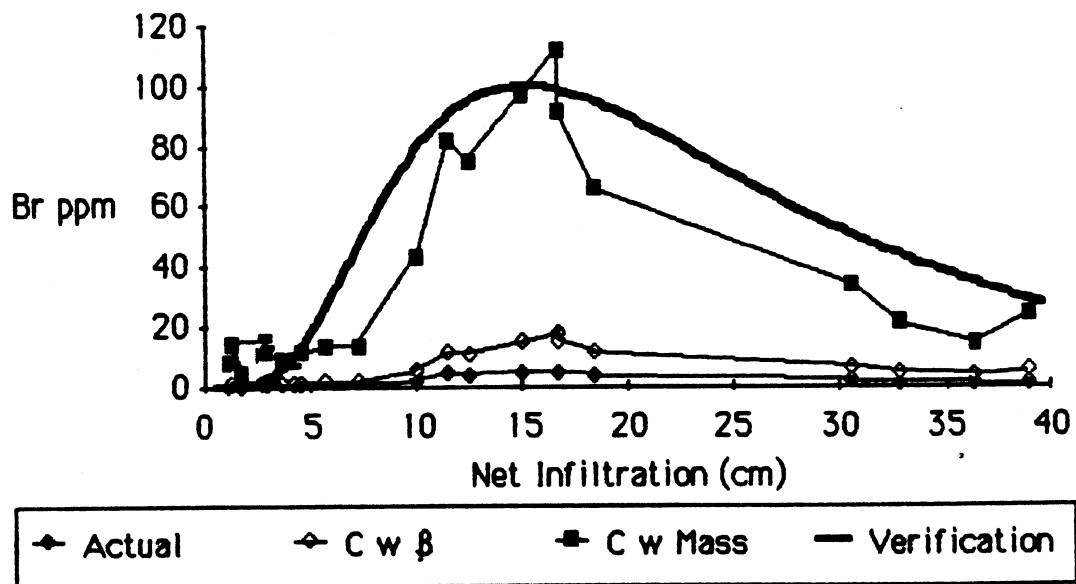


Figure 24. Verification at 6 feet using  $I_3$ .

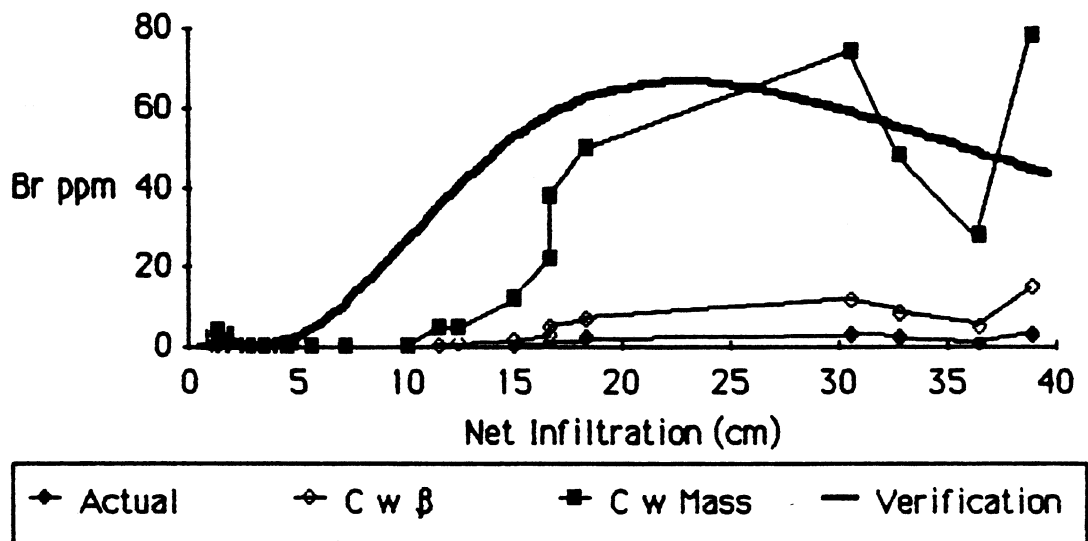


Figure 25. Verification at 9 feet using  $I_3$ .

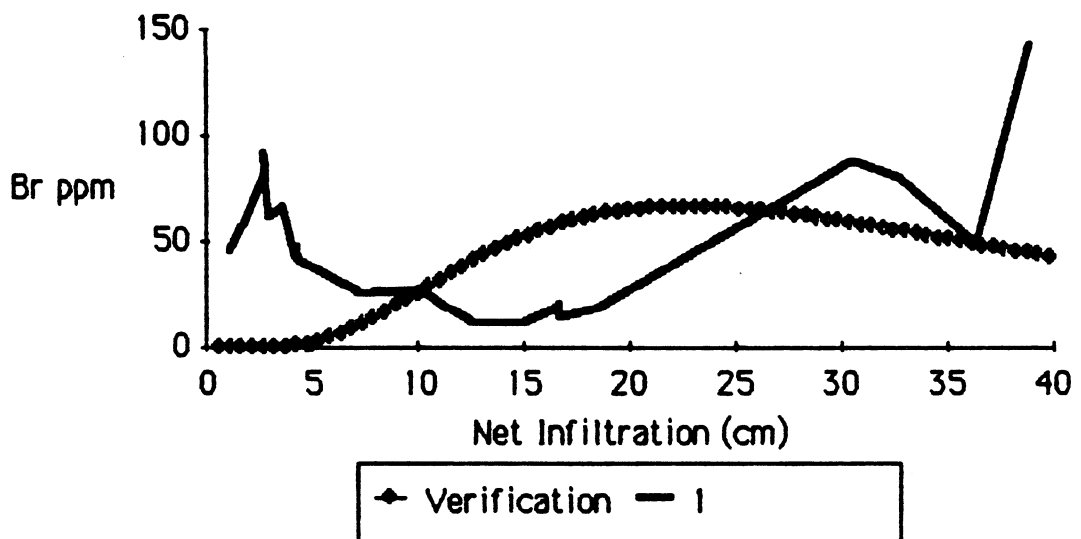


Figure 26. The worst fit.

## 7. Ergodicity

This technique involves equating moments of a distribution derived from one dimension time, time, to another dimension, space. For this reason, the method is heuristically called "ergodic". However, it should be noted that the method does not conform to a rigorous mathematical definition of ergodicity.

Each sampler samples an area adjacent to itself. In the context of the Randomized Plug Flow model, this area cuts across many vertical tubes. Each tube transports tracer at a different rate. Thus, the time series concentration at a sampler is the direct result of the spatial variation of transport amongst the tubes. Low concentrations occur when a small number of tubes deliver tracer to the sampler. Higher concentrations occur when more tubes deliver the tracer to the sampler. If the area that is sampled is large enough to be representative of the field, the center of mass of the time series is a good estimate of the average center of mass for the field. This may indeed be the case in Experiment 1. Using  $I_3$ , the coefficient of variation of centroids for the replicates at 3 feet is 3.8%. Thus, a reasonable estimate of  $\mu_x$  is the natural log of the center of mass of a time series from a single sampler. An estimate of  $\mu$ , based upon  $i$ , is the center of mass of a time series from a single sampler. To estimate  $\sigma_x$ , the natural log of  $i$  replaces  $i$  in the determination of total mass (Tmass) and centroid (Cmass). Then using  $A = \ln i$

$$\sigma_x = (1 / T \text{ mass}) \Sigma (A - C_{\text{mass}})^2 * (\Delta A C / 1000)$$

where  $C_n$  = concentration of bromide (mg/kg) at the  $n^{\text{th}}$  sampling period.  $\sigma$ , based upon  $i$ , was found using relationships between  $\mu$ ,  $\mu_x$ ,  $\sigma$  and  $\sigma_x$  discussed previously. Values of  $\sigma$  and  $\sigma_x$  are given in Table 2. Both  $\sigma_x$  and  $\sigma$ , derived from a single time series, compare well with the model values (based upon fitted  $\sigma_x$  and measured  $\mu_x$ ) found at 3 feet. However, values at 6 and 9 feet are not similar. This may be due to increases in the scale of spatial heterogeneity with depth, caused by increased channelization or instability of flow with depth. Figures 27, 28 and 29 show the TFM output using  $\sigma_x$  and  $\mu_x$  from a single breakthrough curve at 3 feet. They show reasonable agreement with the adjusted sample concentrations.

Table 2				
Sampler Number	$\sigma_x$ Ergodicity	$\sigma$ Ergodicity	$\sigma_x$	$\sigma$
( 9 feet)				
1	1.239	14.218		
2	0.508	6.988		
Model			1.75	25.5
( 6 feet)				
4	0.609	9.055		
5	0.686	8.763		
6	0.791	9.476		
Model			1.63	17
( 3 feet)				
	$\sigma_x$	$\sigma$	$\sigma_x$	$\sigma$
7	0.411	7.019		
8	0.433	7.726		
9	0.438	8.099		
Model			0.6	8.5

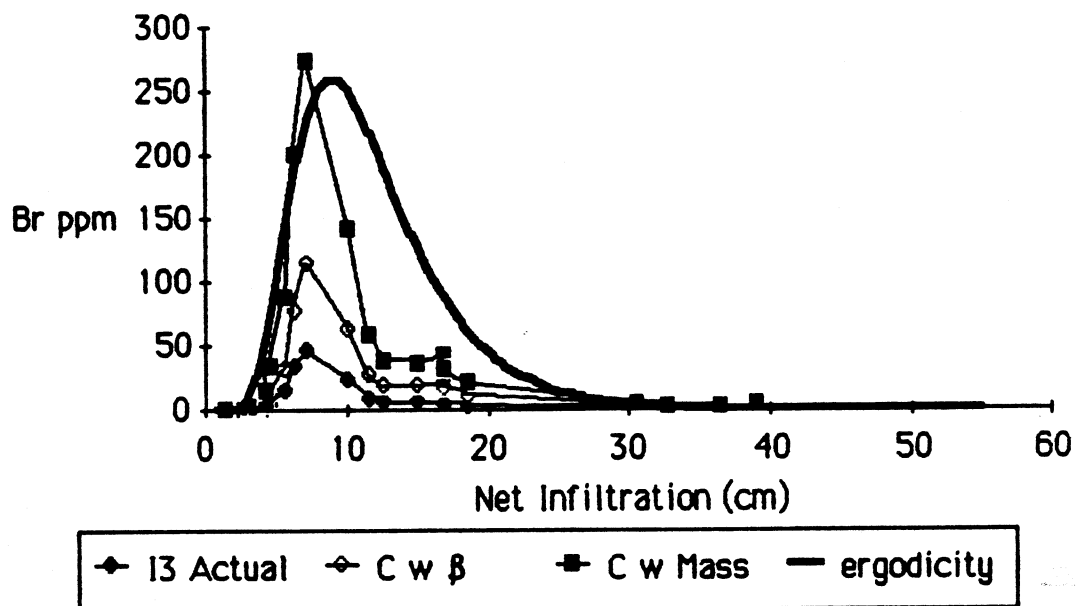


Figure 27. Model output at 3 feet using  $\sigma_x$  and  $\mu_x$  derived from a single time series at 3 feet.

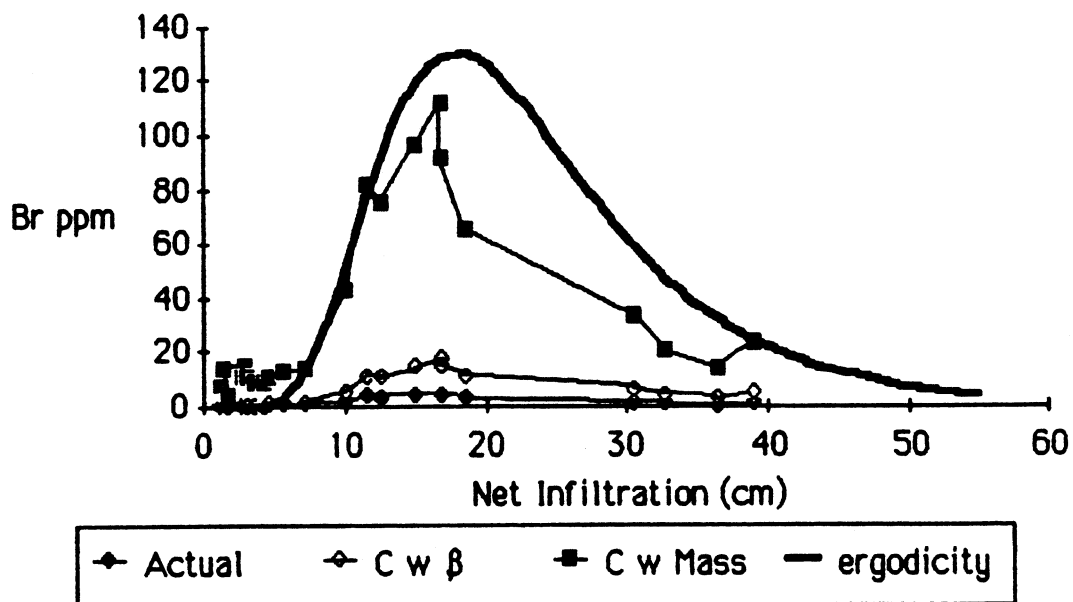


Figure 28. Model output at 6 feet using  $\sigma_x$  and  $\mu_x$  derived from a single time series at 3 feet.

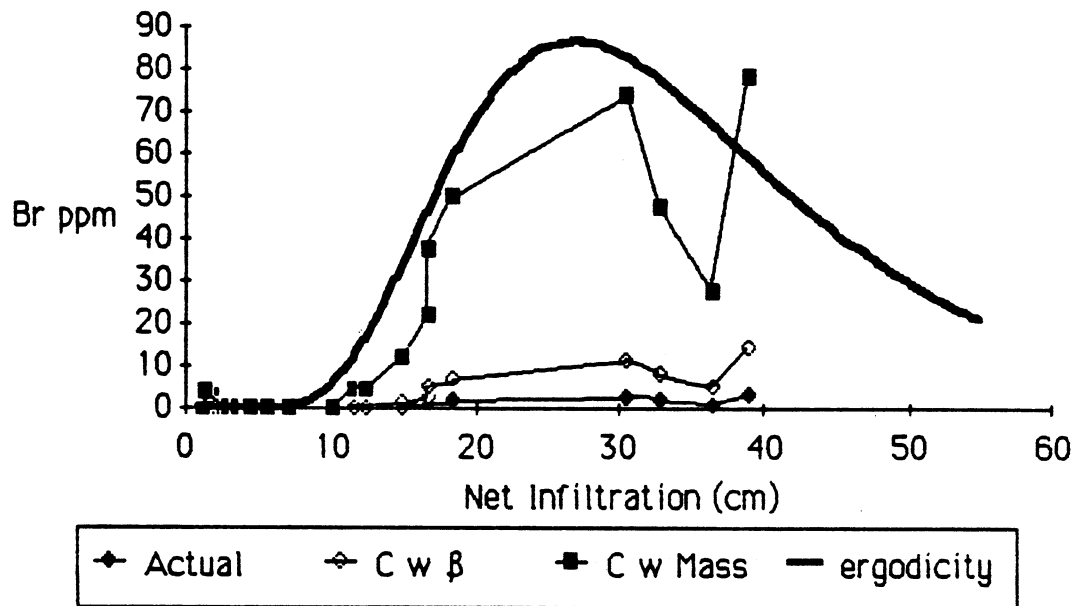


Figure 29. Model output at 9 feet using  $\sigma_x$  and  $\mu_x$  derived from a single time series at 3 feet.

### C. Conclusions

The variance in the transport found between aldicarb and bromide in Plainfield sandy loam is small enough to justify using bromide as a tracer for aldicarb in the unsaturated zone. To predict groundwater contamination using bromide (or aldicarb) data from the unsaturated zone, is not straightforward. The surface of the groundwater collects contaminant as it travels at different rates through the unsaturated zone beneath a field. Since aldicarb degrades, rapid movement (i.e. low probability transfer events) are much more important in determining ground water pollution potential than the average rate of transport beneath a field.



The total mass data show the transport of bromide under the field is greatly affected by transverse dispersivity. This complicates the interpretation of the breakthrough curves under the hills. Tracer traveling vertically down under the hills is also dispersed horizontally. There may be a "fast lane" under the furrows which more rapidly transports the dispersed tracer to the ground water. In such a case, using an uncalibrated  $f_1(i)$  to estimate the quantity of mass transported to the ground water will result in underestimates. This situation will be tested in the following experiment.

The TFM is robust in that it calibrates and verifies well using different estimates of  $I$ . In the following experiments,  $I_3$  will be used exclusively.  $I_3$  is the most accurate estimate of  $I$ . In particular, it is the only estimate which includes ET for late September, October and November. These months are important in the following experiments. Using average weighing lysimeter data to make the estimates of ET may lead to significant errors in any given year. However, some estimate of ET is better than none.

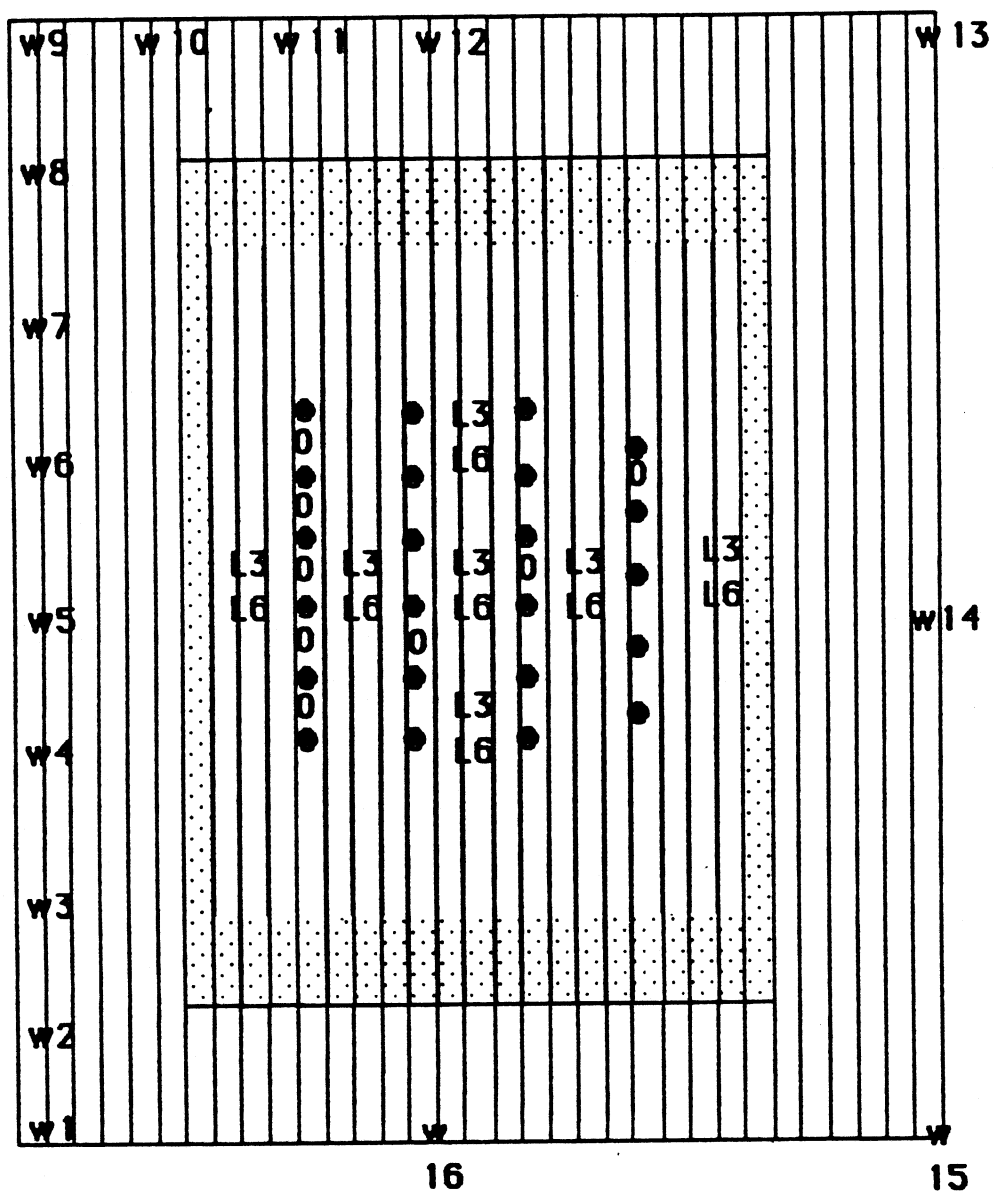
The use of ergodicity to calibrate the TFM worked well, using the time series from a single sampler at 3 feet. Because all of the breakthrough curves are similar at 3 feet, this method appears promising. In the following experiment it will be used on the average breakthrough curve at 3 feet.

## Experiment 2

Hypothesis: The TFM and Randomized Plug Flow models may be used to determine the mass of tracer transported to the water table.

The results from Experiment 1 showed the importance of low probability (rapid movement) transport events in determining ground water pollution potential. The purpose of Experiment 2 is to determine if the TFM and Randomized Plug Flow (RPF) models can be used to quantify these low probability events.

In this section, measured distributions of  $D$  and  $\Theta$  are compared to the log normal models of  $D$  and  $\Theta$ .  $I$  is omitted from this type of comparison because the sample size of  $I$  is too small. Then the models of  $D$  and  $I$  are used to predict  $\Theta$ . This tests the validity of the physical assumptions made in the RPF model. The TFM is calibrated using the distributions of  $I$ ,  $\Theta$  and  $d$  at 3 feet. The calibrated TFM is verified at 6 feet. Once verified, the model is used to find the distribution of  $I$  for  $d_c$  equal to the depth of the water table. The distribution of  $I$  at the water table is also found using the ergodic method described in Experiment 1. The distribution of  $I$ ,  $\Theta$  and  $\%P200$  are then used to calculate the transport of mass to the water table assuming both normal and log normal distributions. The calibration of the TFM is accomplished by adjusting  $\sigma_x$  of the input distribution. This results in "calibrated" distributions of  $I$ ,  $D$  and  $\Theta$ . The calibrated distributions of  $I$  and  $\Theta$  are used to predict the mass transported to the water table and comparisons are made to predictions from uncalibrated distributions (i.e.,  $\sigma_x$  calculated from data).




- w ...wells with two foot screens at the water table
- L3,L6 ...lysimeters installed at 3 and 6 feet respectively.
-  ...area that bromide was sprayed
- 0 ...push cores
- ...bucket auger cores

Figure 30. Conceptual layout for Experiment 2. Refer to Appendices I and L for more precise geometry.

Independently, the transport of mass to the water table is calculated from well samples in the field. The comparison between predictions made on unsaturated zone parameters and field data based on well samples is used to test the hypothesis of Experiment 2. Methods were developed in Appendix A which would allow the use of calibrated or uncalibrated distributions of  $D$  to predict mass transport to the water table. Because of the difficulties found in field methods used to determine  $f(D)$ , predictions from  $f(d)$  were not made.

Both Experiments 1 and 2 use similar methods. In both experiments the potatoes are hilled using 20 inch disks forming parallel hills. Thus bromide transport under the hills is probably similar. As a prologue to the results, this flow system is examined in further detail using calculations of total mass from the cores and soil water samplers.

#### A. Methods

On May 20, 1985, seven soil water samplers were installed at both 3 and 6 feet in a 99' by 120' plot directly under emerging potato plants. The following day the plants were sprayed with 1.11 molar potassium bromide at a rate of 9 ml/ft and the potato plants were hilled using 20 inch disks. The plot was irrigated using a central pivot system and using the Wisconsin Irrigation Scheduling Program. Wells were placed around the field (Figure 30). The wells are outside the region where tracer was sprayed, eliminating the possibility of contamination due to side flow. All wells and soil water samplers have been sampled as in Experiment 1. The field was sampled a total of 15 times between May 20 and November

17, 1985. On August 20, 1985, (92 days after tracer application) twenty-three soil cores were taken in 8 and 12 inch increments using bucket augers following the methods of Wyman (1985). Soils were examined using each core, and the cores were frozen immediately. Samples from the cores were analyzed for gravimetric moisture content (W), bromide (ppm soil solution) and the percent passing through a number 200 sieve using a wet sieve process (XP200). Eight push probe cores were also taken. The cores were used to delineate any fine banding which may have been missed in the bucket auger samples. This was necessary because the bucket auger samples are disturbed. All holes were backfilled using soil from the furrows. This soil should be free of tracer.

Ground water depths were determined in an intensive effort using wells 1, 9, 13 and 15. Depths to ground water were recorded 3 times daily, 5 days a week, September 4 to September 23. Velocities under the plot were determined using the water table slope and hydraulic conductivity from Kimball (1983). This intensive effort was necessary because there are two irrigation wells which may have affected the ground water flow under the plot.

## B. Results

### 1. The Flow Pattern

As discussed in Experiment 1, the transport of tracer under the hills may be complicated by transverse dispersion and higher infiltration occurring in the furrows than in the hills. Although examination of soil cores

showed no extensive horizontal soil structure which might contribute to a complicated flow pattern, considerable local variability in the soil was found. This observation is supported by the  $^{82}\text{Br}$  data. Given the purpose of Experiment 2, there was particular concern with the possibility that tracer transported laterally under the hill would enter the flow system under the furrows. Transport in the unsaturated zone under the furrows, as shown in Experiment 5, is 2 to 3 times faster than under the hills. The accelerated transport is not accounted for because the TFM and RPF models are calibrated using samplers under the hills. Thus, how much mass enters the flow system under the furrow? Appendix I contains the data, methods of analysis and results from the core samples. The average total mass of  $\text{Br}^-$  found in the cores was  $0.0785 \text{ mg/cm}^2$ . Thus, approximately 10% of the applied mass was recovered in the cores taken 92 days after the tracer was applied. There are several possibilities for the fate of the remaining 90% of tracer.

- 1) The cores are approximately 6 feet long. Some tracer flowed out the "bottom" of the cores in the time preceding core sampling.
- 2) The width of the hills is approximately 2 feet at the base. Thus, dilution from  $0.0785 \text{ mg/cm}^2$  to approximately  $0.04 \text{ mg/cm}^2$  may occur due to lateral dispersion in the flow system under the hills without transport under the furrow.
- 3)  $\text{Cl}^-$ , used in the photosynthetic pathways is a required nutrient of potatoes. Although  $\text{Br}^-$  is not a required nutrient, it is actively taken up along with  $\text{Cl}^-$  by the plants. It is difficult to estimate exactly how much  $\text{Br}^-$  is taken up by the plants. However, with

potassium chloride used as a potassium source in fertilizer, the  $\text{Br}^-$  concentrations in situ are probably "swamped" by the  $\text{Cl}^-$  concentrations. This would lead to insignificant quantities of  $\text{Br}^-$  being taken up by the plants.

4) Lateral transport due to transverse dispersion under the hills may carry the  $\text{Br}^-$  into the faster flow system under the furrows. No direct measurement of this quantity was made in Experiment 2.

It is important to note that transverse flow (e.g., due to capillary tension gradients) also occurs from the flow originating in the furrows. This flow would provide a greater flux of soil solution under the hills, which would increase with depth. In particular, the samplers located at 6 feet, which is only 2 feet above the water table, would intercept a large portion of this water flow. This added flux is not accounted for in calculations of total mass and results in a lower total mass. Further, the flux from the furrows would push the center of mass of tracer past the 6 foot sampler faster than would otherwise be the case and alter the time distribution of tracer arrival at 6 feet. The models must provide a close match to data collected at 6 feet to accurately predict mass transport to the water table. Finally, if flux from the furrow into the area under the hill is important, the assumption, made in the  $I_2$  and  $I_3$  estimates of net infiltration, that  $(P_6 - P_3) = P_3$  is in error. With the added flux coming from the furrow and increasing with depth,  $P_6 - P_3$  should be smaller than  $P_3$ .

The real transport of tracer in the experimental plots at Hancock is certainly more complicated than the model. The question that remains is whether the TFM and RPF models, using estimates of spatial heterogeneity and employing random variables, are robust enough to produce reasonable estimates of mass transport to the water table despite the complicated flow system.

## 2) Tests of Assumptions in the RPF Model

The RPF model is based upon

$$i = d/\theta$$

where  $i$  is the net infiltration added at the top of the tube,  $d$  is the depth to the tracer and  $\theta$  is the field capacity of the porous media in the tube. The model assumes that the tracer is applied as a pulse to a single hypothetical tube packed homogeneously with porous media in which there is no dispersion or diffusion. The experimental plot is modeled as a series of these vertical tubes; assuming  $\theta$  is distributed log normally,  $i$  or  $d$  are either random variables or constants as discussed previously. To calibrate  $\theta$  from field data, the average  $\theta$  from each core,  $\bar{\theta}$  was found using methods described in Appendix I. The field capacity is calculated from  $\bar{W} \cdot 1.55 = \bar{\theta}$  where

$\bar{W}$  = mass water/mass of solids averaged over a core;

1.55 = the average bulk dry specific gravity

(mass solids/volume soil)/(mass water/volume water);



$\bar{\theta}$  = volume water /volume soil averaged over a core.

The natural log of  $\bar{\theta}$  was taken for each core and  $\mu_x$  and  $\sigma_x$  calculated.

These two parameters describe the distribution of  $\theta$ . Several assumptions are made by calculating  $f(\theta)$  in this way

1) Using a constant bulk specific gravity probably causes an overestimate of  $\theta$  in the potato hills to the plow layer depth where there is no equipment traffic and the soil has been recently moved (i.e., the average dry specific gravity should be smaller).

2) All samples are assumed to be at field capacity. There were several dry days before sampling August 20 so that this assumption will result in an underestimate of field capacity above the plow layer.

3) Implicit in the use of  $\bar{\theta}$  is the assumption that the scale of heterogeneity of  $\theta$  is larger than a single core (i.e., a core is representative of a single tube, packed with porous media).

However, the scale of a core is probably too large and results in an underestimate of  $\sigma_x$ . One solution to this problem is to replace  $\bar{\theta}$  with  $\theta$  (the volumetric moisture content of a single sample) in the calibration procedure. This scheme will be explored at the end of the chapter.

The distribution of  $d$  is determined using the distance to the centroid of the tracer in each core (Appendix I). Each core is approximately 180 cm long and is segmented into 30 cm intervals. As with the breakthrough curves from the soil water samplers, an alternative

to using numerical approximations to estimate the centroid is to use the depth to the peak concentration.

Using the peak to estimate the centroid is an accurate method at larger times and when the profile is unimodal. Many cores showed bimodal distributions with high concentrations at the surface and again at depth. In addition, the soil water samplers show concentrations rising at 6 feet (180 cm) for several months after the soil cores were taken. This suggests that very little of the bromide had moved beyond the bottom of the cores at the time they were taken. For these reasons, numerical integration to find the centroids of bromide concentration was judged more accurate than using the peak

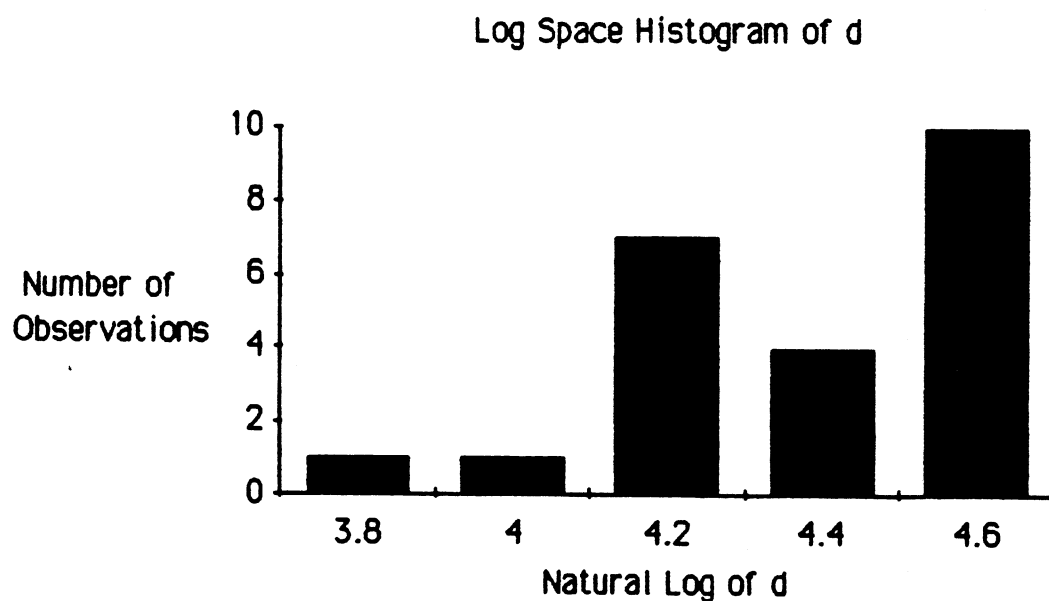


Figure 31. Histogram of observations of the log of the depth to the peak concentration in each core. The center of each interval is shown on the abscissa.

Figure 31 shows a histogram of the natural log of  $d$  from the 23 cores. If  $d$  were distributed log normally, the histogram would be normal. This is clearly not the case. In general, distributions may often appear log normal if the values of the random variable are constrained to be greater than zero and the mean is relatively close to zero. Using numerical integration to find the depth to the centroid of tracer in a core confines the value within the length of the core. Furthermore, the value tends to be in the central third of the core. For example, a triangular distribution of concentration  $C=0, Z=0; C=Max, Z=6$  ft would have the centroid at 4 feet, while a triangular distribution of  $C=Max, Z=0; C=0, Z=6$  ft would have the centroid at 2 feet. Thus, it is unlikely that numerical integration to find the centroid of the tracer concentration to find the centroid would produce data points to the right of 4.6 and make the graph look more normal. However, this may be the result of the method, not a reflection of actual conditions. Figure 32 shows a similar histogram for  $\bar{\theta}$ . Although the graph does not appear to be normal or symmetrical, it may be considered close, given the small sample size and the use of  $\bar{\theta}$  instead of  $\theta$ . Figures 33 and 34 show modeled  $f(d)$  and  $f(\theta)$  distributions (with  $\mu_x$  and  $\sigma_x$  derived from the data) compared to histograms of the field data (normalized so that the sum of all the areas of bars equals one). These figures show fairly good agreement between model and field data.

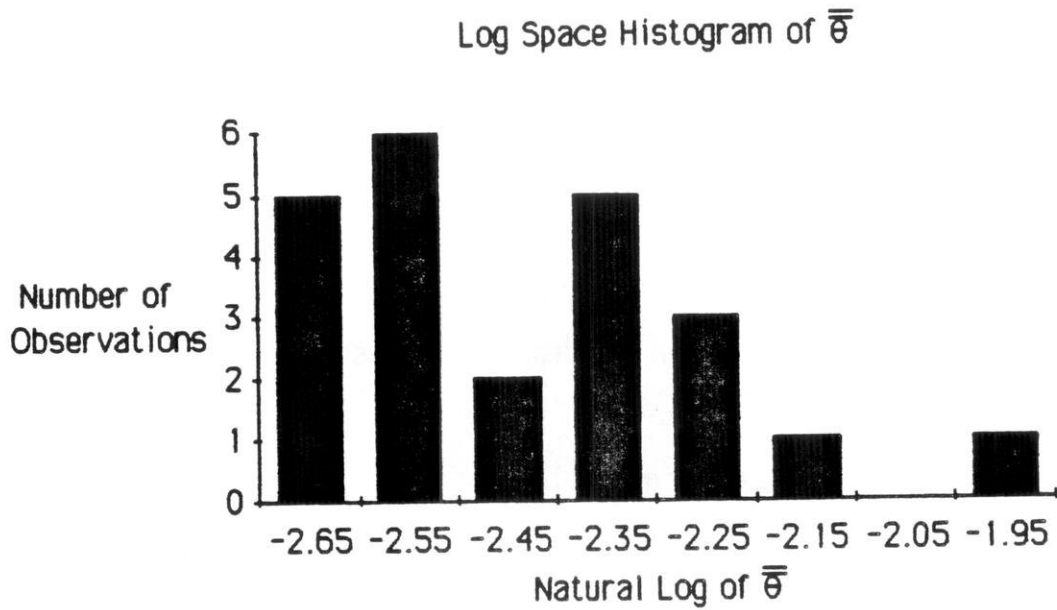


Figure 32. Histogram of the number of observations of the log of the volumetric moisture content. The center of each interval is shown on the abscissa.

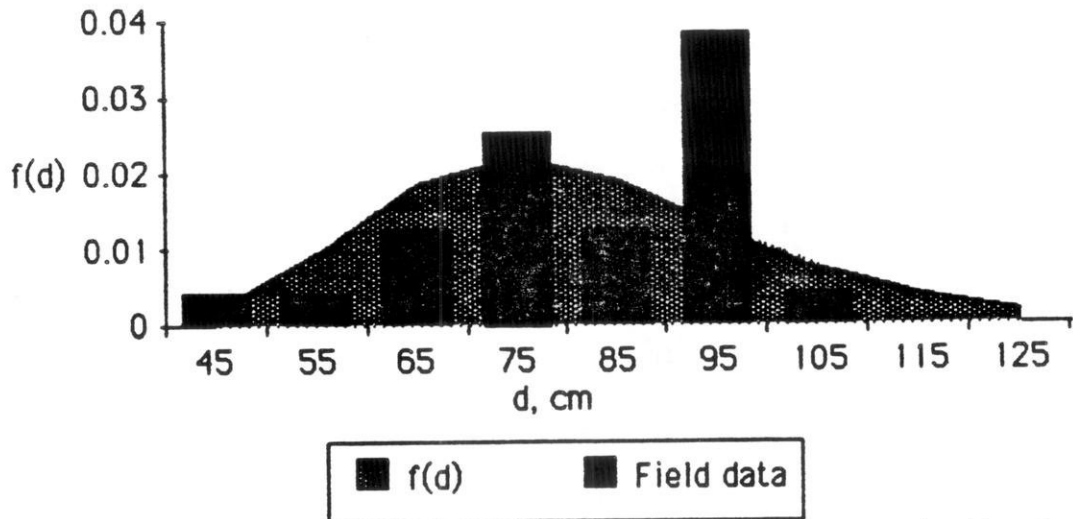


Figure 33. The model of the depth to the peak concentration in a given core is shown in the background. The field data are shown as a histogram in the foreground.

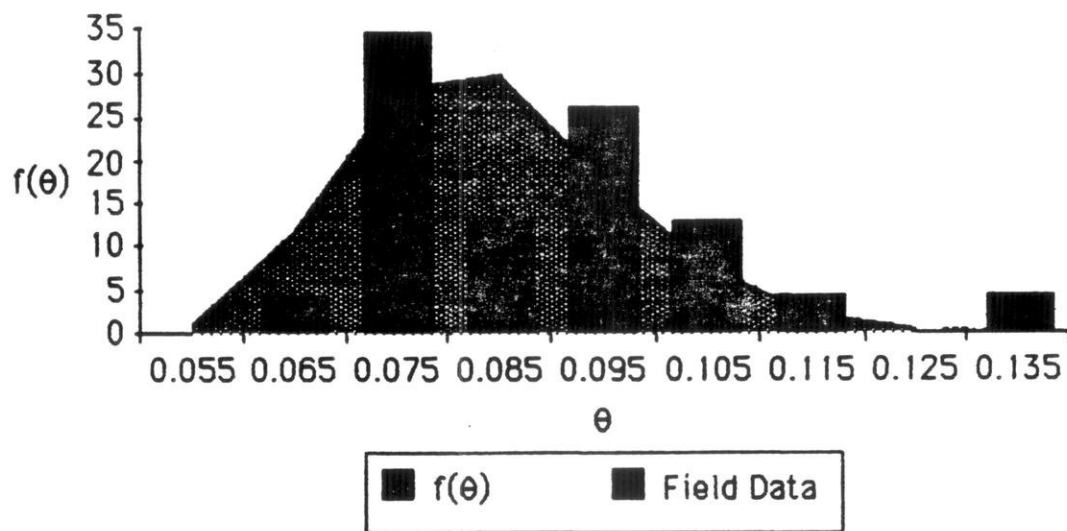


Figure 34. The model of the volumetric water content is shown in the background. The field data are shown in the histogram in the foreground.

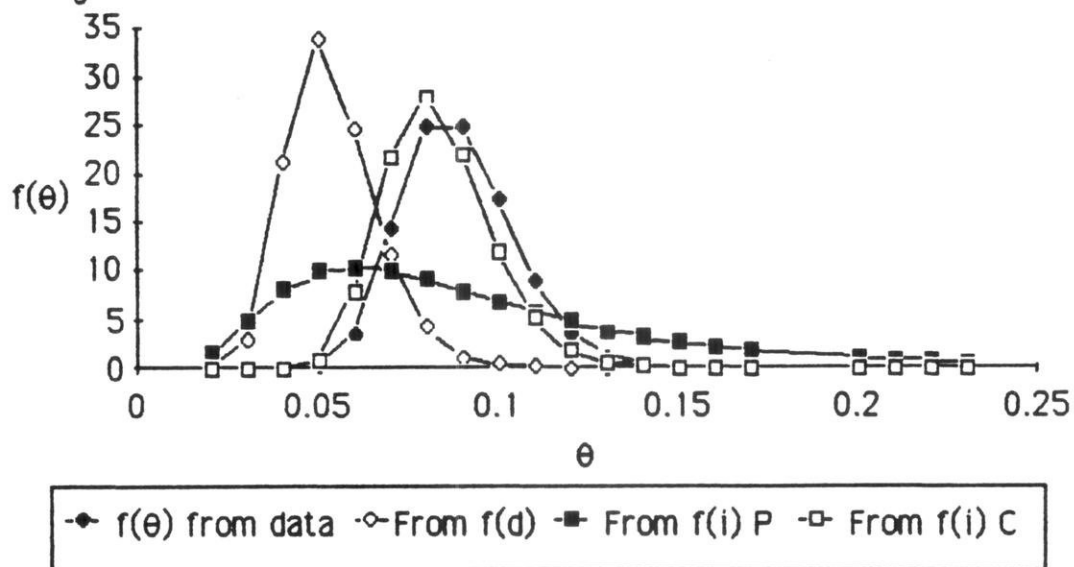


Figure 35. Comparison of the generation of  $f_{\theta}(\theta)$  from 3 independent methods with  $f_{\theta}(\theta)$  from field data.

Figure 35 shows results from the generation of  $\theta$  from three independent sources.  $f(d)$ , determined as described above may be used with Equation 2 to find  $f_{\theta}(\theta)$ .

$$f_{\theta}(\theta) = i_c / \theta^2 f_D(i_c / \theta) \quad (2)$$

where  $i_c$  is the total, net infiltration that had occurred up to the time the cores were taken.  $f_{\theta}(\theta)$  predicted in this manner is shifted relative to the field data, due apparently to underestimates of  $\theta$  from  $i_c/d$ .  $f_D(d)$  should estimate the fraction of  $\theta$  which is mobile. In a recent field study, Guirtzman and Magaritz (1986) found 40% of the moisture was immobile at the surface of the unsaturated zone and 55% immobile at 8.5m. Plainfield loamy sand is only 10 - 15% silt and clay while the soil reported by Guirtzman and Magaritz (1986) is 60% silt and clay so that a direct comparison is impossible. Less immobile water is expected in the Plainfield loamy sand. The data in Figure 35 suggests that approximately one-third of the soil moisture at the experimental plot is immobile.  $f_{\theta}(\theta)$  was also generated using  $f_I(i)$  and Equation 3;

$$f_{\theta}(\theta) = d_c f_I(d_c \theta) \quad (3)$$

where  $d_c$  is the depth to the soil water sampler used to determine  $f_I(i)$ . Figure 35 shows  $f_{\theta}(\theta)$  derived from the distribution of  $i$  determined using two methods. The dark box is  $f_I(i)$  determined using the natural log of the net infiltration ( $I_3$ ) at the time the peak concentration of bromide reached

each soil water sampler at 6 feet. The empty box is  $f_1(i)$  determined using the natural log of the net infiltration ( $I_3$ ) at the time the center of mass of the tracer reached each sampler at 3 feet. Because some of the breakthrough curves at 3 feet (Figure 36) appear to be complete while others do not show obvious peaks, it is difficult to determine which method of calibrating  $f_1(i)$  is more accurate. The use of the center of mass to determine  $f_1(i)$  and predict  $f_\theta(\theta)$  provides a better fit to  $f_\theta(\theta)$  determined using  $\bar{\theta}$  from each core as described above (solid diamond). It is interesting to note that the means of  $f_1(i)$  determined using peaks and  $f_1(i)$  determined using C mass are very similar. This stresses the importance of the standard deviation of the data in this model.

Table 3

	<u>Peaks</u>	<u>Center Mass</u>
$\bar{x}$	8.21	8.772
s	3.865	0.892

### 3) Breakthrough Curves

Figures 36 and 37 contain all the breakthrough curves at 3 and 6 feet respectively. All net infiltration in this experiment was calculated using the  $I_3$  model discussed previously. See Appendix J for values of  $I$ ,  $I_3'$  and  $I_3$ . A large amount of spatial heterogeneity at 3 feet is apparent. Reasons for this heterogeneity include natural variability in soil structure, root density, and micro-relief of the top of the hill, which may all cause spatial heterogeneity in net infiltration. In contrast, the

breakthrough curves at 6 feet are more homogeneous. This may be expected since horizontal tension gradients should mitigate spatial heterogeneity with depth.

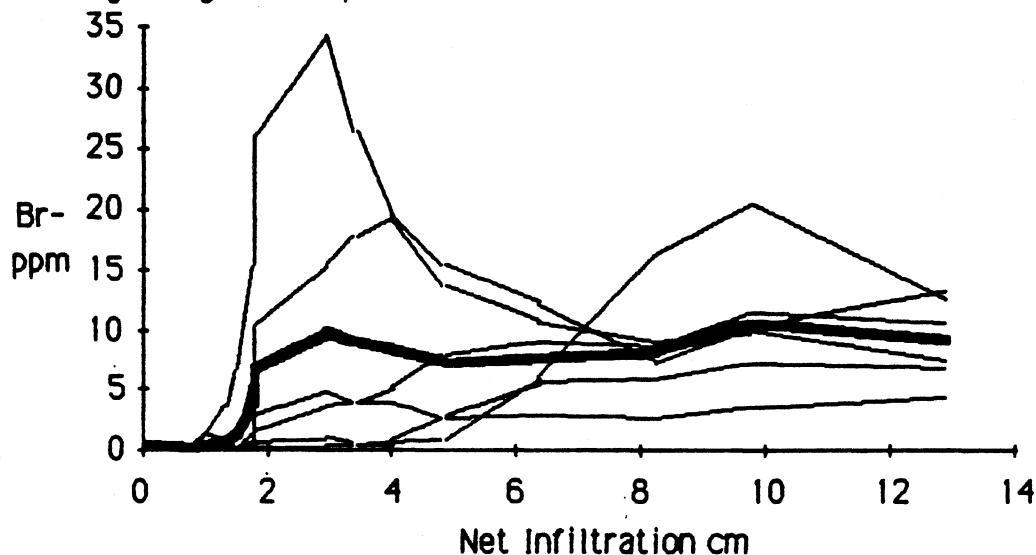


Figure 36. Concentration versus net infiltration ( $I_3$  using peaks) from each sampler at 3 feet. The heavy line is the average trace.

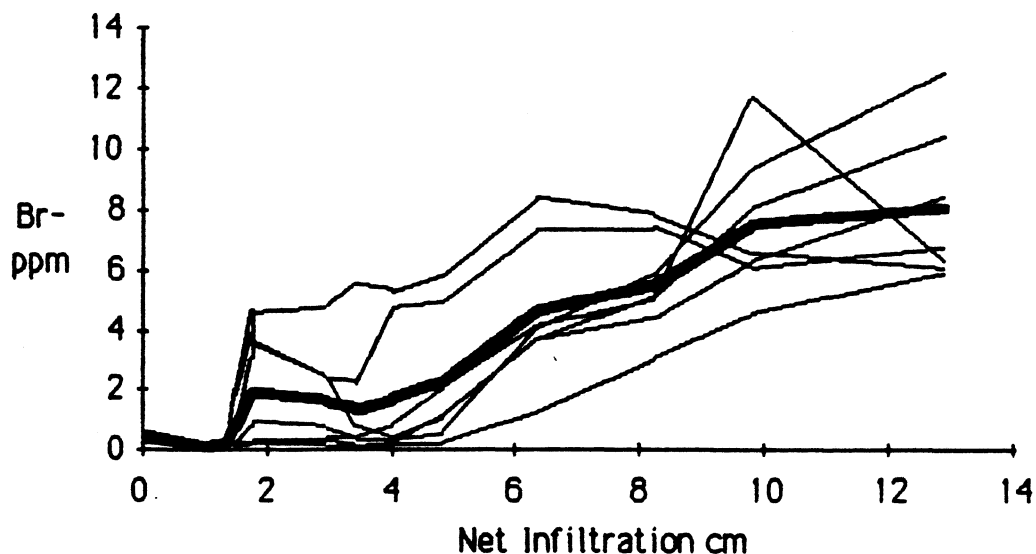


Figure 37. Concentration versus net infiltration ( $I_3$  using peaks) for all samplers at 6 feet. The heavy line is the average trace.



An estimate of  $P_3'$  and  $P_6'$  are required to calculate 1. Since many of the breakthrough curves at 6 feet are still rising at the end of the experiment, total net infiltration at peak concentration was chosen to estimate  $P_6'$  rather than the center of mass. The same estimate is used to determine  $P_3'$ .

#### 4) Transfer Function Model

In Experiment 1, the field data were adjusted so that 100% of the mass of tracer applied was accounted for in the area under the concentration versus net infiltration curve. The TFM calibrated well to these "adjusted" curves but poorly to actual field data. This situation is also found in Experiment 2. The TFM is apparently not useful in predicting the appropriate magnitude of unsaturated zone breakthrough curves in these experiments. This is probably because of lateral transport of moisture and tracer due to the "fast lane - slow lane" flow system and application of tracer in strips.

The model developed in this thesis to predict mass transport to the water table does not require knowledge of absolute concentrations of substances in the unsaturated zone. Only the shape of the unsaturated breakthrough curve is important. Furthermore, assuming a normal or log normal distribution of  $i$ ,  $d$ , or  $\theta$ , only two parameters are required (the mean and standard deviation). Thus the purpose for applying the TFM to the data in Experiment 2 is to determine these parameters from actual breakthrough curves. The accuracy of the calibrated parameters is then

tested by comparing actual and estimated mass transport to the water table.

As in Experiment 1, the standard deviation is used to calibrate the model at 3 feet. The model is then verified at 6 feet. For consistency, three curves are presented with each calibration or verification run as described in Experiment 1; 1) The average breakthrough curve; 2) The average curve adjusted with  $\beta$ ; 3) The average curve adjusted with mass. Since the average curve adjusted with mass is the field data multiplied by a constant, it has the same shape as the field data. Calibration is accomplished by running the TFM model for various  $\sigma_x$  until the "best fit" to the average breakthrough curve shape at 3 feet is obtained. The "best fit" might have been determined by a least squares test. However, given all the sources of error and natural heterogeneity of the system, the curve which looked like the best fit was chosen. Verification runs use the calibrated parameters from the best fit.

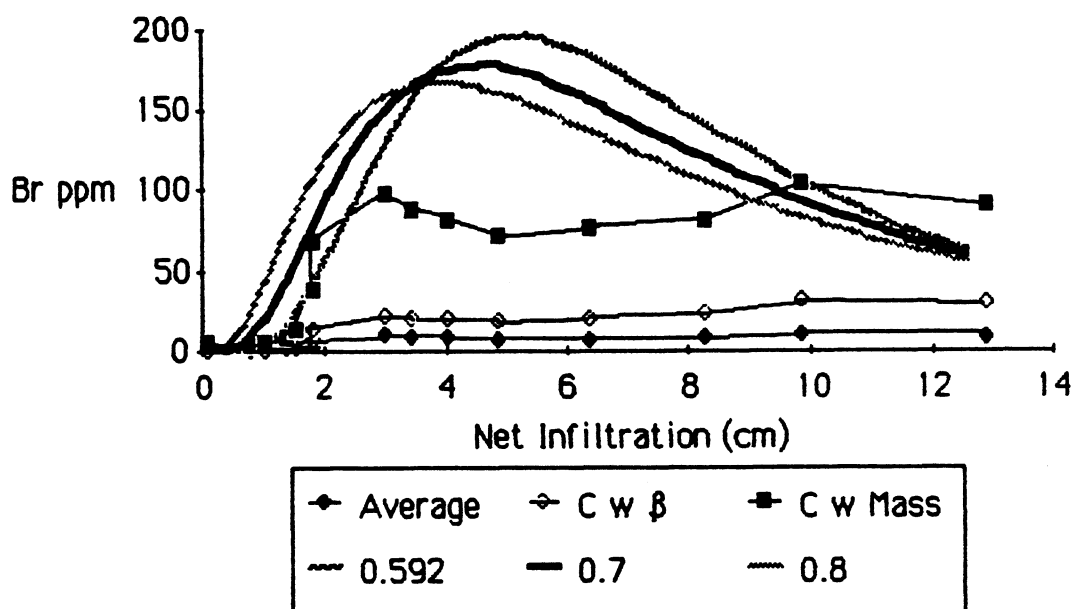


Figure 38. TFM output at 3 feet are shown for three values of  $\sigma_x$  (smooth lines). All three traces use  $\mu_x = 1.98$  taken from  $P_3$  as shown in Appendix J.  $\sigma_x = .592 = \sigma_x$  of  $P_3$ . The line labeled "Average" is the average breakthrough curve at 3 feet. C w  $\beta$  and C w Mass are the average breakthrough curve adjusted as described in the text.

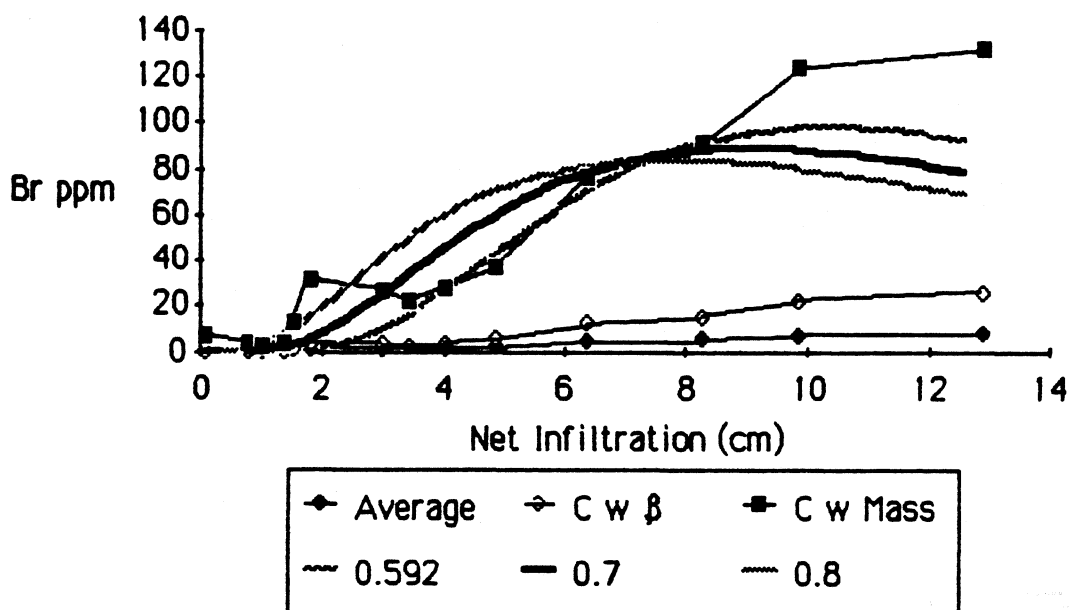


Figure 39. TFM output at 6 feet are shown for three values of  $\sigma_x$  (smooth lines). All three traces use  $\mu_x = 1.98$  taken from  $P_3$  as shown in Appendix J.  $\sigma_x = .592 = \sigma_x$  of  $P_3$ . The line labeled "Average" is the average breakthrough curve at 6 feet. C w  $\beta$  and C w Mass are the average breakthrough curve adjusted as described in the text.

The TFM does not calibrate very well to the average breakthrough curve at 3 feet in any of the following calibrations. This is due to the unusual shape produced by averaging the heterogeneous field data. For this reason, Figures 38 through 47, which show various calibration and verification runs, are given using 3 values of  $\sigma_x$ . Figures 38 and 39 show the calibration and verification runs of the TFM respectively using the net infiltration at the time of peak concentration in the samplers at 3 feet to calibrate the model. From Appendix J,  $\mu_x = 1.98$  and  $\sigma_x = 0.592$ . Both

figures show three values of  $\sigma_x$  including the  $\sigma_x$  from the data. Although higher values of  $\sigma_x$  provide a better calibration at 3 feet, lower values of  $\sigma_x$  provide a better fit at 6 feet. The TFM may also be calibrated using the net infiltration at the centroid of the tracer concentration. This is shown in Figure 40. Here,  $\sigma_x$  of the data was 0.175 and the best fits of the TFM output were found with  $\sigma_x = 0.65$  to 0.75. As discussed previously, the low variance inherent in the centroid data are a problem in using this method of calibration.

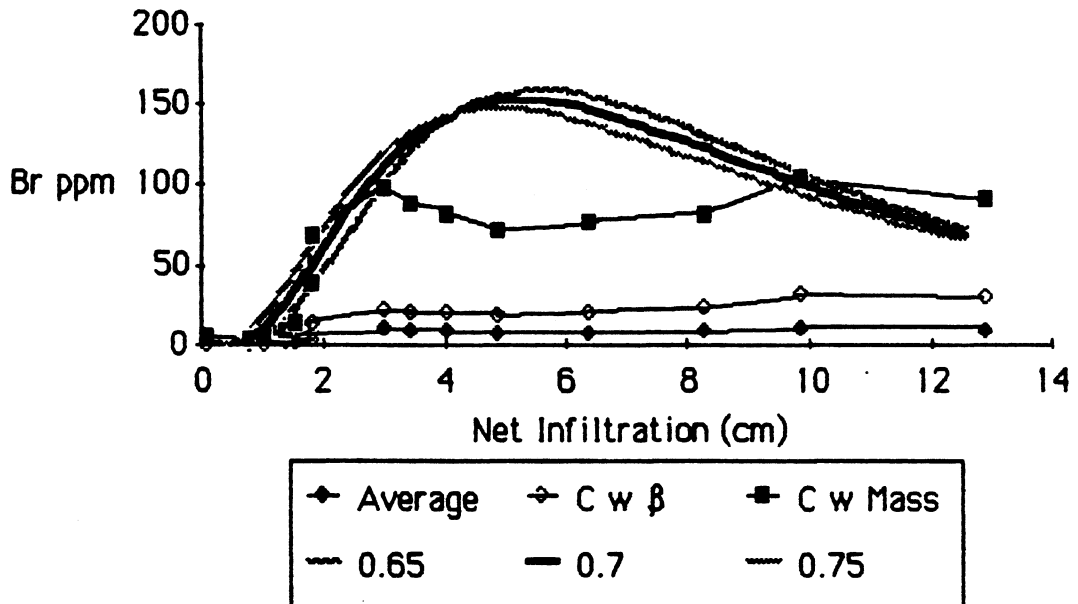


Figure 40. TFM calibration at 3 feet is shown for three values of  $\sigma_x$  (smooth lines). All three traces use  $\mu_x = 2.014$  taken from  $i_3$  using peaks as shown in Appendix J.  $\sigma_x = .175 = \sigma_x$  of  $i_3$  using peaks. The line labeled "Average" is the average breakthrough curve at 3 feet. C w  $\beta$  and C w Mass are the average breakthrough curve adjusted as described in the text.

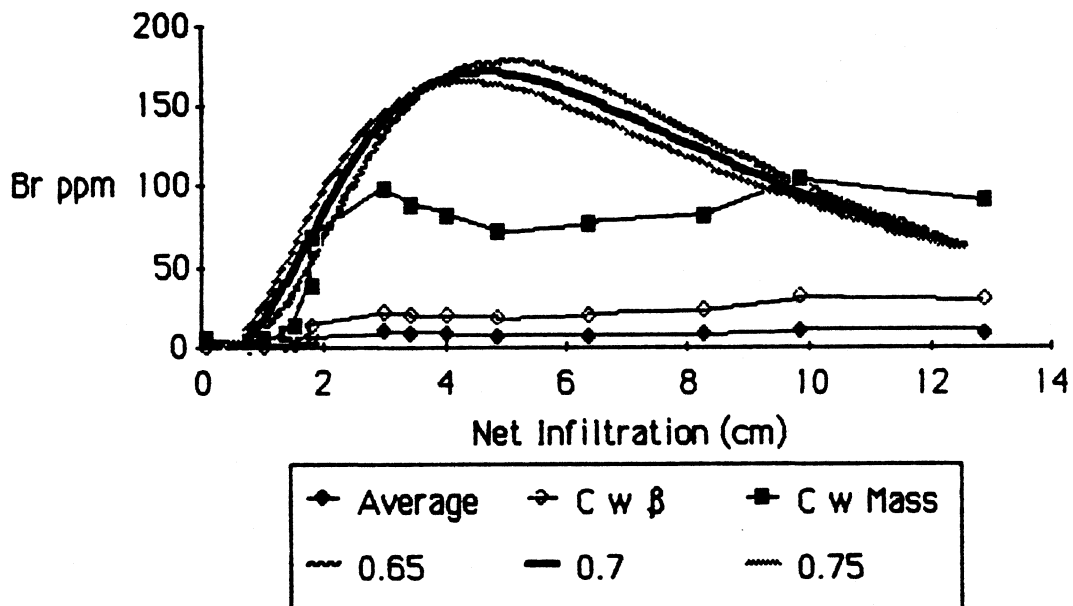


Figure 41. TFM modified to use  $f_{\Theta}(\theta)$  is calibrated at 3 feet. Three values of  $\sigma_x$  (smooth lines) are shown. All three traces use  $\mu_x = -2.501$  taken from  $\bar{\Theta}$  as shown in Appendix I.  $\sigma_x = .1549 = \sigma_x$  of  $\bar{\Theta}$ . The line labeled "Average" is the average breakthrough curve at 3 feet. C w  $\beta$  and C w Mass are the average breakthrough curve adjusted as described in the text.

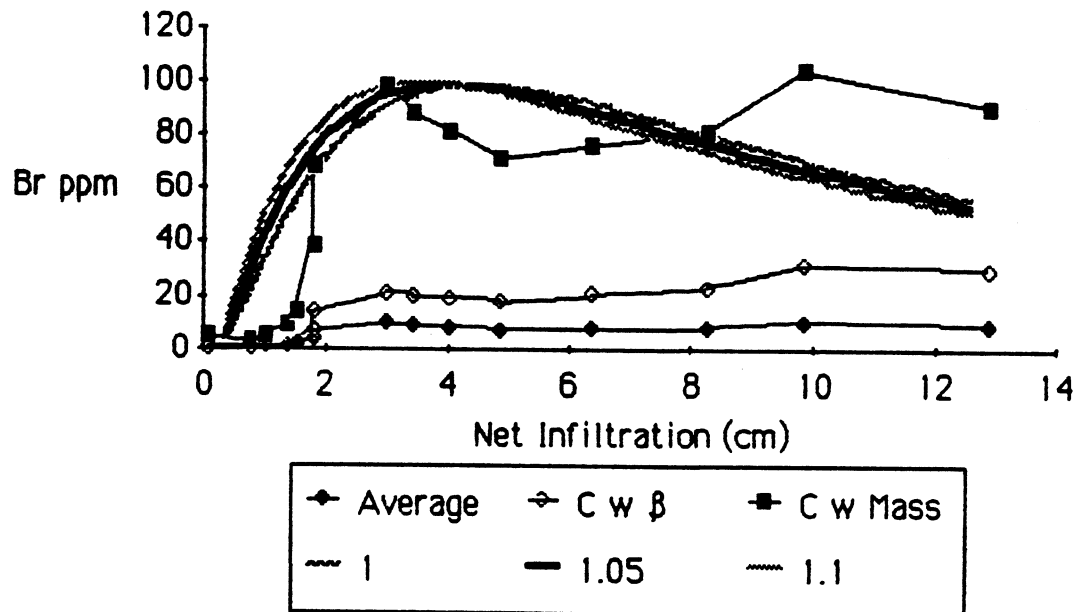


Figure 42. TFM modified to use  $f(d)$  is calibrated at 3 feet. Three values of  $\sigma_x$  (smooth lines) are shown. All three traces use  $\mu_x = 4.373$  taken from D as shown in Appendix I.  $\sigma_x = .229 = \sigma_x$  of D. The line labeled "Average" is the average breakthrough curve at 3 feet. C w  $\beta$  and C w Mass are the average breakthrough curve adjusted as described in the text.

The TFM may be modified to use  $f_{\theta}(\theta)$  through relationships described in Equation 5. The derivation is provided in Appendix A. Figure 41 shows several calibration runs of the TFM modified to use  $f_{\theta}(\theta)$ . As with the previous calibration, a large increase in  $\sigma_x$  was required to provide a desirable fit. This is not unexpected since the scale of the cores is probably larger than the scale of heterogeneity of  $\theta$  which affects transport. Thus, the field data of  $\bar{\theta}$  underestimate  $\sigma_x$ . The TFM may also

be modified to use  $f_D(d)$  instead of  $f_I(i)$ . The derivation of this relation is shown in Appendix A. The calibration run is shown in Figure 42. Again a large increase in  $\sigma_X$  was required to attain a reasonable fit. This is expected because the cores are large compared to the heterogeneity of transport so that the behavior of  $d$  in each core underestimates  $\sigma_X$ .

Verification of the TFM at 6 feet is shown in Figure 43 for all three calibrations discussed above. It is difficult to tell which curve provides the best fit to the average breakthrough curve. Given the errors and heterogeneity of the system, it seems reasonable to conclude that the curves derived from  $f_I(i)$  and  $f_\Theta(\theta)$  are equally good estimators of the average curve shape.  $f_D(d)$  does not seem to be as good a predictor. This is probably because  $\mu_X$  of  $d$  is poorly estimated from the field data as previously discussed.

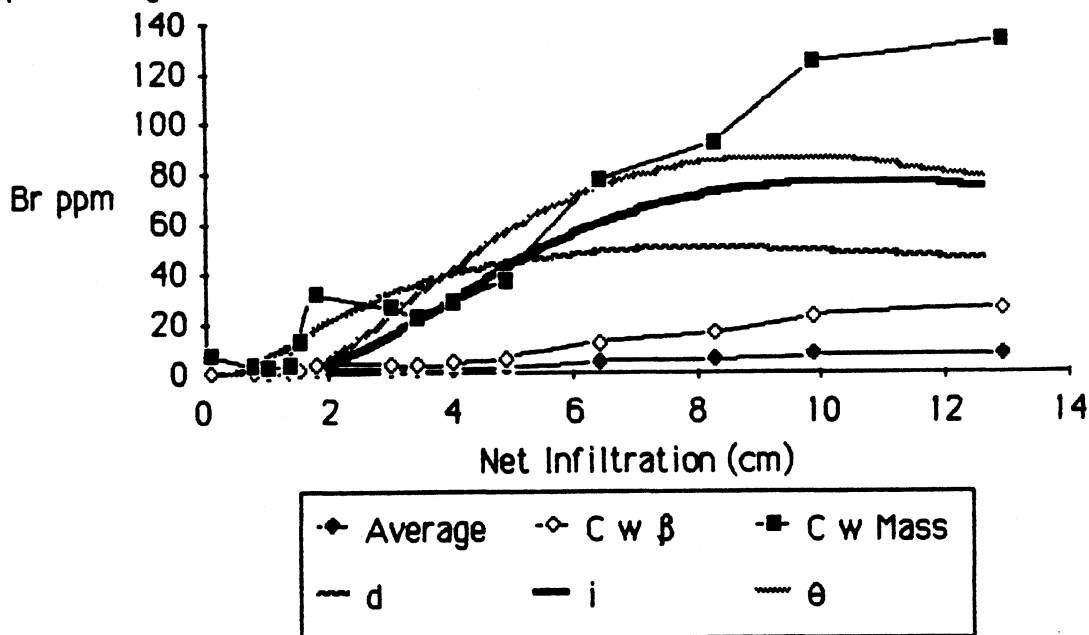


Figure 43. TFM modified to use  $f_D(d)$ ,  $f_\Theta(\theta)$ , or  $f_I(i)$  is verified at 6 feet using  $\sigma_X = 1.05$ ,  $0.7$ , and  $0.7$  respectively. The line



labeled "Average" is the average breakthrough curve at 6 feet. C w  $\beta$  and C w Mass are the average breakthrough curve adjusted as described in the text.

The TFM may also be modified to use time instead of net infiltration as the input data. This is equivalent to assuming a constant net  $i$  per unit time. Thus  $\mu_x$  and  $\sigma_x$  are estimated from the natural log of the values of the centroid of tracer in days from each sampler at 3 feet. In this way,  $f_T(t) \approx \text{LN}(\mu_x, \sigma_x)$  is defined. However, a variable  $\Delta t$ , which is analogous to  $\Delta I$ , defining the duration of the input concentration square pulse is required.  $\Delta t = \Delta I / \text{net infiltration per day}$  was used, where the net infiltration is calculated using  $I_3$ .

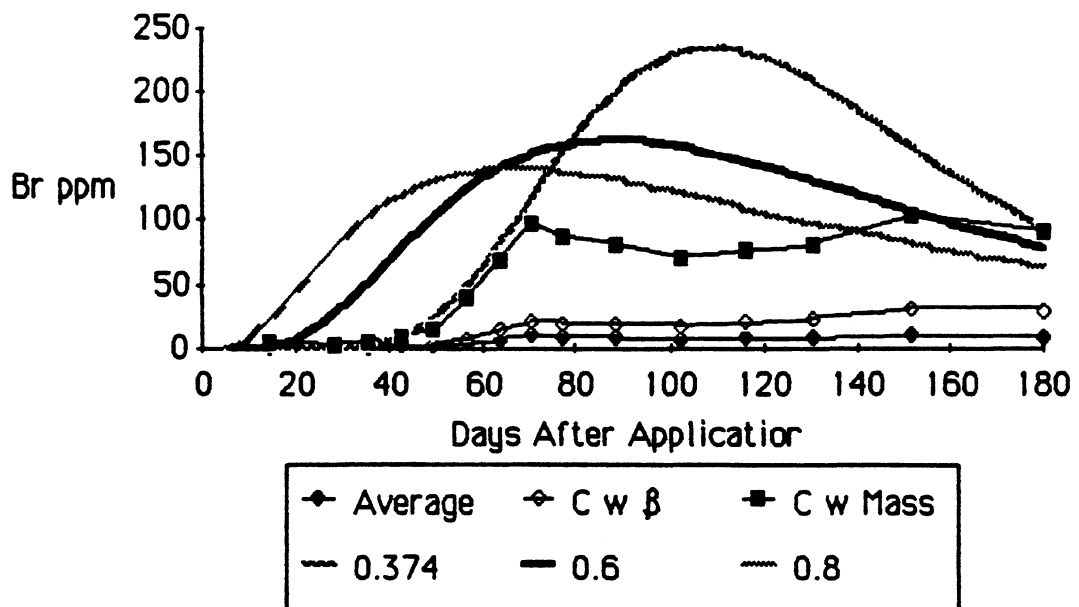


Figure 44. TFM modified to use time is shown for three values of  $\sigma_x$  (smooth lines) are shown. All three traces use  $\mu_x = 4.828$  taken from Peak Days as shown in Appendix J.  $\sigma_x = .374 = \sigma_x$  of Peak

Days. The line labeled Average is the average breakthrough curve at 3 feet. C w  $\beta$  and C w Mass are the average breakthrough curve adjusted as described in the text.

Figure 44 shows the result of a calibration run using the time (days) elapsed when peak concentrations were found at each sampler at 3 feet to calibrate  $f_T(t)$ . The TFM output using  $\sigma_x = 0.374$  from the data is shown as well as  $\sigma_x = 0.6$  and  $0.8$ . It appears that some increase in  $\sigma_x$  would provide a better fit to the shape of the breakthrough curve at 3 feet. Figure 45 shows the verification at 6 feet of the TFM for the same values of  $\sigma_x$  shown in Figure 43. The best fit seems to be provided by the  $\sigma_x$  calculated from the data.

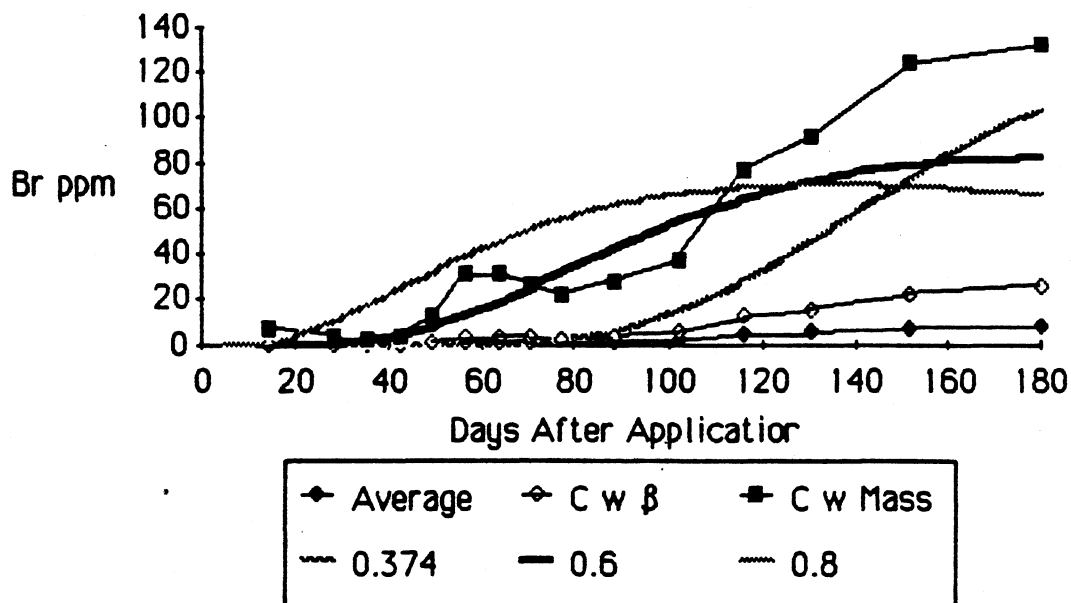


Figure 45. TFM modified to use time instead of infiltration is verified at 6 feet. All three traces use  $\mu_x = 4.828$  taken from Peak Days at 3 feet as shown in Appendix J.  $\sigma_x = .374 = \sigma_x$  of Peak Days

at 3 feet. The line labeled Average is the average breakthrough curve at 6 feet. C w  $\beta$  and C w Mass are the average breakthrough curve adjusted as described in the text.

Using time the TFM may be calibrated by the ergodic method discussed in Experiment 1. Here  $\mu_x$  is estimated from the natural log of the centroid (days) of the average breakthrough curve at 3 feet.  $\sigma_x$  is estimated from the variance about  $\mu_x$  of the average breakthrough curve as a function of the natural log (days) of time. Figures 46 and 47 show the results of using the ergodic method to calibrate the TFM at 3 and 6 feet respectively. Although the method does not produce as desirable results as other calibration methods, it still produces reasonable. It will be used in the following section to predict transport to the water table.

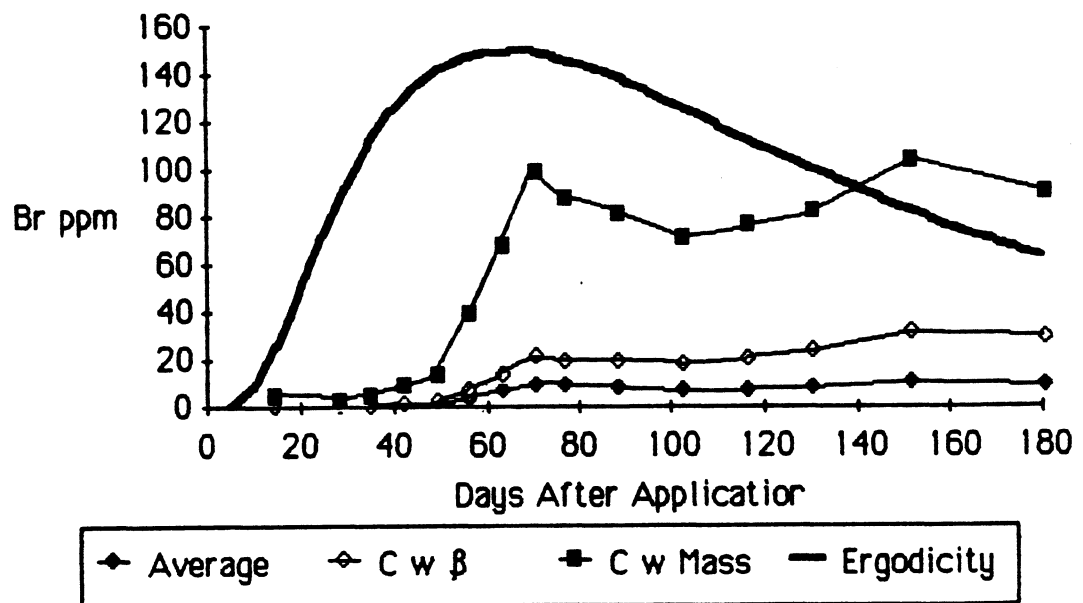


Figure 46. TFM output at 3 feet modified to use time instead of infiltration is shown for  $\mu_x = 4.19$  and  $\sigma_x = .785$  found using the average

breakthrough curve at 3 feet and the ergodic hypothesis as explained in the text. The line labeled "Average" is the average breakthrough curve at 3 feet. C w  $\beta$  and C w Mass are the average breakthrough curve adjusted as described in the text.

The TFM is being used in this section to adjust the parameter  $\sigma_x$ . This adjustment is desirable because the experimental methods used to calibrate  $f_I(i)$ ,  $f_\theta(\theta)$  and  $f_D(d)$  result in underestimates of  $\sigma_x$ . A summary of results from this section are in Table 4.

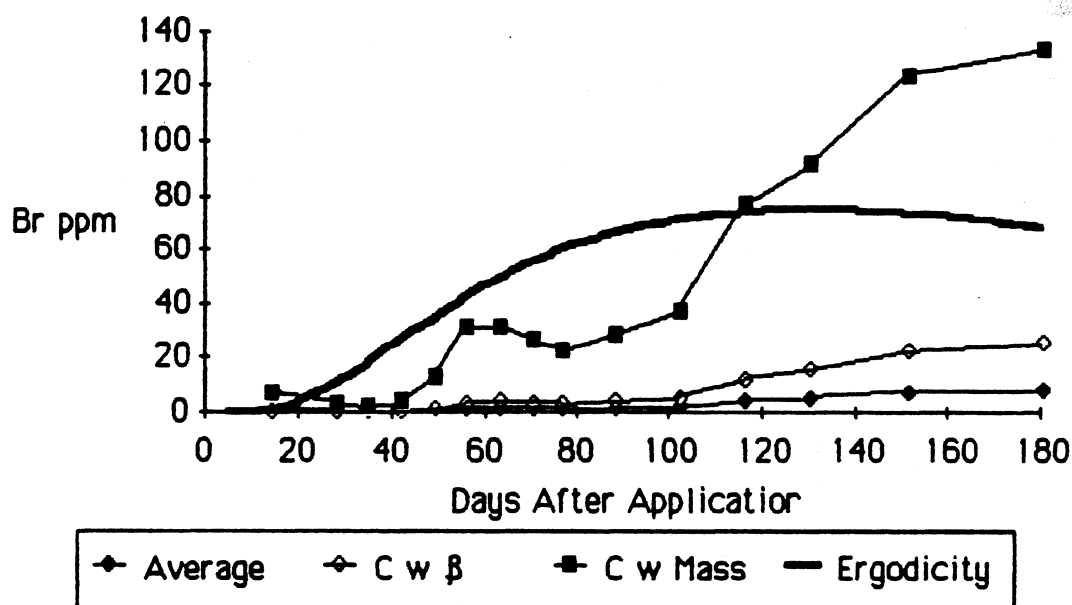


Figure 47. TFM output at 6 feet modified to use time instead of infiltration is shown for  $\mu_x = 4.19$  and  $\sigma_x = .785$  found using the average breakthrough curve at 3 feet and the ergodic hypothesis as explained in the text. The line labeled "Average" is the average breakthrough curve at 6 feet. C w  $\beta$  and C w Mass are the average breakthrough curve adjusted as described in the text.

Table 4

<u>Method</u>	<u><math>\mu_x</math></u>	<u><math>\sigma_x</math></u>	<u><math>\sigma_x</math> calibrated</u>
Infiltration using peaks	1.98	0.592	0.592
Infiltration using centroids	2.01	0.175	0.700
$f_{\theta}(\theta)$	-2.50	0.155	0.700
$f_D(d)$	4.37	0.229	1.05
Time using peaks	4.83	0.374	0.374
Time using ergodicity	4.87	0.785	0.785

#### 5) Prediction of Mass Transported to the Water Table

Bromide concentrations in the wells (Appendix L) show a plume of bromide moving northwest from the field in early summer and changing to west of the field by winter. The well elevation taken in the fall support this change in flow direction. Bromide concentration data suggest that neither of the two irrigation wells in the area affected the groundwater flow pattern past the experimental plot. Well elevation data showed considerable change in direction of groundwater flow during the month of September (Appendix L). A standard deviation of  $12.65^{\circ}$  was found over all. The changes in direction do not seem to be caused by either irrigation well. They may be the result of fluctuations in a local boundary condition (e.g., changes in water level in an irrigation ditch) or measurement error.

Gradients in the field were found to be 0.00148 ft/ft. This compares favorably with  $7.5 \times 10^{-4}$  ft/ft from DeVaul and Green sited in Kimball (1983). From Kimball (1983), the saturated hydraulic conductivity in the Hancock area is 200 ft/day and may be greater at the water table. Using these values, a ground water flow rate of 0.296 ft/day is calculated under the plot. It is important to note that Hillel (1980) shows coefficients of variation of hydraulic conductivity to range from 86% to 190% within the same soil type. The saturated hydraulic conductivity probably contributes the largest error in the following calculations.

The bromide concentrations found in well samples are reported in Appendix L. The minimum concentration reported is 0.08 ppm. The detection limit of the analysis is 0.4 ppm. Thus concentrations reported below this level probably contain higher errors than concentrations above 0.4 ppm. The uncertainty contained in the concentrations below 0.4 ppm and the uncertainty of fluctuations in the ground water flow direction lead to the strategy of calculating a low and high estimation of the mass transported to the water table. To calculate the high estimate, all concentrations presented in Appendix L are employed. The gradient of the ground water elevation is assumed to be constant, perpendicular to the western boundary and at 45 degrees to the northern and southern boundaries (Figure 1, Appendix L). To calculate the low estimate, all concentrations below 0.4 ppm are set to zero and the direction of the gradient is assumed to be constant at 116 degrees from the x axis.

The sum of mass flowing passed all wells as percent of the total mass applied are shown for both high and low mass calculations in Figures

48 through 55. When graphed against net infiltration, a constant value of 0.06993 cm/day (calculated from  $I_3$  using peaks) was used to transfer days to cm of net infiltration for all samples taken after 180 days.

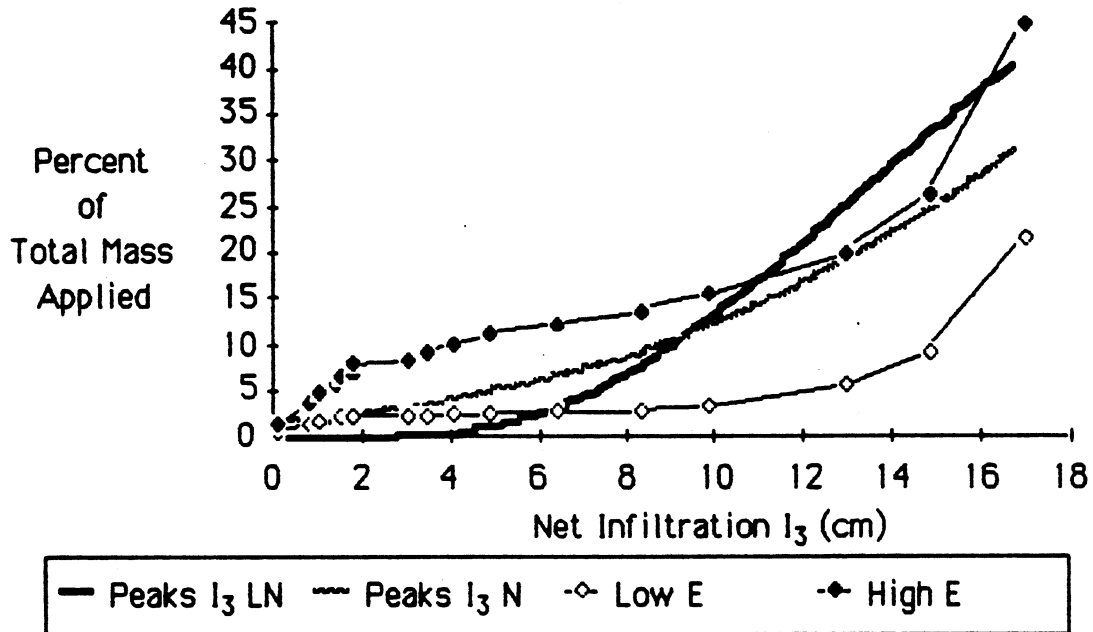


Figure 48. Estimates of the percent mass of bromide transported to the water table as a function of net infiltration. Low and High E are estimates from well samples surrounding the field. Peaks  $I_3$  LN is a prediction based on a log normal model of the net infiltration required to move the peak concentrations to 3 feet. Peaks  $I_3$  N is based on a normal model of the same data.

The purpose for examining the following figures is to judge the usefulness of the transport of mass to the water table predictions. A method might have been derived to quantify the comparison between predicted transport and estimates based on well concentrations. Considering the errors involved in the entire procedure, it was judged that a simple visual comparison is sufficient. All predictions are based on the

calibration of a stochastic model representing the arrival times of tracer at the water table. In Figures 48 through 52, the model is calibrated using the breakthrough curves at 3 feet. Five different methods are compared.

- 1) Infiltration using peaks (Figure 48)
- 2) Infiltration using centroids (Figure 49)
- 3) Infiltration using centroids calibrated using the TFM (Figure 50)
- 4) Peaks in time (Figure 51)
- 5) Ergodicity in time (Figure 52).

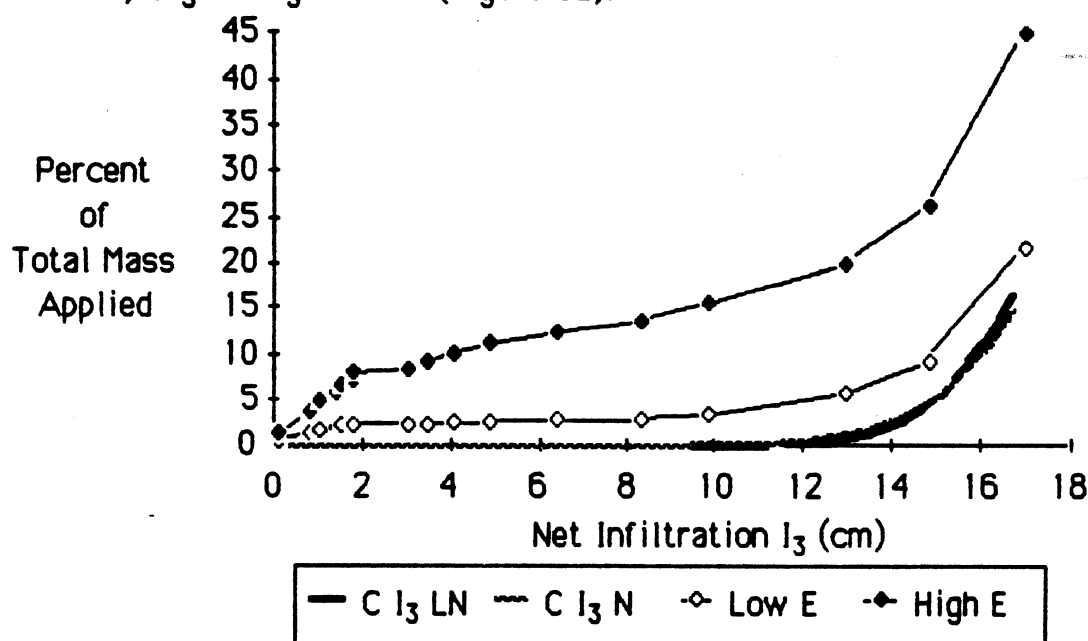


Figure 49. Estimates of the percent mass of bromide transported to the water table as a function of net infiltration. Low and High E are estimates from well samples surrounding the field. C  $I_3$  LN is a prediction based on a log normal model of the net infiltration required to move the center of mass of the breakthrough curves to 3 feet. C  $I_3$  N is based on a normal model of the same data.



All of these methods of finding the two parameters describing  $f_I(i)$  at 3 feet have been discussed in previous sections. Once  $\mu_x$  and  $\sigma_x$  are found at 3 feet, the distribution at the water table (8 feet) is found using the method discussed in Section III and Appendix A. Briefly, the real space values of  $\mu_x$  and  $\sigma_x$  ( $\mu$  and  $\sigma$ ) are scaled by  $d_C/z$ . Since the samplers are at a depth of 3 feet and the water table is at a depth of 8 feet,  $d_C/z = 2.6666$  in this case. A log normal model and a normal model are compared for each of the 5 methods. For the log normal model,  $\mu_x$  and  $\sigma_x$  are required for  $f_I(i)$  at the water table. For a normal model,  $\mu$  and  $\sigma$  are required. The parameters  $(\mu_x, \sigma_x)$  may be transformed to  $(\mu, \sigma)$  and  $(\mu, \sigma)$  transformed to  $(\mu_x, \sigma_x)$  using relations described in Section III and Appendix A. To compare with calibrated results, the following procedures were used to find  $f_I(i)$  at the water table. First,  $\mu_x$  and  $\sigma_x$  are calculated from field data. If appropriate,  $\sigma_x$  is then calibrated using the TFM. The parameters  $\mu$  and  $\sigma$  are calculated from  $\mu_x$  and  $\sigma_x$ . Then  $\mu$  and  $\sigma$  are scaled (multiplied by 2.66). These are the parameters for the normal model of mass transport. The scaled  $(\mu, \sigma)$  may then be transformed to  $(\mu_x, \sigma_x)$  yielding the log normal parameters. Table 5 contains the parameters used to generate Figures 48 through 52.

Table 5

	$\mu_x$	$\sigma_x$	$\mu$	$\sigma$	Figure
Infiltration Peaks	2.01	0.592	23.012	14.908	48
Infiltration Centroids	2.99	0.175	20.20	3.564	49
Infiltration Centroids Cal	2.99	0.7	25.426	20.21	50
Peaks in Time	5.809	0.374	357.33	138.46	51
Ergodicity	5.757	0.785	430.4	397.07	52

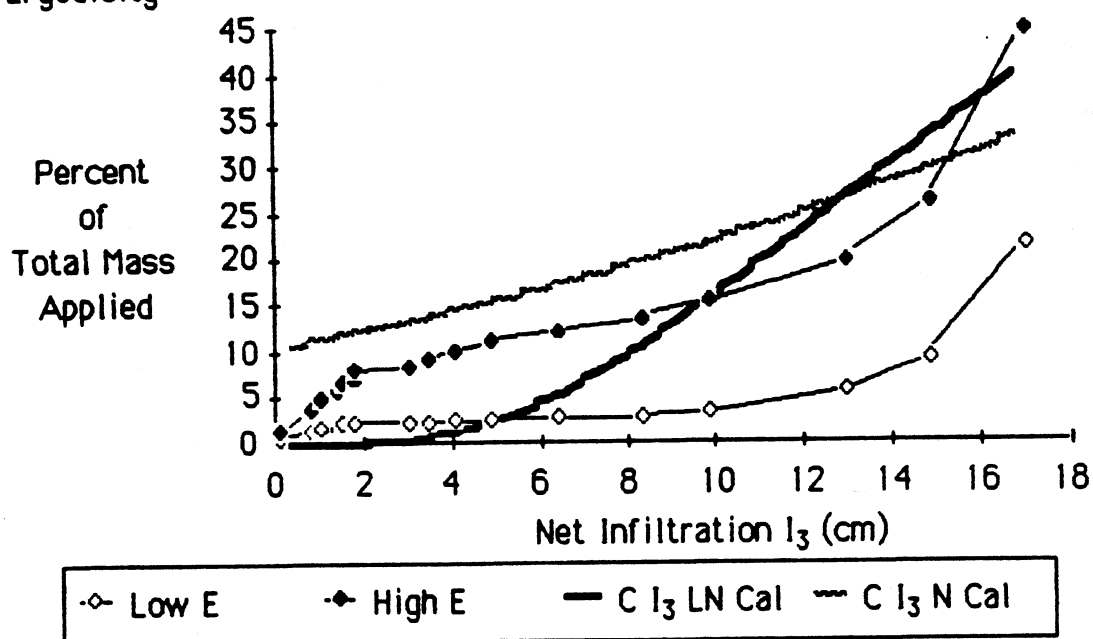


Figure 50. Estimates of the percent mass of bromide transported to the water table as a function of net infiltration. Low and High E are estimates from well samples surrounding the field. C  $I_3$  LN Cal is a prediction based on a log normal model of the net infiltration required to move the center of mass of the breakthrough curves to 3 feet calibrated using the TFM. C  $I_3$  N Cal is based on a normal model of the same data.

Among all the methods, infiltration using centroids provides the worst fit (Figure 49). This is probably because the variance is underestimated using this method. In comparison, adjusting the variance of  $f_1(i)$  using the TFM shown in Figure 50 provides a better fit but seems to overestimate the mass at the water table. Figure 50 also illustrates a major problem in using a normal model. Because the normal model allows finite probabilities for negative values, it may show misleading results for shallow aquifers with high variance of transport in the unsaturated zone. This is the cause of the jump in prediction to over 10% of the mass transported to the water table 5 days following tracer application.

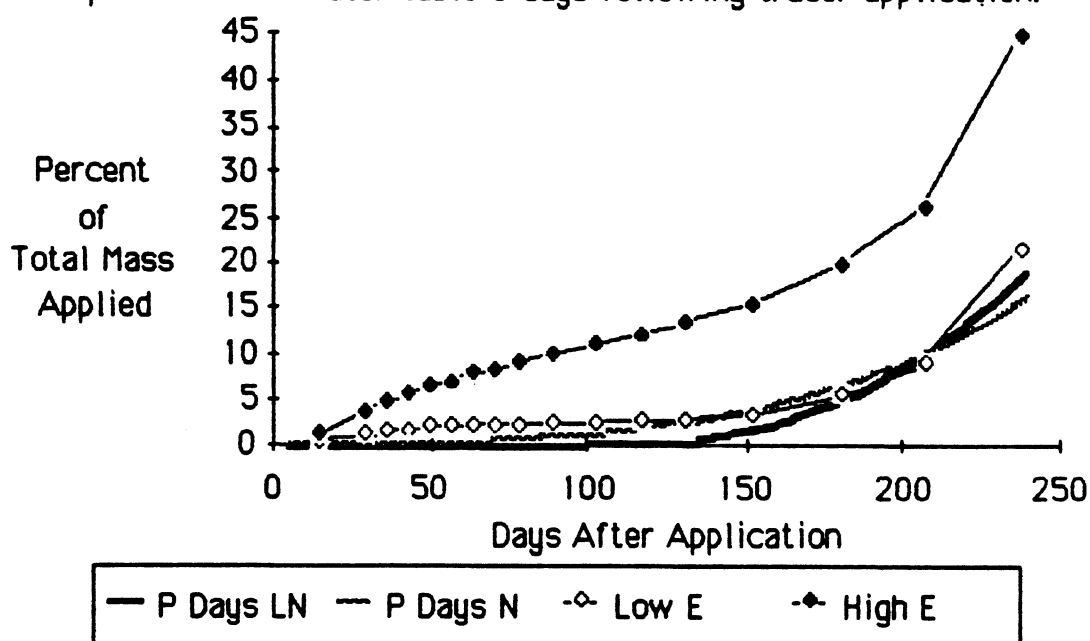


Figure 51. Estimates of the percent mass of bromide transported to the water table as a function of time. Low and High E are estimates from well samples surrounding the field. P Days LN is a prediction based on a log normal model of the days required to move the peak concentrations of bromide to 3 feet. P Days N is based on a normal model of the same data.

Figures 48, 51 and 52 all show reasonable fits to the field data. In all cases, the normal model seems to fit the data better. Because of the difficulty in defining appropriate net infiltration rates directly under the potato plants, it is particularly interesting to note that these data are not used in Figures 51 and 52. The very nice agreement shown in Figure 51 may be fortuitous given that the peak data that  $f_I(i)$  is calibrated with are dependent on sample intervals. Also, many of the breakthrough curves from which "peaks" were taken (Figure 36) show very flat responses. Thus, is it simply error in the system that dictates when these peaks occur? Generally, the normal model calibrated using the ergodic method seems to be most attractive. It provides a good prediction of these data and is derived from numerical methods which analyze the centroid and variance about the mean of the average breakthrough curve at 3 feet. The method does not reduce the input information (i.e. use just peaks or centroids of curves). It may therefore have a higher potential of characterizing the whole system.

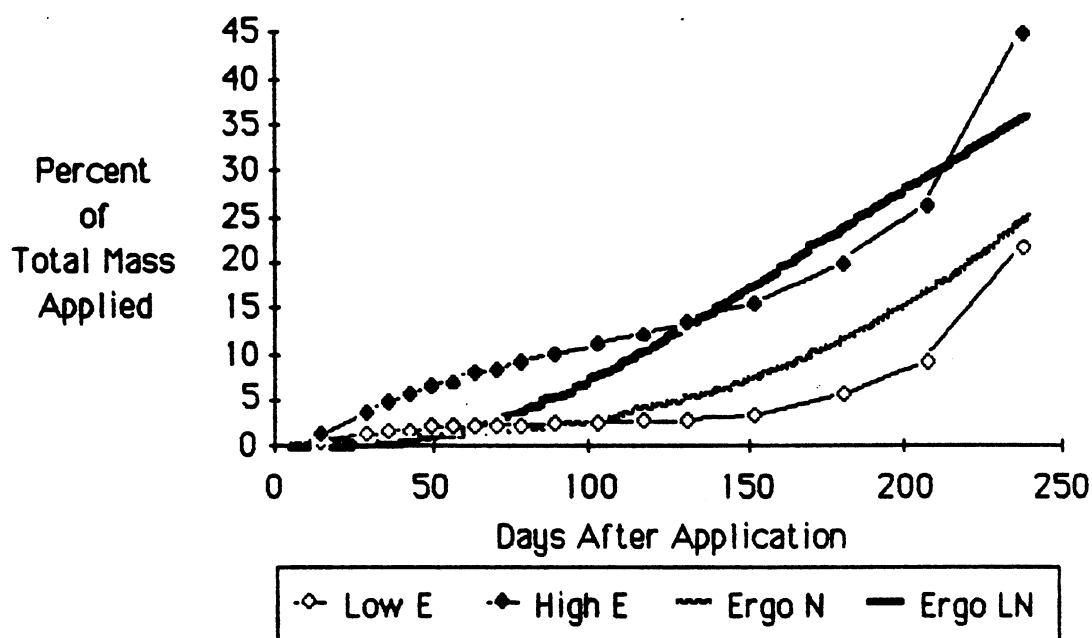


Figure 51. Estimates of the percent mass of bromide transported to the water table as a function of time. Low and High E are estimates from well samples surrounding the field. Ergo LN is a prediction based on a log normal model using the ergodic model described in the text. Ergo N is based on a normal model of the same data.

Figures 53-55 show the results of using the distribution of  $\theta$  in the unsaturated zone to predict the transport of tracer to the water table. Similar to the discussion above, normal and log normal models of  $\theta$  are compared. Five methods of calibrating  $f_{\theta}(\theta)$  are shown

- 1)  $\bar{\theta}$  =  $\theta$  averaged over a core (Figure 53);
- 2) %P200 averaged over a core (Figure 53);
- 3)  $\bar{\theta}$  calibrated using the TFM (Figure 54);
- 4)  $\theta$  in each sample (Figure 55); and

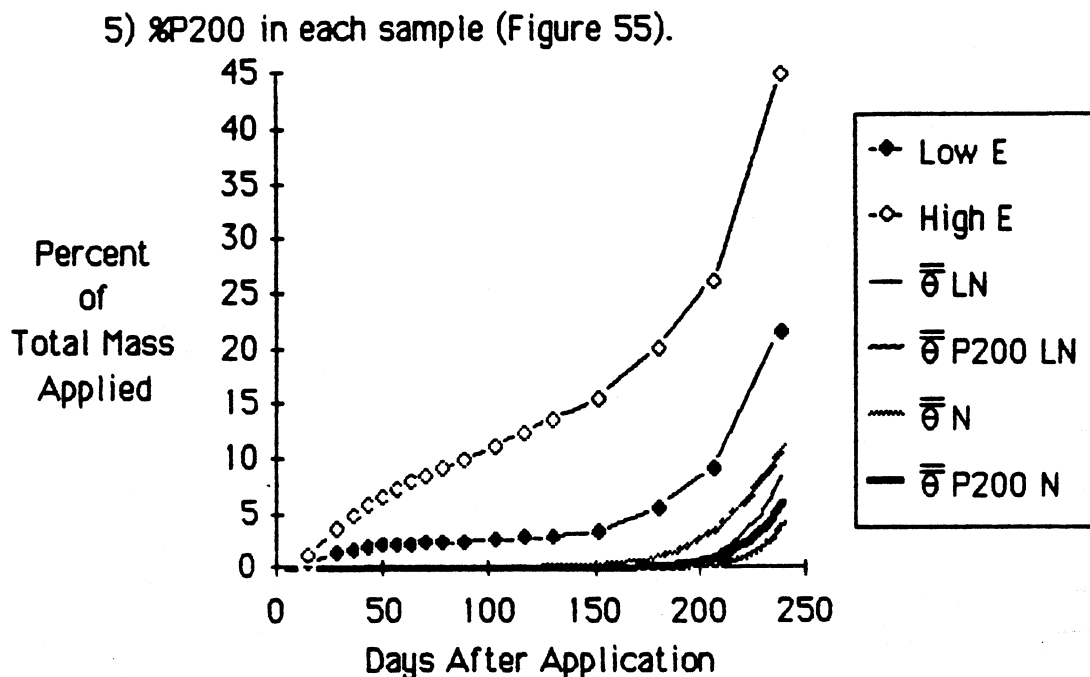


Figure 53. Estimates of the percent mass of bromide transported to the water table as a function of time. Low and High E are estimates from well samples surrounding the field.  $\bar{\theta}$  LN and  $\bar{\theta}$  P200 LN are estimates assuming a log normal model of the distribution of  $\bar{\theta}$  derived from average values of  $\theta$  from each core directly and from %P200 respectively.  $\bar{\theta}$  N and  $\bar{\theta}$  P200 N are predictions assuming a normal model of the same data.

All models operate similarly once they are calibrated. The average net infiltration (0.06993 cm/day) is used as before. The values of  $F_{\theta}(\theta)$  are found where  $\theta = \text{days after application} * (\text{net infiltration/day}) * 1/\text{depth to water table}$ . The method as described in Appendix A, is a simple extension of the plug flow concept. So that  $F_{\theta}(\theta)$  yields the percent of mass transmitted to the water table. In Figures 53-55,  $F_{\theta}(\theta)$  is graphed against the number of days after application.

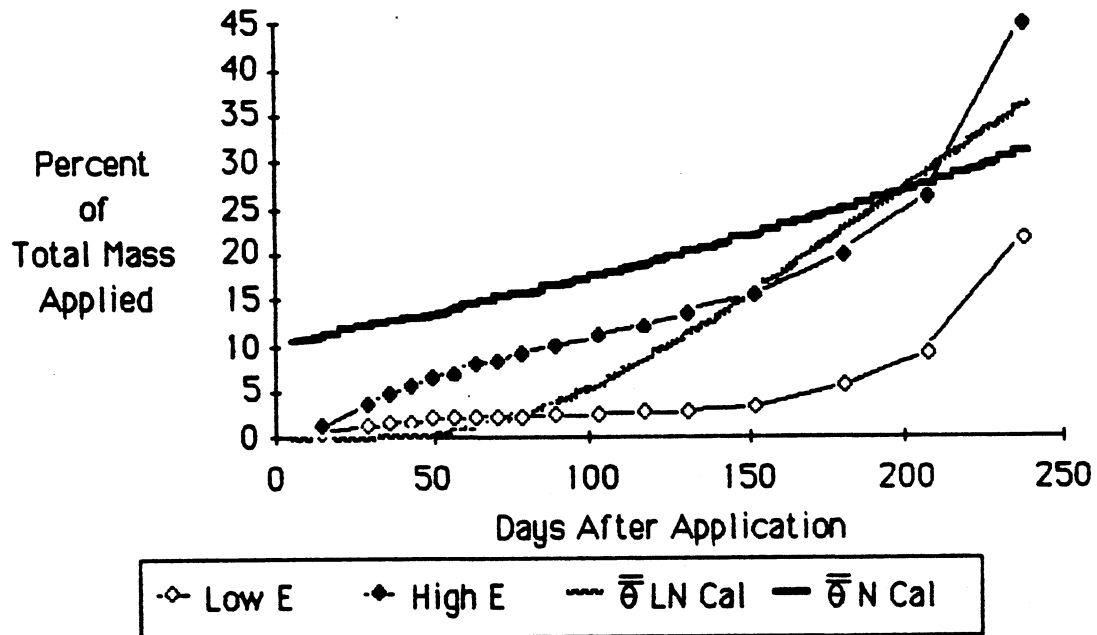


Figure 54. Estimates of the percent mass of bromide transported to the water table as a function of time. Low and High E are estimates from well samples surrounding the field.  $\bar{\theta}$  LN Cal is a prediction based upon a log normal model of  $\bar{\theta}$  calibrated using the TFM.  $\bar{\theta}$  N Cal is a prediction assuming a normal model of the same data.

Figure 53 shows that both log normal and normal models of  $\bar{\theta}$  underestimate the mass arriving at the water table. This is probably due to averaging  $\theta$  or  $\%P200$  in the entire core which results in an underestimate of the variance. As discussed earlier, the distribution of  $\%P200$  provides a very good approximation of  $f_{\theta}(\theta)$  using the regression relation developed in Appendix J.

Figure 53 shows that calibration of  $f_{\theta}(\theta)$  using the TFM somewhat improves estimates of mass transport. The normal model of  $\theta$  greatly overestimates transport close to time = 0. As mentioned above, this will

always be a problem with the normal model for shallow water tables and high variance of parameters.

One option explored in Figure 55 is to determine  $f_{\theta}(\theta)$  using all samples without averaging values for each core. This raises the calculated variance of  $f_{\theta}(\theta)$  and improves the fit to mass transport data. However, it is more difficult to rationalize this approach considering the physical model. Averaging values of  $\theta$  or  $\%P200$  over the cores causes reduction in variance due to the large scale of the cores compared to the scale of parallel tubes. The only argument for using each sample to estimate  $f_{\theta}(\theta)$  is that the scale of the sample is smaller than the scale of the core. Unfortunately, the reduction of scale occurs only in the length of the sample, not the width of the sample. This scale affects the measure of the vertical spatial heterogeneity rather than the desired horizontal variability. However, if the vertical heterogeneity is small and the packed tubes are not modelled as vertical but highly tortuous, which is closer to reality, then using each sample separately to define  $f_{\theta}(\theta)$  may be appropriate.



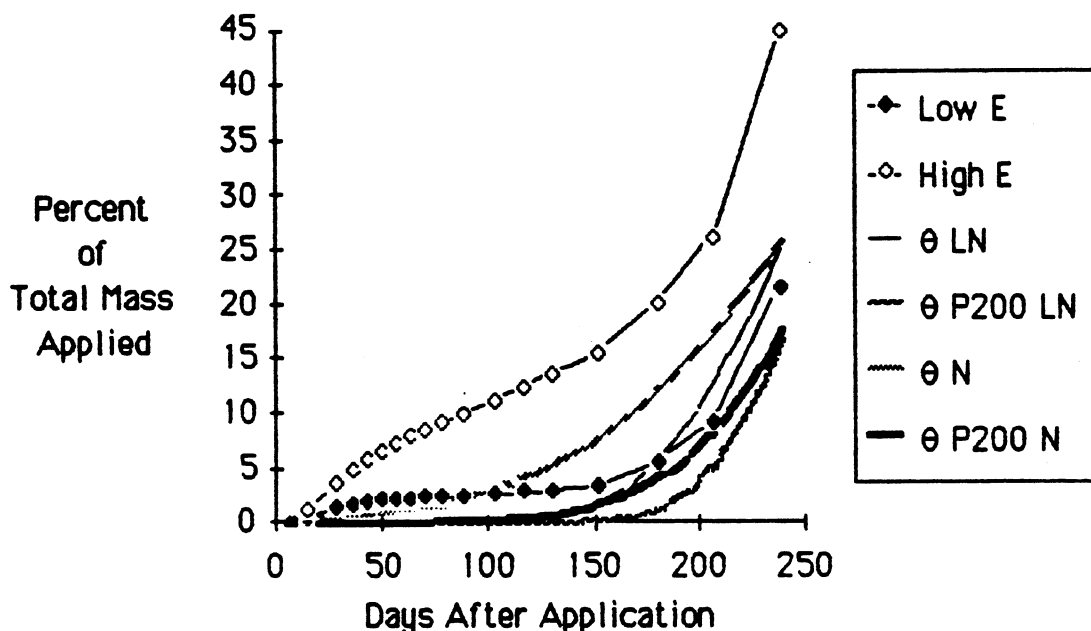


Figure 55. Estimates of the percent mass of bromide transported to the water table as a function of time. Low and High E are estimates from well samples surrounding the field.  $\theta$  LN and  $\theta$  P200 LN are estimates assuming a log normal model of the distribution of  $\theta$  derived from each sample directly and from %P200 respectively.  $\theta$  N and  $\theta$  P200 N are predictions assuming a normal model of the same data.

### Conclusions

Due to the small sample size of  $d$ ,  $\theta$  and  $i$ , it is difficult to determine whether a normal or log normal distribution of the variables is appropriate. The method used to characterize  $f_D(d)$  does not consider tracer lost out of the bottom of the core prior to sampling. It is also biased to finding  $d$  in the central third of the core. For these reasons, the distribution of  $D$  is poorly estimated.

Assuming log normality,  $f_I(i)$  determined from the center of mass of breakthrough curves generates a  $f_\Theta(\theta)$  that is almost identical to  $f_\Theta(\theta)$  generated from field data. This is evidence that the RPF model is modeling the system correctly.

The TFM is found to be a poor predictor of unsaturated zone breakthrough curves of bromide under hilled potatoes in Hancock, Wisconsin. This probably results because of transverse dispersivity and complex tracer transport arising from spatial variability in net infiltration and application of tracer strips along the hills.

The TFM was found to be useful in calibrating the variances of  $f_\Theta(\theta)$  and  $f_I(i)$  centroids. The calibration resulted in an increase of  $\sigma$  or  $\sigma_x$ . This is desirable because field methods of describing  $f_\Theta(\theta)$  and  $f_I(i)$  produce underestimates of the variance. The variance of  $\theta$ ,  $i$  or  $d$  might be better estimated if the scale of sampling is reduced. Averaging of the variable value in large samples causes a reduction in the estimate of variance.

The method to predict mass transported to the water table set forth in this thesis may be a useful tool. Normal distributions and distributions adjusted using the TFM show the best agreement with the percent of mass transported to the ground water determined using well samples. In particular, calibration of the model using the ergodic hypothesis in time, assuming a normal distribution, provided an adequate fit to field data. This procedure avoids the use of net infiltration which is difficult to obtain and minimizes the affects of sample intervals. The method will be used in the following experiment. A normal model allows finite

probability for negative values. For this reason a log normal model is recommended to simulate transport with high variability or transport to shallow water tables.

## V. Model Applications

### Prologue

The following three experiments were conducted at the Hancock Experimental Station in an area where the depth to ground water is approximately 18 feet. The purpose of including them in this thesis is to illustrate the utility of the proposed method in determining ground water pollution potential under a particular set of circumstances.

As discussed previously in Experiment 2, only the shapes of the breakthrough curves are required to calibrate the model. The tracer concentrations are given in dimensionless form so that shape may be more readily determined. Data in ppm Bromide are available in Appendix K. When curves from more than one depth are compared on a single graph, the series of concentrations from a particular sample at 3 feet are divided by the peak concentration in the series and concentrations at 6 feet are divided by twice the peak concentration. In all cases, the model is calibrated using the ergodic method on actual (non-dimensionless) data from the average breakthrough curve at 3 feet.

### Experiment 3

Hypothesis: Different methods of potato culture affect transmission rates of chemicals applied to the surface.

In this experiment, three different methods of potato culture are compared (Figure 56): (1) Bed cultivation; (2) Flat top hill cultivation

using 20 inch disks forming one foot high hills; and (3) Peaked hills using a Lilliston cultivator forming six to eight inch high hills. The evapotranspiration model is used to determine the irrigation schedules. Soil water samplers were installed in a 100' by 300' plot in triplicate at 3' and 6' depths directly under the plants in each method on May 20, 1985. At emergence, 1.66 molar potassium bromide was sprayed at 10 ml/ft in narrow strips which included the emerging potato plants. Where appropriate, potatoes were hilled immediately following tracer application. Both processes were accomplished in a single pass. Samples were taken at 1 week intervals from June 5 to August 17 and were taken at lengthening intervals through December. Samples were analyzed for bromide within 24 hours of sampling.

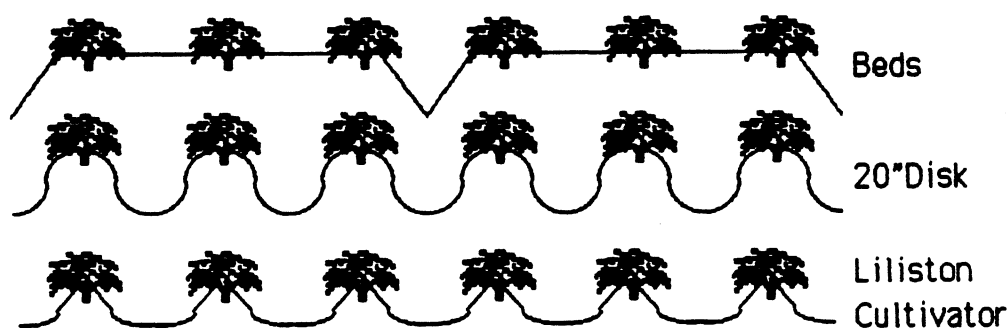


Figure 56. Surface morphology

Because of the difference in surface morphology, each cultivation may affect transport differently. Hills may confine potato roots and present more surface area to wind, causing them to dry out rapidly. This should reverse the direction of solution transport, bringing solute up to the surface. Also, hills rapidly shed excess water into the furrow which diminishes the amount of water leaching through the tracer band.

Graphs of the results will be discussed below for each treatment. Average breakthrough curves will then be compared for 3 and 6 feet. The ergodic methods illustrated in Experiment 2 using the average breakthrough curves from 3 feet will then be used to predict conservative mass transport to the water table.

### Results and Discussion

Figures 57 and 58 contain breakthrough curves from all three cultivation methods. Some samplers ceased working early in the experiment. All treatments, with the exception of bed cultivation, always had at least two soil water samplers operating at a single depth. Figures 57 and 58 show very similar breakthrough curves with higher variability at 3 feet than at 6 feet. Figure 59 shows the average breakthrough curve at 3 feet still rising at the end of the experiment. Due to the small sample size, caution must be taken when interpreting these results.

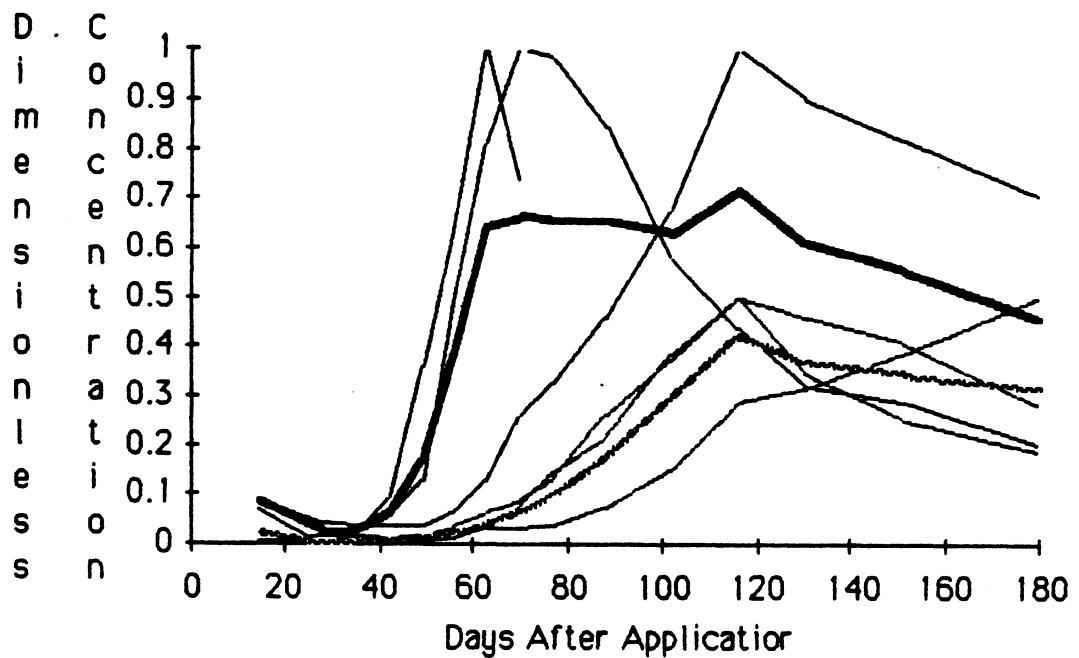


Figure 57. Results from the 20 inch disk treatment. Plain lines are results from 3 feet (concentration/ peak concentration). Dotted lines are results from soil water samplers at 6 feet ( $.5 \times$  concentration/ peak concentration). Thick lines are average breakthrough curves.

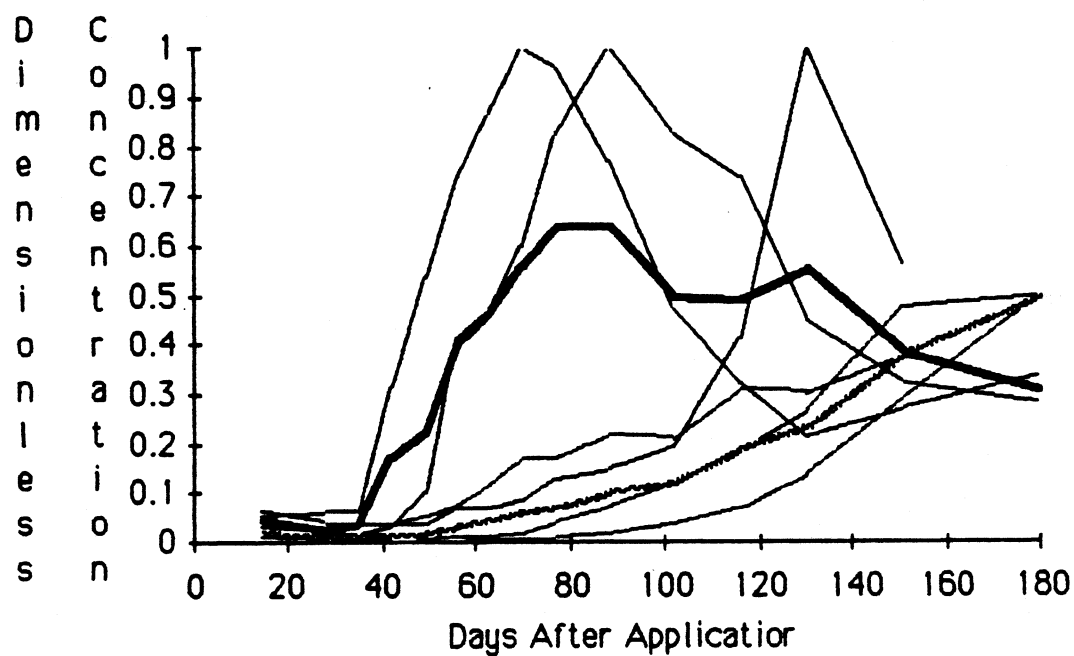


Figure 58. Results from the Lilliston cultivator plot. Plain lines are results from 3 feet (concentration/ peak concentration). Dotted lines are results from soil water samplers at 6 feet ( $.5 \times$  concentration/ peak concentration). Thick lines are average breakthrough curves.



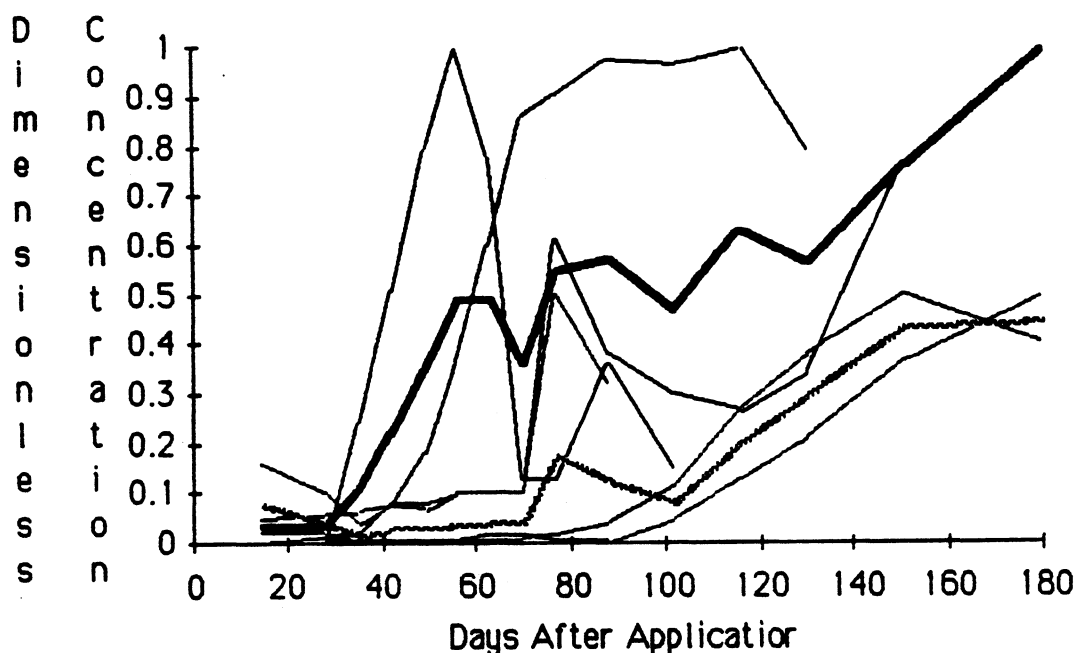


Figure 59. Results from bed cultivation. Plain lines are results from 3 feet (concentration/ peak concentration). Dotted lines are results from soil water samplers at 6 feet ( $.5 \times$  concentration/ peak concentration). Thick lines are average breakthrough curves.

Figures 60 and 61 compare the three breakthrough curves at 3 and 6 feet respectively. The slow transport under the bed cultivation method illustrated by Figure 60 does not seem to be supported by the data at 6 feet. Figure 61 shows that all traces look fairly similar at 6 feet with the possible exception that there is faster transport under the 20 inch disk plot. Many of the breakthrough curves at 6 feet were still rising at the end of the experiment which makes interpretation difficult.

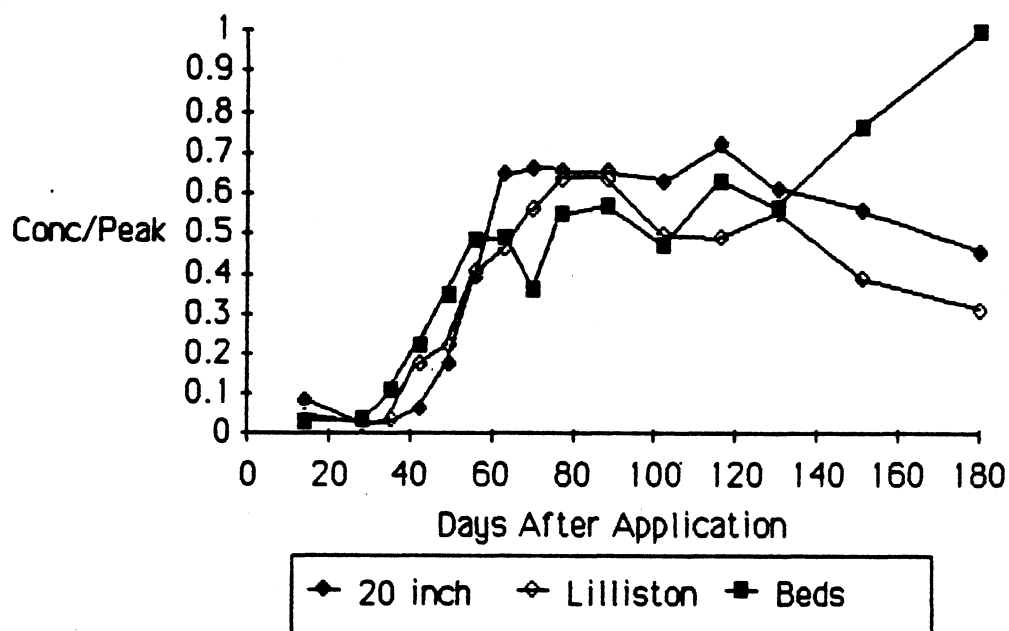


Figure 60. Comparison of average breakthrough curves from 3 feet using the ET irrigation program.

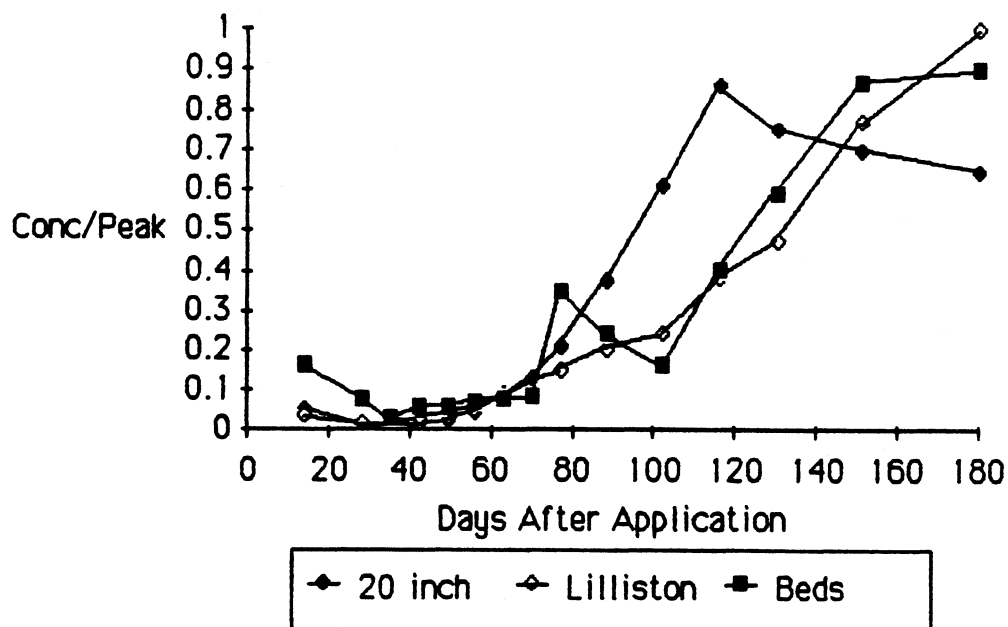


Figure 61. Comparison of average breakthrough curves from 3 feet using the ET irrigation program.

Figure 62 shows the prediction of mass transport to the water table for each of the treatments. The data used to generate the curves are in Appendix K. Since the predictions are based on breakthrough curves at 3 feet, it is not surprising that the bed cultivation method shows the least ground water pollution potential. For reasons discussed above this is probably a misleading result.

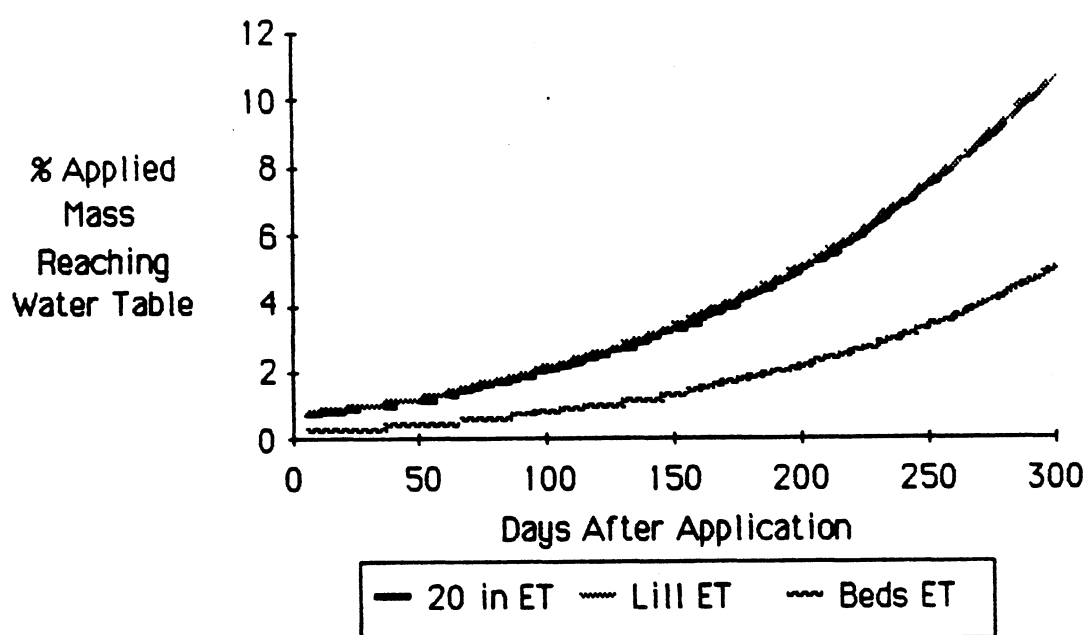


Figure 62. Comparison of transport of applied tracer to the water table predicted using the ergodic method on average breakthrough curves at 3 feet under the ET irrigation schedule.

## Conclusions

The large variability in results within treatments, conflicting results for various depths and failure of several samplers, combined to make the results of this study inconclusive. There certainly seems to be

no large difference in ground water pollution potential in the three methods tested.

#### Experiment 4

Hypothesis: Scheduling irrigation using an evapotranspiration program results in lower transmission rates of chemicals than applying 60% more water than the evapotranspiration program recommends.

Experiment 2 is duplicated in the same field with the exception that 60% more water is applied during irrigation. This experiment will allow quantification of the effects of over irrigation on both average and extreme rates of solute transport.

#### Results

Figures 63-65 show the breakthrough curves for the 20 inch disk, lilliston cultivator and bed cultivation treatment methods using the ET + 60 irrigation schedule. All three treatments show less variability in replicates and fewer sampler failures when more water is applied. At the higher irrigation level, the sources of spatial heterogeneity of bromide transport such as the variability in root density or small-scale variability in infiltration caused by stem flow, leaf drip, or micro-topography are probably swamped by the overabundance of water. This results in low spatial variability in breakthrough curves.

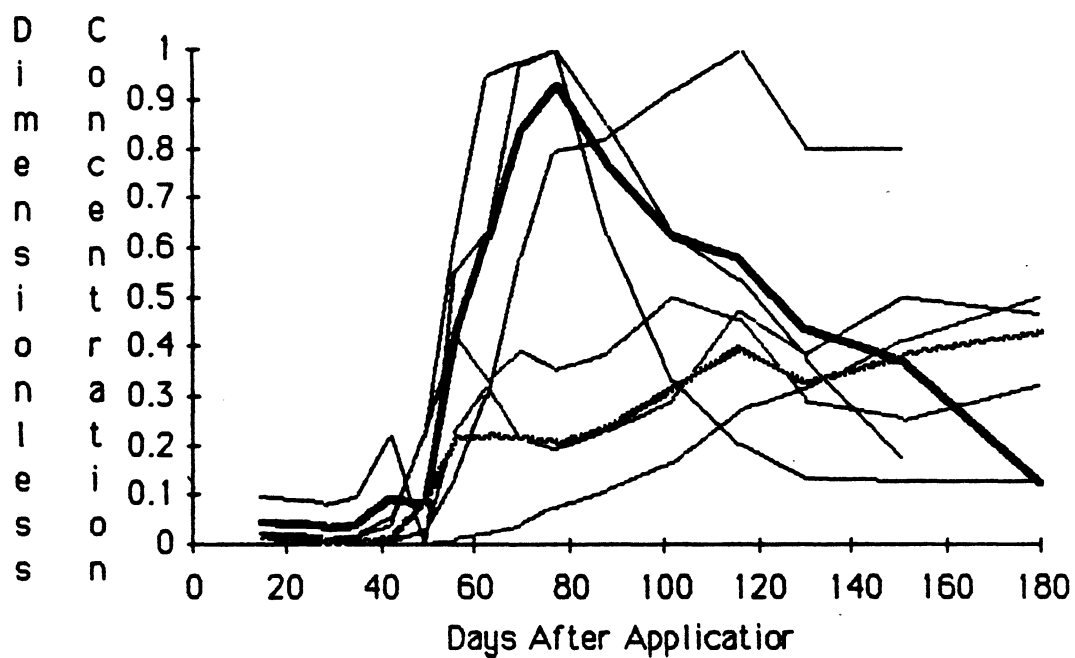


Figure 63. Results from the 20 inch disk treatment under the ET + 60 irrigation schedule. Plain lines are results from 3 feet (concentration/ peak concentration). Dotted lines are results from soil water samplers at 6 feet ( $.5 \times$  concentration/ peak concentration). Thick lines are average breakthrough curves.

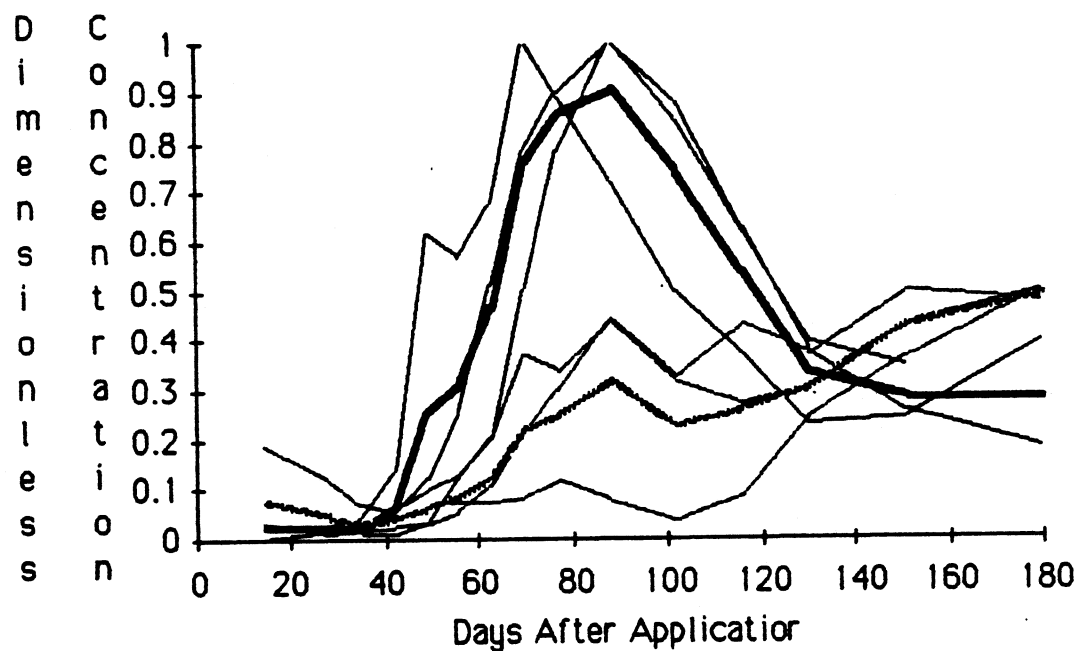


Figure 64. Results from the Lilliston cultivator plot under the ET + 60 irrigation schedule. Plain lines are results from 3 feet (concentration/ peak concentration). Dotted lines are results from soil water samplers at 6 feet ( $.5 \times$  concentration/ peak concentration). Thick lines are average breakthrough curves.

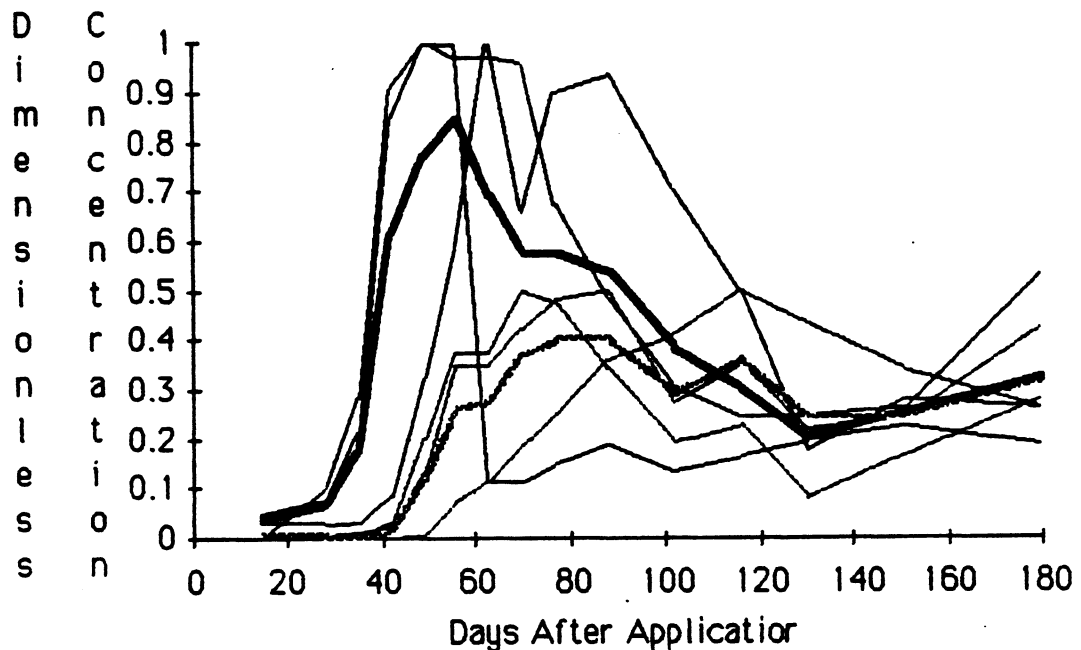


Figure 65. Results from the bed cultivation method. Plain lines are results from 3 feet ( concentration/ peak concentration). Dotted lines are results from soil water samplers at 6 feet (  $.5 \times$  concentration/ peak concentration). Thick lines are average breakthrough curves.

Figures 66-68 compare the average breakthrough curves from ET and ET + 60 irrigation plots for each treatment. The 20 inch disk and lilliston cultivator show little effect of increasing the irrigation 60% at both depths. This result is probably due to the fact that the hills shed most of the excess water. In contrast to these results, Figure 68 shows that 60% more irrigation greatly speeds up the breakthrough curves under the bed treatment at both depths. This seems to follow because the extra water does not drain off the beds but infiltrates through and carries the tracer downward at a more rapid rate. Figure 69 confirms the differences discussed above. Because the standard deviation is large and the mean is

close to zero, the normal model of mass transport to the water table shows an anomalously large jump to 2% five days after application of tracer. This problem with the normal model was discussed in Experiment 2.

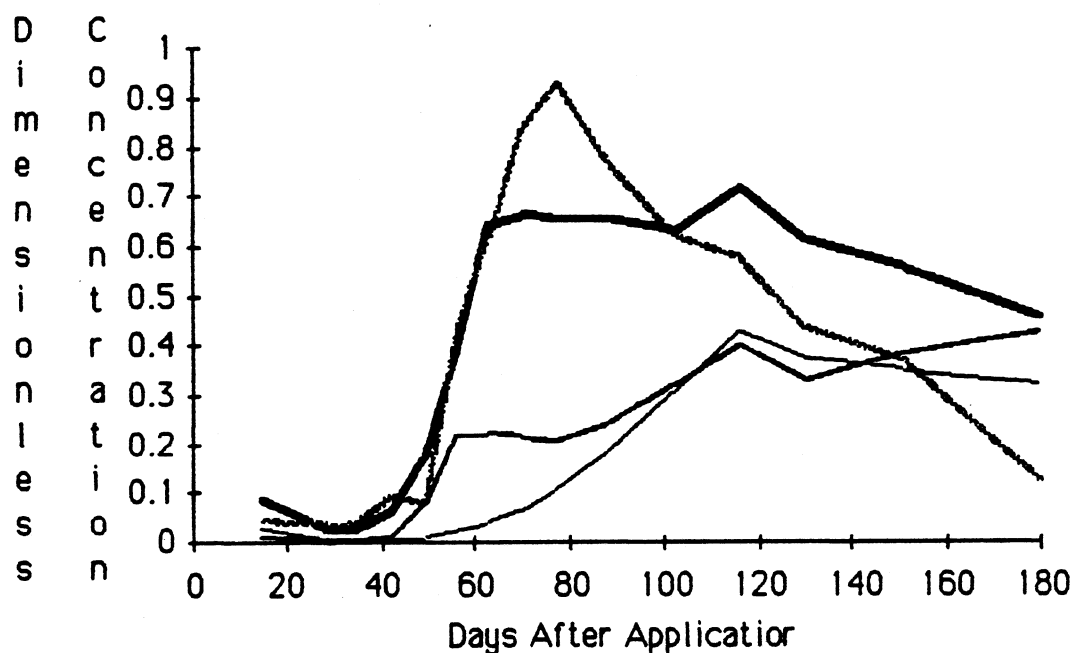


Figure 66. Comparison of average breakthrough curves from 3 (thick lines) and 6 feet (thin lines) between ET (solid lines) and ET + 60 (dotted lines) irrigation schedules using results from the 20 inch disk treatment.



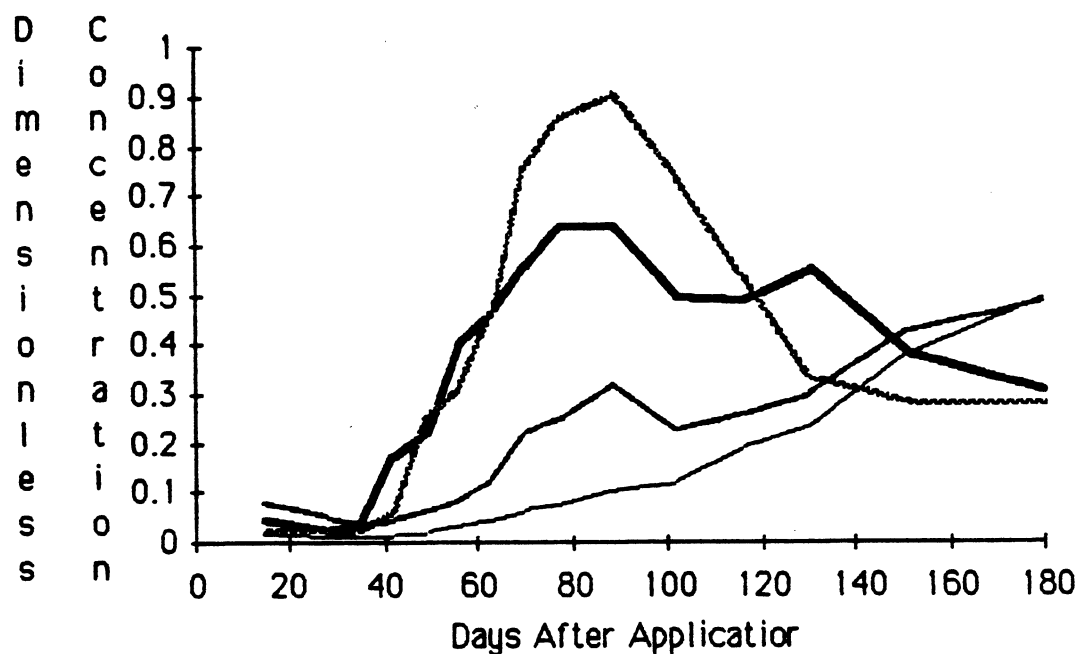


Figure 67. Comparison of average breakthrough curves from 3 (thick lines) and 6 feet (thin lines) between ET (solid lines) and ET + 60 (dotted lines) irrigation schedules using results from the Lilliston cultivator plot.

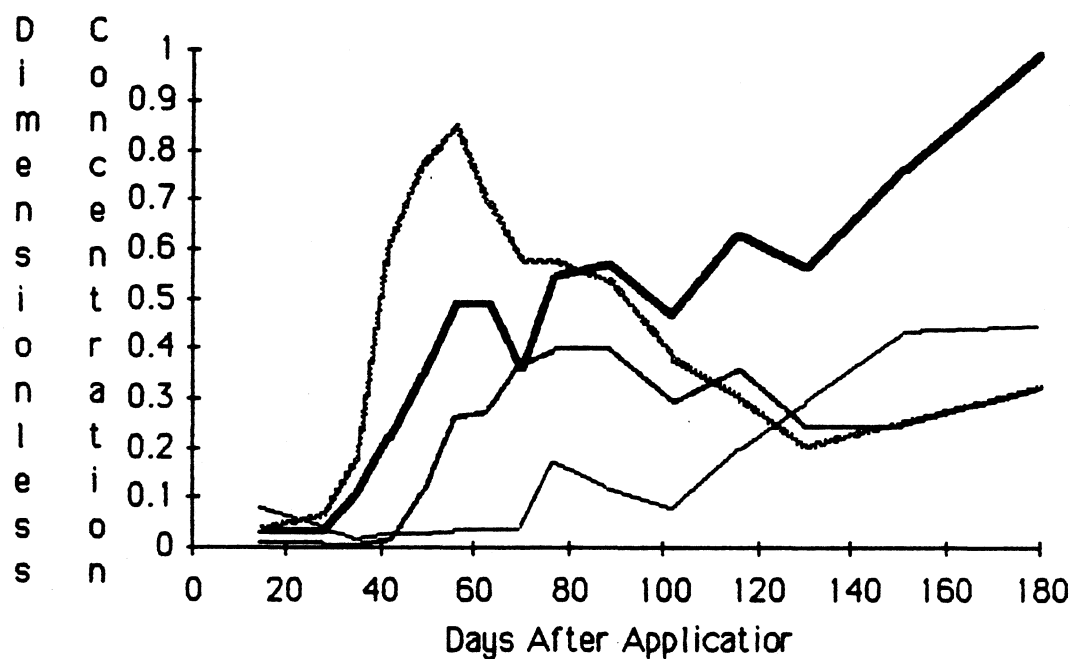


Figure 68. Comparison of average breakthrough curves from 3 (thick lines) and 6 feet (thin lines) between ET (solid lines) and ET + 60 (dotted lines) irrigation schedules using results from the bed cultivation method.

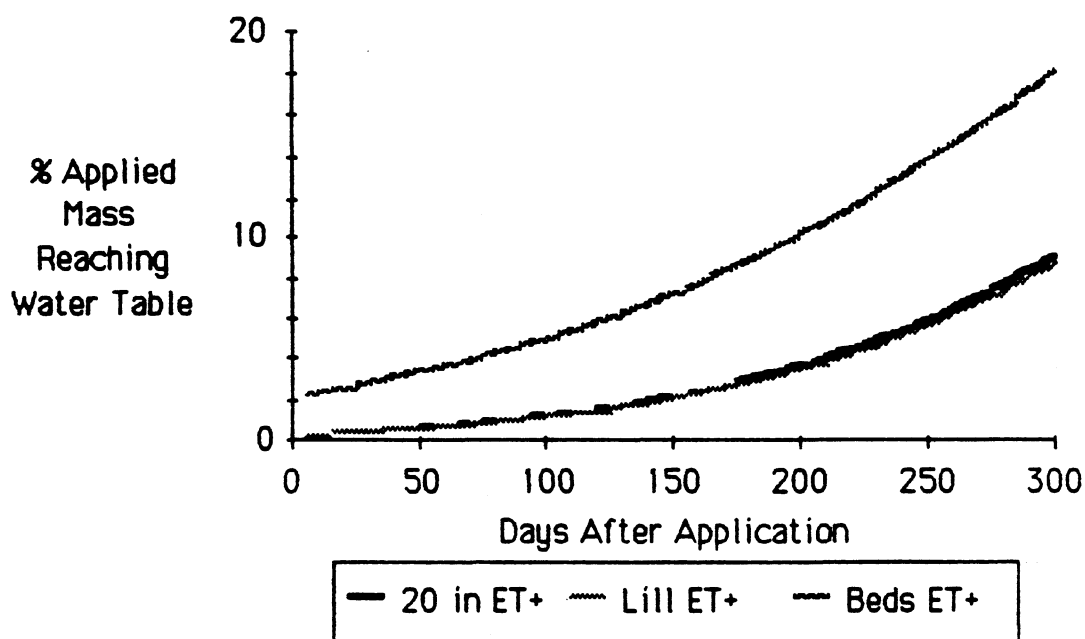


Figure 69. Comparison of transport of applied tracer to the water table predicted using the ergodic method on average breakthrough curves at 3 feet under the ET +60 irrigation schedule.

## Conclusions

Excess irrigation has little or no effect on the transport rates of tracer under the two hilled cultivation methods. In sharp contrast, transport rates under the bed cultivation method are much greater when more water is added. The percent of mass that reaches the water table after 100 days under the beds is more than four times greater than under the other treatments. Apparently, excess water runs off the hill treatments but infiltrates through the beds carrying tracer to depths at an accelerated rate.

## Experiment 5

Hypothesis: The morphology of a surface and placement of a tracer on the surface may significantly affect the rate of transmission of a tracer from the surface to the ground water.

In this experiment, hill cultivation formed using 20 inch disks was employed. Soil water samplers were installed in triplicate at 3 foot and 6 foot depths directly under the furrows in the field on May 20, 1985. At emergence, potassium bromide was sprayed in solution in a narrow strip along the bottom of the furrows at the same rate and concentration as in Experiments 2 and 3.

Samples were taken simultaneously with the other experiments. This experiment includes soil water samplers in the evapotranspiration and evapotranspiration plus 60% areas of the plot. The data generated are modeled and compared with those data showing the transmission rates under the hills in Experiments 2 and 3.

Saffignia et al. (1976) reported highly accelerated transport of rhodamine WT dye in furrows in the upper 0.5 m of soil adjacent to potato plants. The present work should quantify this effect and determine if the effect persists at greater depth. Work by Saffignia (1976), Yule (1976) and Gardner (1978) show that transverse dispersivity is very low in Plainfield sands. This low dispersivity may allow the maintenance of high velocity transport under furrows at depth.

## Results

Figures 70 and 71 show the breakthrough curves of bromide under the furrows with the ET and ET + 60 irrigation schedules, respectively. The replicates show very little variability, probably for the same reasons given in Experiment 4. Figure 72 shows the great difference in transport rates between the 20 inch disk plot and in-furrow application of tracer under the ET irrigation schedule.

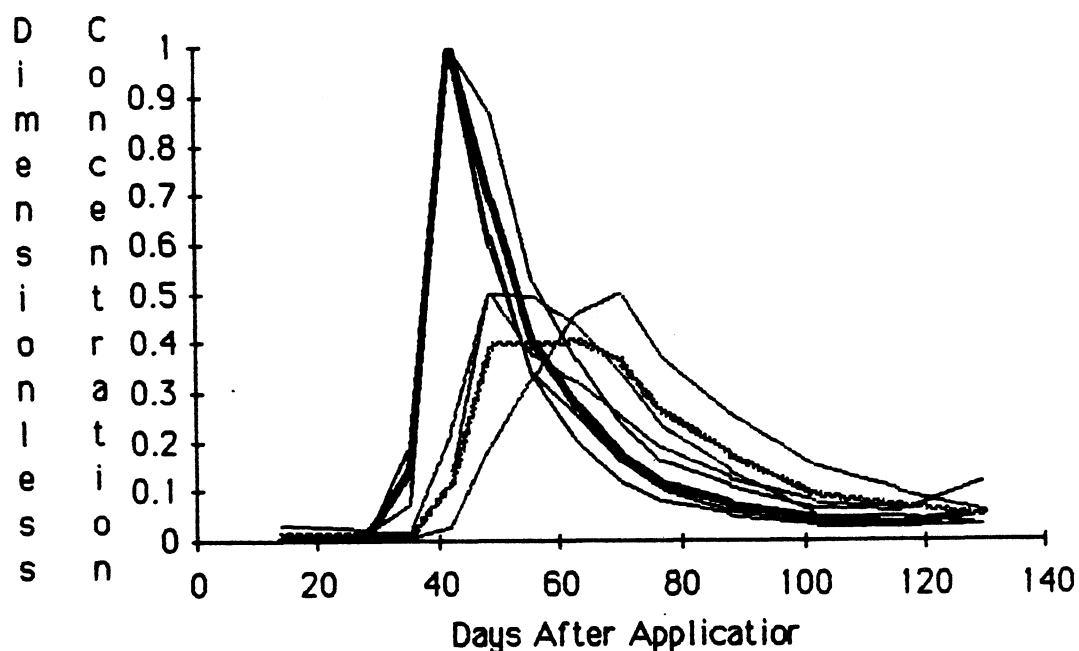


Figure 70. Results from the in furrow application of tracer under the ET irrigation schedule. Plain lines are results from 3 feet (concentration/ peak concentration). Dotted lines are results from soil water samplers at 6 feet ( $.5 \times$  concentration/ peak concentration). Thick lines are average breakthrough curves.

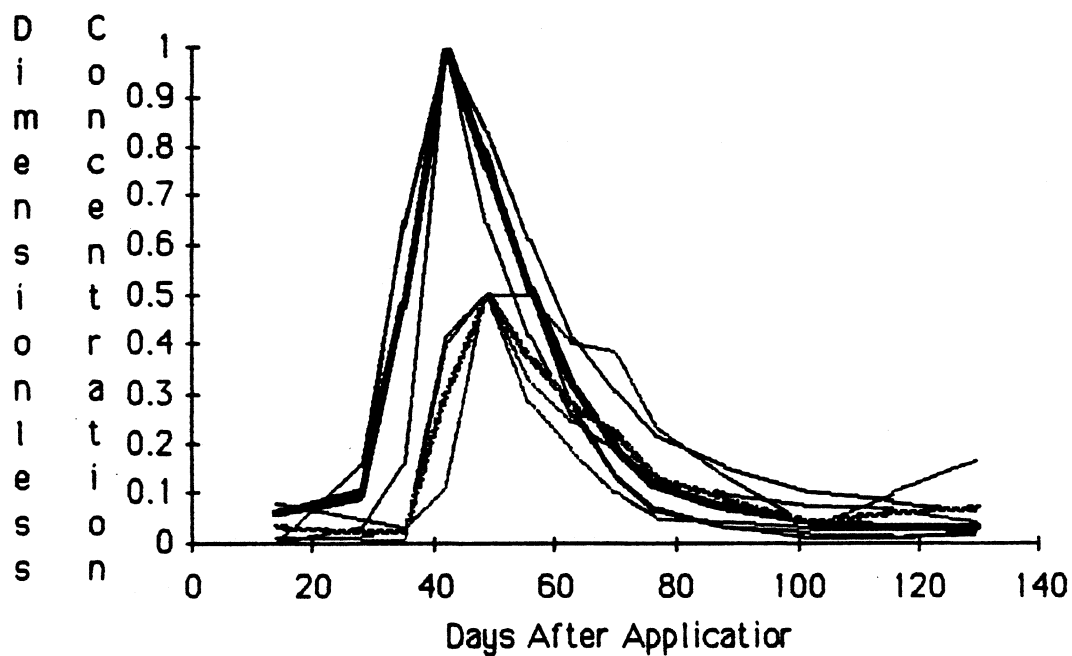


Figure 71. Results from the in furrow application of tracer under the ET + 60 irrigation schedule. Plain lines are results from 3 feet (concentration/ peak concentration). Dotted lines are results from soil water samplers at 6 feet ( $.5 \times$  concentration/ peak concentration). Thick lines are average breakthrough curves.

Table 5  
Centroids in Days at 3 feet

	<u>ET</u>	<u>ET + 60</u>
20 inch disk	101.9	99.05
Lilliston Cultivator	102.8	100.4
Beds	123.1	91.36
In-furrow	52.95	48.36

Table 5 shows the centroids of all three breakthrough curves. It is clear that the greatest decrease in time to the centroid of the tracer is caused by in-furrow application. This is probably due to the occurrence of higher net infiltration in the furrow caused by runoff and lower ET as discussed previously. Figure 73 compares average breakthrough curves under the in-furrow tracer application for ET and ET + 60 irrigation. It is curious that there is no apparent affect at 3 feet. This may be an artifact of the field method employed. Only two samples were taken prior to the occurrence of the peak concentration at 3 feet. The first two samples were taken at two week intervals. Subsequent samples were taken at one week intervals. Each sample represents an average concentration over the sample interval. Thus, separating the time between peaks at 3 feet is difficult. At 6 feet, centroids of 68 and 58 days were found for breakthrough curves under ET and ET + 60 respectively.

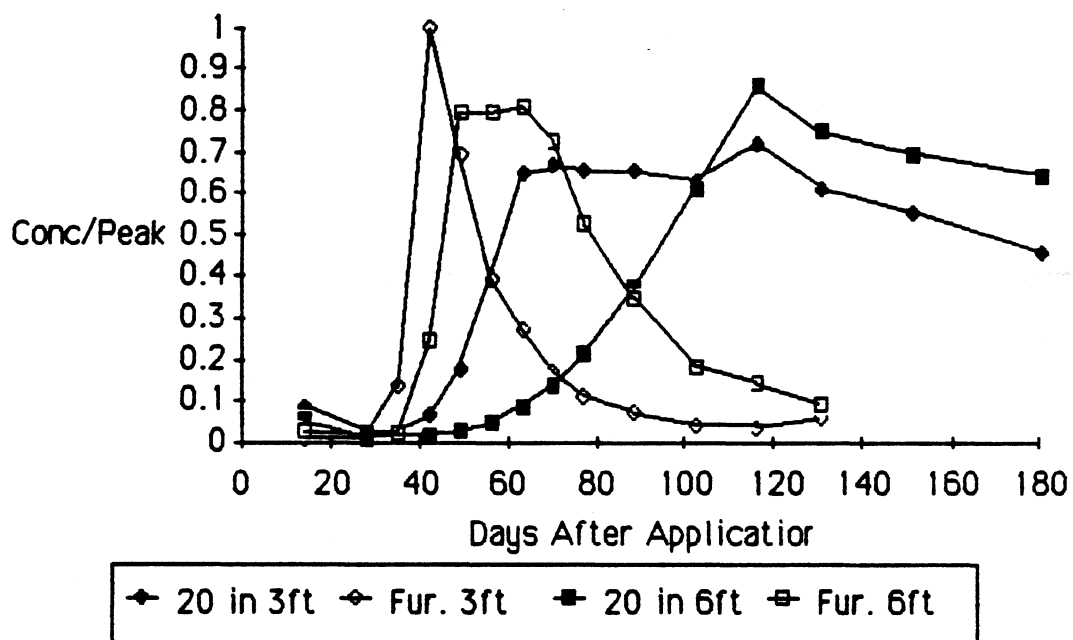


Figure 72. Comparison of average breakthrough curves between 20 inch disc and in furrow application of tracer under the ET irrigation schedule.



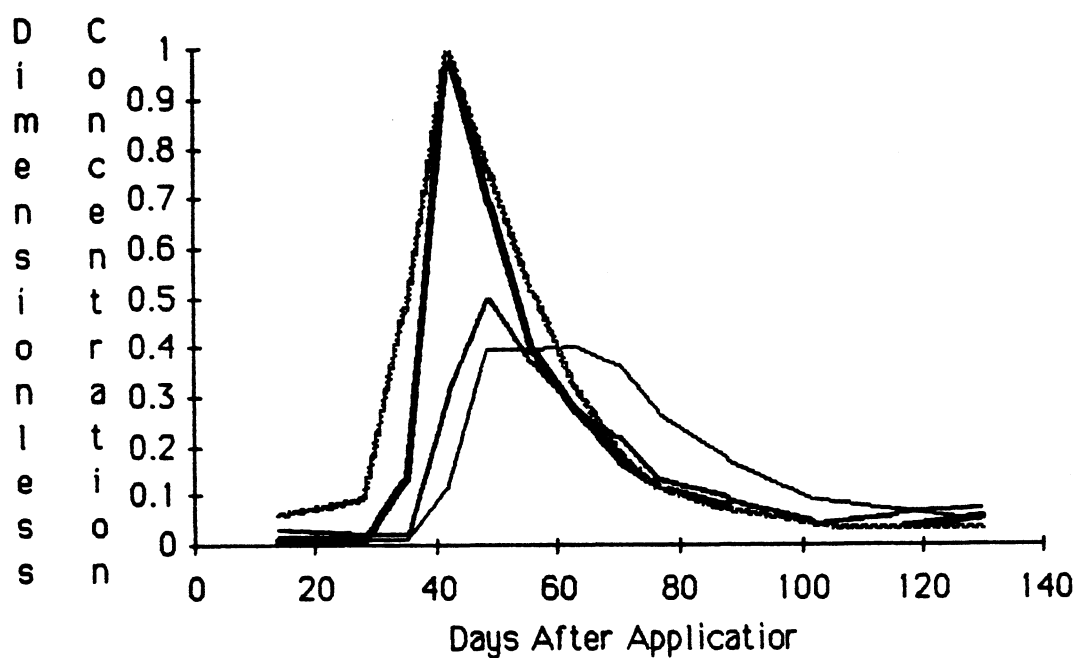


Figure 73. Comparison of average breakthrough curves from in furrow application of tracer between the ET (solid lines) and ET +60 (dotted lines) irrigation schedule. Concentrations at 3 and 6 feet are presented as before.

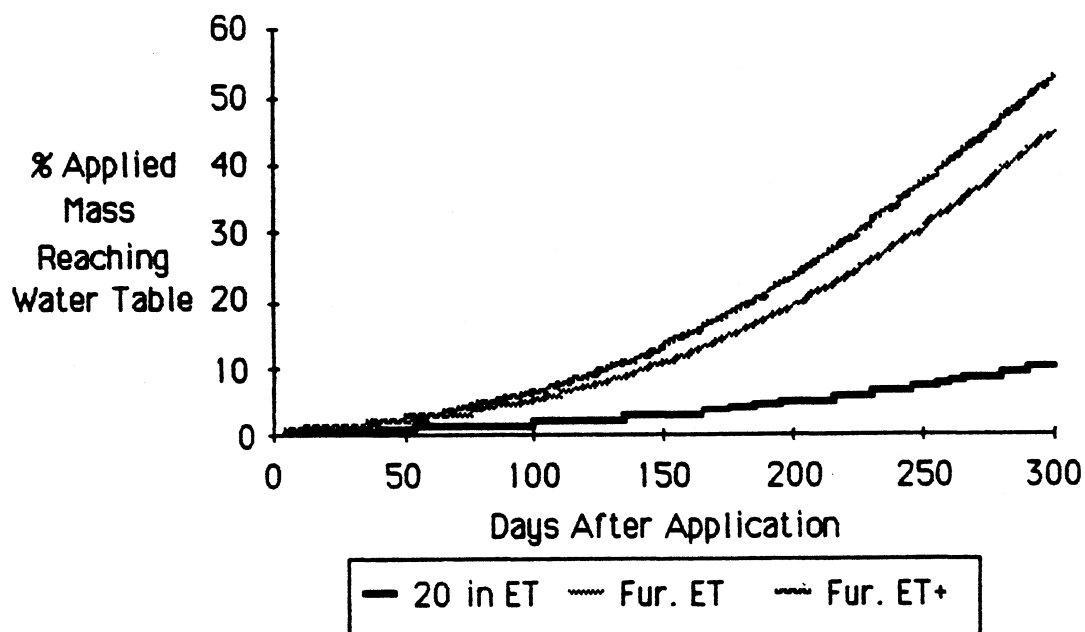


Figure 74. Comparison of transport of applied tracer to the water table predicted using the ergodic method on average breakthrough curves at 3 feet under the ET +60 irrigation schedule.

Figure 74 compares the predicted mass reaching the water table of in-furrow application with the 20 inch disk treatment. At 150 days following application of the tracer, three times more mass is predicted to have contacted the water table under the furrow ET treatment than under the 20 inch disk ET treatment.

## Conclusions

Comparing Figures 62, 69 and 74, it is clear that in-furrow placement of tracer causes the greatest ground water pollution potential. This is probably due to runoff from the hills causing increased gross precipitation as well as lower root density, shading, and wind protection and therefore lowering evapotranspiration losses.

## VI. Summary of Conclusions

The purpose of experiment 1 is to compare the transport of the pesticide aldicarb to potassium bromide through the unsaturated zone and into the ground water. In addition, Experiment 1 is a preliminary experiment, testing methods that were used in following experiments. The conclusions from Experiment 1 affected the design and analysis of following experiments. The variance in the transport found between aldicarb and bromide in Plainfield sandy loam is small enough to justify using bromide as a tracer for Aldicarb in the unsaturated zone. To predict groundwater contamination using bromide (or aldicarb) data from the unsaturated zone, is not straightfoward. The surface of the groundwater collects contaminant as it travels at different rates through the unsaturated zone beneath a field. Since aldicarb degrades, rapid movement (i.e. low probability transfer events) are much more important in determining ground water pollution potential than the average rate of transport beneath a field.

The total mass data show the transport of bromide under the field is greatly affected by transverse dispersivity. This complicates the interpretation of the breakthrough curves under the hills. Tracer traveling vertically down under the hills is also dispersed horizontally. There may be a "fast lane" under the furrows which more rapidly transports the dispersed tracer to the ground water. In such a case, using an uncalibrated  $f_1(i)$  to estimate the quantity of mass transported to the ground water will result in underestimates. This situation will be tested in the following experiment.

The TFM is robust in that it calibrates and verifies well using different estimates of  $I$ . In the following experiments,  $I_3$  will be used exclusively.  $I_3$  is the most accurate estimate of  $I$ . In particular, it is the only estimate which includes ET for late September, October and November. These months are important in the following experiments. Using average weighing lysimeter data to make the estimates of ET may lead to significant errors in any given year. However, some estimate of ET is better than none.

The use of ergodicity to calibrate the TFM worked well, using the time series from a single sampler at 3 feet. Because all of the breakthrough curves are similar at 3 feet, this method appears promising. In the following experiment it will be used on the average breakthrough curve at 3 feet.

The purpose of Experiment 2 is to test predictions of bromide transport to the water table and the assumptions of the Randomized Plug Flow (RPF) model. Due to the small sample size of  $d$ ,  $\theta$  and  $i$ , it is difficult to determine whether a normal or log normal distribution of the variables is appropriate. The method used to characterize  $f_D(d)$  does not consider tracer lost out of the bottom of the core prior to sampling. It is also biased to finding  $d$  in the central third of the core. For these reasons, the distribution of  $D$  is probably poorly estimated.

Assuming log normality,  $f_I(i)$  determined from the center of mass of breakthrough curves generates a  $f_\theta(\theta)$  that is almost identical to  $f_\theta(\theta)$  generated from field data. This is evidence that the RPF model is modeling the system correctly.

The TFM is a poor predictor of unsaturated zone breakthrough curves of bromide under hilled potatoes in Hancock, Wisconsin. This probably results because of transverse dispersivity and complex tracer transport arising from spatial variability in net infiltration and application of tracer strips along the hills.

The TFM was found to be useful in calibrating the variances of  $f_{\theta}(\theta)$  and  $f_I(i)$ . The calibration resulted in an increase of  $\sigma$  or  $\sigma_x$ . This is desirable because field methods of describing  $f_{\theta}(\theta)$  and  $f_I(i)$  produce underestimates of the variance. The variance of  $\theta$ ,  $i$  or  $d$  might be better estimated if the scale of sampling is reduced. Averaging of the variable value in large samples causes a reduction in the estimate of variance.

The method to predict mass transported to the water table set forth in this thesis may be a useful tool. Normal distributions and distributions adjusted using the TFM show the best agreement with the percent of mass transported to the ground water determined using well samples. In particular, calibration of the model using the ergodic hypothesis in time, assuming a normal distribution, provided an adequate fit to field data. This procedure avoids the use of net infiltration which is difficult to obtain and minimizes the affects of sample intervals. A normal model allows finite probability for negative values. For this reason a log normal model is recommended to simulate transport with high variability or transport to shallow water tables.

The purpose of Experiments 3, 4 and 5 are to show the utility of the proposed method in determining ground water pollution potential under a particular set of circumstances. Experiment 3 compares mass transport

to the ground water under 3 methods of potato cultivation, 20 inch disk hills, Lilliston cultivator hills and bed cultivation. Results are inconclusive due to large natural variability and problems with sample apparatus. Experiment 4 compares the effects of over irrigation on the three methods of potato cultivation. Transport under the hill treatments which apparently shed the excess water is not affected by 60% more irrigation. In contrast, over irrigation causes 200% more mass to be predicted to reach the water table under the bed cultivation method within 300 days of tracer application. Experiment 5 compares in furrow placement of tracer to tracer incorporated into hills. Five hundred percent more mass is predicted to reach the water table within 300 days after application of bromide in the furrow.

The RPF model may be calibrated using estimates of readily obtained parameters. It will probably provide good estimates of conservative mass transport to ground water in sandy soils.

## VII. Comments and Recommendations for Further Work

The method to predict conservative mass transport to the water table outlined in this thesis is, apparently new and original. Consequently it will require further examination and change as it becomes mature. The purpose of this section is to point out portions of the method that need further work.

The weakest part of this work is the necessity of calculating and adjusting the net infiltration directly under the potato hills. In addition, increased net infiltration in the furrows, combined with transverse dispersion of tracer, creates a complex flow system. These three factors resulted in the failure of the TFM to calibrate or verify breakthrough curves in the unsaturated zone. However, predictions of mass transport using the "heart" of the TFM model (scaling by  $d_c/Z$ ) provided surprisingly accurate results. Although this method seems to be robust, more attention should be paid to the actual flow system being modeled. In particular, good estimates of infiltration where the substance of interest is placed, are required throughout the study.

The general problem of sample scale should be approached in a future study. Sample intervals at soil water samplers of one week or less should be used at the beginning of any experiment until a "feel" for the rate of movement is developed. Important data may have been lost in several experiments because of initial sample intervals that were too long. The scale of samples should also be considered when calculating

$f(\theta)$ . Relatively small samples of 150 to 200 grams should be collected in such a way that the bulk density of each sample can be found. If there is no pronounced vertical structure, use all samples to determine  $f(\theta)$ . Otherwise use  $\bar{\theta}$  to determine  $f(\theta)$ .

In general, more replicates should be used to include all the natural variability in the field. This seems to be particularly important in drier treatments since these show greater variability in transport. In Experiments 2 through 5 quality may have been traded for quantity. Having fewer replicates made more experiments possible but may have decreased the quality of the results from each experiment. Along these same lines, more time could have been invested to understand the ground water flow patterns under the plot in Experiment 2. However, this added effort (i.e. pump test, more frequent monitoring of the heads) would have compromised some other effort.

#### Enhancements to the Model

Vertical structure may be added to the model. The scale  $d_c/2$  suggested by Jury (1982) and used in this thesis is consistent with a homogeneous profile. Other scales might be used to represent changes in parameters with depth.

The method presented here is limited to predicting transport of conservative solutes. However, it should be fairly straightforward to introduce a retardation factor into the RPF model. The same approach that Rao et al. (1976) proposed, discussed on page 17 should work well. Assuming a pulse input of substance, a first order decay term could be



introduced into the model by multiplying  $e^{-kt}$  by  $f(i)$  or  $f(\theta)$  prior to integration.

The method is very promising. Nevertheless there is plenty of work still to be done in extending the ideas put forth in this thesis.

## VIII. Appendices

### Appendix A

#### Solutions to the TFM and Predictions of Mass Transported to the Water Table

#### Solutions to the TFM

##### Solution using $f_1(i)$

There is a way to represent  $C(i_C, z)$  using error functions which is more convenient for calculation. Consider  $F_1(i_C d_C/z)$  in equation (10).

$$F_1(i_C d_C/z) = \int_0^{i_C} \frac{z}{i d_C \sigma_x \sqrt{2\pi}} \exp - \left[ \frac{\ln(i d_C/z) - \mu_x}{\sqrt{2} \sigma_x} \right] di$$

Let

$$t = \frac{\ln(i d_C/z) - \mu_x}{\sqrt{2} \sigma_x} \quad \text{Then } dt/di = 1/(i\sqrt{2} \sigma_x), \text{ and}$$

$$\begin{aligned} F_1(i_C d_C/z) &= \int_{-\infty}^t \pi^{-.5} e^{-t^2} dt = \int_0^t \pi^{-.5} e^{-t^2} dt - \int_0^{-\infty} \pi^{-.5} e^{-t^2} dt \\ &= .5 \operatorname{erf} t - .5 \end{aligned}$$

Similarly

$$F_1((i_C d_C/z) - (\Delta i_C d_C/z)) = .5 \operatorname{erf} t' - .5$$

Where

$$t' = \frac{\ln((i_c - \Delta i_c) d_c / z) - \mu_x}{\sqrt{2} \sigma_x}$$

Thus the solution to equation (10) can be written

$$C(i_c, z) = \frac{C_0}{2} \left[ \operatorname{erf} \left[ \frac{\ln(i_c d_c / z) - \mu_x}{\sqrt{2} \sigma_x} \right] - \operatorname{erf} \left[ \frac{\ln((i_c - \Delta i_c) d_c / z) - \mu_x}{\sqrt{2} \sigma_x} \right] \right]$$

#### Solution using $f_{\Theta}(\theta)$

Consider  $f_I(i) = (1/d_c) F_{\Theta}(i/d_c)$  from equation 5.

Then

$$F_I(i_c) = \int_0^{i_c} f_I(i) di = 1/d_c \int_0^{i_c} f_{\Theta}(i/d_c) di$$

and

$$F_I(i_c d_c / z) = 1/z \int_0^{i_c} f_{\Theta}(i/z) di$$

This may be expressed in terms of error functions using the method outlined above with

$$t = \frac{\ln(i/z) - \mu_x}{\sqrt{2} \sigma_x} \quad \text{and,} \quad t' = \frac{\ln((i_c - \Delta i_c)/z) - \mu_x}{\sqrt{2} \sigma_x}$$

Solution using  $f_D(d)$

Consider  $f_I(i) = (1/\theta_C) F_D(i/\theta_C)$  from equation 6 where  $\theta_C$  is the average volumetric moisture content in the field.

Then

$$F_I(i_C) = \int_0^{i_C} f_I(i) di = 1/\theta_C \int_0^{i_C} f_D(i/\theta_C) di$$

and

$$F_I(i_C d_C/z) = d_C/z\theta_C \int_0^{i_C} f_D(id_C/z\theta_C) di$$

where  $d_C$  is defined as  $l_C/\theta_C$  and  $l_C$  is the total net infiltration which has occurred between tracer application and core sampling so that

$$F_I(i_C d_C/z) = l_C/z\theta_C^2 \int_0^{i_C} f_D(il_C/z\theta_C^2) di$$

This may be expressed in terms of error functions using the method outlined above with

$$t = \frac{\ln(il_C/z\theta_C^2) - \mu_X}{\sqrt{2} \sigma_X} \quad \text{and,} \quad t' = \frac{\ln((l_C - \Delta l_C)l_C/z\theta_C^2) - \mu_X}{\sqrt{2} \sigma_X}$$

## Predictions of Mass Transported to the Water Table

### Solution Using $f_I(i)$

The probability density function (PDF) of  $I$ ,  $f_I(i)$  is calibrated at some depth  $d_C$  with parameters  $\mu_X$  and  $\sigma_X$  where  $x = \ln(i)$ , and the cumulative distribution function (CDF) of  $I$  is defined as  $F_I(i)$ .

Using

$$\begin{aligned}\mu_I &= \exp(\mu_X + 0.5\sigma_X^2) \\ \sigma_I^2 &= \mu_X^2 (\exp(\sigma_X^2) - 1)\end{aligned}$$

find  $\mu_I$  and  $\sigma_I$ . These parameters scale by  $z/d_C$ . Where  $z$  is the depth to the water table.

$$\begin{aligned}\mu_{IZ} &= (z/d_C) \mu_I \\ \sigma_{IZ} &= (z/d_C) \sigma_I.\end{aligned}$$

Percent mass to the water table may be evaluated using  $\mu_{IL}$  and  $\sigma_{IL}$  assuming a normal distribution by evaluating

$$F_I(i) \approx N(\mu_{IZ}, \sigma_{IZ}).$$

$\mu_I$  and  $\sigma_I$  may be found directly from the data collected at depth  $d_C$ .

However, to allow for straightforward comparison to TFM calibrated distributions (where only  $\mu_X$  and  $\sigma_X$  are available), the method above was always followed in this thesis.

Percent mass to the water table may be evaluated assuming a log normal distribution by evaluating

$$F_I(i) \approx \text{LN}(\mu_{XZ}, \sigma_{XZ}).$$

#### Solution Using $f_\Theta(\theta)$

$f_\Theta(\theta)$  is calibrated using volumetric moisture distributions from core samples.

From  $d_C = i/\theta$ ,  $\theta = i/d_C$ .

Take  $d_C$  as the depth to the water table. Evaluation of the CDF of  $\theta$ ,  $F_\Theta(\theta)$  using  $\theta = i/d_C$  yields the percent mass delivered to the water table after net infiltration ( $i$ ) is applied. This may be calculated using a normal or log normal model of  $\theta$ .

### Solution Using $f_D(d)$

The probability density function (PDF) of  $D$ ,  $f_D(d)$  is calibrated after a net infiltration  $I_C$  has occurred in a field with average field capacity  $\theta_C$ .

Either a log normal distribution, with parameters  $\mu_x$  and  $\sigma_x$  or a normal distribution with parameters  $\mu_d$  and  $\sigma_d$  may be assumed where  $x = \ln(d)$  and the cumulative distribution function (CDF) of  $D$  is defined as  $F_D(d)$ .

To find  $(\mu_d, \sigma_d)$  or  $(\mu_x, \sigma_x)$  at the water table, the random variable  $d$  is scaled by  $z\theta_C/I_C$ . Thus,

$$\mu_{dz} = (z\theta_C/I_C) \mu_d$$

$$\sigma_{dz} = (z\theta_C/I_C) \sigma_d.$$

The parameters  $\mu_{dz}$  and  $\sigma_{dz}$  may be transformed to  $\mu_{xz}$  and  $\sigma_{xz}$  as shown above. The percent mass to the water table as a function of net infiltration is found by evaluating

$$F(I/\theta_C) \approx N(\mu_{dz}, \sigma_{dz}) \text{ or}$$

$$F(I/\theta_C) \approx LN(\mu_{xz}, \sigma_{xz}).$$

## **Appendix B**

### **Experiment I Bromide and Aldicarb Data**

Numbers refer to particular samplers. xx means no sample was taken. Data points that are obvious outliers have been removed from the Aldicarb data set.



3 Feet

DAYS	7 ppm Br-	7 ppb AS	8 ppm Br-	8 ppb AS	9 ppm Br-	9 ppb AS
13	0.08	5.00	0.12	4.00	0.12	10.00
20	0.08	10.00	0.28	0.00	0.28	0.00
23	0.16	0.00	0.16	0.00	0.16	0.00
34	0.16	0.00	0.16	0.00	0.16	0.00
36	0.24	0.00	0.23	0.00	0.23	0.00
37	0.35	0.00	xx	xx	xx	xx
40	0.46	0.00	0.26	0.00	0.26	0.00
42	0.48	0.00	0.56	15.00	0.56	0.00
51	0.84	0.00	0.48	0.00	0.48	0.00
60	2.78	7.00	xx	xx	xx	xx
66	5.93	0.00	xx	xx	xx	xx
73	14.88	185.00	xx	xx	xx	xx
87	34.00	131.00	xx	xx	xx	xx
97	46.40	650.00	48.24	625.00	48.24	0.00
111	24.16	465.00	29.04	950.00	29.04	1665.00
125	10.08	128.00	31.84	300.00	31.84	1120.00
136	6.66	130.00	27.76	340.00	27.76	1025.00
150	6.35	175.00	13.92	360.00	13.92	930.00
166	7.20	83.00	6.72	154.00	8.00	910.00
179	5.44	44.00	5.60	85.00	7.04	770.00
195	3.60	26.00	5.60	83.00	6.40	606.00
292	1.04	9.00	3.84	39.00	3.60	300.00
308	0.70	5.00	2.80	31.00	3.28	307.00
358	0.40	0.00	xx	xx	1.68	288.00
372	0.72	0.00	xx	xx		93.00

6 Feet

DAYS	4 ppm Br-	4 ppb AS	5 ppm Br-	5 ppb AS	6 ppm Br-	6 ppb AS
13	0.08	0.00	0.18	0.00	0.40	7.00
20	0.08	0.00	0.08	0.00	0.24	0.00
23	0.16	0.00	0.16	0.00	0.71	0.00
34	0.16	0.00	0.16	0.00	0.76	0.00
36	0.08	0.00	0.35	0.00	0.54	0.00
37	0.08	0.00	0.44	0.00	0.52	0.00
40	0.23	0.00	0.70	0.00	0.55	0.00
42	0.08	0.00	0.70	0.00	0.44	0.00
51	0.08	0.00	0.96	0.00	0.40	0.00
60	0.08	13.00	0.92	0.00	0.44	0.00
66	0.09	0.00	0.55	0.00	0.55	0.00
73	0.15	0.00	0.29	10.00	0.67	30.00
87	0.15	0.00	xx	xx	xx	xx
97	0.40	20.00	0.26	20.00	0.68	28.00
111	1.53	20.00	1.53	47.00	2.15	90.00
125	2.53	24.00	3.18	15.00	4.10	52.00
136	3.58	20.00	2.65	15.00	3.74	115.00
150	4.20	25.00	2.65	15.00	4.82	110.00
166	4.08	0.00	4.80	34.00	5.60	62.00
179	4.08	70.00	3.44	15.00	4.56	29.00
195	4.00	70.00	1.76	0.00	3.28	50.00
292	2.32	33.00	0.80	5.00	1.68	15.00
308	2.00	0.00	0.46	5.00	1.04	23.00
358	xx	xx	0.24	0.00	0.72	0.00
372	xx	xx	0.80	2.00	1.20	27.00

9 Feet

DAYS	1 ppm Br-	1 ppb AS	2 ppm Br-	2 ppb AS
13	0.46	0.00	0.08	0.00
20	0.58	0.00	0.10	0.00
23	xx	xx	0.16	0.00
34	0.84	0.00	0.08	0.00
36	0.92	0.00	0.08	0.00
37	xx	xx	0.08	0.00
40	0.62	0.00	0.08	0.00
42	0.67	0.00	0.08	10.00
51	0.42	0.00	0.08	8.00
60	0.48	0.00	0.08	0.00
66	0.40	0.00	0.08	0.00
73	xx	xx	0.08	0.00
97	0.26	0.00	0.08	0.00
111	0.28	0.00	0.08	0.00
125	0.18	0.00	0.19	0.00
136	0.12	0.00	0.19	0.00
150	0.12	0.00	0.48	0.00
166	0.20	0.00	0.88	20.00
179	0.14	5.00	1.52	14.00
195	0.18	0.00	2.00	18.00
292	0.88	10.00	2.96	18.00
308	0.80	13.00	1.92	24.00
358	0.48	24.00	1.12	20.00
372	1.44	21.00	3.12	12.00

Well Data

DAYS	1 ppm Br	1 ppb AS	2 ppm Br	2 ppb AS	3 ppm Br	3 ppb AS
20	0.22	0.00	0.08	0.00	0.08	0.00
23	0.16	0.00	0.16	0.00	0.16	0.00
36	0.08	0.00	0.08	0.00	0.08	0.00
37	0.08	0.00	0.08	0.00	0.08	0.00
40	0.08	0.00	0.08	0.00	0.08	0.00
42	0.08	0.00	0.08	0.00	0.08	0.00
51	0.08	0.00	0.08	0.00	0.08	0.00
60	0.08	0.00	0.08	0.00	0.08	0.00
66	0.08	0.00	0.08	0.00	0.08	0.00
97	0.08	0.00	0.08	0.00	0.27	20.00
111	0.08	0.00	0.08	0.00	0.33	6.00
125	0.08	0.00	0.15	12.00	0.82	34.00
136	0.08	0.00	0.17	20.00	0.84	30.00
150	0.08	0.00	0.28	13.00	2.03	55.00
166	0.56	27.00	0.77	49.00	2.64	76.00
179	0.26	8.00	0.96	61.00	4.08	57.00
195	0.08	0.00	1.68	68.00	4.08	44.00
292	0.88	8.00	3.84	32.00	4.16	15.00
308	0.51	5.00	2.96	22.00	4.00	15.00
358	0.80	14.00	1.92	26.00	1.44	13.00
372	1.92	17.00	2.96	21.00	3.12	14.00

## Appendix C

Root density data on Russet Burbank potatoes  
from C. B. Tanner and G.G. Weis

The following forms show root density data as the total length of roots found in a cubic centimeter ( $\text{cm}/\text{cm}^3$ ) on a transect from the center of one furrow across a hill to the center of the next furrow. The number of days past emergence is noted at the top of each group of forms. The parameters length and depth lay out a grid into which the appropriate values of root density are entered. The row labeled " $\text{cm}/\text{cm}^2$ " contains the total root length per  $\text{cm}^2$  encountered in that column. This is calculated

$$\sum \text{Root density (cm/cm}^3\text{)} * \text{Depth of sample (cm)} = \text{Root Density (cm/cm}^2\text{)} \\ \text{column}$$

The row labeled "ratio" is the total root length per  $\text{cm}^2$  divided by the average root length per  $\text{cm}^2$  found in the transect.

The summary at the end of this appendix contains the average values of the ratio described above averaged over the four data points in the furrow and the five points under the hill. Although the entries in this Appendix contain data from two treatments, deep plow and normal tillage, the treatments had little affect on root development. The data are lumped in the summary.

## 9-10 days

length	10	20	30	40	50	60	70	80	90	
			-----hill-----							
depth										
10					0.68					
20	0.16	0.42	0.13	1.26	1.24	0.52	0.3	0.21	0.11	
30	0.2	0.07	0.11	0.14	0.43	0.17	0.25	0.1	0.13	
40				0.18	0.07	0.04				
50										
60										
70										
80										
	3.6	4.9	2.4	15.8	24.2	7.3	5.5	3.1	2.4	cm/cm2
	0.468	0.64	0.31	2.05	3.15	0.95	0.72	0.4	0.31	ratio

length	10	20	30	40	50	60	70	80	90	
			-----hill-----							
depth										
10					0.64					
20	0.1	0.1	0.13	0.17	1.69	1.24	0.36	0.14	0.16	
30	0.03	0.02	0.06	0.07	0.38	0.31	0.14	0.1	0.06	
40				0.03	0.11	0.1				
50										
60										
70										
80										
	1.3	1.2	1.9	2.7	28.2	16.5	5	2.4	2.2	cm/cm2
	0.191	0.18	0.28	0.4	4.13	2.42	0.73	0.35	0.32	ratio

## Deep plow

length	10	20	30	40	50	60	70	80	90	
			-----hill-----							
depth										
10					0.57					
20	0.05	0.2	0.12	0.31	1.3	0.31	0.07	0.05	0.06	
30	0.07	0.03	0.03	0.07	0.13	0.1	0.02	0.02	0.02	
40				0.04	0.1	0.1				
50										
60										
70										
80										
	1.2	2.3	1.5	4.2	21	5.1	0.9	0.7	0.8	cm/cm2
	0.286	0.55	0.36	1	5.01	1.22	0.21	0.17	0.19	ratio

## Deep plow

length	10	20	30	40	50	60	70	80	90	
			-----hill-----							
depth										
10					0.87					
20	0.08	0.1	0.18	0.49	0.66	0.7	0.2	0.2	0.27	
30	0.09	0.05	0.09	0.07	0.51	0.16	0.03	0.03	0.05	
40				0.03	0.22	0.08				
50										
60										
70										
80										
	1.7	1.5	2.7	5.9	22.6	9.4	2.3	2.3	3.2	cm/cm2
	0.297	0.26	0.47	1.03	3.94	1.64	0.4	0.4	0.56	ratio

## 21 days

length	10	20	30	40	50	60	70	80	90	
			-----hill-----							
depth										
10					0.71					
20			0.58	1.05	0.43	0.8	0.28			
30	0.16	0.59	0.88	0.69	0.66	1.45	0.41	0.48	0.28	
40			0.72	1.56	0.85	1.45	0.65			
50				0.13	0.06	0.07				
60										
70										
80										
	1.6	5.9	21.8	34.3	27.1	37.7	13.4	4.8	2.8	cm/cm2
	0.096	0.36	1.31	2.07	1.63	2.27	0.81	0.29	0.17	ratio

length	10	20	30	40	50	60	70	80	90	
			-----hill-----							
depth										
10			0.23	0.54	0.87	0.97	0.14			
20	0.42	0.53	0.9	1.8	1.14	1.1	0.54	0.38	0.17	
30	0.14	0.39	0.87	0.36	0.14	0.22	0.29	0.26	0.22	
40			0.48	0.45	0.1	0.12	0.06			
50				0.12	0.06	0.04				
60					0.07					
70										
80										
	5.6	9.2	24.8	32.7	23.8	24.5	10.3	6.4	3.9	cm/cm2
	0.357	0.59	1.58	2.08	1.52	1.56	0.66	0.41	0.25	ratio



## Deep Plow

length	10	20	30	40	50	60	70	80	90	
			-----hill-----							
depth										
10			0.1	0.48	0.91	0.5	0.29			
20	0.19	0.18	0.35	1.37	1.41	1.7	0.37	0.33	0.32	
30	0.16	0.11	0.73	1.12	0.6	1.33	0.32	0.14	0.09	
40			0.03	0.03	0.06	0.17	0.09			
50				0.03	0.02	0.03				
60					0.03					
70										
80										
	3.5	2.9	12.1	30.3	30.3	37.3	10.7	4.7	4.1	cm/cm2
	0.232	0.19	0.8	2.01	2.01	2.47	0.71	0.31	0.27	ratio

## Deep Plow

length	10	20	30	40	50	60	70	80	90	
			-----hill-----							
depth										
10				0.39	0.69	0.47				
20		0.33	0.34	1.39	1.07	0.9	0.3	0.25		
30	0.12	0.23	0.38	1.63	0.65	0.85	0.3	0.1	0.04	
40			0.05	0.2	0.19	0.39	0.02			
50				0.06	0.01	0.06				
60										
70										
80										
	1.2	5.6	7.7	36.7	26.1	26.7	6.2	3.5	0.4	cm/cm2
	0.095	0.44	0.61	2.89	2.06	2.11	0.49	0.28	0.03	ratio

## 36 days

length	10	20	30	40	50	60	70	80	90	
			-----hill-----							
depth										
10			1.24	1.29	1.88	1.12	0.87			
20	1.24	1.05	0.96	1.58	1.3	1.21	1.04	1.42	0.62	
30	0.23	0.4	0.6	1.08	0.56	0.49	0.38	0.51	0.34	
40			0.03	0.1	0.1	0.09	0.07			
50				0.05	0.1	0.09				
60					0.06					
70										
80										
	14.7	14.5	28.3	41	40	30	23.6	19.3	9.6	cm/cm2
	0.599	0.59	1.15	1.67	1.63	1.22	0.96	0.79	0.39	ratio

length	10	20	30	40	50	60	70	80	90	
			-----hill-----							
depth										
10			0.51	0.7	0.75	0.31	0.72			
20	0.53	0.44	0.65	1.89	2.04	0.7	0.74	0.6	0.68	
30	0.36	0.79	0.8	1.8	1.15	0.99	0.96	0.45	0.23	
40			0.02	0.02	0.1	0.1	0.03			
50				0.14	0.03	0.04				
60					0.23					
70										
80										
	8.9	12.3	19.8	45.5	43	21.4	24.5	10.5	9.1	cm/cm2
	0.411	0.57	0.91	2.1	1.98	0.99	1.13	0.48	0.42	ratio

## Deep Plow

length	10	20	30	40	50	60	70	80	90	
			-----hill-----							
depth										
10			0.47	1.08	1.63	1.27	0.91			
20	0.05	0.36	0.65	0.69	1.32	0.62	1.06	0.5	0.41	
30	0.2	0.66	0.67	2.08	0.28	0.24	1.15	0.26	0.18	
40			0.18	0.06	0.04	0.63	0.65			
50				0.06	0.02	0.06				
60										
70										
80										
	2.5	10.2	19.7	39.7	32.9	28.2	37.7	7.6	5.9	cm/cm2
	0.122	0.5	0.96	1.94	1.61	1.38	1.84	0.37	0.29	ratio

## 62 days

length	10	20	30	40	50	60	70	80	90	
			-----hill-----							
depth										
10				1.81	1.87	1.04				
20			1.92	2.63	4.22	1.83	1.5			
30	1.37	1.05	1.45	2.57	2.46	1.58	1.14	0.97	1.21	
40			1.6	1.82	0.8	0.99	0.79			
50				0.03	0.06	0.04				
60				0.05	0.05	0.05				
70					0.09					
80										
	13.7	10.5	49.7	89.1	95.5	55.3	34.3	9.7	12.1	cm/cm2
	0.333	0.26	1.21	2.17	2.32	1.35	0.83	0.24	0.29	ratio

length	10	20	30	40	50	60	70	80	90	
			-----hill-----							
depth										
10				1.39	1.45	1.27				
20			0.98	0.83	1.97	1.49	1.15			
30	0.66	0.49	0.58	0.79	1.82	1.2	1.14	0.63	1.19	
40			0.63	0.67	0.67	1.28	0.94			
50				0.57	0.35	0.52				
60				0.07	0.03	0.17				
70					0.04					
80										
	6.6	4.9	21.9	43.2	63.3	59.3	32.3	6.3	11.9	cm/cm2
	0.238	0.18	0.79	1.56	2.28	2.14	1.16	0.23	0.43	ratio

length	10	20	30	40	50	60	70	80	90	
			-----hill-----							
depth										
10				1.37	1.93	1.75				
20		3.71	2.97	4.1	1.93	2.2	2.9	2.73		
30	1.85	2.25	2.34	1.91	2.38	2.23	2.09	1.73	1.36	
40			1.9	0.84	1.06	1.2	1.61			
50				0.12	0.17	0.1				
60				0.08	0.22	0.15				
70					0.15					
80										
	18.5	59.6	72.1	84.2	78.4	76.3	66	44.6	13.6	cm/cm2
	0.324	1.05	1.26	1.48	1.37	1.34	1.16	0.78	0.24	ratio

length	10	20	30	40	50	60	70	80	90	
			-----hill-----							
depth										
10				0.99	1.2	1.29				
20			2.08	2.04	2.32	1.9	0.76			
30	1.43	1.84	1.63	1.41	1.51	1.88	1.4	1.08	0.53	
40			0.9	0.84	0.64	1.33	1.36			
50				0.02	0.13	0.9				
60				0.05	0.06	0.02				
70					0.07					
80										
	14.3	18.4	46.1	53.5	59.3	73.2	35.2	10.8	5.3	cm/cm2
	0.407	0.52	1.31	1.52	1.69	2.08	1	0.31	0.15	ratio

### Summary

Average values of the ratio over four data points in the furrow and five data points under the hill.

furrow	0.46	hill	1.44	days	9-10
furrow	0.26	hill	1.59	days	9-10
furrow	0.3	hill	1.56	days	9-10
furrow	0.38	hill	1.5	days	9-10
Average	0.35		1.52		
St Dev	0.08		0.06		

furrow	0.23	hill	1.62	days	21
furrow	0.4	hill	1.48	days	21
furrow	0.25	hill	1.6	days	21
furrow	0.21	hill	1.63	days	21
Average	0.27		1.58		
St Dev	0.07		0.06		

furrow	0.59	hill	1.33	days	36
furrow	0.47	hill	1.42	days	36
furrow	0.32	hill	1.54	days	36
Average	0.46		1.43		
St Dev	0.11		0.09		

furrow	0.27	hill	1.59	days	62
furrow	0.28	hill	1.58	days	62
furrow	0.6	hill	1.32	days	62
furrow	0.35	hill	1.52	days	62
Average	0.38		1.5		
St Dev	0.13		0.11		

## Appendix D

### Weighing Lysimeter Data

The data presented here are monthly summaries for two weighing lysimeters located at Hancock Experimental Station from Tanner (1986). Data labeled Rect and Round are from the rectangular and round weighing lysimeter respectively. The gross infiltration is given neglecting trace precipitation. Negative values of evapotranspiration (ET) are probably due to underestimates of snowfall or drifting snow. Notes are provided to describe conditions on each lysimeter and to explain omissions in the data. Data are presented for bare to weedy soil, crops left standing and potatoes. A summary of the months used in determining  $i_z$  is given at the end of the appendix. All data are in inches of water.

Notes	M/Y	Gross i	Rect ET	Gross i	Round ET
All 1966 to 9/67	3/66	3.96	-0.691	3.96	0.553
Lysimeter left bare	4/66	1.27	0.297	1.27	0.563
Maybe a few weeds	5/66	1.17	0.154	1.17	0.592
	6/66	1.45	1.066	1.45	1.362
	7/66	3.83	3.472	3.83	3.5
	8/66	4.75	1.774	4.75	2.633
	9/66	2.47	0.656	2.47	1.234

	10/66	0.65	0.512	0.65	3.036
	11/66	0.73	0.708	0.73	0.758
	12/66	2.92	2.802	2.92	3.036
	1/67	1.97	1.515	1.97	1.092
	2/67	1.05	0.678	1.05	0.8115
	4/67	2.05	0.277	2.05	0.448
	5/67	1.34	0.709	1.34	0.8
	6/67	7.09	2.84	7.09	4.014
	7/67	1.89	0.876	1.89	2.209
	8/67	11.56	1.188	11.56	1.423
Rye sown but still bare	9/67	2.11	0.949	2.11	1.899
	10/67	3.6	1.882	3.6	1.729
	11/67	0.86	-0.5	0.86	0.236
	12/67	0.94	0.5	0.94	0.71
	2/68	0.44	0.374	0.44	-0.262
	3/68	0.72	1.113	0.72	-0.535
	4/68	3.39	0.495	3.39	1.665
Beans planted 6/68	5/68	6.76	2.342	6.76	3.131
Left standing	9/68	6.45	6.315	6.45	1.554
	10/68	1.19	0.471	1.19	1.02
	11/68	0.54	0.302	0.54	0.437
	12/68	1.73	0.4	1.73	1.672
	1/69	2.03	-1.9	2.03	-0.516
	2/69	0.07	1.045	0.07	-0.818
	3/69	1.14	-1.279	1.14	-3.248



Onions planted 4/69	4/69	2.59	0.716	2.59	-0.79
Left Standing	9/69	3.21	1.952	3.21	
	10/69	4.35	1.005	4.35	
	11/69	0.42	0.586	0.42	0.07
	12/69	0.74	-0.776	0.74	0.66
	1/70	0.48	-0.448	0.48	-0.166
	2/70	0.07	0.158	0.07	-0.537
	3/70	0.7	-0.082	0.7	-2.238
Left bare	4/70	0.93	0.065	0.93	0.491
Possibly weedy	5/70	8.19		8.19	5.086
	6/70	2.07		2.07	-2.543
	7/70	3.11		3.11	2.852
	8/70	1.91		1.91	1.865
	9/70	5.61		5.61	2.47
	10/70	3.3		3.3	1.972
	11/70	2.14		2.14	-0.284
	12/70	0.66		0.66	-0.077
	1/71	0.74		0.74	0.54
	2/71	1.79		1.79	0.352
	3/71	0.66		0.66	-3.356
	4/71	1.59		1.59	-1.991
Potatos planted round	5/71	4.87		4.87	2.946
Potatos planted rect	6/71	7.81	2.344	7.81	6
Heavy irrigation	7/71	10.674	5.691	10.674	9.84
	8/71	11.617	5.701	11.617	8.01

	9/71	16.203	2.897	16.203	2.588
	10/71	6.04	1.205	6.04	-0.105
	11/71	2.72	-0.791	2.72	0.999
	12/71	1.85		1.85	-0.401
Too many problems in 1972	1/73	1.06	-0.796	1.06	-2.575
	2/73	0.78	-0.529	0.78	0.07
	3/73	4.54	0.156	4.54	-2.855
	4/73	14.922	0.878	14.922	1.206
Potatos planted	5/73	6.75	0.272	6.75	1.682
	6/73	5.05	3.821	7.1	3.722
	7/73	6.403	6.297	8.94	6.37
	8/73	6.53	4.51	8.421	4.77
Vines killed	9/73	3.383	2.207	3.96	1.34
	10/73	2.2	0.929	2.2	1.48
	11/73	1.55	0.083	1.55	0
	12/73	1.23	-0.329	1.23	0
	1/74	0.67	-0.511	0.67	-0.121
	2/74	0.52	-1	0.52	-0.203
Rect in wheat	3/74	2.86	-0.53	2.86	0.012
Round bare	4/74			2.44	-3.586
	5/74			3.55	2.108
	6/74			3.94	1.881
	7/74			3.15	2.59
	8/74			3.27	2.51
	9/74	1.56	0.22	1.56	1.446

Rect stubble disked and	10/74	2.42	0.665	3.05	2.603
round used in leaching	11/74	2.73	0.594	6.25	0.027
	12/74	1.24	-0.496	1.24	0.778
Winter negative or	9/75	1.235	1.499	1.235	0.497
not working	10/75	0.41	0.873	0.41	0.3
Fall bare	11/75	2.275	-0.06	2.275	2.29
	12/75	0.85	-0.071	0.85	-0.727
	1/76	0.97	-0.746	0.97	0.805
	2/76	1.18	-0.947	1.18	-2.989
	3/76	4.03	1.399	4.03	0.35
Potatos planted	4/76	3.455	0.524	3.455	0.025
	5/76	1.38	0.392	1.38	0.441
	6/76	7.375	2.887	7.375	5.118
	7/76	10.365	5.991	10.365	3.138
	8/76	9.127	5.994	9.127	5.479
Vines killed	9/76	2.827	2.67	2.827	1.498
	10/76	1.295	1.115	1.295	1.046
	11/76	0.455	0.892	0.455	0.335
	12/76	0.25	-0.277	0.25	0.202
	1/77	0.43	-0.061	0.43	0.389
	2/77	1.16	-0.324	1.16	-1.133
	3/77	3.405	-0.495	3.405	-2.021
	4/77	3.035	-0.369	3.035	-1.165
Corn 5-9/77	10/77	2.245	0.871	2.245	0.167
	11/77	2.99	-0.016	2.99	1.21

Corn 5-10/78	12/77	1.965	-1.1858	1.965	-0.978
	1/78	0.945	-1.287	0.945	-0.573
	2/78	0.29	0.321	0.29	-0.582
	3/78	0.225	-0.785	0.225	-3.62
	4/78	4.26	0.628	4.26	1.11
	10/78	1.92	1.237	1.92	0.344
	11/78	4.11	2.045	4.11	3
	12/78	0.87	-0.506	0.87	0.62

### Summary

The behavior of ET/Gross i from the data above. Negative entries are ignored.

#### April

	Average	Stan Dev
Rect	0.110	0.094
Round	0.184	0.215
Combined	0.147	0.166

#### May

Rect	0.166	0.199
Round	0.494	0.141
Combined	0.330	0.237

## June

Rect	0.369	0.306
Round	0.391	0.732
Combined	0.380	0.539

## September

Rect	0.543	0.407
Round	0.443	0.295
Combined	0.493	0.350

## October

Rect	0.571	0.549
Round	0.827	1.255
Combined	0.699	.957

## November

Rect	0.471	.652
Round	0.461	.389
Combined	0.466	.525

## December

Rect	0.143	.303
Round	0.483	.440
Combined	0.313	.408

**Addendum to Appendix D**  
**Comparison of Coefficients of Variation**  
**for**  
**Each Usable Month**  
**Data are from Tanner (1986).**

Month	(T=0) Gross i (T=0) CV	Rect ET CV	(T=0) Gross i (T=0) CV	Round ET CV	Rect Ratio	Round Ratio
4	1.085	0.543	1.068	0.712	0.483	0.704
5	0.834	1.065	0.755	0.788	0.593	0.122
6	0.875	0.642	0.696	0.581	0.417	0.371
7	0.333	0.844	0.27	0.195	0.457	0.156
8	0.817	0.28	0.798	0.269	0.804	0.603
9	1.083	0.593	1.065	0.422	0.681	0.506
10	0.014	0.003	0.014	0.008	0.005	0.011
11	0.677	0.849	0.844	1.061	0.978	0.647
Mean	0.715	0.602	0.689	0.505	0.552	0.39
StDev	0.37	0.338	0.37	0.347	0.292	0.266
CV	0.518	0.562	0.537	0.688	0.528	0.681

### Appendix E

#### Net Infiltration During Experiment I

Given below are three estimates of total net infiltration  $I_1$ ,  $I_2$ ,  $I_3$ . Explanations of methods are given in the text. The  $\alpha_0$  used to determine  $I_2$  is 0.441. The  $\alpha_0$  used to determine  $I_3$  is 0.318.

$$i = \text{Gross } i - ET$$

Notes	Days	Gross $i$	ET	$i$	$I_1$	$I_2$	$I_3$	$\alpha_{00}$
5/29	0	2.54						
	13	5.79	2.34	3.45	3.45	1.53	1.10	1
	20	3.99	2.08	1.91	5.36	2.37	1.70	1
	23	0.20	1.57	-1.37	3.99	1.76	1.27	1
	34	10.69	5.87	4.83	8.81	3.89	2.80	1
	36	0.51	0.97	-0.46	8.36	3.69	2.66	1
	37	1.22	0.30	0.91	9.27	4.09	2.95	1
	40	1.17	1.19	-0.03	9.25	4.08	2.94	1
	42	2.29	0.41	1.88	11.13	4.91	3.54	1
	51	6.83	4.72	2.11	13.23	5.84	4.21	1
	60	3.71	3.84	-0.13	13.11	5.79	4.17	1
	66	3.15	2.24	0.91	14.02	6.19	4.46	1
	73	6.35	2.87	3.48	17.50	7.73	5.57	1
	87	7.26	5.38	1.88	19.38	8.56	6.17	1
	97	6.43	3.40	3.02	22.40	9.89	7.13	1
9/5 Day 99	111	9.07		9.07	31.47	13.90	10.01	1
Plants killed	125	4.52		4.52	35.99	18.42	11.48	0.324
	136	2.95		2.95	38.94	21.36	12.43	0.324
	150	7.65		7.65	46.58	29.01	14.91	0.324
	166	5.33		5.33	51.92	34.34	16.64	0.324
	179	0.00		0.00	51.92	34.34	16.64	0.324
	195	2.46		2.46	54.38	36.81	18.33	0.687
	292	12.14		12.14	66.52	48.95	30.47	1
	308	2.67		2.67	69.19	51.61	32.69	0.834
	358	5.46		5.46	74.65	57.08	36.35	0.67
	372	4.04		4.04	78.69	61.11	38.86	0.62

## Appendix F

### Summary of Total Mass, Center of Mass and Log Space Parameters Experiment I

#### Definitions and Methods

#### **I<sub>1</sub>, I<sub>2</sub>, I<sub>3</sub>**

The three estimates of net infiltration stated in the text (pages 66-69).

#### **T mass**

The total mass of bromide was found by numerically integrating the concentration of bromide over the total quantity of moisture flowing past the soil water samplers.

$$\sum_{n=1}^N \frac{\text{mg Br}_n}{\text{Kg Solution}} * \frac{1 \text{ kg solution}}{1000 \text{ cm}^3} \Delta i_n \text{ cm} * I = T \text{ Br mg} \frac{\text{cm}^2}{\text{cm}^2}$$

With  $\Delta i$  the flux during the  $n^{\text{th}}$  sample period. This numerical integration approximates the following analytical integration:

$$\int_0^{\infty} C * \rho * u \, dt = M/A$$



Where  $C$  is the mass per unit mass concentration,  $\rho$  is the density of solution,  $u$  is the flow rate,  $t$  is the time,  $M$  is the mass, and  $A$  is the horizontal cross sectional area. Comparing the analytical expression with the numerical expression we can see that several assumptions were made in evaluating the integral:

- 1) All bromide has flowed past the soil water sample by the time the last sample is taken.
- 2) The solution density is constant and equal to  $1\text{gm/cm}^3$ .
- 3) The soil water samplers average the concentration within  $\Delta i$  (i.e., the  $C(i)$  relation is linear or constant in each  $\Delta i$ ).
- 5) The bromide is applied uniformly to the surface.

T AS (total mass as aldicarb sulfone) is calculated similarly yielding T AS as  $\mu\text{g/cm}^2$ .

### Centroid

The centroid or center of mass of the bromide is found by numerically integrating the product of  $i$  and mass in the sample as

$$\frac{1}{TBr} \sum_{n=1}^N (i_{cm} - (\Delta i_{cm}/2)) * mg Br_n * \frac{1 \text{ Kg H}_2\text{O}}{1000 \text{ cm}^3} * \Delta i_n \text{ cm} = C \text{ mass cm}$$

Where  $\Delta i_n$  is the flux during the  $n^{\text{th}}$  sample period, and  $i$  is the total flux up to and including the sample flux. This numerical integration approximates the following analytical integration:

$$(1/T \text{ Br}) \int_0^{\infty} t * C * \rho u \, dt = C \text{ mass cm}$$

The assumptions and definitions are as above.  $P_3$  and  $P_6$  are variables presented in the text.  $P_3 = C \text{ mass at 3 feet}$ .  $P_6 = C \text{ mass at 6 feet}$ .

### **Peak Values**

The value of  $I$  when the sample with the highest concentration was taken.

### **Sampler Number**

Each sampler was numbered. Samplers 1 and 2 are replicates at 9 feet. Samplers 4, 5, and 6 are replicates at 6 feet. Samplers 7, 8, and 9 are replicates at 3 feet.

## Mass and Moment Parameters for Bromide and Aldicarb

I<sub>1</sub> Model

	T Br	T AS	Br	AS	Br Peak, AS Peak,	
9 feet	mg/cm <sup>2</sup>	µg/cm <sup>2</sup>	C Mass, cm	C Mass, cm	cm	cm
1	3.24E-02	2.87E-01	40.29	66.58	78.70	74.70
2	6.46E-02	5.78E-01	57.27	57.77	78.70	69.20
Average	4.85E-02	4.33E-01	48.78	62.18	78.70	71.95
Stan Dev	2.28E-02	2.06E-01	12.01	6.23	0.00	3.89
6 feet						
4	1.37E-01	1.17E+00	45.61	45.65	51.90	53.20
5	1.07E-01	1.04E+00	41.00	34.90	51.90	31.50
6	1.65E-01	3.19E+00	41.91	37.88	46.60	38.90
Average	1.36E-01	1.80E+00	42.84	39.48	50.13	41.20
Stan Dev	2.91E-02	1.21E+00	2.44	5.55	3.06	11.03
3 Feet						
7	6.62E-01	1.00E+01	28.23	29.22	22.40	22.40
8	1.15E+00	2.11E+01	29.07	29.46	22.40	31.50
9	1.16E+00	4.27E+01	29.53	39.85	22.40	31.50
Average	9.90E-01	2.46E+01	28.94	32.84	22.40	28.47
Stan Dev	2.84E-01	1.66E+01	0.66	6.07	0.00	5.25

I<sub>2</sub> Model

	T Br	T AS	Br	AS	Br Peak, AS Peak,	
9 feet	mg/cm <sup>2</sup>	μg/cm <sup>2</sup>	C Mass, cm	C Mass, cm	cm	cm
1	2.49E-02	2.87E-01	33.46	49.01	61.10	57.10
2	6.31E-02	5.59E-01	40.89	42.18	61.10	51.60
Average	4.40E-02	4.23E-01	37.17	45.59	61.10	54.35
Stan Dev	2.70E-02	1.92E-01	5.25	4.83	0.00	3.89

## 6 feet

4	1.27E-01	1.04E+00	29.94	31.06	34.30	35.60
5	9.43E-02	7.29E-01	26.55	22.78	34.30	13.90
6	1.46E-01	2.59E+00	27.65	24.18	29.00	21.36
Average	1.23E-01	1.45E+00	28.05	26.01	32.53	23.62
Stan Dev	2.62E-02	9.97E-01	1.73	4.43	3.06	11.03

## 3 Feet

7	3.92E-01	6.07E+00	17.28	17.36	9.89	9.89
8	7.49E-01	1.30E+01	18.10	17.95	9.89	13.90
9	7.66E-01	3.43E+01	18.66	25.98	9.89	13.90
Average	6.36E-01	1.78E+01	18.01	20.43	9.89	12.56
Stan Dev	2.11E-01	1.47E+01	0.69	4.81	0.00	2.32

I<sub>3</sub> Model

	T Br mg/cm <sup>2</sup>	T AS μg/cm <sup>2</sup>	Br C Mass, cm	AS C Mass, cm	Br Peak, AS Peak, cm	cm
9 feet						
1	1.98E-02	2.38E-01	20.91	29.01	38.90	36.40
2	5.17E-02	4.21E-01	24.39	25.30	38.90	32.70
Average	3.58E-02	3.30E-01	22.65	27.15	38.90	34.55
Stan Dev	2.26E-02	1.30E-01	2.46	2.62	0.00	2.62
6 feet						
4	6.96E-02	7.12E-01	19.02	19.55	16.60	17.50
5	4.36E-02	3.82E-01	16.05	13.33	16.60	10.00
6	7.27E-02	1.23E+00	17.21	14.46	14.90	12.40
Average	6.20E-02	7.74E-01	17.43	15.78	16.03	13.30
Stan Dev	1.60E-02	4.26E-01	1.50	3.31	0.98	3.83
3 Feet						
7	2.25E-01	3.31E+00	10.07	9.84	7.12	7.12
8	4.07E-01	7.18E+00	11.03	10.45	7.12	10.00
9	4.15E-01	1.77E+01	11.38	16.46	7.12	10.00
Average	3.49E-01	9.40E+00	10.82	12.25	7.12	9.04
Stan Dev	1.08E-01	7.45E+00	0.68	3.66	0.00	1.66

Log Space Parameters for Bromide

Depth	Center of Mass		Peaks	
	Average	Stan Dev	Average	Stan Dev
$I_1$				
3 Feet	3.365	0.023	3.109	0
6 Feet	3.756	0.056	3.913	0.062
9 Feet	3.872	0.249	4.366	0
$I_2$				
3 Feet	2.891	0.039	2.292	0
6 Feet	3.333	0.061	3.479	0.097
9 Feet	3.611	0.142	4.113	0
$I_3$				
3 Feet	2.38	0.064	1.963	0
6 Feet	2.856	0.085	2.773	0.062
9 Feet	3.117	0.109	3.661	0

**Appendix G**  
**% Applied Bromide Recovered in the Samplers**  
**Experiment 1**

The % applied Bromide is calculated by dividing the T Br given in Appendix F (mg/cm<sup>2</sup>) by the amount of Bromide applied per unit area (1.32 mg/cm<sup>2</sup>). Values also are given for the percent of bromide recovered using  $I_3$  corrected for transverse dispersion. These values are entered as  $C I_3$ . The corrections were made according to equation 11 in the text. Values of  $\beta$  used to correct the samples from each sampler are given at the end of this appendix. All entries are fractions, (1=100%).

9 Feet

	$I_1$	$I_2$	$I_3$	$C I_3$
1	0.02	0.02	0.01	0.05
2	0.05	0.05	0.04	0.15

6 feet

	$I_1$	$I_2$	$I_3$	$C I_3$
4	0.10	0.10	0.05	0.18
5	0.08	0.07	0.03	0.11
6	0.12	0.11	0.05	0.18

3 Feet

	$I_1$	$I_2$	$I_3$	$C I_3$
7	0.50	0.30	0.17	0.46
8	0.87	0.57	0.31	0.87
9	0.88	0.58	0.31	0.90

### Values of $\beta$ for Each Sample Period

The columns are not all the same length because all samplers did not always work. To find a particular  $\beta$  for a particular sample period and sampler match the column entries with bromide or aldicarb data.

1	2	4	5	6	7	8	9
1.05	1.05	1.05	1.05	1.05	1.05	1.05	1.05
1.27	1.27	1.27	1.27	1.27	1.27	1.27	1.27
1.48	1.37	1.37	1.37	1.37	1.37	1.37	1.37
1.64	1.51	1.51	1.51	1.51	1.51	1.51	1.51
1.69	1.64	1.64	1.64	1.64	1.64	1.64	1.64
1.74	1.66	1.66	1.66	1.66	1.66	1.70	1.70
1.83	1.70	1.70	1.70	1.70	1.70	1.74	1.74
1.98	1.74	1.74	1.74	1.74	1.74	1.83	1.83
2.09	1.83	1.83	1.83	1.83	1.83	2.47	2.47
2.34	1.98	1.98	1.98	1.98	1.98	2.61	2.61
2.61	2.09	2.09	2.09	2.09	2.09	2.77	2.77
2.77	2.18	2.18	2.18	2.18	2.18	2.90	2.90
2.90	2.38	2.32	2.47	2.47	2.32	3.04	3.04
3.04	2.61	2.47	2.61	2.61	2.47	3.17	3.17
3.17	2.77	2.61	2.77	2.77	2.61	3.31	3.31
3.31	2.90	2.77	2.90	2.90	2.77	3.44	3.44
3.44	3.04	2.90	3.04	3.04	2.90	3.90	3.90
3.90	3.17	3.04	3.17	3.17	3.04	4.32	4.32
4.32	3.31	3.17	3.31	3.31	3.17		4.54
4.54	3.44	3.31	3.44	3.44	3.31		4.75
4.75	3.90	3.44	3.90	3.90	3.44		
	4.32	3.90	4.32	4.32	3.90		
	4.54	4.32	4.54	4.54	4.32		
	4.75		4.75	4.75	4.54		
					4.75		



## Appendix H

### Transfer Function Program Listing

This program is written in Pascal and is designed to be run on a Macintosh 512K computer. The code was developed and compiled using TML Pascal.

```
PROGRAM transferfunction (input, output) ;
{$T APPL JSB!}
LABEL 1;
```

```
TYPE
```

```
    Oneday = record
        day : integer;
        conc : real;
    end;
    Store = array [1..1000] of Oneday;
    head = string [15];
```

```
VAR
```

```
    f : TEXT;
    dat : Store;
    Concin, Deli, Aver, Stdev, Caldepth, Intdepth, Netprecip : real;
    Sim : integer;
    Title : head;
    Ans : char;
```

```
FUNCTION Pwr(x : real; p : integer) : real;
```

```
VAR
```

```
    z : real;
```

```
BEGIN
```

```
    z := Exp (p * Ln(Abs (x))) ;
    If (odd(p)) and (x,0) then Pwr := -z
        else Pwr := z;
```

```
END;
```

```
FUNCTION Erf(x : real) : real;
```

CONST

a1 = 0.0705230784;  
 a2 = 0.0422820123;  
 a3 = 0.0092705272;  
 a4 = 0.0001520143;  
 a5 = 0.0002765672;  
 a6 = 0.0000430638;

VAR

ans : char;  
 z : real;  
 i : integer;

BEGIN

  If x < 0 then i := 0  
     else i := 1;  
 x := Abs (x);  
 z := 1 + a1 \* x + a2 \* Pwr(x,2) + a3 \* Pwr(x,3) + a4 \* Pwr(x,4) +  
 cont.       a5 \* Pwr(x,5) + a6 \* Pwr(x,6);  
 z := Pwr(z,16);  
 z := 1 - (1/z);  
 If i = 1 then Erf := z  
     else Erf := -z;

END;

PROCEDURE Readinfo (var Concin, Deli, Aver, Stdev, Calsepth, Intdepth,  
 cont.       Netprecip : real;  
             var Sim : Integer;  
             var Titile : head;

CONST

pi = 3.141592654

BEGIN

  Writeln ('Remember, use consistent units');  
 Writeln ('What was the concentration of the applied tracer');

```

        Readln (Concin);
    Writeln ('What was the depth of water applied with tracer?');
        Readln (Deli);
    Writeln ('What was the average of the natural log of the net?');
    Writeln ('precipitation required to move the peak concentrations');
    Writeln ('to your soil water samplers?');
        Readln (Aver);
    Writeln ('What was the standard deviation of the same data?');
        Readln (Stdev);
    Writeln ('At what depth were those soil water samplers?');
        Readln (Caldepth);
    Writeln ('What depth are you interested in?');
        Readln (Intdepth);
    Writeln ('What was or will be the average net precip');
    Writeln ('over the simulation period?');
        Readln (Netprecip);
    Writeln ('How many days to simulate?');
        Readln (Sim);
    Writeln ('Name for the data file?');
        Readln (Title);
    Writeln ('I am starting now');

```

END;

PROCEDURE Simulation (var Concin, Deli, Aver, Stdev, Caldepth, Intdepth,  
cont.

```

        Netdepth : real;
        var dat : Store;
        var Sim : Integer);

```

CONST

```

    Rt2 = 1.4142;

```

VAR

```

    ans : char;
    Toti, x, y, c : real;
    d : Integer;

```

BEGIN

```

    d := 0;

```

```

REPEAT
    d := 5 + d;
    Toti := d * Netprecip;
    x := (Ln (Toti * Caldepth/Intdepth) - Aver) / (Rt2 * Stdev);
    y := (Ln ((Toti - Deli) * Caldepth/Intdepth) - Aver) / Rt2 *
cont.      Stdev);
    x := Erf (x);
    y := Erf (y);
    c := (Concin / 2) * (x - y);
        With dat[d] do begin
            day := d;
            conc := c;
            end;
    UNTIL d > Sim;
    Readln (Ans);
END;

PROCEDURE Maildata (var dat : Store;
                    var Sim : Integer;
                    var Title : head);

VAR
    i : integer;
    answer : char;

BEGIN
    i := 0;
    Open (f, Title);
    REPEAT
        i := i + 5;
        With dat[i] do begin
            Writeln (f, day, 'char (9)', conc : 6.5);
            end;
        UNTIL i > (Sim - 5);
    Close (f);
    Writeln ('All done');
end;

BEGIN

```

```
1:  Readinfo (Concin, Deli, Aver, Stdev, Caldepth, Intdepth, Netprecip,  
cont.           Sim, Title);  
    Simulation (Concin, Deli, Aver, Stdev, Caldepth, Intdepth, Netprecip,  
cont.           dat, Sim);  
    Maildata (dat, Sim, Title);  
  
        WriteIn ('Do again? (y,n)');  
        ReadIn (Ans);  
        if Ans = 'y' then goto 1  
  
END.
```

## Appendix I

### Core Data

Cores were taken on 8/20/85 at the Giford.G40 plot at Hancock Experimental station, Hancock Wisconsin.

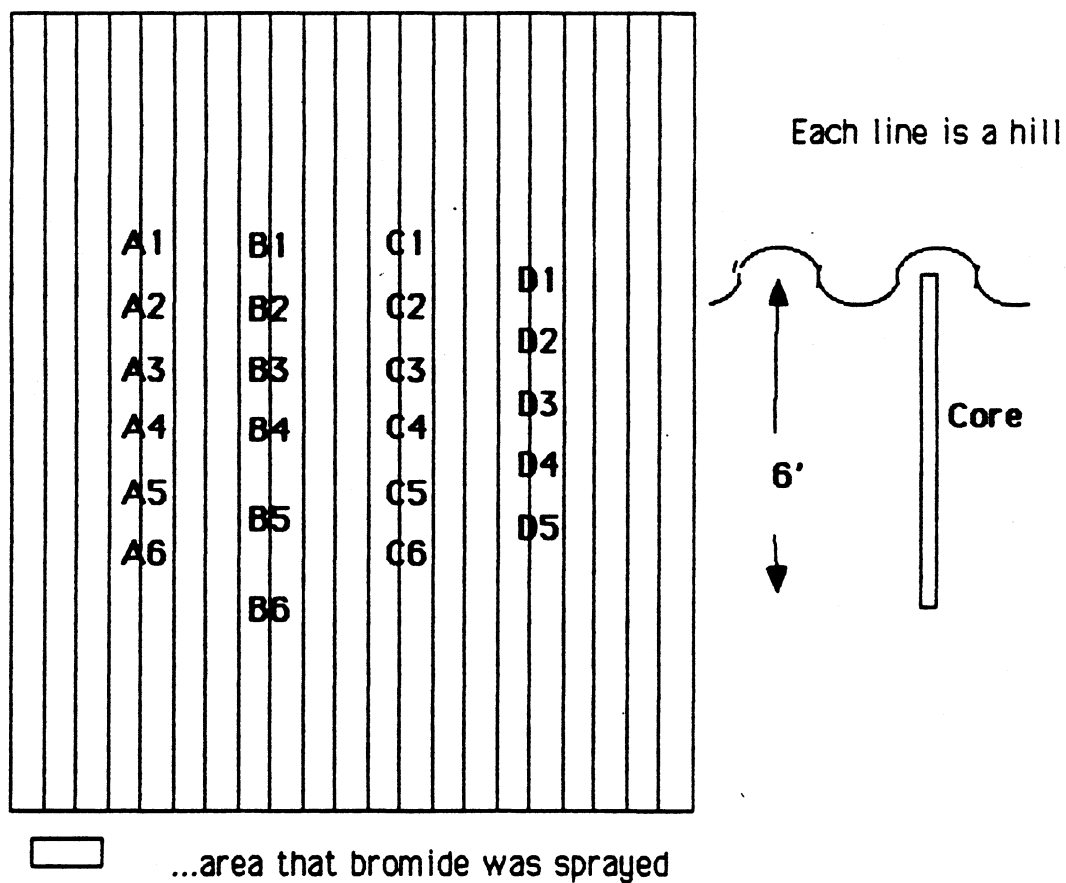


Figure 1. Placement of cores.

## Definitions and Methods

### **Core**

Each core was taken using a three inch bucket auger. The placement of the cores in the field are shown in Figure 1 of this appendix.

### **Depth**

The depth (d) of a particular sample is the lowest point in that sample. Thus each sample is representative of an interval in the core from the depth of the previous sample to the depth of the sample.

### **W**

W is the mass of water per unit mass of dry porous media. It is found by weighing approximately 190 g of sample before and after drying for 24 hours at 103° C.  $\bar{W}$  is W averaged over a core.

### **$\theta$**

$\theta$  is the volumetric water content calculated from W as follows;

$$\theta(\text{cm}^3/\text{cm}^3) = W(\text{g/g}) * 1.55 (\text{g/cm}^3 \text{ Dry Bulk Density}) * 1\text{cm}^3/\text{g H}_2\text{O}$$

The value 1.55 for dry bulk density is from USDA (1967).  $\bar{\theta}$  is  $\theta$  averaged over a core.

**Br- raw**

This is the Bromide ( $\mu\text{moles/liter}$ ) in the extracted solution from the sample. To make the extracted solution a sample of approximately 60 g is mixed with 10 to 15 mls of deionized water using a vortex mixer. The sample is then centrifuged for 15 to 30 minutes. Five to ten clear milliliters of supernatant are removed from the centrifuge for analysis using methods described in the text.

**Br- (ppm)**

The Bromide as parts per million in the soil water in situ is found by:

$$\frac{(S * W) + (C * 1 \text{ ml/g}) * \text{Br- raw} * .08 \text{ ppm}}{S * W} = \frac{\text{Br- ppm}}{1 \mu\text{m/liter}}$$

Where: S is the weight of the sample in grams; and  
C is the amount of added water in milliliters.

The method assumes that all Br- is in solution in the soil water in situ and that 1 ml of deionized water is equivalent to 1 g.

**Total Br**

Total Br was found by numerically integrating the concentration of bromide over the depth of the core. The bold value at the bottom of the column is the total Br- as  $\text{mg/cm}^2$  of surface.



$$\sum \frac{\text{mg Br}}{\text{Kg soln}} * \frac{\Delta d \text{ cm}^3 \text{ soil}}{\text{cm}^2 \text{ soil}} * \frac{\theta \text{ cm}^3 \text{ soln}}{\text{cm}^3 \text{ soln}} * \frac{1 \text{ Kg soln}}{1000 \text{ cm}^3 \text{ soln}} = \text{Total Br } \frac{\text{mg}}{\text{cm}^2}$$

This numerical integration approximates the following analytical integration;

$$\int_{-\infty}^{\infty} C * \rho \, dx = M/A$$

Where C is the mass per unit mass concentration,  $\rho$  is the density, x is the distance, M is the mass, and A is the cross sectional area. By comparing the analytical expression with the numerical expression we can see several assumptions were made in evaluating the integral.

- 1) No bromide has been removed from the bottom of the core.
- 2) The moisture content is constant through the core.
- 3) The bulk density is constant through the core.
- 4) The bromide is applied uniformly to the surface.
- 5) The density of the soil solution is 1g/cm.

### Centroid

The centroid or center of mass of the bromide is found by numerically integrating the product of depth and mass in a core;

$$\sum (d \text{ cm} - (\Delta d \text{ cm}/2)) * \frac{\text{mg Br}}{\text{Kg soln}} * \frac{\Delta d \text{ cm}^3}{\text{cm}^2} * \frac{\theta \text{ cm}^3 \text{ soln}}{\text{cm}^3 \text{ soln}} * \frac{1 \text{ Kg soln}}{1000 \text{ cm}^3} * \frac{1 \text{ cm}^2}{1 \text{ Br mg}}$$

= Centroid (cm)

This numerical integration approximates the following analytical integration;

$$\int_{-\infty}^{\infty} X * C * \rho \, dx = M/A$$

Where the assumptions and definitions are as above with the addition that C(X) is assumed linear in each sample.

### **%P200**

%P200 is the mass of dry sample that passes through a number 200 sieve in a wet sieve process divided by the total dry mass of the sample.

Percents are given as fractions, 1 = 100%.

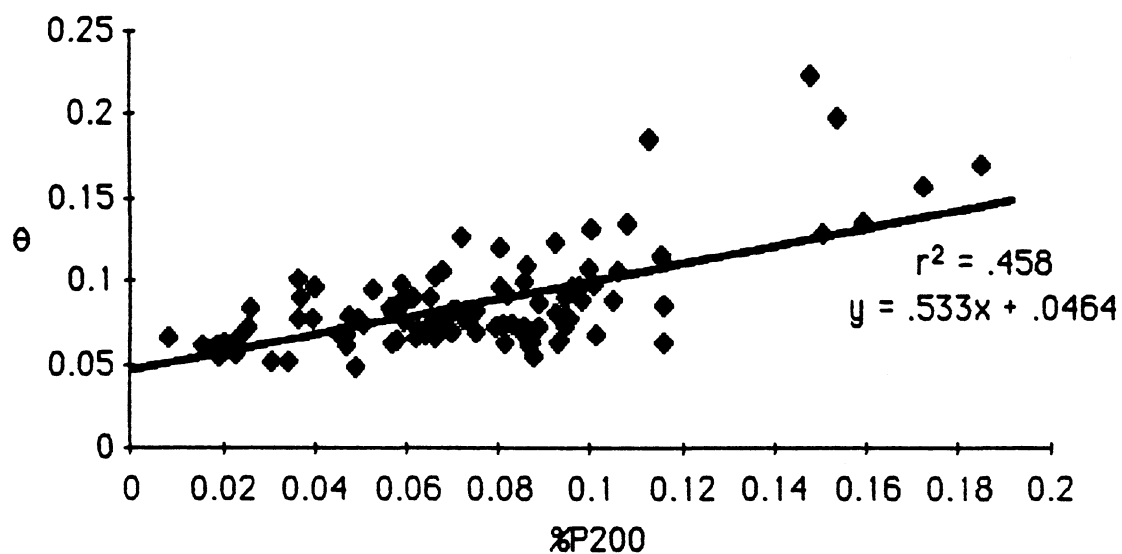


Figure 2. Regression of  $\theta$  on %P200.

Sample	depth	W W	BR Raw	Br ppm SW	P200 %
A1	32	0.0691	6	2.487	0.0996
A1	56	0.0527	11	5.6065	0.0707
A1	80	0.0403	8	5.1585	0.0197
A1	109	0.0422	32	20.458	0.008
A1	132	0.0398	14	9.2627	0.0184
A1	152	0.0352	4	2.962	0.0189
A1	183	0.0537	6	3.3204	0.0258
A2	32	0.0464	23	11.461	0.0793
A2	58	0.0488	7	3.3994	0.0673
A2	80	0.0526	12	5.4571	0.0749
A2	102	0.0578	16	6.7282	0.0941
A2	130	0.0573	15	6.1926	0.06
A2	158	0.0639	21	8.0883	0.0855
A2	180	0.0818	13	4.2348	0.0718

A3	35	0.0571	30	14.002	0.0979
A3	62	0.0556	6	2.8442	0.0888
A3	92	0.0477	4	2.1621	0.0502
A3	120	0.0688	6	2.5769	0.1056
A3	145	0.0772	7	2.6526	0.0804
A3	170	0.0799	10	3.6915	0.092

A4	35	0.0405	8	5.4413	0.0814
A4	60	0.0446	6	3.9024	0.0696
A4	90	0.0397	10	7.1822	0.0468
A4	120	0.0414	12	8.3092	0.0226
A4	150	0.0579	8	4.2489	0.0368
A4	180	0.0632	5	2.3629	0.0586

A5	45	0.0469	14	7.5526	0.0885
A5	75	0.0422	18	10.581	0.0658
A5	105	0.0489	12	6.2751	0.0652
A5	140	0.0504	14	6.8718	0.0731
A5	170	0.0507	8	4.0463	0.0471

A6	37	0.0439	14	9.0667	0.0855
A6	65	0.0487	2	1.2111	0.0591
A6	95	0.054	1.5	0.8227	0.056
A6	125	0.0614	7	3.6678	0.0522
A6	155	0.0871	9	3.2316	0.1078
A6	185	0.0657	14	6.1066	0.036

B1	34	0.0441	25	15.507	0.1008
B1	58	0.0477	17	9.8937	0.0805
B1	80	0.0457	9	5.7793	0.0623
B1	100	0.0433	10	5.9432	0.0641
B1	125	0.062	10	4.3917	0.0971
B1	145	0.0518	5	2.5824	0.0567
B1	162	0.0742	7	2.7549	0.1153

B1	184	0.0395	3	1.9514	0.0151
B2	38	0.0463	16	7.9854	0.0942
B2	60	0.0406	7	4.1235	0.0568
B2	85	0.0368	3	1.6981	0.0228
B2	110	0.0331	1	0.6083	0.0304
B2	130	0.0423	5	2.5268	0.0618
B2	150	0.0494	5	2.4072	0.0675
B2	170	0.0578	3	1.2763	0.0615
B3	32	0.0393	18	11.642	xx
B3	55	0.0413	9	5.344	xx
B3	80	0.0298	6	4.9034	xx
B3	95	0.0673	10	4.1898	xx
B3	120	0.0998	16	5.0555	xx
B3	140	0.0626	13	5.7546	xx
B3	160	0.0476	4	2.2239	xx
B3	180	0.0347	2	1.5471	xx
B4	36	0.0466	21	10.636	0.0855
B4	60	0.0528	3	1.3783	0.0695
B4	80	0.0573	8	3.3277	0.1046
B4	100	0.0619	10	4.1079	0.08
B4	120	0.0563	11	4.8372	0.0583
B4	140	0.0502	14	6.6007	0.0492
B4	170	0.062	17	7.3595	0.04
B5	37	0.0478	40	22.928	0.0827
B5	60	0.0494	5	3.1863	0.036
B5	80	0.0627	7	3.6202	0.1007
B5	105	0.0506	8	4.8763	0.0946
B5	130	0.0736	15	6.4435	0.1152
B5	150	0.0844	16	6.4725	0.0999
B5	170	0.0667	16	7.7756	0.0659

B6	36	0.045	17	9.9768	xx
B6	62	0.0516	5	2.6082	xx
B6	90	0.0523	7	3.6231	xx
B6	110	0.0726	17	7.201	xx
B6	130	0.0922	16	5.1329	xx
B6	150	0.1041	23	6.7365	xx
B6	170	0.1017	21	6.3208	xx
C1	39	0.0416	16	11.271	0.0867
C1	63	0.0416	4	2.8135	0.0578
C1	95	0.0593	5	2.6621	0.0818
C1	125	0.1194	8	2.4223	0.1128
C1	152	0.1441	13	3.6343	0.1479
C1	180	0.1278	16	4.7999	0.1532
C2	38	0.0444	12	7.4356	0.0751
C2	65	0.0437	3	1.9986	0.0456
C2	97	0.0332	1	0.7542	0.0343
C2	129	0.062	7	3.101	0.0956
C2	165	0.0708	6	2.4467	0.0859
C3	39	0.0405	26	19.628	0.087
C3	71	0.0475	3	1.9489	0.0649
C3	110	0.0439	8	4.9194	0.0466
C3	146	0.0577	9	4.5006	0.0652
C3	180	0.0686	10	4.3543	0.0677
C4	35	0.0358	8	5.6555	0.0874
C4	65	0.042	7	4.5433	0.093
C4	100	0.0867	7	2.5877	0.1592
C4	141	0.1097	5	1.5571	0.1849
C4	180	0.0499	8	4.8009	0.0391

C5	38	0.0403	37	23.366	0.0928
C5	75	0.0434	5	2.9734	0.0448
C5	110	0.1013	21	6.5617	0.1723
C5	170	0.0553	11	5.1519	0.0576
C6	40	0.0403	9	5.6721	0.1156
C6	70	0.0318	6	4.6445	0.0489
C6	110	0.0547	12	5.9161	0.1157
C6	145	0.0831	17	6.093	0.1505
C6	180	0.0427	9	5.4773	0.0229
D1	40	0.0502	8	4.0883	0.095
D1	80	0.0518	4	1.9958	0.092
D1	120	0.0387	8	5.0593	0.0233
D1	160	0.0471	11	6.0724	0.0253
D2	45	0.0399	13	8.4684	0.0865
D2	70	0.0498	7	3.8031	0.0721
D2	115	0.0516	5	2.6402	0.0562
D2	150	0.0465	7	3.806	0.0331
D2	180	0.0428	4	2.4429	0.0084
D3	35	0.0438	10	4.9888	0.0919
D3	60	0.0453	3	1.4523	0.1123
D3	80	0.0496	7	3.1746	0.1621
D3	105	0.0699	21	7.6818	0.1415
D3	135	0.0871	27	8.494	0.1162
D3	160	0.1044	18	5.0119	0.1853
D3	180	0.0648	10	3.7415	0.0651
D4	38	0.0437	35	21.416	0.099

D4	60	0.0414	5	3.0686	0.052
D4	79	0.0424	8	4.758	0.0625
D4	100	0.0645	6	2.5877	0.1158
D4	130	0.0696	5	2.2907	0.1
D4	150	0.1074	2	0.6599	0.1983
D4	170	0.0674	0	0	0.0724

D5	40	0.0425	12	7.2899	0.1179
D5	70	0.0513	5	2.6156	0.0983
D5	110	0.0753	8	2.979	0.1084
D5	150	0.1072	17	5.1245	0.205
D5	180	0.0607	5	2.2826	0.0545

C5	38	0.0406	40	25.596	0.0928
C5	38	0.0407	41	26.206	0.0995
C5	38	0.0402	39	25.149	0.1059
C5	38	0.041	42	25.548	xx
C5	38	0.0397	xx	xx	xx

C5	75	0.0419	9	5.6023	0.0448
C5	75	0.0424	7	4.3235	0.0368
C5	75	0.041	7	4.4451	xx
C5	75	0.0414	7	4.4082	xx
C5	75	0.0412	xx	xx	xx

C5	110	0.0956	25	8.0992	0.1723
C5	110	0.096	22	7.1418	0.1659
C5	110	0.0974	23	7.75	xx
C5	110	0.0961	25	8.3568	xx
C5	110	0.1041	25	7.9145	xx





## Averages for Each Core

$\bar{W}$ M/M	T Br mg/cm <sup>2</sup>	Centroid cm	$\bar{\theta}$ L/L	$\overline{D200}$	$\bar{\theta}$ Predicted
0.0476	0.087	91.29	0.0737	0.0373	0.0663
0.0584	0.1	90.44	0.0905	0.0761	0.087
0.0644	0.077	62.07	0.0998	0.0858	0.0921
0.0479	0.0634	88.57	0.0742	0.0526	0.0744
0.0478	0.0657	97.91	0.0741	0.0679	0.0826
0.0601	0.0889	61.81	0.0932	0.0661	0.0816
0.051	0.0382	55.6	0.0791	0.074	0.0858
0.0438	0.0741	75.72	0.0678	0.0564	0.0764
0.0528	0.0798	86.57	0.0819	0.0696	0.0835
0.0553	0.1289	72.02	0.0857	0.085	0.0917
0.0622	0.1032	97.35	0.0964	0.1067	0.1033
0.0742	0.0936	98.55	0.115	0.0673	0.0823
0.089	0.0413	71.95	0.1379	0.0663	0.0817
0.0508	0.0915	70.28	0.0788	0.0589	0.0778
0.0516	0.0539	91.43	0.08	0.0513	0.0737
0.0648	0.1183	67.28	0.1005	0.1249	0.113
0.0601	0.0769	98.42	0.0931	0.1	0.0997
0.0505	0.0468	88.58	0.0783	0.1168	0.1087
0.047	0.0525	71.07	0.0728	0.1127	0.1065
0.0461	0.0949	106.8	0.0715	0.0919	0.0954
0.0664	0.0767	40.86	0.1029	0.0907	0.0948
0.0623	0.0742	92.53	0.0966		
0.0674	0.0634	88.57	0.1045		
Average	Average	Average	Average	Average	Average
0.0575	0.0778	81.12	0.0891	0.079	0.0885
StDev	StDev	StDev	StDev	StDev	StDev
0.0107	0.0233	16.58	0.0166	0.0235	0.0126

## Log space

$\bar{W}$ M/M	T Br mg/cm <sup>2</sup>	Centroid cm	$\bar{\theta}$ L3/L3	$\overline{D200}$	$\bar{\theta}$ Predicted
-3.045	-2.442	4.514	-2.607	-3.289	-2.714
-2.841	-2.303	4.505	-2.403	-2.575	-2.442
-2.743	-2.564	4.128	-2.305	-2.456	-2.385
-3.039	-2.758	4.484	-2.6	-2.945	-2.598
-3.04	-2.723	4.584	-2.602	-2.689	-2.494
-2.811	-2.42	4.124	-2.373	-2.716	-2.506
-2.975	-3.264	4.018	-2.537	-2.604	-2.455
-3.129	-2.603	4.327	-2.691	-2.875	-2.571
-2.941	-2.528	4.461	-2.503	-2.665	-2.483
-2.895	-2.049	4.277	-2.457	-2.465	-2.389
-2.778	-2.271	4.578	-2.34	-2.238	-2.27
-2.601	-2.369	4.591	-2.163	-2.698	-2.498
-2.419	-3.186	4.276	-1.981	-2.714	-2.504
-2.98	-2.392	4.253	-2.541	-2.832	-2.554
-2.963	-2.921	4.516	-2.525	-2.971	-2.608
-2.736	-2.134	4.209	-2.298	-2.08	-2.18
-2.812	-2.566	4.589	-2.374	-2.303	-2.306
-2.985	-3.061	4.484	-2.547	-2.147	-2.22
-3.059	-2.946	4.264	-2.62	-2.183	-2.24
-3.076	-2.355	4.671	-2.638	-2.387	-2.35
-2.712	-2.567	3.71	-2.274	-2.4	-2.356
-2.775	-2.601	4.528	-2.337		
-2.697	-2.758	4.484	-2.258		
Average	Average	Average	Average	Average	Average
-2.872	-2.599	4.373	-2.434	-2.582	-2.434
StDev	StDev	StDev	StDev	StDev	StDev
0.175	0.318	0.229	0.175	0.3079	0.1411

## Appendix J

Results from Giford plot 1985  
Bromide sprayed at .779 mg/cm<sup>2</sup> on 5/21/85

### Definitions and Methods

#### **Days**

Days after bromide was applied. The sample period is the value of Days minus the previous value of Days.

#### **52,54...**

The bromide in parts per million found in the solution collected from soil water sampler number 52, or 54, etc.

For all other information refer to Appendix F

Data collected at 3 feet  
Bromide in ppm

DAYS	52	54	56	58	60	62
14	0.48	0.64	0.48	0.64	0.48	0.32
28	0.24	0.32	0.32	0.32	0.4	0.16
35	0.16	1.36	0.08	0.16	1.36	0.08
42	0.24	0.88	0.24	0.24	3.84	0.08
49	1.12	0.08	0.08	0.24	6.88	0.24
56	5.76	0.8	0.32	0	15.3	1.36
63	10.32	0.72	0.24	1.52	26	2.8
70	15.28	1.04	0.4	3.68	34.5	4.96
77	17.84	0.56	0.56	4	26.5	4.08
88	19.52	0.64	0.96	4.08	19.1	5.28

102	15.28	0.88	2.88	2.64	13.5	8
116	12.08	6.08	5.68	2.88	10.6	9.12
130	7.36	16.2	6	2.64	9.04	8.48
151	10.4	20.5	7.36	3.52	9.84	11.5
180	13.28	12.5	6.88	4.4	7.36	10.6

	$I_1$					
T mass mg/cm <sup>2</sup>	0.524	0.37	0.19	0.14	0.59	0.34
Centroid cm	25.65	34	32.7	27.8	20.5	30
Natural Logs	3.245	3.53	3.49	3.33	3.02	3.4
Average	<b>3.335</b>					
Std Dev	<b>0.185</b>					

	$I_2$					
T mass mg/cm <sup>2</sup>	0.127	0.09	0.05	0.03	0.14	0.08
Centroid cm	6.197	8.21	7.9	6.71	4.96	7.24
Natural Logs	1.824	2.1	2.07	1.9	1.6	1.98
Average	<b>1.914</b>					
Std Dev	<b>0.184</b>					

	$I_3$					
T mass mg/cm <sup>2</sup>	0.288	0.31	0.15	0.09	0.27	0.23
Centroid cm	14.02	15.1	15.5	14.9	11	14.9
Natural Logs	2.641	2.71	2.74	2.7	2.4	2.7
Average	<b>2.649</b>					
Std Dev	<b>0.127</b>					

### $I_3$ using Peaks

T mass mg/cm <sup>2</sup>	0.142	0.114	0.057	0.04	0.154	0.099
Centroid cm	6.95	8.858	8.636	7.559	5.51	8.008
Natural Logs	1.939	2.181	2.156	2.023	1.707	2.08
Average	<b>2.014</b>					
Std Dev	<b>0.175</b>					

Number of days to the centroid of bromide distribution at 3 feet.

Centroid Days	114.3	137.7	134	119.7	98.78	127.8
Average	122.1					
Std Dev	14.34					
Natural Logs	4.739	4.925	4.898	4.785	4.593	4.851
Average	<b>4.798</b>					
Std Dev	<b>0.122</b>					

Days after application of bromide when  $P_3$  occurred.

Peaks Days	70	88	151	151	151	180
Average	<b>131.8</b>					
Std Dev	<b>42.82</b>					
Natural Logs	4.248	4.477	5.017	5.017	5.017	5.193
Average	<b>4.828</b>					
Std Dev	<b>0.374</b>					

Value of  $I_3$  using peaks when  $P_3$  occurred

$P_3$	4.002	2.971	9.796	9.796	9.796	12.9
Average	<b>8.21</b>					
Std Dev	<b>3.865</b>					
Natural Logs	1.387	1.089	2.282	2.282	2.282	2.557
Average	<b>1.98</b>					
Std Dev	<b>.592</b>					

Data collected at 6 feet  
Bromide in ppm

DAYS	51	53	55	57	59	61	63
14	0.32	0.4	0.48	0.64	0.56	0.48	0.4
28	0.16	0.08	0.24	0.32	0.24	0.24	0.16
35	0.08	0	0.24	0.16	0.16	0.24	0.08
42	0.16	0.16	0.4	0.24	0.24	0.24	0.24
49	2.08	0.16	1.84	0.24	0.8	0.24	0.08
56	4.64	0.32	3.92	0.8	3.12	0.32	0.24
63	3.6	0.24	3.52	0.96	4.56	0.4	0.24
70	2.4	0.32	2.4	0.72	4.8	0.48	0.08
77	2.24	0.08	0.8	0.4	5.52	0.48	0.08
88	4.72	0.16	0.4	0.48	5.28	0.88	0.24
102	4.96	0.24	0.64	1.12	5.84	2.08	1.12
116	7.36	1.28	4.08	3.68	8.4	4.16	3.68
130	7.44	3.12	5.92	5.12	7.84	5.12	4.4
151	6.08	4.56	9.36	8.08	6.56	11.8	6.32
180	6.8	5.92	12.6	10.5	6	6.24	8.48

	$I_1$						
T mass mg/cm <sup>2</sup>	0.239	0.11	0.25	0.21	0.26	0.19	0.17
Centroid cm	29.21	36.4	34.4	35.3	27.5	33.5	35.5
Natural Logs	3.375	3.59	3.54	3.56	3.31	3.51	3.57
Average	<b>3.495</b>						
Std Dev	<b>0.108</b>						

	$I_2$						
T mass mg/cm <sup>2</sup>	0.058	0.03	0.06	0.05	0.06	0.05	0.04
Centroid cm	7.055	8.77	8.29	8.52	6.63	8.07	8.58
Natural Logs	1.954	2.17	2.12	2.14	1.89	2.09	2.15
Average	<b>2.073</b>						
Std Dev	<b>0.108</b>						

	$I_3$						
T mass mg/cm <sup>2</sup>	0.157	0.1	0.21	0.17	0.16	0.15	0.14
Centroid cm	14.35	17.1	16.9	17	13.5	15.4	17
Natural Logs	2.664	2.84	2.83	2.83	2.6	2.74	2.83
Average	<b>2.762</b>						
Std Dev	<b>0.097</b>						

	$I_3$ using peaks						
T Mass mg/cm <sup>2</sup>	0.068	0.034	0.077	0.063	0.074	0.057	0.052
Centroid cm	7.769	9.598	9.179	9.37	7.297	8.796	9.394
Natural Logs	2.05	2.262	2.217	2.238	1.987	2.174	2.24
Average	<b>2.167</b>						
Std Dev	<b>0.106</b>						

Number of days to the centroid of bromide distribution at 3 feet.

Centroid Days	121.8	144	138.2	141.2	118.3	135.8	142.5
Average	<b>134.5</b>						
Std Dev	<b>10.33</b>						
Natural Logs	4.802	4.97	4.929	4.95	4.773	4.911	4.959
Average	<b>4.899</b>						
Std Dev	<b>0.079</b>						

Days after application of bromide when  $P_3$  occurred.

Peaks in Days	130	116	151	180	180	180	180
Average	<b>159.6</b>						
Std Dev	<b>27.43</b>						
Natural Logs	4.868	4.754	5.017	5.193	5.193	5.193	5.193
Average	<b>5.059</b>						
Std Dev	<b>0.184</b>						



Value of  $I_3$  using peaks when  $P_6$  occurred

$P_6$	8.241	8.241	9.796	12.9	12.9	12.99	12.9
Average	<b>10.83</b>						
Std Dev	<b>2.337</b>						
Natural Logs	2.109	2.109	2.282	2.557	2.557	2.557	2.557
Average	<b>2.362</b>						
Std Dev	<b>.223</b>						

## Average Curves and Ergodicity Results

3ft	6ft		3ft	6ft	
0.507	0.469		Total Mass mg/cm <sup>2</sup>		
0.293	0.206		.101	.061	
0.533	0.137				
0.92	0.24	3ft	6ft	3ft	6ft
1.44	0.777				
3.92	1.909	Centroids $I_3$ cm		Centroids Days	
6.933	1.931	7.3	8.66	118.7	133
9.973	1.6				
8.92	1.371	$\sigma$	$\sigma$	$\sigma$	$\sigma$
8.267	1.737	3.79	3.35	42.4	39.5
7.2	2.286				
7.747	4.663	$\sigma_x$	$\sigma_x$	$\sigma_x$	$\sigma_x$
8.293	5.566	.619	.596	.7885	.987
10.52	7.531				
9.173	8.069				

Formulation of  $I_3$  Using Peaks in the Place of Centroids

$\alpha_{00}=0.324$  for the last 3 data points.

DAYS	$I_1$	$i_1$	$i_3'$	$I_3'$	$i_3$	$I_3$
				0	0	0
14	0.279	0.279	0.279	0.279	0.065	0.065
28	3.302	3.023	3.023	3.302	0.706	0.771
35	4.318	1.016	1.016	4.318	0.237	1.008
42	5.791	1.473	1.473	5.791	0.344	1.352
49	6.426	0.635	0.635	6.426	0.148	1.5
56	7.569	1.143	1.143	7.569	0.267	1.767
63	7.442	-0.13	0	7.569	0	1.767
70	12.6	5.156	5.156	12.73	1.204	2.971
77	14.48	1.88	1.88	14.61	0.439	3.41
88	17.02	2.54	2.54	17.15	0.593	4.002
102	20.57	3.556	3.556	20.7	0.83	4.833
116	27.1	6.528	6.528	27.23	1.524	6.357
130	32.92	5.817	1.885	29.11	1.885	8.241
151	37.72	4.801	1.555	30.67	1.555	9.796
180	47.3	9.576	3.103	33.77	3.103	12.9

**Appendix K**  
Results from Experiments 3, 4, and 5.  
Bromide (ppm)

20 inch Disk ET

Days	---	3 FEET	---	---	6 FEET	---	Av 3ft	Av 6ft
14	1.28	0	0	0.4	1.04	0.08	0.427	0.507
28	0.64	0.64	0.64	0.24	0	0.24	0.64	0.16
35	0.56	0.8	0.88	0.32	0.24	0.16	0.747	0.24
42	0.56	3.36	1.92	0.64	0.16	0.08	1.947	0.293
49	0.56	12.4	4.24	0.96	0.24	0.24	5.733	0.48
56	0.96	21.84	16	2	0.32	0.56	12.93	0.96
63	1.92	34.4	26.64	3.28	0.48	1.6	20.99	1.787
70	3.84	25.28	32.64	4.64	0.48	3.6	20.59	2.907
77	4.8	xx	32.08	6.8	0.56	6.64	18.44	4.667
88	6.8	xx	27.68	13.44	1.12	9.84	17.24	8.133
102	10	xx	18.96	19.2	2.24	17.36	14.48	12.93
116	14.72	xx	14.4	25.6	4.24	22.48	14.56	17.44
130	13.28	xx	10.56	23.52	4.64	15.68	11.92	14.61
151	12.08	xx	9.44	20.8	5.68	11.36	10.76	12.61
180	10.4	xx	6.64	14.24	7.36	8.24	8.52	9.947

20 inch Disk ET + 60

Days	---	3 FEET	---	---	6 FEET	---	Av 3ft	Av 6ft
14	1.12	0.8	0.96	0.56	0.48	0.4	0.96	0.48
28	0.96	0.56	0.56	0.08	0.16	0.08	0.693	0.107
35	1.2	0.4	0.96	0.64	0.24	0.08	0.853	0.32
42	2.56	0.4	2.48	1.6	0.4	0.08	1.813	0.693
49	xx	1.52	10	8.24	0.88	0.08	3.84	3.067
56	6.4	6.72	28.08	15.52	8.8	0.4	13.73	8.24
63	7.36	15.36	43.52	12.24	12.4	0.8	22.08	8.48
70	11.36	29.76	44.8	14.48	8.4	1.44	28.64	8.107

77	11.68	40.24	45.84	13.12	7.52	2.56	32.59	7.733
88	9.92	41.84	28.64	14.4	9.12	3.68	26.8	9.067
102	7.36	46.48	15.36	18.4	11.6	5.52	23.07	11.84
116	6.24	50.8	9.28	16.8	18.64	9.04	22.11	14.83
130	4.4	40.48	6.08	10.72	15.12	10.48	16.99	12.11
151	2.08	40.4	5.84	9.36	19.68	13.68	16.11	14.24
180	xx	xx	5.68	12.08	18.4	16.56	5.68	15.68

## Ergodicity ET

	$\mu$	$\sigma$	$\mu_x$	$\sigma_x$		$\mu$	$\sigma$
3ft	101.9	41.79	4.624	0.587	Water Table	611.4	250.74
6ft	122.3	35.57	4.807	0.738	Water Table	366.9	106.7

## Ergodicity ET + 60

	$\mu$	$\sigma$	$\mu_x$	$\sigma_x$		$\mu$	$\sigma$
3ft	99.05	36.88	4.596	0.649	Water Table	594.3	221.3
6ft	120.6	42.46	4.793	0.687	Water Table	361.8	127.4

## Lilliston ET

Days	---	3 FEET	---	---	6 FEET	---	Av 3ft	Av 6ft
14	1.84	1.28	1.44	0.56	0.32	0.72	1.52	0.533
28	xx	0.8	0.56	0.32	0.08	0.32	0.68	0.24
35	2.32	xx	0.64	0.32	0.32	0.24	1.48	0.293
42	10.8	xx	2.08	0.64	0.32	0.08	6.44	0.347
49	18.32	0.72	6.08	0.96	0.16	0.24	8.373	0.453
56	24.96	1.44	23.84	1.36	0.32	0.64	16.75	0.773
63	29.68	1.36	26.96	2.08	0.16	0.56	19.33	0.933
70	34.16	1.68	34.96	2.96	0.16	0.88	23.6	1.333
77	32.8	2.56	47.92	3.04	0.24	2.24	27.76	1.84
88	26.32	2.96	58	3.84	0.4	3.84	29.09	2.693

102	16.16	3.84	48	3.68	0.96	6.24	22.67	3.627
116	10.96	8.24	42.8	5.44	1.84	9.92	20.67	5.733
130	7.28	19.84	26.08	5.28	3.6	13.92	17.73	7.6
151	9.28	11.12	18.64	6.64	7.6	24.8	13.01	13.01
180	11.52	xx	16.24	8.72	12.96	26	13.88	15.89

## Lilliston ET +60

Days	---	3 FEET	---	---	6 FEET	---	Av 3ft	Av 6ft
14	xx	1.84	0.48	0.48	0.8	1.52	1.16	0.933
28	0.64	1.2	0.56	0.4	0.24	0.96	0.8	0.533
35	0.88	0.96	0.96	0.64	0.4	0.56	0.933	0.533
42	2.24	1.04	2.8	1.44	0.64	0.4	2.027	0.827
49	4.8	3.2	12.48	2.16	0.88	0.56	6.827	1.2
56	9.84	10.32	11.52	2.8	1.52	0.64	10.56	1.653
63	19.68	16.96	13.76	4.4	2.8	0.64	16.8	2.613
70	30	41.84	20.24	8	5.44	0.72	30.69	4.72
77	34.4	64.72	18	7.36	7.68	0.96	39.04	5.333
88	38.08	82.4	14.56	9.52	11.36	0.64	45.01	7.173
102	32	72.32	10.08	6.88	8.4	0.32	38.13	5.2
116	23.52	51.52	7.52	5.92	11.12	0.72	27.52	5.92
130	15.12	31.04	4.64	6.64	9.52	2	16.93	6.053
151	13.28	21.12	4.96	9.36	12.8	2.96	13.12	8.373
180	xx	14.72	8	10.8	12.16	4.08	11.36	9.013

## Ergodicity ET

	$\mu$	$\sigma$	$\mu_x$	$\sigma_x$		$\mu$	$\sigma$
3ft	102.8	42.54	4.633	0.75	Water Table	616.8	255.5
6ft	139	36.58	4.934	0.913	Water Table	417	219.7

## Ergodicity ET + 60

	$\mu$	$\sigma$	$\mu_x$	$\sigma_x$		$\mu$	$\sigma$
3ft	100.4	37.27	4.609	0.646	Water Table	602.4	223.6
6ft	121.1	44.55	4.797	1.007	Water Table	363.3	133.5

## Beds ET

Days	---	3 FEET	---	---	6 FEET	---	Av 3ft	Av 6ft
14	0.4	xx	0.96	xx	0.16	0.64	0.68	0.4
28	0.32	xx	1.12	0.24	0.56	0.4	0.72	0.4
35	0.4	1.84	1.2	0.08	0.24	0.16	1.147	0.16
42	1.6	3.84	1.44	0.16	0.24	0.32	2.293	0.24
49	3.76	6	1.28	0.16	0.16	0.32	3.68	0.213
56	7.44	7.52	1.92	0.08	0.48	0.4	5.627	0.32
63	12.24	5.84	1.92	0.32	0.56	0.4	6.667	0.427
70	17.52	0.96	1.92	0.32	0.96	0.4	6.8	0.56
77	18.4	0.96	11.68	0.08	1.84	2	10.35	1.307
88	19.84	2.72	7.28	0	4.4	1.28	9.947	1.893
102	19.6	1.12	5.68	1.04	11.52	xx	8.8	6.28
116	20.32	xx	5.04	2.8	27.84	xx	12.68	15.32
130	16	xx	6.56	4.64	38.64	xx	11.28	21.64
151	xx	xx	14.56	8	50.8	xx	14.56	29.4
180	xx	xx	19.04	10.88	40.56	xx	19.04	25.72

## Beds ET +60

Days	---	3 FEET	---	---	6 FEET	---	Av 3ft	Av 6ft
14	0.96	xx	1.2	0.32	0.48	0.4	0.72	0.4
28	1.52	1.36	1.12	0.16	0.16	0.24	1.333	0.187
35	4.32	3.84	1.36	0.24	0.4	0.08	3.173	0.24
42	17.04	12.24	3.44	1.44	0.88	0.08	10.91	0.8
49	20	13.44	12.72	9.12	5.36	0.56	15.39	5.013
56	19.36	13.44	22.8	16.8	13.2	3.36	18.53	11.12

63	19.36	1.52	38.8	16.8	13.36	5.28	19.89	11.81
70	19.12	1.52	25.6	22.24	16.24	8.72	15.41	15.73
77	13.52	2	34.96	21.28	18.4	11.52	16.83	17.07
88	9.68	2.56	36.4	15.2	19.04	16.56	16.21	16.93
102	6.16	1.84	27.28	8.64	10.48	18.96	11.76	12.69
116	4.96	2.24	19.36	10.24	13.52	22.96	8.853	15.57
130	4.96	2.64	6.8	3.6	8.4	20	4.8	10.67
151	5.28	3.04	10.88	7.52	9.28	15.6	6.4	10.8
180	10.72	2.48	10.24	12.64	16.4	12	7.813	13.68

## Ergodicity ET

	$\mu$	$\sigma$	$\mu_x$	$\sigma_x$		$\mu$	$\sigma$
3ft	123.1	44.56	4.813	0.787	Water Table	738.6	267.4
6ft	139.6	30.73	4.939	0.662	Water Table	418.8	92.2

## Ergodicity ET + 60

	$\mu$	$\sigma$	$\mu_x$	$\sigma_x$		$\mu$	$\sigma$
3ft	91.36	45.66	4.515	0.651	Water Table	548.2	274.0
6ft	110.8	43.65	4.708	0.602	Water Table	332.4	131.0

## In Furrow ET

Days	---	3 FEET	---	---	6 FEET	---	Av 3ft	Av 6ft
14	0.56	0.56	0.32	0.64	0.08	0.64	0.48	0.453
28	0.56	0.48	0.32	0.32	0.48	0.32	0.453	0.373
35	2.56	10	6.8	0.32	0.56	0.24	6.453	0.373
42	34.56	66.08	36.4	4.48	4.56	1.76	45.68	3.6
49	20.4	40.64	31.68	10.24	18.72	12.24	30.91	13.73
56	11.68	21.68	19.04	7.68	18.4	20.8	17.47	15.63
63	8.8	13.28	13.2	6.56	16.24	29.28	11.76	17.36
70	5.52	8	8.64	5.2	12.64	31.84	7.387	16.56

77	3.6	5.2	5.84	3.84	8.64	23.68	4.88	12.05
88	2	3.2	4	2.56	5.28	16.4	3.067	8.08
102	1.04	2.08	2.4	1.6	1.92	9.44	1.84	4.32
116	0.88	1.76	2.08	1.28	1.92	6.24	1.573	3.147
130	1.12	2.32	4.24	0.96	1.28	3.68	2.56	1.973

Days	---	3 FEET	---	---	6 FEET	---	Av 3ft	Av 6ft
14	xx	xx	1.84	0.4	0.48	0.4	1.84	0.427
28	5.12	1.68	3.12	0.24	0.72	0.24	3.307	0.4
35	20.8	8	19.04	0.4	1.04	0.16	15.95	0.533
42	32.64	50.16	29.36	15.84	19.12	0.56	37.39	11.84
49	27.12	39.68	18.96	20	22.8	2.4	28.59	15.07
56	19.92	25.44	12.32	13.2	12.88	2.4	19.23	9.493
63	13.52	13.84	7.6	9.84	8.32	1.92	11.65	6.693
70	10	6.88	3.84	7.28	4.56	1.84	6.907	4.56
77	6.96	3.52	1.92	4.64	2.32	1.12	4.133	2.693
88	4.96	1.52	0.96	3.84	2	0.64	2.48	2.16
102	3.28	0.8	0.32	2.96	1.36	0.16	1.467	1.493
116	2.64	0.64	0.4	2.56	1.2	0.48	1.227	1.413
130	2	1.28	0.64	1.68	1.04	0.8	1.307	1.173

## Ergodicity ET

	$\mu$	$\sigma$	$\mu_x$	$\sigma_x$		$\mu$	$\sigma$
3ft	52.95	22.74	3.969	0.42	Water Table	317.7	136.4
6ft	68.22	23.07	4.223	0.543	Water Table	204.7	69.2

## Ergodicity ET + 60

	$\mu$	$\sigma$	$\mu_x$	$\sigma_x$		$\mu$	$\sigma$
3ft	48.36	21.08	3.879	0.609	Water Table	290.2	126.5
6ft	58.35	24.69	4.066	0.562	Water Table	175.1	74.1



## Appendix L

Well Concentrations in ppm Br  
xx means no sample was taken  
Official limit to detection is 0.4 ppm

The purpose of the well data is to calculate the total mass of bromide arriving at the water table as a function of time or net infiltration during Experiment 2. Wells were installed using two foot screens at the water table. The height of the wells were adjusted throughout the study to keep the intersection of water table and well within the screened portion. This was accomplished by pounding or pulling the well to a depth where it yielded approximately 2 - 300 ml before running dry. This adjustment took place prior to sample removal. During November, December and January, wells were bailed to obtain samples. During all other months, wells were sampled using a suction pump.

A total of 13 wells were installed surrounding the experimental plot in the Gifford field during Experiment 2 (Figure 30 page 88). Because of unanticipated flow patterns and limitations of resources, all of the wells did not remain in place for the duration of the experiment. Using county water table maps, the flow under the experimental sight was found to be westward. For this reason, wells 1 through 9 were installed prior to tracer application on the west side of the field. Within the first 63 days of sampling it became apparent that some of the bromide plume was moving across the northern boundary of the plot. After sampling on day

63, wells 2, 3 and 5 were removed and reinstalled as wells 10, 11 and 12. Wells 13, 14, 15 and 16 were installed after sampling on day 88.

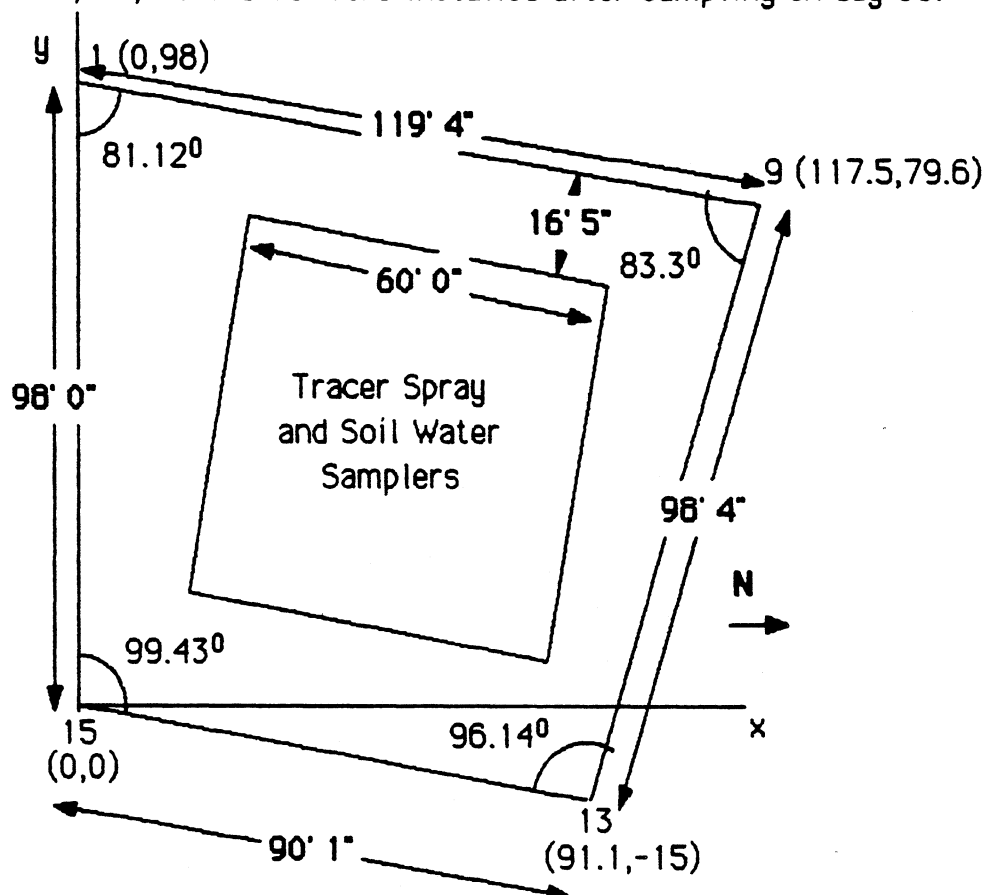


Figure 1. Exact geometry and placement of wells.

### Methods and Definitions

#### **Well heights above datum**

The relative heights of the top of wells 1, 9, 13 and 15 were found using an auto level. Distances from the tops of the wells to the water table were determined using a popper. The lengths reported are distances from an arbitrary datum located beneath the water table.

### Direction of gradient

The direction of the water table gradient was found using heights from all possible combinations of three out of four wells located at the corners of the field. To do this, each well was first located on an arbitrary horizontal  $x, y$  axis (Figure 1). At any point in time the water table is described at a well by three parameters  $(x, y, z)$  where  $z$  is the height of the water table above the datum. The equation of the plane which runs through three points is found using the following procedure;

- 1) Choose three well heights A, B, C described by coordinates  $(x, y, z)$ .
- 2) Choose the point with the minimum distance to the other two points as the origin (i.e. A).
- 3) Subtract the coordinates of A from each of the other two points. This results in vectors  $N1$  and  $N2$ .
- 4) Take  $N1 \times N2 = N3$ . Thus,  $N3$  is a vector perpendicular to the plane.
- 5) Then write  $N3 \cdot (P - A) = 0$  where  $P$  is any point with coordinates  $x, y, z$ .
- 6) Write the equation of the plane in the form  $z = ax + by + c$ .

The direction of the (Deg) gradient is found as degrees from the positive  $x$  axis by

$$\text{Acos} (-a/ |\nabla H|) = \text{Deg when } b < 0$$

or

$$\text{Acos} (-a/ |\nabla H|) + 180 = \text{Deg when } b > 0$$

### The Magnitude of the Gradient

The magnitude of the gradient is determined by

$$|\nabla H| = (a^2 + b^2)^{1/2}$$

### Estimates of Percent Total Mass to Ground Water

The low estimate assumptions:

- 1) There is a constant flow direction of  $115^\circ$  from the x axis;
- 2) There is a constant gradient of 0.00144 ft/ft (G);
- 3) The hydraulic conductivity is 200 ft/day (K);
- 4) Sample concentrations represent average concentrations in the top 2 ft (Z) of aquifer and all of the tracer remains in the top 2 feet;
- 5) There is a linear change in concentration with distance from one well to the adjacent well; and
- 6) All concentrations below 0.4 ppm = 0.

The percent of mass flowing past any two adjacent wells on the west side of the field is calculated as

$$\frac{T(\text{day}) * K(\text{ft}) * G(\text{ft}) * Z(\text{ft}) * D(\text{ft}) * (C_1 + C_2) (\text{gm}) * \cos 34.88^\circ}{2 (\text{ft}^3) \text{ total mass applied}}$$

where  $D$  is the distance between two adjacent wells,  $C_1$  and  $C_2$  are concentrations of bromide in the wells and  $T$  is the number of days from application of the tracer.

The percent of mass flowing past any two adjacent wells on the south side is calculated as above replacing  $\cos 34.88^\circ$  with  $\cos 64^\circ$ . All other concentrations are ignored.

The high estimate assumptions:

- 1) Flow is perpendicular to the western boundary and at  $45^\circ$  to both the northern and southern boundaries of the field;
- 2) All concentrations of bromide are included; and
- 3) All other assumptions are the same as above.

Calculations are the same as above replacing the cosine term with 1.0 ( $\cos 90^\circ$ ) for perpendicular transport and 0.707 ( $\cos 45^\circ$ ) for  $45^\circ$  transport across a boundary.

DAYS	1	2	3	4	5	6	7	8
14	0.24	0.16	0.4	0.4	0.48	0.56	0.56	0.96
28	0.24	0.08	0.24	0.32	0.48	0.16	0.8	0.8
35	0.24	0	0	0.24	0.4	0.16	0.64	0.72
42	0.32	0.08	0.16	0.08	0.16	0.24	0.96	1.44
49	0.08	0.16	0.08	0.08	0.08	0.16	0.32	0.32
56	0.16	0.24	0.24	0.16	0.08	0.24	0.24	0.32
63	0.24	0.08	0.08	0.08	0.08	0.08	0	0.16
70	0.24	xx	xx	0.16	xx	0.16	0.24	0.24
77	0.16	xx	xx	0.08	xx	0.16	0.08	0.24
88	0.24	xx	xx	0.16	xx	0.08	0.16	0.08

102	0.4	xx	xx	0.16	xx	0.08	0.08	0.08
116	0.56	xx	xx	0.24	xx	0.16	0.16	0.24
130	0.08	xx	xx	0.24	xx	0.16	0.24	0.16
151	0.4	xx	xx	0.4	xx	0.4	0.32	0.24
180	0.96	xx	xx	0.8	xx	0.56	0.64	0.56
206	0.64	xx	xx	1.68	xx	1.04	0.64	0.56
237	0.48	xx	xx	8	xx	7.12	0.88	0.56

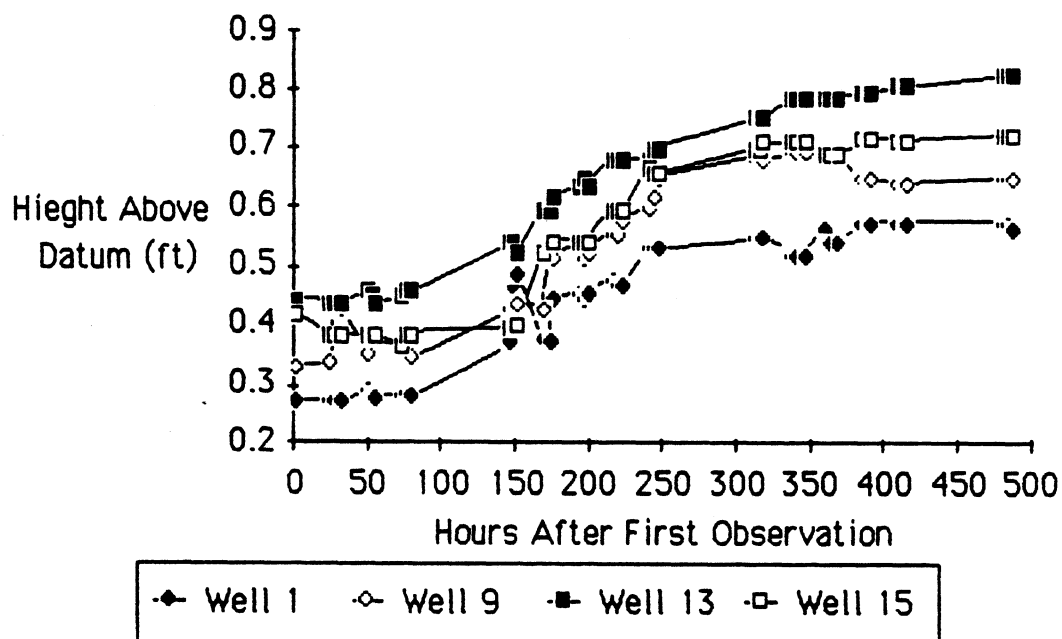
DAYS	9	10	11	12	13	14	15	16
14	0.8	xx	xx	xx	xx	xx	xx	xx
28	0.8	xx	xx	xx	xx	xx	xx	xx
35	0.72	xx	xx	xx	xx	xx	xx	xx
42	0.4	xx	xx	xx	xx	xx	xx	xx
49	0.64	xx	xx	xx	xx	xx	xx	xx
56	0.72	xx	xx	xx	xx	xx	xx	xx
63	0.8	xx	xx	xx	xx	xx	xx	xx
70	0.56	0.24	0.8	0.08	xx	xx	xx	xx
77	0.96	0.16	0.88	0.32	xx	xx	xx	xx
88	0.4	0.56	0.4	0.64	xx	xx	xx	xx
102	0.16	0.64	0.08	0.24	xx	0	xx	0.08
116	0.24	0.64	0.24	0.56	xx	0.08	xx	0.24
130	0.08	0.48	0.16	0.32	xx	0.08	xx	0.24
151	0.16	0.48	0.24	0.24	xx	0.16	xx	0.32
180	0.16	0.72	0.24	0.24	xx	0.24	xx	0.56
206	0.24	0.56	0.24	0.16	0.24	0.24	0.16	0.48
237	0.16	0.32	0.24	0.24	0.24	0.16	0.24	0.32

## Well Heights Above Datum (ft)

Date	Hour	Hours From First Sample	Well 1	Well 9	Well 13	Well 15
------	------	----------------------------	--------	--------	---------	---------

9/3	9	0	0.27192	0.33388	0.44563	0.42388
9/4	9	24	0.27192	0.33908	0.44042	0.38742
9/4	12	27	0.27192	0.43283	0.44042	0.38742
9/4	16	31	0.27192	0.43283	0.44042	0.38742
9/5	10	49	0.29275	0.35471	0.46125	0.38742
9/5	13	52	0.28233	0.38075	0.45083	0.38742
9/5	16	55	0.27713	0.38075	0.44042	0.38742
9/6	9	72	0.28233	0.37033	0.45083	0.36658
9/6	13	76	0.28754	0.35992	0.46125	0.38742
9/6	16	79	0.28233	0.3495	0.46125	0.38742
9/9	11	146	0.37608	0.43283	0.54458	0.39783
9/9	13	148	0.46983	0.43804	0.54458	0.39783
9/9	16	151	0.49067	0.43804	0.52375	0.40304
9/10	9	168	0.38129	0.43283	0.59667	0.52283
9/10	14	173	0.37608	0.51617	0.59667	0.54367
9/10	16	175	0.449	0.51617	0.6175	0.54367
9/11	10	193	0.45942	0.537	0.63833	0.54367
9/11	13	196	0.449	0.51617	0.64875	0.54367
9/11	16	199	0.45942	0.52658	0.63833	0.54367
9/12	8	215	0.48025	0.55783	0.68	0.59575
9/12	12	219	0.46983	0.55783	0.68	0.59575
9/12	16	223	0.46983	0.57867	0.68	0.59575
9/13	9	240	0.53233	0.5995	0.68	0.66867
9/13	12	243	0.53233	0.62033	0.70083	0.65825
9/13	16	247	0.53233	0.65158	0.70083	0.65825
9/16	9	312	0.55317	0.68283	0.75292	0.69992
9/16	12	315	0.55317	0.68283	0.75292	0.69992
9/16	14	317	0.55317	0.68283	0.75292	0.71033
9/17	10	337	0.52192	0.69325	0.78417	0.71033
9/17	13	340	0.52192	0.69325	0.78417	0.71033
9/17	16	346	0.52192	0.69325	0.78417	0.71033
9/18	9	360	0.56358	0.69325	0.78417	0.6895
9/18	12	363	0.54275	0.69325	0.78417	0.6895
9/18	16	367	0.54275	0.69325	0.78417	0.6895
9/19	9	384	0.574	0.65158	0.79458	0.71554
9/19	13	388	0.574	0.65158	0.79458	0.71554
9/19	16	391	0.574	0.65158	0.79458	0.71554

9/20	9	408	0.574	0.64117	0.805	0.71033
9/20	13	412	0.574	0.64117	0.805	0.71033
9/20	16	415	0.574	0.64117	0.805	0.71033
9/23	9	480	0.574	0.65158	0.82583	0.72075
9/23	12	483	0.574	0.65158	0.82583	0.72075
9/23	16	487	0.56358	0.65158	0.82583	0.72075



Magnitude of Gradient 146, 148 and 151 are removed

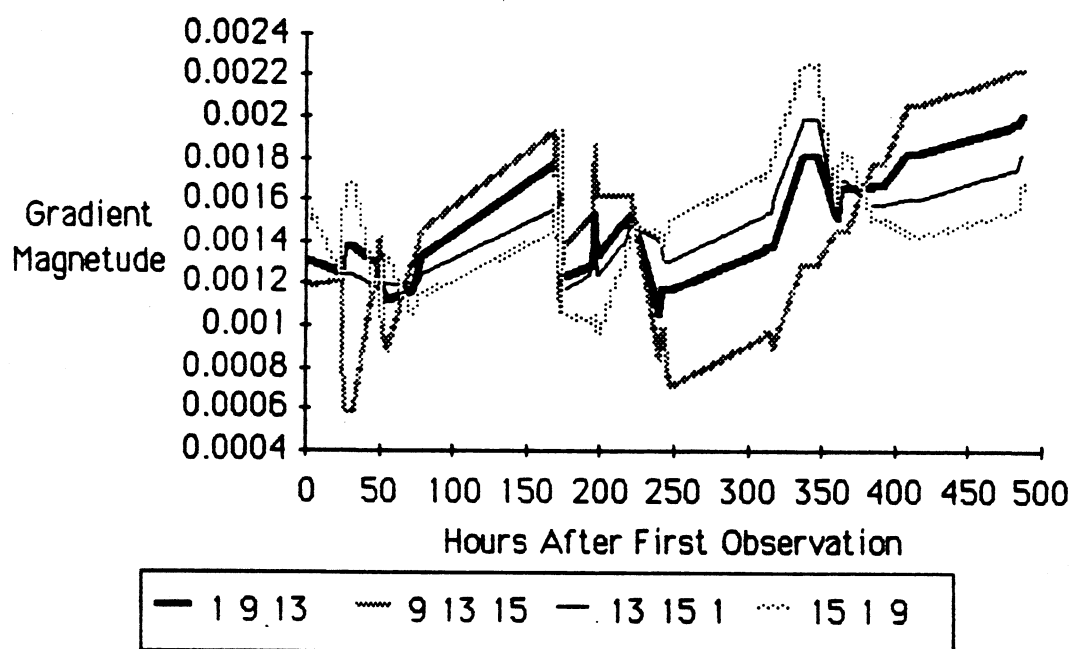
Hours	1 9 13	9 13 15	13 15 1	15 1 9
0	0.00131	0.00119	0.00155	0.00158
24	0.00124	0.00124	0.00124	0.00124
27	0.00137	0.00059	0.00124	0.00167
31	0.00137	0.00059	0.00124	0.00167
49	0.00126	0.00142	0.00116	0.00104
52	0.00116	0.00105	0.00119	0.00126
55	0.00113	0.00088	0.00119	0.00133
72	0.00117	0.0013	0.00116	0.00106
76	0.00126	0.00138	0.0012	0.00112



79	0.00134	0.00147	0.00124	0.00115
168	0.00178	0.00193	0.00155	0.00146
173	0.00152	0.00105	0.00174	0.00194
175	0.00124	0.00138	0.00116	0.00105
193	0.00129	0.00154	0.00124	0.00101
196	0.00153	0.00186	0.00138	0.00105
199	0.00134	0.00162	0.00124	0.00096
215	0.00148	0.00163	0.00139	0.00127
219	0.00153	0.00163	0.00147	0.0014
223	0.00147	0.00146	0.00147	0.00148
240	0.00105	0.00085	0.0014	0.00144
243	0.00117	0.00099	0.00131	0.0014
247	0.00118	0.00072	0.00131	0.00152
312	0.00138	0.00097	0.00153	0.00173
315	0.00138	0.00097	0.00153	0.00173
317	0.00138	0.00089	0.00162	0.00182
337	0.00181	0.00129	0.00198	0.00224
340	0.00181	0.00129	0.00198	0.00224
346	0.00181	0.00129	0.00198	0.00224
360	0.00152	0.00146	0.00153	0.00157
363	0.00166	0.00146	0.00169	0.00183
367	0.00166	0.00146	0.00169	0.00183
384	0.00167	0.00177	0.00157	0.00151
388	0.00167	0.00177	0.00157	0.00151
391	0.00167	0.00177	0.00157	0.00151
408	0.00183	0.00206	0.00161	0.00144
412	0.00183	0.00206	0.00161	0.00144
415	0.00183	0.00206	0.00161	0.00144
480	0.00197	0.00222	0.00175	0.00156
483	0.00197	0.00222	0.00175	0.00156
487	0.00201	0.00222	0.00183	0.00168
Average	0.0015	0.00142	0.00149	0.0015
Stdev	0.00027	0.00045	0.00024	0.00033
Overall	Av	Stdev	CV	
	0.00148	0.00033	0.22346	

# Magnetude of gradient in average direction

Average	0.00144	0.00141	0.00146	0.00148
Stdev	0.00027	0.00047	0.00025	0.00033
Overall	Av	Stdev	CV	
	0.00145	0.00034	0.23248	



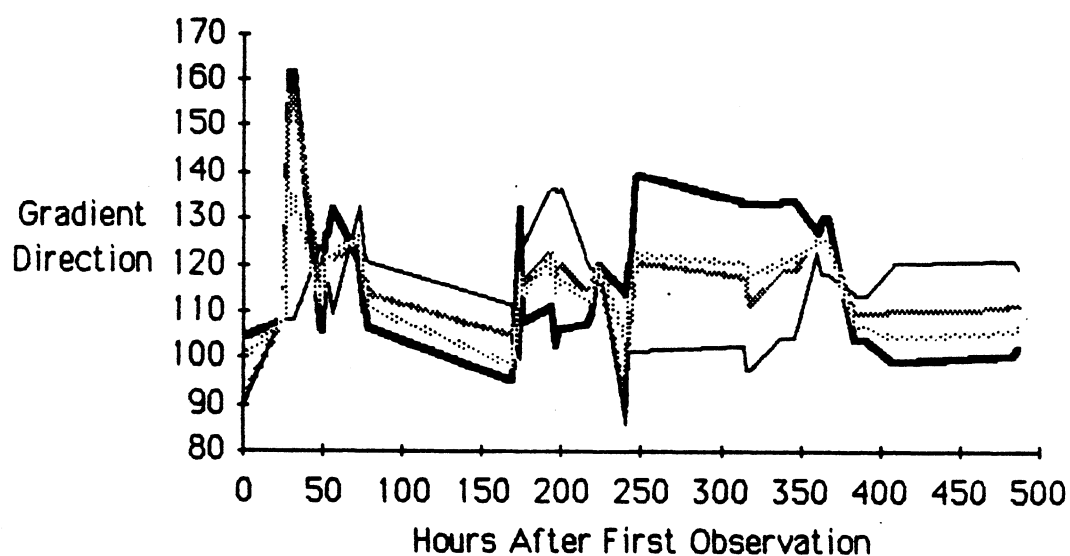
## Direction of gradient in degrees from x axis

146 148 and 151 are removed

Hours	1 9 13	9 13 15	13 15 1	15 1 9
0	104.492	91.9659	89.3003	100.405
24	108.213	108.158	108.121	108.185
27	161.204	156.919	108.121	135.145
31	161.204	156.919	108.121	135.145
49	105.451	114.782	123.919	111.271
52	126.563	121.539	115.769	121.981
55	131.815	121.063	109.318	122.084
72	120.198	125.277	132.272	125.542
76	109.873	116.027	122.158	114.122
79	106.129	113.611	120.512	110.633

168	95.1947	104.977	111.541	98.3785
173	131.862	113.526	99.8666	118.392
175	108.213	116.027	123.919	113.517
193	111.467	122.36	136.178	121.439
196	102.754	118.149	135.773	113.517
199	106.129	119.847	136.178	116.943
215	107.288	114.662	121.723	111.982
219	110.065	114.662	118.955	113.088
223	119.75	119.368	118.955	119.432
240	113.499	88.9145	85.6127	104.274
243	120.198	108.41	101.172	113.088
247	139.305	120.371	101.172	122.341
312	133.321	116.961	102.528	120.125
315	133.321	116.961	102.528	120.125
317	133.321	111.599	97.1366	117.988
337	133.752	118.768	104.317	121.036
340	133.752	118.768	104.317	121.036
346	133.752	118.768	104.317	121.036
360	126.954	125.146	122.709	125.074
363	130.652	125.146	117.81	124.938
367	130.652	125.146	117.81	124.938
384	104.065	109.401	113.475	106.733
388	104.065	109.401	113.475	106.733
391	104.065	109.401	113.475	106.733
408	99.0636	110.421	120.133	104.274
412	99.0636	110.421	120.133	104.274
415	99.0636	110.421	120.133	104.274

480	100.438	111.422	121.123	105.877
483	100.438	111.422	121.123	105.877
487	102.695	111.422	118.932	107.248
Average	117.582	116.463	114.103	114.981
Stdev	16.7026	12.1145	11.8305	8.92101
Overall	Av	Stdev	CV	
	115.782	12.6523	0.10928	



— 1 9 13    - - - 9 13 15    - . - 13 15 1    . . . 15 1 9

### Deleted Values

#### Direction of Gradient

146	102.799	130.978	171.97	153.647
148	66.9602	132.138	337	258
151	52.9324	132.672	328.74	250.99

#### Magnitude of Gradient

146	0.00129	0.00206	0.00159	0.0005
148	0.00109	0.00203	0.00188	0.00075
151	0.00094	0.00166	0.00172	0.00095

## Estimates of Percent Total Mass to Ground Water

Days	Low	High
14	0.00528918	0.01264403
28	0.01297655	0.03667839
35	0.01567407	0.0471489
42	0.01901357	0.05698196
49	0.02108462	0.06518927
56	0.02157329	0.07222681
63	0.02211945	0.07950669
70	0.02260813	0.08423164
77	0.02315429	0.09022156
88	0.02392221	0.09970633
102	0.02547235	0.11119077
116	0.02735587	0.12303196
130	0.02845459	0.1353571
151	0.03288961	0.1545334
180	0.0559612	0.19973704
206	0.09216652	0.260779
237	0.21594495	0.44949599

## IX. Bibliography

- Barcelona, M.J., Helfrich, J.A. and E.E. Garske. 1985. Sampling tubing effects on ground water samples. *Anal. Chem.* 57: 460-464.
- Bear, J. 1972. *Dynamics of fluids in porous media*. American Elsevier.
- Beeson, K.C. 1941 The mineral composition of crops with particular reference to the soils in which they were grown. United States Department of Agriculture, Miscellaneous Publication No. 369.
- Beven, K. and P. German. 1982. Macropores and water flow in soils. *Water Resources Research* 18(5): 1311-1325.
- Biggar, J.W. and D.R. Nielson. 1976. Spatial variability of the leaching characteristics of a filed soil. *Water Resources Research* 12(1): 78-84.
- Boast, C.W. 1973. Modeling the movement of chemicals in soils by water. *Soil Science* 115(3): 224-230.
- Bohn, H.L., B.L. McNeal and G.A. O'Connor. 1979. *Soil Chemistry*. John Wiley and Sons. pp. 94-101.
- Bressler, E. 1973a. Anion exclusion and coupling effects in nonsteady transport through unsaturated soils: II Laboratory and numerical experiments. *Soil Science Society America Proceedings* 382: 213-218.
- Bressler, E. 1973. Simultaneous transport of solutes and water under transient unsaturated flow conditions. *Water Resources Research* 9,4: 975-986.
- Bressler, E. and G. Dagan. 1982. Modeling of water flow and solute transport in unsaturated heterogeneous fields. *Proc. of the Symp. on Unsaturated Flow and Transport Modeling*. Seattle, Wash. March 23-24. Prepared for NRC by Battelle Pacific Northwest Labs.

- Burns, I.G. 1975. An equation to predict the leaching of surface-applied nitrate. *J. Agric. Sci.* 85: 443-454.
- 1976. Equations to predict the leaching of nitrate uniformly incorporated to a known depth or uniformly distributed throughout a soil profile. *J. Agric. Sci.* 86: 305-313.
- Cassel, D.K., M.Th. Van Genuchten and P.J. Wierenga. 1975. Predicting anion movement in disturbed and undisturbed soils. *Soil Science Society America* 39(6): 1015-1019.
- Chesters, G. 1982. *Aldicarb in groundwater*. Water Resources Center, University of Wisconsin - Madison.
- Childs, E.C. 1969. *An Introduction to the Physical Basis of Soil Water Phenomena*. John Wiley and Sons.
- Coats, K.H. and B.D. Smith. 1964. Dead end pore volume and dispersion in porous media. *Society of Petroleum Engineers Journal*, March: 73-84.
- Davis, S.N., G.M. Thompson, H.W. Bentley and G. Stiles. 1980. Groundwater tracers - A short review. *Ground Water* 18(10): 14-23
- Diment, G.A. and K.K. Watson. 1985. Stability analysis of water movement in unsaturated porous materials. 3. Experimental studies. *Water Resources Research* 21(7): 979-984.
- Enfield, C.G., R.F. Carsel, S.Z. Cohen, T. Phan and D.M. Walters. 1982. Approximating pollutant transport to ground water. *Ground Water* 20(6): 711-722.
- England, C.B. 1974. Comments on "A technique using porous cups for water sampling at any depth in the unsaturated zone". By W. Wood and reply. *Water Resources Research* 10(5): 1049-1050.
- Freeze, R.A. and J.A. Cherry. 1979. *Groundwater*. Prentice Hall Inc.
- Fischer, H.B. et al. 1979. *Mixing in inland and coastal waters*. Academic Press. New York.

- Gardner, W.R. and R.H. Brooks. 1956. A descriptive theory of leaching. In: Stembach. 295-304.
- Gaudet, J.P., H. Jegat, G.Vachaud and P.J. Wierenga. 1977. Solute transfer and exchange between mobile and stagnant water, through unsaturated sand. *Soil Sciences Society Journal* 41(4): 665-671.
- Gelhar, . 1981. Analysis of longitudinal dispersion in unsaturated flow. 1. The analytical method. *Water Resources Research* 17,1: 122-130.
- Ghuman, B.S., S.M. Verma and S.S. Prihar. 1975. Effect of application rate, Initial soil wetness, and redistribution time on salt displacement by Water. *Soil Science Society American Proceedings* 39: 7-10.
- Gillham, R.W., E.A. Sudicky, J.A. Cherry and E.O. Frind. 1984. An advection-diffusion concept for solute transport in heterogeneous unconsolidated geologic deposits. *Water Resources Research* 20(3): 369-378.
- Guirtzman, H. and M. Mordeckai. 1986. Investigation of water movement in the unsaturated zone under an irrigation area using environmental tritium. *Water Resources Research* 22(5): 635-642.
- Hillel, D. 1982. *Introduction to Soil Physics*. Academic Press Inc.
- Hillel, D. 1980. Applications of soil physics. Academic Press. N.Y.
- Holley, E.R. and Y.H. Tsai. 1977. Comment on "Longitudinal dispersion in natural channels" by T.J.Day. *Water Resources Research* 13(2): 505-511.
- Holley, E.R. and Y.H. Tsai. 1978. Effects of separation zones on temporal moments. for longitudinal mixing in rivers. *Proceedings of the International Symposium on Environmental Effects of Hydraulic Engineering Works*. Knoxville, Tennessee. Eds: E.E. Driver and W.O. Wunderlich.
- Jim, T.C.Yeh, L.W. Gelhar and A.L. Gutjhar. 1985a. Stochastic analysis of unsaturated flow in heterogeneous soils. 1. *Water Resources Research* 21(4): 447-471.



- \_\_\_\_\_. 1965b. Stochastic analysis of unstaured flow in heterogeneoud soils. II. *Water Resources Research* 21(4): 447-471.
- \_\_\_\_\_. 1965c. Stochastic analysis of unstaured flow in heterogeneous soils. *Water Resources Research* 21(4): 447-471.
- Jones, R. 1984. Personal communications. Union Carbide Agricultural Products Division.
- Jury, W.A. 1982. Simulation of solute transport using a transfer-function model. *Water Resiurces Research* 18(2): 363-368.
- Jury, W.A. 1983. Chemical Mobility and reactivity in soil systems (Chapter 4) ASA, SSSA, Madison, Wisc.
- Jury, W.A. 1985. Spatial varianbility of soil physical parameters in soulte migration: A critical literature review - An iterim report. *Electric Power Research Institute, Inc.*
- Jury, W.A. and G. Sposito. 1985. A field calibration and validation of solute transport model for the unsaturated zone. *Soil Science Society America Journal*. Submitted for publication.
- Jury, W.A. and L.H. Stolzy. 1982. A field test of the transfer function model for predicting solute trnsport. *Water Resources Research* 18(2): 369-355?
- Jury, W.A., G. Sposito and R.E. White. 1985. A transfer-function model of solute transport through soil. 1. Fundamental concepts. *Water Resources Research* (In press).
- Jury, W.A., H. Fluhler and L.H. Stolzy. 1977. Influence of soil properties, leaching, fracton and plant water uptake on solute concentration distribution. *Water Res. Res.* 12(3): 645-650.
- Kimball, C.G. 1983. The thermal, chemical and physical effects on the hydrogeologic system in the sand plain of Wisconsin from water source Heat pump disgcharge via a return well. Masters Thesis, University of Wisconsin.

- Krause, R.T. 1980. Multiresidue method for determining N-Methylcarbamate insecticides in crops, using high performance liquid chromatography. *J. Assoc. Off. Anal. Chem.* 63(5): 1114-1124.
- Kurtz, L.T. and S.W. Melsted. 1973. Movement of chemicals in soils by water. *Soil Science* 115,3: 231-239.
- Lesczynski, D.B. 1969. A comparison of field and laboratory conductivity measurements on Plainfield sand. M.S. Thesis. University of Wisconsin.
- Linsley, \_\_\_\_, \_\_\_\_, Kohler and \_\_\_\_. Paulhaus. 1982. To be entered.
- McMahon, M.A. and G.W. Thomas. 1974. Chloride and titrated water flow in disturbed and undisturbed soil cores. *Soil Sci Soc* 38 (5): 727-732.
- Miller, E.E. 1981. Personal communications. University of Wisconsin-Madison.
- Miller, E.E. and A. Klute. 1967. *Irrigation of Agricultural Lands*. Edited by R.M. Hagan et al. American Society of Agronomy. Chapter 13, pp. 209-244.
- Molz, F.J., O. Guven and J. Melville. 1983. An examination of scale dependent dispersion coefficients. *Ground Water* 21 (6): 715-725
- Nielson, D.R. and J.W. Biggar. 1961. Miscible displacement: I Experimental information. *Soil Science Society America Proceedings* 25: 1-5.
- \_\_\_\_\_. 1962. Miscible displacement: II Behavior of Tracers. *Soil Science Society America Proceedings* 26: 125-128.
- \_\_\_\_\_. 1962. Miscible displacement: III Theoretical considerations. *Soil Science Society Proceedings*: 216-221.
- \_\_\_\_\_. 1963. Miscible displacement: IV Mixing in glass beads. *Soil Science Society Proceedings*: 10-13.
- Pye V.I. and R. Patrick. 1983. Groundwater Contamination in the United States. *Science* 19: 713-718.

- Rao, P.S.C., J.M. Davidson and L.C. Hammond. 1976. Residual management by land disposal. Proceedings of the Hazardous Waste Research Symposium. EPA 600/9-76-015. Edited by W.H. Fuller. U.S. EPA Cincinnati, Ohio.
- Reynolds, E.R.C. 1966. The percolation of rainwater through soil demonstrated by fluorescent dyes. *J Soil Sci* 17: 127-132.
- Rothschild, E.R., R.J. Manser and M.P. Anderson. 1982. Investigation of aldicarb in ground water in selected areas of the Central Sand Plain of Wisconsin. *Ground Water* 20: 437-445.
- Saffigna, P.G., C.B. Tanner and D.R. Keeney. 1976. Non-uniform infiltration under potato canopies caused by interception stemflow and hilling. *Agronomy Journal* 68: 337-342.
- Schuller, R.M., J.P. Gibb and R.A. Griffin. 1981. Recommended sampling procedures for monitoring wells. *Ground Water Monitoring Review (Spring)*: 42-46.
- Sinawong, S. and S.A. El-Swaify. 1974. Predicting exchangeable sodium ration in irrigated tropical vertisols. *Soil Science Society America Proceedings* 38: 732-731?
- Smart, P.L. and I.M.S. Laidlaw. 1977. An evaluation of some fluorescent dyes for water tracing. *Water Resources Research* 13: 15-33.
- Sposito, G., R.E. White, P.R. Darrah and W.A. Jury. 1985. A transfer-function model of solute transport through soil. 3. The convection-dispersion equation. *Water Resources Research* (In press).
- Stumm, W. and J.J. Morgan. 1981. *Aquatic Chemistry*. John Wiley and Sons. p. 611.
- Swartzendruber, D. and D. Hillel. 1973. *Physical Aspects of Soil Water and Salt in Ecosystems*. Edited by A Hadas et al. Springer Verlag A1: p.3-17
- Tanner, C. 1986. Personal communication.
- Tanner, C. and \_\_\_\_ Weis. 1986. To be entered.

- Tsai, Y.H. and E.R. Holley. 1979. Temporal and spatial moments for longitudinal mixing in prismatic channels with storage in separation zones. Hydraulic Engineering Series, Report No. 35. Dept. of Civil Engineering, University of Illinois at Urbana-Champaign. Champaign, Ill.
- United States Department of Agriculture. 1967. Soil survey laboratory data and descriptions for some soils of Wisconsin. Soil Conservation Service, U.S. Department of Agriculture in cooperation with Wisconsin Agricultural Experiment Station
- Vincent, P.J. and J.V. Clarke. 1982. Dyestuff penetration in soils at vegetation boundaries: The effect of the canopy. *J. of Hydrology* 59: 149-160.
- Warrick, A.W. and A. Amoozegar-Fard. 1977. Soil water regimes near porous cup water samplers. *Water Resources Research* 13 (1): 203-207.
- Warwick, A.W. J.W. Biggar and D.R. Nielson. 1971. Simultaneous solute and water transfer for an unsaturated soil. *Water Resources Research* 7,5: 1216-1225.
- Wehtje, G., L.N. Mielke, J.R.C. Leavitt and J.S. Schepers. 1984. Leaching of atrazine in the root zone of an alluvial soil in Nebraska. *J. Environ. Qual.* 4(13): 507-513.
- Westrich, B. 1976. Simulation of mass exchange in dead zones for steady and unsteady flow conditions. *International Symposium on Unsteady Flow in Open Channels*. April 12-15. University of Newcastle-Upon-Tyne, England.
- White, I., P.M. Columbera and J. R. Philip. 1977. Experimental studies of wetting front instability induced by gradual changes in pressure gradient and by heterogeneous porous media. *Soil Science Society America Proceedings* 41: 483-489.
- White, R.E., J.S. Dyson, R.A. Haigh, W.A. Jury and G. Sposito. 1985. A transfer-function model of solute transport through soil. 2. Illustrative applications. *Water Resources Research* (In press).

- Wilson, L.G. 1979. Monitoring in the vadose zone; A review of technical elements and methods. *Environmental Monitoring and Systems Laboratory Office of Research and Development*. U.S. EPA, Las Vegas, Nevada. GE - Kaman Tempo \*GE 79 TMP-55.
- Wilson, J.L. and L.W. Gelhar. 1981. Analysis of longitudinal dispersion in unsaturated flow 1. The analytical method. *Water Resources Research* 17: 122-130.
- Wyman, A.J. 1985. Movement of Aldicarb residues in soil. *Environmental Toxicology and Chemistry* (In press).
- Yaglom, A.M. 1962. *Theory of Stationary Random Functions*. Prentice Hall Inc. New Jersey.
- Yates, W.E. and N.B. Akesson. 1963. Fluorescent tracers for quantitative microresidue analysis. *Transactions of the ACSE* 104
- Yule, D.F. 1976. Longitudinal and transverse dispersion coefficient in unsaturated Plainfield sand. M.S. Thesis. University of Wisconsin-Madison.
- Yule, D.F. and W.R. Gardner. 1978. Longitudinal and transverse dispersion coefficients in Plainfield sand. *Water Resources Research* 14(4): 582-588.

89072249105



b89072249105a

050833- A Simple Stochastic  
Model Predicting Con-  
servative Mass Transport  
Through the Unsaturated  
Zone into Ground Water



89072249105



B89072249105A